THE GLIOBLASTOMA INVASION: PROTEASES, MICROENVIRONMENT AND STEM CELLS

Barbara Breznik, MPharm

Doctoral Dissertation
Jožef Stefan International Postgraduate School
Ljubljana, Slovenia

Supervisor: Prof. Tamara Lah Turnšek, PhD, National Institute of Biology, Ljubljana, Slovenia
Co-Supervisor: Prof. Cornelis J.F. van Noorden, PhD, Academic Medical Center, Amsterdam, The Netherlands

Evaluation Board:
Prof. Boris Turk, PhD, Chair, Jožef Stefan Institute, Ljubljana, Slovenia
Prof. Janko Kos, PhD, Member, Jožef Stefan Institute and Faculty of Pharmacy, University of Ljubljana, Slovenia
Prof. Radovan Komel, Member, PhD, Medical Faculty, University of Ljubljana, Slovenia

MEDNARODNA PODIPLOMSKA ŠOLA JOŽEFA STEFANA
JOŽEF STEFAN INTERNATIONAL POSTGRADUATE SCHOOL



Barbara Breznik, MPharm

THE GLIOBLASTOMA INVASION: PROTEASES, MICROENVIRONMENT AND STEM CELLS

Doctoral Dissertation

INVAZIJA MOŽGANSKEGA TUMORJA GLIOBLASTOMA: PROTEAZE, MIKROOKOLJE IN MATIČNE CELICE

Doktorska disertacija

Supervisor: Prof. Tamara Lah Turnšek, PhD

Co-Supervisor: Prof. Cornelis J.F. van Noorden, PhD

Ljubljana, Slovenia, February 2018

Acknowledgments

Firstly, I would like to thank my supervisor Prof. Tamara Lah Turnšek for giving me the opportunity to work in her research group at the Department of Genetic Toxicology and Cancer Biology at the National Institute of Biology in Ljubljana. I am thankful for her valuable advice and support during my PhD training, as well as for navigating me through the exciting world of science. Moreover, I would like to thank her for revising and correcting this thesis and all other manuscripts.

I am exceptionally thankful to my co-supervisor Prof. Cornelis J.F. van Noorden for giving me the opportunity to work in his laboratory at the Department for Medical Biology at the Academic Medical Center in Amsterdam and for his enthusiastic guidance through histological techniques. Furthermore, I would like to thank him for all the encouraging and positive advice and discussions, as well as for all manuscript revisions during my PhD.

I am grateful to the members of the evaluation board: Prof. Boris Turk, Prof. Janko Kos and Prof. Radovan Komel, for the revision of this doctoral dissertation.

This dissertation would not be possible without our collaboration with medical doctors at the Faculty of Medicine and the University Clinical Centre in Ljubljana. I would like to thank pathologists Clara Limbaeck and Jernej Mlakar at the Institute of Pathology, Faculty of Medicine, for providing us with paraffin-embedded tumour sections. Also, I am thankful to neurosurgeons Andrej Porčnik and Prof. Roman Bošnjak from the Department of Neurosurgery, University Clinical Centre Ljubljana, for providing us with tumour tissue samples and information about patients.

I would like to thank my co-workers Neža, Urška, Helena, Jana, Martina, Klara, Mateja V., Mateja B., Matjaž, Katja, Bojana, Monika, Ana T., Ana R., Katra, Miloš, and Prof. Metka Filipič for their unselfish help, fruitful discussions and a friendly environment. I would also like to thank the students Miha, Monika Š., Monika G., Barbara H., and Barbara Ž. B. for their technical assistance with the experiments. Moreover, I would like to thank the people from Amsterdam: Vashendriya, Mohammed, Rens, Karoline, and Daisy, for their kind welcome at the AMC, our discussions and for their help with immunohistochemistry and microscopy.

Moreover, I would like to thank Prof. Janko Kos and Ana Mitrović for providing us with antibodies and selective protease inhibitors.

This doctoral dissertation was funded by the Slovenian Research Agency, Programme P10245 (TTL) and an ARRS Young Researcher Grant, by the Operational Program for Italy-Slovenia, INTERREG project CB134-GLIOMA, and by the Dutch Cancer Society, grant UVA 2014-6839 (MK).

In the end, I would like to express my gratitude to my family and friends for their endless support and love.

Abstract

Proteases are involved in different processes of cancer progression by cleaving peptide bonds and thus modifying proteins. One of the processes is the invasive spread of the brain tumour glioblastoma (GBM). Besides single GBM cell invasion into surrounding brain parenchyma, GBM is characterized by significant heterogeneity. In this thesis, the GBM invasion is addressed in relation to invasion-associated proteases and the heterogeneous nature of GBM. Four GBM subtypes have been identified on the basis of clinical behaviour and patient's survival. GBM cell heterogeneity is a consequence of both different cancer cells and different stromal cells, such as mesenchymal stem cells (MSCs).

It was shown that GBM cell lines U87 and U373 differ in their invasive properties, with the U87 cell line being more invasive and expressing higher levels of proteases. It was proven that the effects of tumour-infiltrating MSCs on GBM cell invasion is GBM cell type-specific. MSCs increased the invasion of U373 cells and inhibited the invasion of U87 cells. MSCs enhanced invasion of U373 cells via overexpression of proteases, such as cathepsin B, calpain1, uPA/uPAR, MMP-2, -9 and -14, and increased activities of some of these proteases, whereas selective protease inhibitors had no effect on U87 cell invasion upon MSC co-culturing. New selective cathepsin B inhibitors were tested and GBM cell type-specific inhibition of cell migration in MSC and GBM cell co-cultures was demonstrated, implicating the importance of addressing the GBM heterogeneity when testing novel anti-GBM drugs. By monitoring GBM cell invasion upon their co-injection with MSCs into the brain of zebrafish embryo, GBM cell type-dependent responses to MSCs were confirmed *in vivo*. It was demonstrated that zebrafish embryos are an excellent model for studying GBM heterogeneity.

The research described in this thesis was focused on the expression of the lysosomal cysteine cathepsins B, K and X, which were found to be upregulated in GBM tissue. High cathepsin X mRNA levels were associated with poor GBM patient survival. Moreover, it was found that cathepsins K and X were heterogeneously expressed and that GBM subtype–dependent expression had predictive value with respect to overall survival, indicating the importance of taking into account GBM heterogeneity when exploring novel biomarkers.

Therapy-resistant GBM stem cells (GSCs) reside in specific tumour tissue niches and contribute to the heterogeneity of GBM. It was demonstrated that cathepsin X, K and B are localized in GSC niches both in paraffin and cryostat GBM tissue sections. *In vitro*, it was demonstrated that SDF-1α induces chemotactic responses of CXCR4- and CXCR7-positive GSCs supporting the concept that this cytokine recruits GSCs to niches. Moreover, it was shown that cathepsin K can cleave SDF-1α at the N-terminal site and thus inhibits its chemotactic effects on CXCR4/7-positive GSCs. This implies that cathepsin activity may facilitate the invasion of GSCs out of their niches. The clinical relevance of this finding is supported by correlations that were observed between mRNA expression of cathepsins and GSC niche markers in GBM tissues. In summary, previously unknown roles of proteases in GBM pathobiology, such as mediation of GBM-MSC interactions and regulation of GSC invasion from their niches were demonstrated.

Povzetek

Proteaze so s cepitvijo peptidnih vezi in posledično modifikacijo številnih proteinov udeležene v različnih procesih napredovanja raka, vključno z invazivnostjo možganskega tumorja glioblastoma (GBM). Poleg invazije posameznih celic GBM v okoliško možganovino je za GBM značilna heterogenost. V tej doktorski nalogi invazivnost GBM obravnavamo v povezavi s proteazami in heterogeno naravo GBM. Na podlagi stopnje preživetja in kliničnega obnašanja so bili identificirani 4 podtipi GBM. Celična heterogenost GBM je posledica prisotnosti različnih rakavih celic in stromalnih celic, kot so mezenhimske matične celice (MSC).

Pokazali smo, da se celični liniji GBM U87 in U373 razlikujeta v invazivnih lastnostih. Celična linija U87 je namreč bolj invazivna in izraža višji nivo proteaz kot celična linija U373. Dokazali smo, da je učinek v tumor infiltrirajočih celic MSC na invazijo celic GBM specifičen glede na vrsto celic GBM. MSC so povečale invazijo celic U373 in zmanjšale invazijo celic U87. MSC so povečale invazijo celic U373 preko povečanega izražanja proteaz, kot so katepsin B, kalpain 1, uPA/uPAR, MMP-2, -9 in -14, in preko povečane aktivnosti nekaterih proteaz. Nasprotno pa selektivni inhibitorji proteaz niso imeli učinka na invazijo celic U87 ob so-gojenju z MSC. Testirali smo tudi nove selektivne inhibitorje katepsina B ter dokazali celično specifično inhibicijo migracije celic v ko-kulturi celic GBM in MSC, kar nakazuje na pomembnost obravnavanja heterogenosti GBM pri testiranju novih protitumorskih učinkovin. S spremljanjem invazije celic GBM ob njihovem ko-injiciranju z MSC v možgane zarodkov rib cebric, smo potrdili različen odziv celic GBM na MSC *in vivo*, ki je odvisen od vrste celic GBM. Prikazali smo, da so zarodki rib cebric odličen model za študijo heterogenosti GBM.

V študiji predstavljene doktorske naloge smo se osredotočili na izražanje lizosomalnih cisteinskih katepsinov B, K in X, ki so povišano izraženi v tkivu GBM. Visok mRNA nivo katepsina X je bil povezan s slabšim preživetjem bolnikov z GBM. Poleg tega smo ugotovili heterogeno izražanje katepsinov K in X ter da je napovedna vrednost za preživetje izražanja katepsinov odvisna glede na GBM podtip. Vse to nakazuje na pomembnost upoštevanja heterogenosti GBM pri raziskovanju novih bioloških označevalcev.

Na terapijo odporne GBM matične celice (GSC) prebivajo v specifičnih tumorskih tkivnih nišah ter prispevajo k heterogenosti GBM. Z uporabo tako parafinskih kot zamrznjenih rezin tkiv GBM smo odkrili, da so katepsini B, K in X lokalizirani v nišah GSC. Prikazali smo, da SDF-1α sproži kemotaktični odziv CXCR4- in CXCR7-pozitivnih celic GSC *in vitro*. Ta rezultat podpira koncept, da citokin SDF-1α rekrutira GSC v niše. Poleg tega smo pokazali, da katepsin K cepi SDF-1α na N-terminalnem koncu in s tem inhibira njegov kemotaktični učinek na CXCR4/7-pozitivne GSC. To pomeni, da aktivnost katepsinov lahko pospeši invazijo GSC iz njihovih niš. Kliničen pomen teh izsledkov je potrjen z opaženimi korelacijami med mRNA izražanjem katepsinov in označevalcev niš GSC v tkivih GBM.

V doktorski dizertaciji smo dokazali doslej nepoznane vloge proteaz v patobiologiji GBM, kot sta mediacija interakcij med celicami GBM in MSC ter regulacija invazije GSC iz njihovih niš.

Contents

List of Tables **xv**

Abbreviations **xvii**

1 Introduction **1**
1.1 Glioblastoma ... 1
1.2 Glioblastoma: A Heterogeneous Disease ... 1
1.2.1 Molecular Subtypes of Glioblastoma ... 2
1.2.2 Intra-Tumoural Heterogeneity ... 3
1.2.3 Glioblastoma Microenvironment ... 4
1.2.3.1 Glioblastoma Stem Cells ... 4
1.2.3.2 Glioblastoma Stem Cell Niches ... 5
1.3 Glioblastoma Invasion ... 6
1.3.1 Proteases ... 6
1.4 Advanced Models for Studying Cancer Progression: from *in vitro* Three Dimensional (3D) Cellular to *in vivo* Zebrafish Xenotransplantation Models ... 7
1.5 Scientific Problems and Aims of this Thesis ... 8
1.5.1 The Invasion of Various GBM Cell Lines and the Effects of MSCs ... 9
1.5.2 Studying MSC-GBM Interactions in Zebrafish Embryo Model ... 9
1.5.3 Expression of Cathepsins K and X in Glioblastoma Tissues ... 9
1.5.4 Cathepsins in GSC Niches ... 10
1.6 Research Hypothesis ... 10
1.7 Publications Included and Candidate' s Contributions ... 12

2 Scientific Publications **15**
2.1 Proteases and Cytokines as Mediators of Interactions Between Cancer and Stromal Cells in Tumours ... 15
2.2 Mesenchymal Stem Cells Differentially Affect the Invasion of Distinct Glioblastoma Cell Lines ... 27
2.3 Imaging of Human Glioblastoma Cells and Their Interactions with Mesenchymal Stem Cells in the Zebrafish *(Danio rerio)* Embryonic Brain ... 46
2.4 Addition of 2-(Ethylamino)Acetonitrile Group to Nitroxoline Results in Significantly Improved Anti-Tumor Activity *in vitro* and *in vivo* ... 56
2.5 Cathepsins K and X in Glioblastoma Progression and Survival (in Revision) ... 69
2.6 Cysteine Cathepsins B, X and K Expression in Peri-Arteriolar Glioblastoma Stem Cell Niches (in Revision) ... 85
2.7 Cathepsin K Cleavage of SDF-1α Inhibits its Chemotactic Activity Towards Glioblastoma Stem-Like Cells ... 111

3 Discussion and Conclusions **123**

Appendix A Supplementary Material of Included Publications ... 127

A.1 Supplementary Material of Publication 2.2. 127
A.2 Supplementary Material of Publication 2.5. 138
A.3 Supplementary Material of Publication 2.6. 148

Appendix B Permissions for Reproduction of Included Publications.....154
B.1 Permission for Reproduction of Publication 2.7. 154

References **155**

Bibliography **165**

Biography **167**

List of Tables

Table 1.1: Genetic changes and characteristics of different GBM subtypes (adopted from Philips et al., 2006; Verhaak et al., 2010; Van Meir et al., 2010). 3

Abbreviations

2D	... Two-dimensional
3D	... Three-dimensional
ABC transporters	... ATP-binding cassette transporters
CAF	... Cancer-associated fibroblast
CNS	... Central nervous system
CSC	... Cancer stem cell
CSF-1R	... Colony-stimulating factor 1 receptor
CXCR4/7	... Chemokine receptor type 4/7
EC	... Endothelial cell
ECM	... Extracellular matrix
EMT	... Epithelial to mesenchymal transition
GBM	... Glioblastoma
GSC	... Glioblastoma stem cell
HSC	... Hematopoietic stem cell
IDH1/2	... Isocitrate dehydrogenase 1/2
IL	... Interleukin
MGMT	... The O-6-methylguanine-DNA methyltransferase
MMP	... Matrix metalloprotease
mRNA	... Messenger ribonucleic acid
NF-kB	... Nuclear factor kappa-light-chain-enhancer of activated B cells
qRT-PCR	... Quantitative real-time polymerase chain reaction
SDF-1α	... Stromal-derived factor 1α
SMA	... Smooth muscle actin
TAM	... Tumour-associated macrophage
TCGA	... The Cancer Genome Atlas
TGF-β	... Transforming growth factor beta
TME	... Tumour microenvironment
uPA	... Urokinase-type plasminogen activator, urokinase
uPAR	... Urokinase-type plasminogen activator receptor
WHO	... World Health Organization

Chapter 1

Introduction

1.1 Glioblastoma

Malignant diffuse gliomas are brain tumours of neuroepithelial tissue and are classified according to histopathological and molecular features. As they can arise from different types of glial cells, we distinguish astrocytomas, oligoastrocytomas and oligodenrogliomas. Glioblastoma (GBM), WHO grade IV astrocytoma, represents the most commonly-occurring and biologically aggressive form of primary brain tumours (Louis et al., 2016). The annual incidence of GBM is 3.2 cases per 100,000 (Gallego, 2015). GBM is characterized by nuclear atypia, cellular pleomorphism, mitotic activity, vascular thrombosis, microvascular proliferation, and necrosis (Ohgaki & Kleihues, 2013). The median survival of patients with GBM after diagnosis is only 15 months despite multimodality treatment comprising of surgery, radiotherapy and temozolomide therapy (Czarnek et al., 2016). The reasons for poor patient survival and tumour recurrence are infiltrative invasion of individual GBM cells into the surrounding healthy parenchyma, high resistance to therapy and the tumour heterogeneity (Verhaak et al., 2010; Bonavia et al., 2011; Cuddapah et al., 2014; Gallego, 2015).

In the 2016 World Health Organization classification of tumours of the central nervous system classification (CNS WHO) (Louis et al., 2016), GBM were classified for the first time into isocitrate dehydrogenase (IDH)-wild type and IDH-mutant GBM, which are synonyms for primary GBM and secondary GBM, respectively. Secondary GBM have a mutation in either the IDH1 or IDH2 gene and the IDH1 mutation is a reliable diagnostic marker of secondary GBMs (Ohgaki & Kleihues, 2013). Primary GBM, which occur in approx. 90% of all GBM cases, develop rapidly de novo, mostly in elderly patients. Meanwhile, secondary GBM progress from low-grade diffuse gliomas in younger patients and have a significantly better prognosis (Louis et al., 2016). Primary and secondary GBM have similar morphological and biological hallmarks of GBM. Furthermore, therapy resistance and consequently tumour recurrence is inevitable in both GBM types, although with significantly different rates.

1.2 Glioblastoma: A Heterogeneous Disease

Tumour heterogeneity is a well-known characteristic of cancers and is crucial for cancer spreading and resistance to therapy. GBM is a heterogeneous type of tumour with inter- and intra-tumoural heterogeneity, both at the molecular and cellular level (Ohgaki & Kleihues, 2013). Therapy responses of GBM patients are impossible to predict on the basis of histopathology only. At present, more advanced and personalized medicine approaches

are becoming available to understand pathobiology of GBM and to improve the treatment of GBM.

1.2.1 Molecular Subtypes of Glioblastoma

Based on genomic profiling of 206 patient samples, The Cancer Genome Atlas (TCGA) research network defines 4 molecular subtypes of GBM: proneural, neural, classical and mesenchymal subtype. These GBM subtypes differ in the expression pattern of signature genes and signalling-pathway alterations, which drive GBM pathogenesis. It has been speculated that GBM of different subtypes have a different cause or different cells of origin (Verhaak et al., 2010). The final goal of this classification is the development of more effective and personalized therapeutic strategies for each subtype of GBM tumours. Detailed genetic changes and characteristics of each GBM subtype are listed and described in Table 1.1. The studies imply that secondary GBM (IDH-mutated) have a proneural expression pattern, whereas primary GBMs show all expression profiles such as proneural, neural, classical and mesenchymal (Verhaak et al., 2010; Ohgaki & Kleihues, 2013). Recently, three GBM-intrinsic transcriptional subtypes were revealed: the proneural, classical and mesenchymal subtypes by Wang et al. (2017). The classification of these subtypes is based on gene expression in GBM cells only, because the expression of genes in tumour-associated microenvironment was filtered out.

Table 1.1: Genetic changes and characteristics of different GBM subtypes (adopted from Philips et al., 2006; Verhaak et al., 2010; Van Meir et al., 2010).

GBM subtype	Genetic changes and characteristics
Proneural	*PDGFRA* amplification *IDH1* point mutation *PIK3A/PIK3R1* mutations *TP53, CDKN2A* and *PTEN* loss/mutation Proneural marker expression (*SOX, DCX, DLL3, ASCL1, TCF4*) Oligodendrocytic marker expression (*PDGFRA, OLIG2, TCF3, NKX2-2*) HIF, PI3 kinase and *PDGFRA* pathways activation Younger patients
Neural	*EGFR* amplification/overexpression Gene signature of normal brain Neuron marker expression (*NEFL, GABRA1, SYT1, SLC12A5*)
Classical	*EGFR* mutation/amplification/overexpression *PTEN* loss/mutation *CDKN2A* loss *NES* overexpression (neural precursor and stem cell marker) Notch (*NOTCH3, JAG1, LFNG*) and Sonic hedgehog (*SMO, GAS1, GLI2*) pathway activation
Mesenchymal	*NF1* loss/mutation *TP53* loss/mutation *PTEN* loss/mutation Mesenchymal marker overexpression (*MET, CHI3L1, CD44, MERTK*) TNF family and NFkB pathway activation Higher necrosis High infiltration of immune cells

Genomic profiling-based GBM classification is clinically relevant for patients by predicting the disease outcome and their response to treatment. Aggressive therapy (chemo- and radiotherapy) reduced mortality in classical and mesenchymal subtypes, but it did not change the survival of proneural subtype (Verhaak et al., 2010).

Further investigations of genome, transcriptome, miRNAs, DNA methylation status and proteomic profiling of different GBM subtypes brought new insights in GBM classification and the prediction of patient responses to treatment. For example, DNA methylation of the O-6-methylguanine-DNA methyltransferase (MGMT) gene promoter was found to be a predictive biomarker for the treatment response of the classical subtype only and not for the other subtypes (Brennan et al., 2013).

1.2.2 Intra-Tumoural Heterogeneity

Intra-tumoural heterogeneity is one of the major reasons of unreliable predictions with respect to therapy responses and outcome of the treatment, as TCGA classification of whole GBM tumours did not have sufficient predictive significance (Renovanz & Kim, 2014; Ellis et al., 2015; Segerman et al., 2016). Genomic and transcriptomic profiling of whole GBM tumours showed only small differences in prognosis and therapy response among different GBM subtypes (Verhaak et al., 2010; Brennan et al., 2013). Recently,

different molecular subtypes were found in one and the same GBM tumour at regional and at single cell levels, implicating that different cancer cell subclones with diverse biological behaviour co-exist within the same tumour (Patel et al., 2014; Segerman et al., 2016). Chemotherapy can even further enhance this heterogeneity by causing additional mutations in signalling pathways within the tumour mass (Johnson et al., 2014). Moreover, interactions between distinct GBM cells can lead to GBM progression and therapeutic resistance as described by Ricklefs et al. (2016) and Motaln et al. (2015).

In addition to already described cell-autonomous factors (e.g., genomic and epigenomic heterogeneity), intra-tumoural heterogeneity can be governed by non-cancer cell-autonomous factors (e.g., stromal heterogeneity), which refers to the presence of extracellular matrix (ECM) and distinct non-cancerous cell populations within the GBM mass, such as endothelial cells (ECs), infiltrating immune cells, fibroblasts and other cell types (Cassidy et al., 2015). How these stromal factors that represent the GBM microenvironment affect GBM progression is discussed in the following section.

1.2.3 Glioblastoma Microenvironment

The hypothesis of tumour microenvironment (TME) has its origins in 1889, when the English surgeon Sir James Paget compared tumour cells with the seed of plants as they are both carried in all directions; but they can only live and grow if they fall on congenial soil. He hypothesized that metastatic cells can thrive only where conditions are in some way favourable (Mueller & Fusenig, 2004). Now it is proven that cancer progression is a result of intensive intercellular interactions between cancer cells and non-cancerous stromal cells within the tumour and its surrounding supporting tissue, called TME or stroma. Cancer cells in the TME coexist with ECs, pericytes, immune cells, fibroblasts and mesenchymal stem cells (MSCs) that infiltrate the tumour mass (Hannahan & Coussens, 2012; Hossain et al., 2015). In GBM, also brain-specific cell types including microglia, neurons, astrocytes, glial and neuronal progenitors, are present, dynamically communicating with glioma cells to promote tumour growth and therapy resistance (Placone et al., 2015; Quail & Joyce, 2017). Furthermore, non-cellular components such as soluble factors (growth factors, cytokines) and insoluble matrix-forming proteins of the ECM, participate in a complex network within TME (Quail & Joyce, 2017).

Various promising approaches to target components of the TME and/or to normalize the TME in GBM are investigated in preclinical and clinical studies (Quail & Joyce, 2017). For example, repolarization and re-education of tumour-promoting macrophages and microglia can be achieved by colony-stimulating factor 1 receptor (CSF-1R) inhibitors, which are already in clinical trials for recurrent GBM (Butowski et al., 2015). Although these studies are in early stages, they show clinical potential of selectively targeting TME components in GBM, either via monotherapy or as a part of multimodal treatment regimens.

1.2.3.1 Glioblastoma Stem Cells

Cancer stem cells (CSCs) are a small population of tumorigenic and self-renewing cancer cells that contribute to tumour initiation, progressive tumour growth and therapeutic resistance (Van Meir, 2010; Borovski et al.,2011; Podergajs et al., 2016; Ludwig et al., 2017). CSCs are resistant to conventional therapies due to active DNA damage response mechanisms, the ability to evade cell death and high expression of ATP-binding cassette (ABC) transporters (Bao, 2006; Borovski, 2011; Tajnsek, 2013; Rama, 2014). The theory of CSCs, which hypothesize that the tumours are initiated by a subtype of stem-like cells, originates back in the 19th century. In recent years, the stochastic and hierarchical models

of carcinogenesis have been challenged by a mixed CSC model (Bjerkvig et al., 2009), which includes the features of both, the stochastic and hierarchical model, to explain tumour development, as has been reviewed in detail by Tajnsek and co-workers (2013). CSCs may arise in different ways: from normal stem cells/progenitors or from already differentiated cells, which undergo mutations, dedifferentiate and re-acquire stem-like properties (Van Meir et al., 2010; Tajnsek et al., 2013). CSCs are defined by three functional characteristics *in vitro* and *in vivo*: sustained self-renewal, persistent proliferation and tumour initiation upon secondary transplantation (Lathia et al., 2015). Clear-cut characterization of CSCs is not available since CSCs in different tumour types are defined by different markers and CSCs can arise from multiple populations. Moreover, CSCs show inherent phenotypic plasticity and adaptability to the microenvironment clues (Plaks et al., 2015).

Numerous markers of GBM stem cells (GSCs) have been identified such as surface proteins CD133, CD15, CD44, integrin α6, L1CAM, transcriptional factors SOX2, NANOG, Olig2 and intermediate filament nestin (Singh et al., 2003; Lathia et al., 2010; Ludwig et al., 2017). Recently, transmembrane protein CD9 has been reported as potential selective GSC marker that can allow discrimination between GSCs and normal neural stem cells (Podergajs et al., 2016). Although CD133-negative glioma cells can have tumour-initiating potential, cell surface glycoprotein CD133 (also named prominin-1) remains the most commonly used cell surface marker for isolation and identification of GSCs (Beier et al., 2007; Wang et al., 2008; Campos et al., 2010; Ludwig et al., 2017).

1.2.3.2 Glioblastoma Stem Cell Niches

GSC differentiation state and quiescence are regulated by external (extrinsic) factors, which include the host immune system and factors in GSC niches. These are specific microenvironments, where GSCs are maintained and protected against therapy (Lathia et al., 2015). Moreover, dynamic interactions of GSCs with non-neoplastic stromal cells and the ECM within niches create a supportive microenvironment for GSC survival, growth and immune surveillance (Borovski, 2011; Tajnšek, 2013; Gattazzo, 2014; Hambardzumyan & Bergers, 2015; Plaks et al., 2015). Various cell types, both cancerous and stromal, within the CSC niche promote CSC stemness through cell-cell interactions and paracrine signalling. For example, cancer-associated fibroblasts (CAFs) with increased cytokine production activate Wnt and Notch signalling pathways, which are both implicated in stem cell maintenance (Plaks et al., 2015). Another activated pathway in CSCs is NF-kB, promoted by stromal MSC-derived SDF-1α, IL-6 and IL-8 (Cabarcas et al., 2011). On the other hand, CSCs directly modulate the cells of the immune system to create an immune-suppressive environment within the niche. CSC-secreted TGF-β and IL-10 suppress the function of tumour-associated macrophages (TAMs) and generate the immunosuppressive M2 TAM phenotype (Wu et al., 2010). Moreover, cross-talk between ECs and GBM cells is crucial for angiogenesis and GSC propagation in the niches (Roos et al., 2017).

Within GBM, morphologically and functionally distinct GSC niches such as perivascular, hypoxic and invasive niches can be found. With GBM invasion and growth also the switch between different niches can occur. For example, expanding tumour growth triggers hypoxia and subsequent vascularization, consequently transforming the hypoxic niche into a perivascular niche (Hambardzumyan & Bergers, 2015). In the perivascular niche, GSCs reside close to abnormal blood vessels (Calabrese, 2007; Borovski, 2011), whereas in the vascular-invasive niche GBM cells migrate along blood vessels, enabling invasion deep into the brain parenchyma (Cuddapah, 2014; Hambardzumyan & Bergers, 2015).

1.3 Glioblastoma Invasion

GBM cells individually or in small clusters invade into the brain parenchyma, up to 4-7 cm away from the tumour bulk, thus preventing complete surgical removal of the GBM cells (Mentlein et al., 2012). Because the GBM cell-specific properties enable diffuse infiltration and their survival during conventional treatment approaches, GBM cells are also called guerrilla warriors (Claes et al., 2007). Gliomas frequently home and migrate along nerve tracts, meninges and blood vessels (Claes et al., 2007; Mentlein et al., 2012; Cuddapah et al., 2014). Already in 1939, neuropathologist Scherer (1938) described that gliomas migrate along existing brain structures, also called "secondary structures". He was the first to describe preferential sites of glioma homing and invasion: brain parenchyma (around neurons), blood vessels, white matter tracts and below the margins of the pia mater. Although glioma cells are extremely invasive, gliomas rarely metastasize outside the brain (Cuddapah et al., 2014).

GBM invasion differs from invasion of other cancer types into parenchyma or stroma, because of the different composition of brain ECM. In the compact cellular environment of brain tissue, extracellular space presents only 20% of the tissue volume, whereas network of neuronal and glial cells fills the rest (Rauch, 2007). The extracellular space of brain is composed of a ternary network of the glycosaminoglycan hyaluronic acid, proteoglycans of the lectican family, which are connected directly or through linker proteins, and tenascins interspersed in the structures that connect the network to cell surfaces (Rauch, 2004). Brain ECM resembles that of cartilage, but without a collagen component. The collagens are found in the brain only around blood vessels and at the surface of pia mater, where a conventional basal lamina is present (Rauch, 2007; Mentlein et al., 2012). This is a network of collagen type IV, laminin, heparin sulfate, proteoglycans and nidogen/entactin (Kalluri, 2004).

GBM cell movement in the brain is thus defined as a mesenchymal type of migration. Mesenchymal migration strategy is a five-step process, which begins with pseudopod protrusions at the leading edge, cell-matrix interactions via integrins and formation of focal contacts, followed by recruitment of surface proteases and proteolysis of surrounding ECM, contraction of intracellular actin-myosin and detachment of the trailing edge. This process was initially described in details by Friedl & Wolf (2003). Besides mesenchymal protease-driven cell movement, amoeboid type of movement can be utilized by the GBM cells. This amoeboid type of movement can occur without the formation of mature focal contacts and proteolytic activity (Friedl & Wolf, 2011). Plasticity and flexibility of GBM cells enable adaption of cellular programs and movements to specific circumstances during tumour progression such as epithelial-to-mesenchymal transition (EMT), or from mesenchymal-to-amoeboid type of movement (MAT transition) (Ulrich et al., 2009; Meng et al., 2014; Ye & Weinberg, 2015).

1.3.1 Proteases

Proteases (also called proteinases, proteolytic enzymes or peptidases) irreversibly catalyse the hydrolysis of peptide bonds by attacking the carbonyl group of the peptide bond. Each protease is assigned to a family on the basis of similarities in the primary structure, and families that are homologous are grouped together in clans. A clan comprises of proteases with the same catalytic mechanism, based on the active site amino acid, i.e. aspartic, cysteine, glutamic, metallo, asparagine, serine and threonine proteases. Besides, there are also proteases of which the active site amino acid is unknown or are mixed (Rawlings et al., 2016). Both intracellular and secreted proteases degrade proteins completely or provide limited proteolysis to control various physiological processes such as cell cycle progression,

cell death, tissue remodelling, homeostasis, wound healing and immune responses (López-Otín & Bond, 2008).

Protease activity is tightly regulated under normal physiological conditions at different levels to preserve homeostasis, from genetic and epigenetic factors controlling gene expression, protein biosynthesis, and posttranslational modifications that affect trafficking and compartmentalization of proteins, to zymogen activation. Ultimately, activity is also controlled by the abundance of selective endogenous protease inhibitors (Lah et al., 2006; Turk et al., 2012). Collectively, the complex network and interactions between proteases, their inhibitors and substrates are called the degradome (López-Otín & Overall, 2002), the functionality of which is dependent on cellular context and tissue physiology. Furthermore, proteases are involved in a highly-organized network of proteolytic events and a hierarchical cascade of steps, which Turk et al. *(*2012*)* described as protease signalling, where the initial proteolytic step does not cause complete substrate degradation, but rather activation of signalling pathways, thus initiating a chain of reactions that lead to specific biological effects.

In humans, more than 1200 known and putative proteases genes have been identified (Rawlings et al., 2016), representing ~ 7 % of the genome (Verbovšek et al., 2015). When homeostasis is challenged, protease–inhibitor–substrate balances may become disrupted, resulting in altered protease signalling. This may be either the cause or the consequence of a disease state, as is the case in various inflammatory conditions, neurodegenerative and cardiovascular diseases, viral infections, osteoporosis and cancer. Protease signalling is coupled to other types of cellular signalling, altogether being involved in various biological and pathological processes. A typical example in cancer is the interplay between proteases and cytokines (Mason & Joyce, 2011) that modulates angiogenesis, ECM composition and integrity, cancer cell invasion and other signalling pathways in the TME. During tumour progression, deregulation of protease homeostasis plays a highly relevant role (Lah et al., 2006; Verbovšek et al., 2015), where cancer cells and stromal cells are part of a complex proteolytic network within the TME (Mason & Joyce, 2011; Olson & Joyce, 2015), having both pro- and anti-tumorigenic effects (Lah et al., 2006; López-Otín & Matrisian, 2007). The role of different proteases in cancer is described recently in a review paper (Breznik et al., 2017a) in Section 2.1.

1.4 Advanced Models for Studying Cancer Progression: from *in vitro* Three Dimensional (3D) Cellular to *in vivo* Zebrafish Xenotransplantation Models

In the past, studies of tumour pathobiology were dependent on two-dimensional (2D) cell culture investigations and/or rodent model systems. Yet, cells that are grown in 2D monolayers *in vitro* differ significantly in their morphology, cell-cell and cell-matrix interactions, and differentiation from cells that are grown in 3D cultures, which mimics physiological conditions in organisms much better. Moreover, 3D models enable the acceleration of translational research from reductionist 2D *in vitro* systems to whole-animal systems. (Yamada & Cukierman 2007; Kimlin et al., 2013; Rape et al., 2014). Sophisticated 3D multicellular spheroid systems, using different ECM and scaffolds, are an emerging tool to model complex cellular heterogeneity, interactions and microenvironmental conditions of tumours *in vivo* (Kimlin et al., 2013; Thorma et al., 2014; Breslin et al., 2016). Multicellular 3D tumour spheroids that mimic cancer cell-stromal cell interactions have been shown to be a powerful tool for studying cancer progression mechanisms, developing

new anti-tumour agents and screening their efficiency as part of preclinical studies (Kimlin et al., 2013; Rape et al., 2014; Thorma et al., 2014).

Animal modelling is an essential tool for cancer research studies and translational oncology. In addition to widely-used rodent models (Huszthy et al., 2012; Welker et al., 2016), alternative vertebrate models such as zebrafish (*Danio rerio*) are becoming frequently used in cancer research (White et al., 2013; Eden et al., 2015; Vittori et al., 2015). Originally, zebrafish have been used in developmental biology and genetics (White et al., 2013), but more recently zebrafish and their embryos have been exploited to investigate cancer processes such as proliferation, invasion, angiogenesis and metastasis (Vittori et al., 2015; Wang et al., 2015) as well as to screen anti-cancer compounds (Zhang et al., 2014; MacRae & Peterson, 2015). Zebrafish embryos are an excellent experimental system because of several advantages, as discussed by Vittori et al. (2015). Zebrafish are ethically less problematic and can serve as a simple, relatively high throughput and cheap animal model. Zebrafish reproduce rapidly and allow a daily production of large numbers of embryos in a small facility (Vittori et al., 2015). Transparency and small size of zebrafish embryos makes these embryos appropriate for *in vivo* imaging of tumour progression directly at single-cell resolution in a real time (Tobia et al., 2013; White et al., 2013). Xenotransplantation of human cancer cells into zebrafish embryos has another benefit as these animals have not yet developed an immune system and thus immunosuppression is not needed (White et al., 2013; Vittori et al., 2015). Taken together, 3D tumour cell cultures and zebrafish xenotransplantation models contribute to a better and more thorough understanding of cancer progression. These model systems allow studies of important elemental processes of tumour development, including cell-cell interactions, cancer cell-microenvironment interactions and cancer heterogeneity, and can be thus utilized as additional tools to other model systems for preclinical validation studies.

1.5 Scientific Problems and Aims of this Thesis

Invasion is a key process of GBM progression. Invasion of GBM cells into surrounding brain parenchyma is associated with the activity of proteases, which are involved in different steps of GBM progression besides ECM degradation (Kenig et al., 2010; Gole et al., 2012; Sayegh et al., 2014). Many studies have been focused on therapeutic targeting of various types of proteases involved in GBM cell invasion. Most relevant players in pericellular protease activity of GBM cells are lysosomal cathepsins, such as cathepsins B and S, calpains, the serine protease urokinase-type plasminogen activator (uPA) and its receptor uPAR and specific matrix metalloproteases (MMPs) (Mentlein et al., 2012; Rao Malla et al., 2013; Sayegh et al., 2014). All these proteases enable cancer cell invasion by direct degradation of the ECM or indirectly by activating other proteases as part of the proteolytic cascade. However, little or nothing is known about the expression and the role of other cysteine cathepsins, such as K and X, in GBM progression.

The aim of the present doctoral dissertation was to explore the involvement of different proteases in GBM progression, taking the heterogeneity of GBM into consideration. MMPs, serine and cysteine proteases are studied: (a) in various GBM cell lines, (b) in GBM cells and stromal MSCs upon their interactions, (c) in GBM tissues of different subtypes, and (d) in special GBM microenvironments, such as GSC niches.

1.5.1 The Invasion of Various GBM Cell Lines and the Effects of MSCs

The heterogeneous nature of GBM is reflected in the diverse GBM cell types and the presence of non-cancerous stromal cells in the GBM microenvironment (Bonavia et al., 2011; Segerman et al., 2016).

The first aim was to compare GBM subtypes (TCGA) and the invasion properties of the generally used and phenotypically distinct GBM cell lines U87 MG and U373, respectively. GBM cell invasion and expression of different invasion-related proteases were studied in 3D *in vitro* invasion models and qRT-PCR, flow cytometry and Western blot, respectively.

MSCs in bone marrow or endogenous brain tissue are attracted by signalling molecules secreted by GBM tumours (Behnan et al., 2014; Hossain et al., 2015). The effects of MSCs on GBM progression are poorly understood. Besides being part of the GBM microenvironment, MSCs have been suggested as therapeutic vectors to treat GBM. However, treatment with MSCs is not yet an approved therapeutic strategy because of opposite effects of MSCs that have been observed on growth and invasion of GBM and ill-defined molecular mechanisms of their interactions (Motaln et al., 2012; Barcellos-de-Souza et al., 2013; Kološa et al., 2015). Moreover, the involvement of proteases in MSC-GBM interactions has not been explored so far.

The second aim was to evaluate the effect of MSC-GBM interactions on cell invasion *in vitro* by measuring cell invasion in 3D co-culture models and by analysing the expression of cysteine proteases, serine proteases and metalloproteases in cells and media of co-cultures.

The third aim was to determine the anti-invasive properties of specific selective protease inhibitors in monocultures and co-cultures of GBM cells and MSCs.

1.5.2 Studying MSC-GBM Interactions in Zebrafish Embryo Model

As the critical step in translational oncology remains the bridge from *in vitro* cell cultures to *in vivo* animal models, as a preclinical phase I step, a zebrafish embryo xenotransplantation model can be employed for studying GBM progression and cancer-stromal cell interactions. As described above, the most important benefit of zebrafish as a tumour model is the transparency of the embryos that allows visualization of tumour progression at single-cell resolution in real time (Vittori et al., 2015).

The fourth aim was to establish zebrafish embryo model for studying MSC-GBM interactions and to explore the effects of cellular cross-talk between MSCs and GBM cells during invasion *in vivo*.

1.5.3 Expression of Cathepsins K and X in Glioblastoma Tissues

Cathepsins D, B, L and S are the most extensively studied lysosomal cathepsins in cancers and are involved in various processes in GBM progression, such as angiogenesis, invasion and apoptosis (Fukuda et al., 2005; Flannary et al., 2006; Kenig et al., 2011; Gole et al., 2012). These cathepsins are over-expressed in GBM tissue, as compared to gliomas of lower grades and normal brain. Moreover, cathepsins B and S are also prognostic factors for GBM survival (Fukuda et al., 2005; Strojnik et al., 1999; 2005; Flannary et al., 2006). However, very little or nothing is known of expression patterns and the roles of cathepsins K and X in GBM progression, whereas both are important in progression of several other types of tumours (Vižin et al., 2012; Verbovšek et al., 2015; Kos et al., 2015). Recently, cathepsin K has been identified as one of the highest up-regulated proteases in GBM tissue

and GBM cells using in silico approach, as compared to normal brain and astrocytes, respectively (Verbovšek et al., 2014).

The fifth aim was to explore cathepsins K and X expression pattern in GBM tissue at gene end protein level and its prognostic value for GBM survival. The aim was also to determine the expression of both cathepsins in GBMs of different subtype and to correlate cathepsins expression with survival of different subtypes.

1.5.4 Cathepsins in GSC Niches

In the GBM microenvironment, GSCs are a tumour-initiating and therapy-resistant population of GBM cells. They are maintained and protected in special GBM regions, so-called GSC niches (Hira et al. 2015; Hambardzumyan & Bergens, 2015). These niches have been identified in close proximity of tumour vasculature as interactions between ECs and GSCs promote GSC stemness and malignancy (Calabrese et al., 2007; Zhu et al., 2011; Roos et al., 2017). Hira et al. (2015; in press) have shown that GSC niches are localized in hypoxic areas around arterioles in GBM. However, there are still a lot of open questions with respect to molecular mechanisms in GSC niches, for example, which proteins and signalling pathways are crucial for GSC trafficking to and out of their niches.

Stromal-derived factor 1α (SDF-1α/CXCL12) is a chemotactic cytokine, belonging to a CXC cytokine subgroup and binds to chemokine receptor type (CXCR) 4 and 7. SDF-1α/CXCR4 axis is involved in tumour angiogenesis and proliferation, apoptosis and migration of cancer cells by activating downstream signalling pathways, such as, MAPK/ERK, NF-kB, PI3 and PKC (Domanska et al., 2013). Moreover, SDF-1α is a key factor for the retention and maintenance of CSCs in their niches (Hira et al., 2015) and the SDF-1α/CXCR4 signalling axis has been identified as mediator of GSC resistance to radiotherapy (Goffart et al., 2017). It has already been shown that cathepsins B, K an X can cleave SDF-1α *in vitro* with different efficiency. Functional inactivation of SDF-1α by cathepsin B, K and X cleavage inhibited its chemoattractive capacity toward hematopoietic stem cells (HSCs) (Staudt et al., 2010; 2012). Since high expression of cathepsins B, K and X was observed in the proximity of tumour vasculature in GBM tissue, it was speculated that similar mechanisms may occur in GSC niches and that cathepsins are involved in the regulation of GSC migration/invasion out of their niches.

The sixth aim was to localize cathepsins B, K and X in peri-arteriolar GSC niches in cryostat and paraffin-embedded GBM tissue sections. Furthermore, it was also aimed to confirm the role of one of the cathepsins, cathepsin K, in GSC invasion via cleavage and inactivation of chemotactic cytokine SDF-1α.

1.6 Research Hypothesis

1. **Two established GBM cell lines U87 MG and U373 differ in genotype and their invasion properties. Specifically, it is hypothesized that:**
   - U87 and U373 cell lines belong to two distinct GBM subtypes (TCGA) on the basis of transcriptome analysis.
   - U87 and U373 cell lines differ in the expression of pro-invasive proteases and in invasive behaviour *in vitro.*

2. **MSC-GBM cell interactions differentially affect the invasion of GBM cell lines via invasion-related proteases such as cathepsins, calpains, uPA/uPAR and MMPs *in vitro.* Specifically, it is hypothesized that:**

- MSCs differently affect invasive behaviour of two distinct GBM cell lines (U87 MG and U373).
- The distinct GBM cell lines impact invasive behaviour of MSCs differentially.
- Cell invasion in co-cultures depends on the expression and activity of proteases, involved in specific protease signalling pathways, in the two GBM cell lines.
- Established selective protease inhibitors (CA-074, Nitroxoline) and new selective protease inhibitors (Compound 17) of cathepsin B inhibit cell invasion in MSC-GBM co-cultures.

3. **GBM progression studies in zebrafish embryo model confirm the effect of MSCs on GBM cell invasion *in vivo*. Specifically, it is hypothesized that**:
   - The invasion of distinct GBM cell lines alone and in the presence of MSCs also differs *in vivo.*
   - The zebrafish embryo model is a suitable tool for studying cancer-stromal cell interactions *in vivo.*

4. **Cathepsins K and X expression is up-regulated in GBM tissue, as compared to gliomas of lower grades and normal brain, and correlates with GBM survival. Specifically, it is hypothesized that:**
   - The expression levels of cathepsin K and X are upregulated in GBM vs. normal brain and lower-grade gliomas, and the highest expression levels of both cathepsins are associated with the mesenchymal GBM subtype.
   - Cathepsins K and X are heterogeneously expressed in GBM tissue at the protein level.
   - High expression levels of cathepsins K and X at mRNA and protein levels correlate with poor survival of GBM patients.
   - Prognostic values of cathepsins K and X expression levels depend on the GBM subtype.

5. **Cathepsins B, K and X are present in peri-arteriolar GSC niches. One of the cathepsins, cathepsin K promotes invasion of GSCs out of their niches by inactivation of chemotactic cytokine SDF-1α. Specifically, it is hypothesized that:**
   - Cathepsins B, K and X are expressed and active in peri-arteriolar GSC niches, which are positive for GSC markers CD133 and nestin, smooth muscle cell marker smooth muscle actin (SMA) and cytokine SDF-1α.
   - GBM and GSC cell lines express CXCR receptors 4 and 7.
   - Cathepsin K inactivates SDF-1α by cleaving its active N-terminal site.
   - Cathepsin K cleavage of SDF-1α prevents its chemotactic activity towards GSCs *in vitro.*
   - CXCR4 inhibitor inhibits the invasion of GSCs *in vitro.*

1.7 Publications Included and Candidate' s Contributions

Three groups of proteases, the cysteine proteases, serine proteases and metalloproteases, and their role in cancer progression are described in details **in the first manuscript** *"Proteases and cytokines as mediators of interactions between cancer and stromal cells in tumours"*. In particular, the role of proteases in the TME, stromal cells and cellular cross-talk within the tumours are discussed. Moreover, this review summarizes the interplay between proteases and cytokines in tumour stroma that regulates cancer development and spreading. The PhD candidate is the first author of this publication. The candidate wrote the review paper based on existing literature, previous work in the research group of the supervisor and her own data on proteases in MSC-GBM interactions.

In the second manuscript *"Mesenchymal stem cells differentially affect the invasion of distinct glioblastoma cell lines"* the difference in genotype and phenotype of various established GBM cell lines are analysed. Furthermore, the effects of MSCs on the expression of various proteases and invasive behaviour of different GBM cells were studied. PhD candidate is the first author of this publication and she wrote the manuscript. The candidate performed and designed all *in vitro* experiments on cell lines using RT-PCR, Western blot, flow cytometry and fluorescent microscopy. The candidate also analysed and interpreted all data, as well as interpreted bioinformatics studies, which were performed by the co-workers in the research group.

In the third manuscript *"Addition of 2-(ethylamino)acetonitrile group to nitroxoline results in significantly improved anti-tumor activity in vitro and in vivo"* the addition of a 2-(ethylamino)acetonitrile group to nitroxoline (compound 17) was tested whether it improved anti-invasive and anti-cancer activities *in vitro* and *in vivo*. The effects of these selective inhibitors of cathepsin B on GBM cell invasion and migration were tested in monocultures and co-cultures with MSCs. The PhD candidate is the coauthor of this publication. She designed and performed the experiments on MSC-GBM co-cultures, as well as analysed and interpreted these data. The candidate drafted the corresponding part of the manuscript.

The fourth manuscript *"Imaging of human glioblastoma cells and their interactions with mesenchymal stem cells in zebrafish (Danio rerio) embryonic brain"* describes the development and establishment of a zebrafish embryo model to study GBM cell invasion and the interactions between GBM cells and stromal cells *in vivo*. A carbocyanine-compatible clearing protocol was applied for the observation of cells in deep layers of tissues for example to study GBM cell invasion and MSC-GBM cell interactions in zebrafish embryo brain. The PhD candidate is the coauthor of this publication. The candidate designed the study, prepared the cells for experiments, analysed and interpreted the data.

In the fifth manuscript *"Cathepsins K and X in glioblastoma progression"* mRNA and protein expression of cathepsins K and X was studied in human GBM tissues and its association with GBM patient survival. Furthermore, it was studied whether cathepsins K and X protein expression was found in special regions around arterioles and whether their mRNA expression correlated with mRNA expression of GSC niche markers. The PhD candidate is the first author of this publication and she wrote the first draft of the manuscript. The candidate analysed and interpreted the data of cathepsin mRNA expression in GBM using public transcriptomic datasets. Moreover, she designed, performed and analysed the immunohistochemical studies.

In the sixth manuscript *"Cysteine cathepsins B, X and K are expressed in peri-arteriolar glioblastoma stem cell niches"* localization pattern of the cathepsin B and the less explored cathepsins K and X in GSC niches within human GBM tissue were studied using immunohistochemistry. As cathepsin K has already been identified in GSC niches,

expression of the two other cathepsins, B and X, was determined in peri-arteriolar GSC niches. Furthermore, the activities of cathepsins were analyzed in cryostat GBM sections using metabolic mapping and fluorogenic substrates. The PhD candidate is the first author of this publication and she drafted the manuscript. She designed and performed immunohistochemistry and metabolic mapping experiments, as well as analysed and interpreted the data.

In the seventh manuscript *"Cathepsin K cleavage of SDF-1α inhibits its chemotactic activity towards glioblastoma stem-like cells"* it was investigated whether SDF-1α is a niche factor that through its interactions with CXCR4 and/or its second receptor CXCR7 on GSCs facilitates their homing in niches. Furthermore, it was aimed to show that SDF-1α cleavage by cathepsin K inactivates SDF-1α and inhibits its chemotactic activity towards GSCs. It is shown that cathepsin K can cleave and inactivate SDF-1α. The PhD candidate is the co-author of this publication. She designed and performed 2D/3D invasion experiments and CXCR mRNA/protein expression experiments. Moreover, she analysed and interpreted the data.

Chapter 2

Scientific Publications

2.1 Proteases and Cytokines as Mediators of Interactions Between Cancer and Stromal Cells in Tumours

Barbara Breznik, Helena Motaln, Tamara Lah Turnšek

Biological Chemistry 2017; 398(7): 709–719. DOI 10.1515/hsz-2016-0283

DE GRUYTER Biol. Chem. 2017; 398(7): 709–719

Review Open Access

Barbara Breznik, Helena Motaln and Tamara Lah Turnšek*

Proteases and cytokines as mediators of interactions between cancer and stromal cells in tumours

DOI 10.1515/hsz-2016-0283
Received September 12, 2016; accepted December 14, 2016; previously published online December 20, 2016

Abstract: Proteolytic enzymes are highly relevant in different processes of cancer progression. Their interplay with other signalling molecules such as cytokines represents important regulation of multicellular cross-talk. In this review, we discuss protease regulation mechanisms of cytokine signalling in various types of cancer. Additionally, we highlight the reverse whereby cytokines have an impact on protease expression in an autocrine and paracrine manner, representing complex feedback mechanisms among multiple members of these two protein families. The relevance of the protease-cytokine axis is illustrated in glioblastoma, where interactions between normal mesenchymal stem cells and cancer cells play an important role in this very malignant form of brain cancer.

Keywords: cellular cross-talk; glioblastoma; invasion; mesenchymal stem cells; protease-cytokine signalling.

Introduction

Proteases (also termed proteolytic enzymes, proteinases and peptidases) irreversibly catalyse the hydrolysis of peptide bonds by attacking the carbonyl group of the peptide bond. Each protease is assigned to a family on the basis of similarities in the primary structure, and families that are homologous are grouped together in clans. A clan comprises proteases with the same catalytic mechanism, based on the active site amino acid, i.e. aspartic, cysteine, glutamic, metallo, serine, threonine, but there are also proteases where these are unknown or mixed in addition to the asparagine peptide lyases (Rawlings et al., 2016). Proteases are deposited in the comprehensive MEROPS database, where on June 2016 over 4400 protease genes were described (http://merops.sanger.ac.uk/about/merops.shtml). Intracellular and secreted proteases are responsible for both total protein degradation and limited proteolysis that control various key physiological processes such as cell cycle progression, cell death, tissue remodelling, homeostasis, wound healing and immune responses (López-Otín and Bond, 2008).

To preserve homeostasis under normal physiological conditions, protease activity is tightly regulated at different levels, from genetic and epigenetic factors controlling gene expression and protein biosynthesis, and post-translational modifications that affect trafficking and compartmentalisation of proteins, to zymogen activation. Ultimately, activity is also controlled by the abundance of selective endogenous protease inhibitors (Lah et al., 2006; Turk et al., 2012). Collectively, the complex network and interactions between proteases, their inhibitors and substrates is called the degradome (López-Otín and Overall, 2002), the functionality of which is dependent on cellular context and tissue physiology. Furthermore, proteases are involved in a highly organised network of proteolytic events and a hierarchical cascade of steps, which Turk et al. (2012) described as protease signalling, where the initial proteolytic step does not cause complete substrate degradation, but rather its activation, thus initiating a chain of reactions that lead to specific biological effects.

In humans, 1208 and 1857 known and putative proteases and protease inhibitor genes have been identified, respectively (Rawlings et al., 2016), representing ~7% of the genome (Verbovšek et al., 2014, 2015). When

*Corresponding author: Tamara Lah Turnšek, Department of Genetic Toxicology and Cancer Biology, National Institute of Biology, Večna pot 111, SI-1000 Ljubljana, Slovenia; Jožef Stefan International Postgraduate School, Jamova 39, SI-1000 Ljubljana, Slovenia; and Department of Biochemistry, Faculty of Chemistry and Chemical Engineering, University of Ljubljana, Večna pot 113, SI-1000 Ljubljana, Slovenia, e-mail: Tamara.Lah@nib.si
Barbara Breznik: Department of Genetic Toxicology and Cancer Biology, National Institute of Biology, Večna pot 111, SI-1000 Ljubljana, Slovenia; and Jožef Stefan International Postgraduate School, Jamova 39, SI-1000 Ljubljana, Slovenia
Helena Motaln: Department of Genetic Toxicology and Cancer Biology, National Institute of Biology, Večna pot 111, SI-1000 Ljubljana, Slovenia

©2017, Barbara Breznik et al., published by De Gruyter.
This work is licensed under the Creative Commons Attribution-NonCommercial-NoDerivatives 3.0 License.

Unauthenticated
Download Date | 6/13/17 3:10 PM

homeostasis is challenged, the protease-inhibitor-substrate balances may become disrupted, resulting in altered protease signalling. This may be either the cause or the consequence of a diseased state, as is the case in various inflammatory conditions, neurodegenerative and cardiovascular diseases, viral infections, atherosclerosis and osteoporosis. In cancer, the altered protease signalling is termed the "cancer degradome" (López-Otín and Overall, 2002). Protease signalling is coupled to other types of cellular signalling, altogether being involved in various biological and pathological processes. Typical examples in cancer are the interplay between kinases and proteases (López-Otín and Hunter, 2010), and between proteases and cytokines (Mason and Joyce, 2011) that modulate angiogenesis, extracellular matrix (ECM) composition and integrity, cancer cell invasion and other signalling pathways in the tumour microenvironment (TME). In tumour progression, the deregulation of protease homeostasis plays a highly relevant role (Lah et al., 2006; López-Otín and Bond, 2008; Verbovšek et al., 2014, 2015), where cancer and stromal cells contribute to a complex proteolytic network within the TME (Mason and Joyce, 2011), having both pro- and anti-tumorigenic effects (López-Otín and Matrisian, 2007).

The role of various protease classes in cancer

The most extensively studied class of proteases in cancer are matrix metalloproteases (MMPs), which are the zinc-dependent endopeptidases, classified on the basis of protein-domain structure and sequence homology into the four main subclasses: collagenases (MMP-1, MMP-8 and MMP-13), MMPs of the stromelysin subclass (MMP-3, MMP-10, MMP-11, MMP-7 and MMP-26), gelatinases (MMP-2 and MMP-9) and membrane-type MMPs, termed MT1-MMP to MT6-MMP, alternatively classified as MMP14-17, MMP-24, and MMP-25 (Cathcart et al., 2015; Rawlings et al., 2016). These MMPs directly degrade ECM proteins, but differ in substrate specificity. MMPs are counteracted by their endogenous tissue inhibitors TIMPs (1–4), nearly all of them playing a distinct role in cancer progression (Yamamoto et al., 2015). Besides the MMP activity regulation by TIMPs, extracellular MMP activity is also regulated by their binding to ECM proteins and cell surface molecules, such as integrins (β1 subunit) and tetraspanins and by endocytotic trafficking (Yamamoto et al., 2015). A related protease family consists of a disintegrin and metalloprotease with thrombospondin motifs (ADAMTSs), which mostly act in the pericellular milieu. These proteases can be secreted by cancer and stromal cells and may contribute to modifying the TME by multiple mechanisms, related to both oncogenic and tumour-protective functions (Cal and López-Otín, 2015).

Another frequently investigated class of proteases in cancer progression are the serine proteases, subdivided with respect to their substrate specificity as trypsin-like and chymotrypsin-like serine endopeptidases (Rawlings et al., 2016). Among these serine endopeptidases, the plasminogen/plasmin activator system and kallikreins have received most attention in oncology. Urokinase-type plasminogen activator (uPA), its receptor (uPAR) and serpin inhibitors PAI-1 and -2 comprise the cancer membrane degradome system, which activates plasminogen to plasmin, a feedback activator of PAs and various MMPs that then degrade ECM proteins (Lah et al., 2006; Mason and Joyce, 2011). In concert with cysteine cathepsins, uPA/uPAR signalling induces activation of a proteolytic cascade, which facilitates cancer cell invasion. Besides proteolytic activity, the uPA/uPAR system has important proteolyisis independent functions in cancer cell invasion, as plasma membrane linked uPAR interacts directly with integrins and vitronectin, thereby mediating cell adhesion and migration (Rao Malla et al., 2013). Because expression of uPA, uPAR and PAI-1 is increased in many types of cancers, they were among the first proteins that were proposed as prognostic biomarkers for cancer patients, in particular for breast cancer (Schrohl et al., 2003; Lah et al., 2008).

Human tissue kallikreins (hKs) comprise the family of 15 homologous secreted serine proteases with trypsin or chymotrypsin-like activities and are aberrantly expressed in different types of cancers, as recently reviewed (Avgenis and Scorilas, 2016). The best known is hK3 (prostate-specific antigen, PSA) used as a biomarker for detection and prognosis of prostate cancer, although its relevance is questionable, as it is also highly increased in inflammation that is not related to neoplasms (Diamandis 2012). Despite the fact that roles of distinct hKs in cancer are not completely understood, studies indicates that hK-mediated pericellular proteolysis may be important in cancer cell invasion, angiogenesis and growth in particular due to modulating the activities of various cytokines, growth factors and other proteases (Avgenis and Scorilas, 2016). As mentioned above (López-Otín and Matrisian, 2007), not all proteases are tumour promoting and, for example, Strojnik et al. (2009) found downregulation of hK6 in glioma progression, although expression of this kallikrein in tumours had no impact on patients' survival.

Unauthenticated
Download Date | 6/13/17 3:10 PM

Originally recognised by their intralysosomal activity, cysteine proteases such as papain-like cathepsins and caspases are now known to be active in other subcellular compartments as well extracellularly, and cysteine proteases and caspases are implicated in cancer development and progression. Human cysteine cathepsins comprise an 11-member family: cathepsins B, C, F, H, K, L/V, O, S, Z, X and W (Kos et al., 2015; Rawlings et al., 2016). Although initially associated with increased metabolism and lysosomal protein degradation in cancer cells, diverse and distinct other functions of cathepsins have later been revealed, for example, their involvement in resistance development to therapeutics (Olson and Joyce, 2015). The expression pattern of cathepsins in different types of cancer is rather diverse and again, not all cathepsins are pro-tumorigenic in all cancers. For example, Reinheckel et al. (2012) demonstrated that cathepsin L possesses tumour suppressor anti-proliferative activity in the Rip1-Tag2 mouse model, but enhances tumorigenesis in APC^{min} and K14-HPV16 mice. We found that in glioblastoma cathepsin L upregulation has an anti-apoptotic effect by increasing caspase 3 synthesis (Kenig et al., 2011), supporting earlier reports that cathepsin L facilitates drug resistance (Lankelma et al., 2010).

Caspases are the most relevant proteases in initiation and execution of apoptosis and altered apoptotic signalling pathways are one of the hallmarks of cancer (Hanahan and Weinberg, 2011). The caspase cascade is initialised by caspases 2, -8, -9 and -10, which in various pathways directly or indirectly activate effector caspases -3, -6 and -7 triggering apoptosis (Mason and Joyce, 2011). Downregulation of caspases can lead to impaired apoptosis, higher cancer cell survival and therapy resistance. For example, progression of some types of cancer, including glioblastoma, has been associated with a lack of caspase-8 expression. On the other hand, caspase-8 was found to be upregulated in other types of cancers and promotes malignancy probably by its other non-apoptotic functions such as inducing NF-κB signalling, altering endosomal trafficking, regulating autophagy and enhancing cellular adhesion and migration (Stupack 2013).

The interplay between mitochondrial and lysosomal compartments in cell death has been established as well as a distinct role of lysosomal cathepsins in apoptosis (Droga-Mazovec et al., 2008). Cysteine cathepsins B, L, S and K cleave Bid and Bcl-2 homologues, which can when released from damaged lysosomes not only affect mitochondrial membrane integrity, but also enhance caspase activity through degradation of the caspase endogenous inhibitor XIAP. Therefore, the cellular compartment and context of lysosomal protease activity dictates the substrate targets and pro- versus anti-tumorigenic functions.

Proteases in stromal cells

An additional complexity of the role of proteases in cancer is related to their expression and regulation in tumour-associated stromal cells, including endothelial cells, fibroblasts, immune cells and mesenchymal stem cells (Hanahan and Weinberg, 2011). As active participants in TME, these stromal cell support cancer cell proliferation, invasion, metastasis and drug resistance (Bougnaud et al., 2016). However, the expression pattern of proteases in stromal cells and their processing may differ from that of cancer cells, and thus may have a different impact on tumour progression (Olson and Joyce, 2015). For example, Gocheva et al. (2010) observed that cathepsins B and S secreted from tumour-associated macrophages (TAMs) in a Rip1-Tag2 pancreatic neuroendocrine tumour (PanNET) mouse model are predominantly responsible for pancreatic tumour growth, angiogenesis and invasion *in vivo*. In contrast, cathepsin L expressed by cancer cells has a pancreatic neuroendocrine tumour promoting role. This indicates that there are different and even opposite effects of proteases expressed by cancer and stromal cells, depending on the type of cancer. In other words, the heterogeneity and plasticity of the tumour in response to cancer cell evolution may differentially affect the protease web, depending on the cellular context. As a consequence, selective pressure resulting from these cellular cross-talks is also pushing cancer cells to compensation of one type of protease, when this protease is not expressed or inhibited, by the activation of other protease(s), as was suggested by Akkari et al. (2016). It was demonstrated that high amounts of cathepsin X are present in TAMs as a functional compensation of cathepsin B and cathepsin S depletion in RT2 PanNET mouse model (cathepsin $B^{-/-}S^{-/-}$ RT2 mice). Interestingly, this compensation occurs in a tumour stage-dependent manner, empasizing the plasticity of the TME.

These phenomena may be a reason that protease inhibitors, such as MMP inhibitors, failed in clinical trials as anti-cancer agents, because resistance to specific protease inhibitors may be due to compensation by non-targeted types of protease(s) (Cathcart et al., 2015). For example, enhanced invasion of MMP-9-deficient tumours is associated with homing of cathepsin B-expressing leukocytes to invasive tumour fronts, facilitating invasion (Shchors et al., 2013). Finally, inefficacy of protease

Unauthenticated
Download Date | 6/13/17 3:10 PM

inhibitors may be due to non-proteolytic roles of proteases such as their interaction with other proteins (Kessenbrock et al., 2015). For example, TAM-derived and cancer cell-derived pro-form of cathepsin X promotes cancer cell adhesion and migration through binding to the RGD domain of integrins on cancer cell membranes (Kos et al., 2015). Furthermore, inhibitors that target the hemopexin domain (HPX) in MMPs, which is located at the C-terminal of most MMP members and is crucial for protein-protein interactions, block tumour growth (Kessenbrock et al., 2015). Taken together, it means that the cellular context, the redundancy and selectivity of proteases make therapeutic targeting of proteases in cancer difficult.

Protease signalling: cytokines as protease substrates

Cytokines are a heterogeneous group of small soluble signalling molecules comprising chemokines, interleukins (ILs), interferons (IFNs) and some growth factors such as TGF-β (Seruga et al., 2008). Cytokines exert their function via binding to their membrane-associated receptors. Each group of cytokines binds to corresponding receptors, classified as type I and II cytokine receptors, immunoglobulin, TNF, TGF-β and chemokine receptors (Borish and Steinke, 2003). Cytokines are secreted by both cancer cells and stromal cells, and act as means of communication among these cells. Cytokines can act in autocrine or paracrine manners to exert their functions such as regulating cell proliferation in the TME. Additionally, cytokines enhance cancer cell invasion and tumour angiogenesis by inducing the expression of invasion-associated proteolytic enzymes (Kenig et al., 2010; Sevenich and Joyce, 2014) as is discussed in the next chapter.

Chemotactic cytokines – chemokines play a crucial role by regulating recruitment of immune cells to tumours. The chemokine subfamily is classified according to the position of the first cysteines at the NH_2-terminus of the protein into four groups: CXC, CC, C and CX3C. Chemokine receptors are G-protein-coupled receptors and bind to more than one type of chemokine. These chemokine receptors are grouped into four classes depending on the type of binding of the chemokine: CXCR, CC, CX3CR1, XCR1. The chemokine receptors CXCR4, CXCR5, CXCR6, CCR6, CCR9 and CX3CR1 bind only one ligand (Borish and Steinke, 2003). During cancer progression the protease network interferes with chemokine signalling and thus affects recruitment and proliferation of immune cells to the tumours, where they can have either pro- or anti-inflammatory and even immunosuppressive activity. However, there is a high redundancy among chemokines with respect to target cell selectivity and in many cases it is difficult to ascribe a distinct role to a single chemokine (Wolf et al., 2008).

Proteases affect cytokine expression by different signalling pathways and affect their activity post-translationally by proteolytic processing. For example, cathepsin S functions as transcriptional mediator of the pro-inflammatory chemokine CCL2/MCP-1 *via* type I transmembrane glycoprotein CD74 in cancer cells. Within endosomes, cathepsin S is the key protease responsible for the cleavage of CD74 and liberation of its intracellular domain (CD74-ICD), being then translocated into the nucleus, where it interacts with NFκB, that in turn regulates the expression of CCL2/MCP-1, among others. Accordingly, downregulation of cathepsin S expression in cancer cells reduces macrophage recruitment to the tumour site and correlates with reduced tumour growth in mice (Wilkinson et al., 2015). Hu et al. (2014) demonstrated that activation of the uPA-uPAR axis in cancer cells increases gene expression and protein secretion of IL-4 via ERK1/2 signalling and TGF-β by a thus far unknown mechanism. Both cytokines are responsible for increased mobilisation and polarisation of macrophages towards the M2 status, which promotes tumour progression.

Proteases selectively cleave cytokines leading either to activation or inactivation of cytokine function or altered receptor specificity (Wolf et al., 2008). Some cytokines thus require proteolytic activation to exert their function. For example, both MMP-8, -9, and cathepsin L process IL-8 into an up to 30-fold more active conformation after N-terminal cleavage (Van Den Steen et al., 2003). Moreover, a positive feedback loop is created as IL-8 induces MMP-8 and -9 release from inflammatory cells, which contributes to ECM degradation. Additionally, elevated levels of IL-8 in glioma cells trigger the epithelial-mesenchymal transition (EMT) and enhances their invasiveness (Zhang et al., 2015). Other examples are ADAM-17 and MMPs, such as MMP-2, -9 and -14, that convert the inactive stromal macrophage and T cell membrane-bound precursor of TNF-α into the soluble pro-inflammatory cytokine. Active TNF-α then increases infiltration of tumour-promoting macrophages into the tumour. TNF-α also increases cancer cell proliferation *via* the transcription factor NF-κB (Kessenbrock et al., 2010).

On the other hand, proteases may inactivate cytokines and alter their receptor binding, impairing cancer progression. For example, MMPs, such as MMP-1, -2, -3, -9, -13 and -14, cleave CXCL12/SDF-1α that results in loss of its ability to bind to its receptor CXCR4 (Manicone and McGuire, 2008).

Unauthenticated
Download Date | 6/13/17 3:10 PM

This specific MMP activity inhibits local chemotaxis of endothelial cells of existing vessels and prevents tumour angiogenesis (Yamada et al., 2015). Reduced chemotactic activity of tumours towards lymphocytes, expressing CXCR4 receptors, was found to be caused by cleavage of its ligand CCL22, by the tumour-derived serine protease CD26/dipeptidyl-peptidase IV (Mortier et al., 2016).

Proteases regulate cytokine bioavailability by proteolytic processing of ECM proteins, that are the essential cytokine binding partners. By limited proteolytic processing of the ECM, active cytokines are liberated. Extracellular MMP-2 and membrane-associated MMP-14 indirectly activate TGF-β by releasing its binding to latent TGF-β-binding protein 1 (LTBP-1), which is an ECM component (Kessenbrock et al., 2010). TGF-β signalling in combination with cathepsin B activity in direct co-cultures of human melanoma cells and fibroblasts *in vitro* activates the fibroblasts in a similar manner as stromal fibroblasts are activated *in vivo*, thereby inducing cancer cell invasion (Yin et al., 2012). In addition, proteases orchestrate recruitment of leukocytes and promote tumour-associated inflammation by modulating cell surface proteoglycans. For example, MMP-7 shedding of heparin sulphate proteoglycan syndecan-1 releases the CXCL1-syndecan-1 complex from the cell surface to generate a chemokine gradient for recruitment of tumour-promoting neutrophils into the tumour (Wolf et al., 2008).

Proteases are also key players in the formation of metastatic and cancer stem cell niches. For example, MMP-9 is involved in pre-metastatic niche formation by cleaving the cytokine c-KitL (soluble Kit ligand, stem cell ligand), which releases c-KitL from the surface of stromal cells such as endothelial cells and fibroblasts at secondary tumour sites distant to the primary tumour. This cytokine then recruits hematopoietic progenitor cells from the bone marrow into the niche to create a metastasis-supporting TME, which sustains metastatic cell growth (Kessenbrock et al., 2010). An example of proteases that contribute to cancer stem cell niche formation are MMPs and cathepsin K. The latter has been associated with periarteriolar stem cell niches where it co-localises with CXCL12/SDF-1α (Hira et al., 2015). This chemokine attracts glioblastoma cells into niches, where the cells become glioblastoma stem-like cells. It is hypothesised that focal activation and N-terminal SDF-1α cleavage by cathepsin K inactivates this chemokine, which possibly induces release of stem cells from the niche and promotion of glioblastoma stem-like cell invasion as well as their differentiation (Verbovšek et al., 2015).

Taken together, proteases affect cytokine signalling in various ways; proteases directly activate or inactivate cytokines by proteolytic cleavage or liberate cytokines from the ECM. As a consequence, cytokines (a) affect recruitment and proliferation of immune cells, (b) impact proliferation and migration of cancer cells, and (c) sustain metastatic niches and cancer stem cell niches and thus affect tumour cell homing. Proteases, released from both, cancer cells and stromal cells are responsible for the fine tuning of cytokine function in the complex TME, as shown in Figure 1.

Cytokine signalling affects protease activity

Cytokines, as major mediators of paracrine cell signalling, are potent regulators of protease activity, virtually affecting all types of cells in the TME (Figure 1). Pro-inflammatory cytokines stimulate expression, secretion and activation of MMPs in cancer cells, as well as in various stromal cell types (Sevenich and Joyce, 2014). Stromal cells secrete cytokines, which induce the expression of MMPs in cancer cells and thus promote their invasion, as was illustrated by Kenig et al. (2010) in an *in vitro* glioma and endothelial cell co-culture. Endothelial cell-derived SDF-1α upregulates the expression of MMP-9 together with cathepsins B and S in glioblastoma cells that enhance invasiveness. Similar observations were made *in vivo* by Wang et al. (2013) when co-injecting endothelial and hepatocellular carcinoma cells into nude mice and found an increased tumorigenicity of the carcinoma cells. This was associated with expression of MMP-2 and -9 in hepatocellular carcinoma cells, induced by the cellular cross-talk *via* secreted CCL2/MCP-1, IL-8 and IL-16 (Wang et al., 2013).

A vast body of literature describes infiltrating inflammatory cells, such as macrophages, dendritic cells, mast cells, as well as neutrophils and B and T lymphocytes that produce a variety of pro-inflammatory cytokines, inducing MMP activity in the TME. For example, macrophage-derived IL-1β induces the expression of MMP-1, -3, -10 and -14 in metastatic renal cell carcinoma *via* a mechanism dependent on activation of the transcription factor CCAAT-enhancer binding protein β (CEBPβ) by IL-1β (Petrella and Vincenti, 2012). On the other hand, cancer cells upregulate by secretion of soluble cytokines the activity of MMPs in stromal cells. For example, IL-6 is one of the major inflammatory cytokine in cancer progression. IL-6, produced by breast cancer cells induces expression and secretion of MMP-2 and -9 and cathepsin B from tumour-associated monocytes *in vitro* (Mohamed et al., 2010).

Unauthenticated
Download Date | 6/13/17 3:10 PM

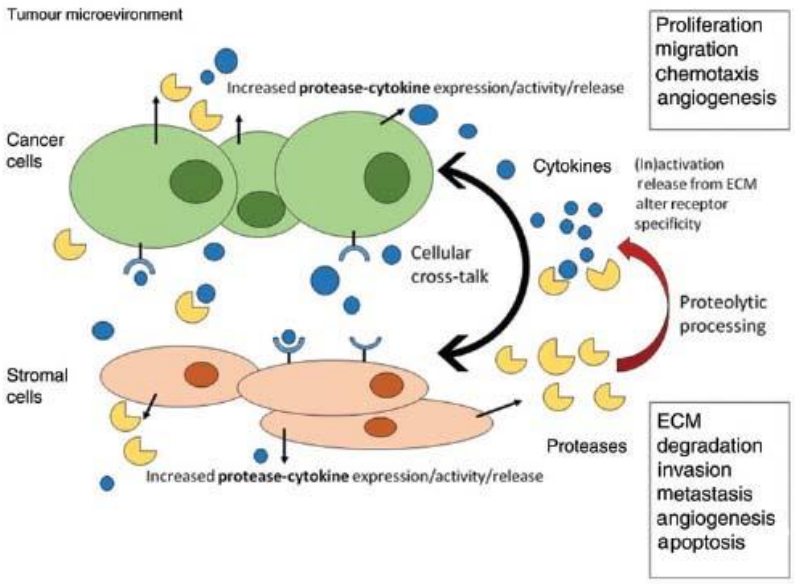


Figure 1: Proteases and cytokines as mediators of cellular cross-talk in the tumour microenvironment that promotes tumour progression. Schematic presentation of interactions between cancer and stromal cells within the tumour microenvironment, that are mediated by the protease-cytokine interplay. Cytokines induce protease expression and activity in stromal and cancer cells as well as induce their release, whereas proteases can also induce cytokine expression. Proteases by proteolytic processing alter cytokine activity, their receptor specificity and/or their bioavailability that may lead to altered cancer cell and stromal cell proliferation and migration, recruitment of other cell types such as immune cells, fibroblasts and mesenchymal stem cells to the tumour site and angiogenesis of the tumour. On the other hand, increased activity of proteases in tumour stroma affects ECM degradation, invasion, metastasis, angiogenesis and apoptosis.

Fibroblasts are an important component of the TME and are a source of cytokines. For example, a dynamic interplay between colon cancer cells and fibroblasts *via* activated TGB-β signalling leads to activation of serine protease uPA, its inhibitor PAI-1 and some types of MMPs, as well as the autocrine TGF-β loop in normal fibroblasts, transforming them in cancer-associated fibroblasts (CAFs), playing an important role in various types of cancer (Hawinkels et al., 2014).

Cathepsins in the TME may originate from various cell types (Mohamed et al., 2010; Mason and Joyce, 2011). Pro-inflammatory IL-4 upregulates cathepsin B and S expression in TAMs that enhances pancreatic cancer cell invasion *in vivo* and *in vitro*, and promotes pancreatic cancer growth as well as angiogenesis in a PanNET mouse model (Gocheva et al., 2010). Increased levels of cathepsin K in fibroblasts enhances invasiveness of squamous cancer cells in fibroblast/cancer cells co-cultures *in vitro* by cancer cell derived IL-1α (Xie et al., 2011).

Cytokine-regulated activity of cathepsin L (Lankelma et al., 2010; Kenig et al., 2011) and cathepsin B (Bruchard et al., 2013) has been reported to be important in the development of chemo-resistance. It has been also shown (Tuomela et al., 2013) that cancer cells take DNA from dead cancer cells, killed by chemo-therapy, inducing expression of Toll-like receptor TLR9. This was mediated by MMP-13 activation and downregulation of TIMP-3 expression.

Taken together, cytokines that are secreted into the TME from endothelial cells, immune cells and fibroblasts affect the expression of all classes of proteases in an autocrine and paracrine manner usually to promote tumour progression.

Case study: interactions between mesenchymal stem cells and glioblastoma

An additional component of the TME are mesenchymal stem cells (MSCs), although their exact role in brain tumour and progression is still not fully understood (Barcellos-de-Souza et al., 2013). Tumour-secreted cytokines and growth factors such as TGF-β, VEGF and IL-8 (Motaln et al., 2012)

Unauthenticated
Download Date | 6/13/17 3:10 PM

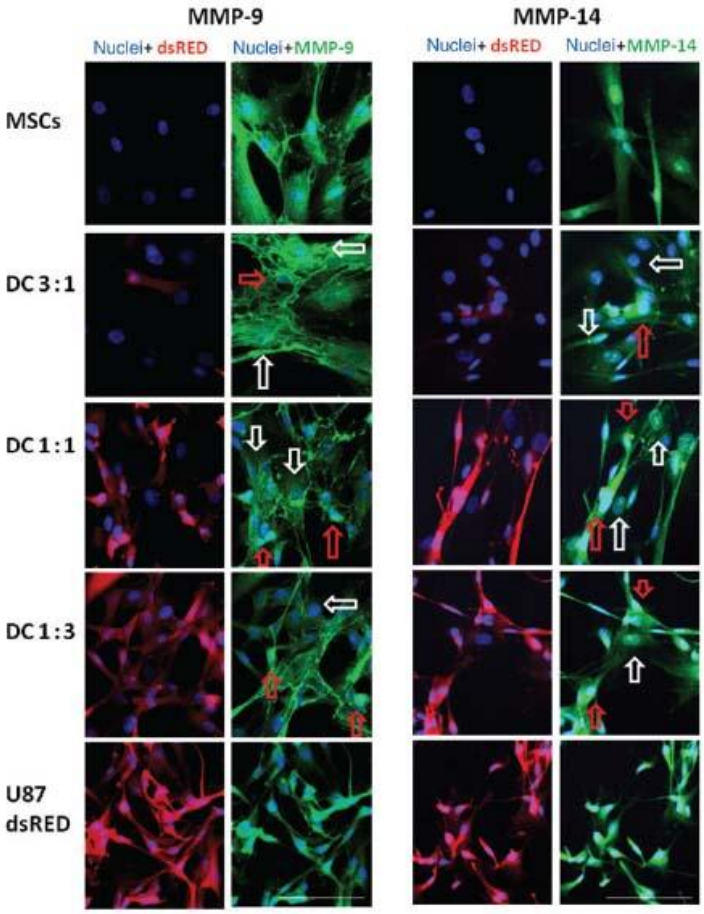


Figure 2: Localization of MMP-9 and MMP-14 in MSCs, U87dsRED cells and their direct co-cultures (DC).
After 3 days of direct co-culturing in three different MSC-U87dsRED ratios (DC 1:3, 1:1 and 3:1), immunocytochemistry was performed. Cells were fixed using 4% paraformaldehyde (Sigma-Aldrich, St. Louis, MO, USA), permeabilized with 0.1% Triton X-100 (Sigma-Aldrich) and incubated with anti-MMP-9 (1:100 dilution) or anti-MMP-14 (1:200) primary antibody (both Abcam, Cambridge, UK), followed by incubation with secondary antibody conjugated with Alexa Fluor 488 (green; Applied Biosystems, Carlsbad, CA, USA). Cell nuclei were stained with DAPI (4′,6-diamidino-2-phenylindole; Life technologies, Carlsbad, MO, USA) and analysed by inverted fluorescence microscope Nikon (Tokyo, Japan; 200× original magnification; scale bar=100 μm). Images taken from DAPI and dsRED (blue nuclei, red U87 cells) and DAPI and MMP-9/MMP-14 (blue nuclei, green antibody) were merged, respectively. White arrows indicate protease expression in MSCs and red arrows in U87dsRED cells.

mediate tropism and homing of MSCs from bone marrow or endogenous brain tissue niche to the brain tumour glioblastoma (Schichor et al., 2012). Due to their high expression of cytokines and their receptors, MSCs play an important immunomodulatory role in TME. Furthermore, we showed that MSCs in the presence of glioblastoma cells overexpress and secrete a range of cytokines and chemokines such as TGF-β, IL-1α and β, IL-6, IL-8, CCL2, CCL13, CCL20, CCL26, CXCL1-2, CXCL6, CXCL12, in particular CCL2/MCP1 (Motaln et al., 2012; Motaln and Turnsek, 2015). Increased levels of inflammatory cytokines enhance in autocrine manner expression of proteases such as MMP-2, -9 and -14 in MSCs that promote MSC motility towards the tumour (Ries et al., 2007). Ho et al. (2009) showed that MMP-1 is crucial for MSC migration toward glioma *in vivo*, as well as *in vitro*. MMP-1 cleaves G-protein-coupled receptor PAR1 on MSC surface, triggering intracellular signalling, which promotes MSC glioma tropism. Gutova et al. (2008) confirmed that MSC tropism is also mediated through uPA and uPAR overexpression in GBM cells, besides increased levels of cytokines IL-6, IL-8 and CCL2/MCP-1 in conditioned medium of glioblastoma cells.

Unauthenticated
Download Date | 6/13/17 3:10 PM

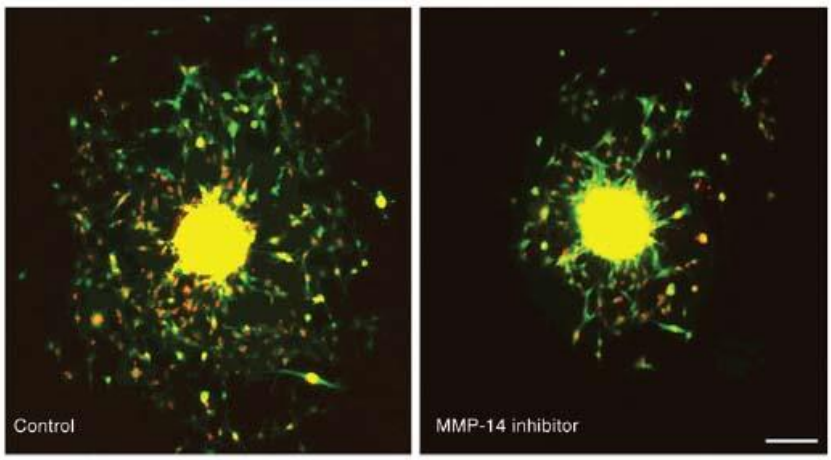


Figure 3: Invasion of DiI-labelled MSCs (red) and U373 eGFP cells (green) out of mixed spheroids upon treatment with a selective inhibitor of MMP-14.
For monitoring of invasion of MSCs and GBM cells out of MSC/GBM mixed spheroids, MSCs were labelled prior to spheroid formation with the fluorescent dye Vybrant DiI (Molecular Probes, Eugene, OR, USA). For mixed spheroid formation, DiI-MSCs and U373 eGFP cells were mixed in a 1:1 ratio and seeded in medium containing 4% methylcellulose (Sigma-Aldrich) in U-bottomed 96-well plates (BD Biosciences, San Jose, CA, USA), which were centrifuged at 850 *g* for 90 min, and then incubated overnight. Generated MSC/GBM mixed spheroids were transferred in laminin-coated wells and treated with MMP-14 inhibitor NSC405020 (Tocris Bioscience, Bristol, UK) in a final non-cytotoxic concentration 10 μM, diluted in 0.1% DMSO, or with control (0.1% DMSO). Cell invasion was monitored using an inverted fluorescence microscope with NIS elements software (Nikon; 40× original magnification; scale bar=200 μm) after 72 h. Images taken using either TRITC (red DiI-MSCs) or FITC (green U373 eGFP cells) philtres were merged, respectively.

Glioblastoma-associated MSCs also affect endothelial cells and immune cells in stroma, thus increasing intra-tumoural protease activity, which facilitates tumour progression. Macrophages, which express high levels of cathepsins B, L and S are attracted to tumours by cytokines such as IL-6 and CCL2/MCP-1 that are secreted by activated MSCs (Akkari et al., 2016). Furthermore, the MSCs promote macrophage polarisation into the tumour promoting M2 type, that is associated with immunosuppressive effects (Jia et al., 2016).

MSCs may enhance cancer cell invasion in a paracrine manner *via* protease activty regulation, as Swamydas et al. (2013) showed *in vitro*. MSCs in mammary cancer cells activate MMP-9, -13 and -14 through chemokines CCL-5 and CCL-9. Therefore, we were interested whether protease expression and activity is also affected by direct cross-talk between bone marrow-derived MSCs and glioblastoma cells. To analyse the cellular origin of invasion-related proteases MMP-9 and -14 in direct co-cultures of bone marrow-derived MSCs and glioblastoma cells and to distinguish between the two cell types in the direct co-culture set up, we used U87 cells, which stably expressed dsRED fluorescent protein (U87 dsRED). Our preliminary results of immunocytochemical analysis of MSC/U87 direct co-culture shows that both MSCs and U87 cells are important sources of proteases such as MMP-9 and -14 (Figure 2). This indicates that MSC-derived MMPs also contributed to the complex proteolytic signalling in the glioblastoma TME, possibly regulating ECM degradation and enabling glioblastoma cell invasion into surrounding healthy brain parenchyma. Furthermore, our unpublished findings indicate that direct cross-talk between MSCs and GBM cells in 3D-spheroids indeed enhances U373 cell invasion *via* MMP-14 upregulation, as a selective MMP-14 protease inhibitor decreases both MSCs and U373 cell invasion out of MSC/U373 mixed spheroids (Figure 3). As secretion of CCL2/MCP-1, which is an activator of MMPs via ERK 1/2signalling (Yang et al., 2016), is increased in direct MSC and glioblastoma co-cultures (Motaln and Turnsek, 2015), it is possible that paracrine signalling through CCL2 enhances MMP activity and drives glioblastoma cell invasion.

Conclusions

Proteases are key regulators of cancer progression and metastasis, and proteases in cancer cells as well as in stromal cells, such as fibroblasts, MSCs, immune cells and endothelial cells, are all part of the TME. These

Unauthenticated
Download Date | 6/13/17 3:10 PM

non-neoplastic cells actively contribute to the proliferative and invasive behaviour of cancer cells by secretion of proteases and cytokines. As proteases and cytokines exhibit both tumour-promoting and tumour-suppressive functions, it is important to develop therapeutic strategies that target tumour-promoting functions and restore those that suppress tumorigenesis.

Acknowledgements: We are grateful to Dr. Belinda Parker, Latrobe Institute for Molecular Science, La Trobe University, Melbourne, Australia, for reviewing the manuscript and for her valuable comments. We thank Mrs. Monika Golob for technical assistance with the immunocytochemical analysis. This work was supported by the ARRS project J1-4274, ARRS Programme P1-0245 (all to T.T.L.) and the ARRS Young Researcher grant (to B.B.).

References

Akkari, L., Gocheva, V., Quick, M.L., Kester, J.C., Spencer, A.K., Garfall, A.L., Bowman, R.L., and Joyce, J.A. (2016). Combined deletion of cathepsin protease family members reveals compensatory mechanisms in cancer. Genes Dev. *30*, 220–232.

Avgenis, M. and Scorilas, A. (2016). Kallikrein-related peptidases (KLKs) as emerging therapeutic targets: focus on prostate cancer and skin pathologies. Expert Opin. Ther. Targets *20*, 801–818.

Barcellos-de-Souza, P., Gori, V., Bambi, F., and Chiarugi, P. (2013). Tumor microenvironment: bone marrow-mesenchymal stem cells as key players. Biochim. Biophys. Acta *1836*, 321–335.

Borish, L.C. and Steinke, J.W. (2003). Cytokines and chemokines. J. Allergy Clin. Immunol. *111*, S460–S475.

Bougnaud, S., Golebiewska, A., Oudin, A., Keunen, O., Harter, P.N., Mäder, L., Azuaje, F., Fritah, S., Stieber, D., Kaoma, T., et al. (2016). Molecular crosstalk between tumour and brain parenchyma instructs histopathological features in glioblastoma. Oncotarget, *7*, 31955–31971.

Bruchard, M., Mignot, G., Derangère, V., Chalmin, F., Chevriaux, A., Végran, F., Boireau, W., Simon, B., Ryffel, B., Connat, J.L., et al. (2013). Chemotherapy-triggered cathepsin B release in myeloid-derived suppressor cells activates the Nlrp3 inflammasome and promotes tumor growth. Nat. Med. *19*, 57–64.

Cal, S. and López-Otín, C. (2015). ADAMTS proteases and cancer. Matrix Biol. *44–46*, 77–85.

Cathcart, J., Pulkoski-Gross, A., and Cao, J. (2015). Targeting matrix metalloproteinases in cancer: bringing new life to old ideas. Genes Dis. *2*, 26–34.

Diamandis, E.P. (2012). The failure of protein cancer biomarkers to reach the clinic: why, and what can be done to address the problem? BMC Med. *10*, 87.

Droga-Mazovec, G., Bojic, L., Petelin, A., Ivanova, S., Romih, R., Repnik, U., Salvesen, G.S., Stoka, V., Turk, V., and Turk, B. (2008). Cysteine cathepsins trigger caspase-dependent cell death through cleavage of bid and antiapoptotic Bcl-2 homologues. J. Biol. Chem. *283*, 19140–19150.

Gocheva, V., Wang, H.W., Gadea, B.B., Shree, T., Hunter, K.E., Garfall, A.L., Berman, T., and Joyce, J.A. (2010). IL-4 induces cathepsin protease activity in tumor-associated macrophages to promote cancer growth and invasion. Genes Dev. *24*, 241–255.

Gutova, M., Najbauer, J., Frank, R.T., Kendall, S.E., Gevorgyan, A., Metz, M.Z., Guevorkian, M., Edmiston, M., Zhao, D., Glackin, C.A., et al. (2008). Urokinase plasminogen activator and urokinase plasminogen activator receptor mediate human stem cell tropism to malignant solid tumors. Stem Cells *26*, 1406–1413.

Hanahan, D. and Weinberg, R.A. (2011). Hallmarks of cancer: the next generation. Cell *144*, 646–674.

Hawinkels, L.J., Paauwe, M., Verspaget, H.W., Wiercinska, E., van der Zon, J.M., van der Ploeg, K., Koelink, P.J., Lindeman, J.H., Mesker, W., ten Dijke, P., et al. (2014). Interaction with colon cancer cells hyperactivates TGF-β signaling in cancer-associated fibroblasts. Oncogene *33*, 97–107.

Hira, V.V., Ploegmaker, S.K.J., Grevers, F., Verbovšek, U., Silvestre-Roig, C., Aronica, E., Tigchelaar, W., Turnšek, T.L., Molenaar, R.J., and Van Noorden, C.J. (2015). CD133$^+$ and Nestin$^+$ glioma stem-like cells reside around CD31$^+$ arterioles in niches that express SDF-1α, CXCR4, osteopontin and cathepsin K. J. Histochem. Cytochem. *63*, 481–493.

Ho, I.A., Chan, K.Y., Ng, W.H., Guo, C.M., Hui, K.M., Cheang, P., and Lam, P.Y. (2009). Matrix metalloproteinase 1 is necessary for the migration of human bone marrow-derived mesenchymal stem cells toward human glioma. Stem Cells *27*, 1366–1375.

Hu, J., Jo, M., Eastman, B.M., Gilder, A.S., Bui, J.D., and Gonias, S.L. (2014). uPAR induces expression of transforming growth factor β and interleukin-4 in cancer cells to promote tumor-permissive conditioning of macrophages. Am. J. Pathol. *184*, 3384–3393.

Jia, X.H., Feng, G.W., Wang, Z.L., Du, Y., Shen, C., Hui, H., Peng, D., Li, Z.J., Kong, D.L., and Tian, J. (2016). Activation of mesenchymal stem cells by macrophages promotes tumor progression through immune suppressive effects. Oncotarget *7*, 20934–20944.

Kenig, S., Alonso, M.B., Mueller, M.M., and Lah, T.T. (2010). Glioblastoma and endothelial cells cross-talk, mediated by SDF-1, enhances tumour invasion and endothelial proliferation by increasing expression of cathepsins B, S, and MMP-9. Cancer Lett. *289*, 53–61.

Kenig, S., Frangež, R., Pucer, A., and Lah, T. (2011). Inhibition of cathepsin L lowers the apoptotic threshold of glioblastoma cells by up-regulating p53 and transcription of caspases 3 and 7. Apoptosis *16*, 671–682.

Kessenbrock, K., Plaks, V., and Werb, Z. (2010). Matrix metalloproteinases: regulators of the tumor microenvironment. Cell *141*, 52–67.

Kessenbrock, K., Wang, C.Y., and Werb, Z. (2015). Matrix metalloproteinases in stem cell regulation and cancer. Matrix Biol. *44–46*, 184–190.

Kos, J., Vižin, T., Fonović, U.P., and Pišlar, A. (2015). Intracellular signaling by cathepsin X: molecular mechanisms and diagnostic and therapeutic opportunities in cancer. Semin. Cancer Biol. *31*, 76–83.

Lah, T.T., Durán Alonso, M.B., and Van Noorden, C.J. (2006). Antiprotease therapy in cancer: hot or not? Exp. Opin. Biol. Ther. *6*, 257–279.

Lah, T.T., Obermajer, N., Duran Alonso, M.B., Kos, J. (2008). Cystein cathepsins and cystatins as caner biomarkers. In: The Cancer Degradome: Proteases and Cancer Biology, D. Edwards et al.,

Unauthenticated
Download Date | 6/13/17 3:10 PM

eds. (New York: Springer Science and Business Media), pp. 575–613.

Lankelma, J.M., Voorend, D.M., Barwari, T., Koetsveld, J., Van der Spek, A.H., De Porto, A.P., Van Rooijen, G., and Van Noorden, C.J. (2010). Cathepsin L, target in cancer treatment? Life Sci. *86*, 225–233.

López-Otín, C. and Bond, J.S. (2008). Proteases: multifunctional enzymes in life and disease. J. Biol. Chem. *283*, 30433–30437.

López-Otín, C. and Hunter, T. (2010). The regulatory crosstalk between kinases and proteases in cancer. Nat. Rev. Cancer *10*, 278–92.

López-Otín, C. and Matrisian, L.M. (2007). Emerging roles of proteases in tumour suppression. Nat. Rev. Cancer *7*, 800–808.

López-Otín, C. and Overall, C.M. (2002). Protease degradomics: a new challenge for proteomics. Nat. Rev. Mol. Cell Biol. *3*, 509–519.

Manicone, A.M. and McGuire, J.K. (2008). Matrix metalloproteinases as modulators of inflammation. Semin. Cell Dev. Biol. *19*, 34–41.

Mason, S.D. and Joyce, J.A. (2011). Proteolytic networks in cancer. Trends Cell Biol. *21*, 228–237.

Mohamed, M.M., Cavallo-Medved, D., Rudy, D., Anbalagan, A., Moin, K., and Sloane, B.F. (2010). Interleukin-6 increases expression and secretion of cathepsin B by breast tumor-associated monocytes. Cell. Physiol. Biochem. *25*, 315–324.

Mortier, A., Gouwy, M., Van Damme, J., Proost, P., and Struyf, S. (2016). CD26/dipeptidylpeptidase IV-chemokine interactions: double-edged regulation of inflammation and tumor biology. J. Leukoc. Biol. *99*, 955–969.

Motaln, H. and Turnsek, T.L. (2015). Cytokines play a key role in communication between mesenchymal stem cells and brain cancer cells. Protein Pept. Lett. *22*, 322–331.

Motaln, H., Gruden, K., Hren, M., Schichor, C., Primon, M., Rotter, A., and Lah, T.T. (2012). Human mesenchymal stem cells exploit the immune response mediating chemokines to impact the phenotype of glioblastoma. Cell Transplant. *21*, 1529–1545.

Olson, O.C. and Joyce, J.A. (2015). Cysteine cathepsin proteases: regulators of cancer progression and therapeutic response. Nat. Rev. Cancer *15*, 712–729.

Petrella, B.L. and Vincenti, M.P. (2012). Interleukin-1β mediates metalloproteinase-dependent renal cell carcinoma tumor cell invasion through the activation of CCAAT enhancer binding protein β. Cancer Med. *1*, 17–27.

Rao Malla, R., Gopinath, S., Alapati, K., Gorantla, B., Gondi, C.S., and Rao, J.S. (2013). Knockdown of cathepsin B and uPAR inhibits CD151 and α3β1 integrin-mediated cell adhesion and invasion in glioma. Mol. Carcinog. *52*, 777–790.

Rawlings, N.D., Barrett, A.J., and Finn, R. (2016). Twenty years of the MEROPS database of proteolytic enzymes, their substrates and inhibitors. Nucleic Acids Res. *44*, D343–D3450.

Reinheckel, T., Peters, C., Krüger, A., Turk, B., and Vasiljeva, O. (2012). Differential impact of cysteine cathepsins on genetic mouse models of *de novo* carcinogenesis: cathepsin B as emerging therapeutic target. Front. Pharmacol. *3*, 133.

Ries, C., Egea, V., Karow, M., Kolb, H., Jochum, M., and Neth, P. (2007). MMP-2, MT1-MMP, and TIMP-2 are essential for the invasive capacity of human mesenchymal stem cells: differential regulation by inflammatory cytokines. Blood *109*, 4055–4063.

Schichor, C., Albrecht, V., Korte, B., Buchner, A., Riesenberg, R., Mysliwietz, J., Paron, I., Motaln, H., Turnšek, T.L., Jürchott, K., et al. (2012). Mesenchymal stem cells and glioma cells form a structural as well as a functional syncytium *in vitro*. Exp. Neurol. *234*, 208–219.

Schrohl, A.S., Holten-Andersen, M., Sweep, F., Schmitt, M., Harbeck, N., Foekens, J., Brünner, N.; European Organisation for Research and Treatment of Cancer (EORTC) Receptor and Biomarker Group. (2003). Tumor markers: from laboratory to clinical utility. Mol. Cell. Proteomics *2*, 378–387.

Seruga, B., Zhang, H., Bernstein, L.J., and Tannock, I.F. (2008). Cytokines and their relationship to the symptoms and outcome of cancer. Nat. Rev. Cancer *8*, 887–899.

Sevenich, L. and Joyce J.A. (2014). Pericellular proteolysis in cancer. Genes Dev. *28*, 2331–2347.

Shchors, K., Nozawa, H., Xu, J., Rostker, F., Swigart-Brown, L., Evan, G., and Hanahan, D. (2013). Increased invasiveness of MMP-9-deficient tumors in two mouse models of neuroendocrine tumorigenesis. Oncogene *32*, 502–513.

Strojnik, T., Kavalar, R., Zajc, I., Diamandis, E.P., Oikonomopoulou, K., and Lah, T.T. (2009). Prognostic impact of CD68 and kallikrein 6 in human glioma. Anticancer Res. *29*, 3269–3279.

Stupack, D.G. (2013). Caspase-8 as a therapeutic target in cancer. Cancer Lett. *332*, 133–140.

Swamydas, M., Ricci, K., Rego, S.L., and Dréau, D. (2013). Mesenchymal stem cell-derived CCL-9 and CCL-5 promote mammary tumor cell invasion and the activation of matrix metalloproteinases. Cell Adh. Migr. *7*, 315–324.

Tuomela, J., Sandholm, J., Kaakinen, M., Patel, A., Kauppila, J. H., Ilvesaro, J., Chen, D., Harris, K.W., Graves, D., and Selander, K.S. (2013). DNA from dead cancer cells induces TLR9-mediated invasion and inflammation in living cancer cells. Breast Cancer Res. Treat. *142*, 477–487.

Turk, B., Turk, D., and Turk, V. (2012). Protease signalling: the cutting edge. EMBO J. *31*, 1630–1643.

Van Den Steen, P.E., Wuyts, A., Husson, S.J., Proost, P., Van Damme, J., and Opdenakker, G. (2003). Gelatinase B/MMP-9 and neutrophil collagenase/MMP-8 process the chemokines human GCP-2/CXCL6, ENA-78/CXCL5 and mouse GCP-2/LIX and modulate their physiological activities. Eur. J. Biochem. *270*, 3739–3749.

Verbovšek, U., Motaln, H., Rotter, A., Atai, N.A., Gruden, K., Van Noorden, C.J., and Lah, T.T. (2014). Expression analysis of all protease genes reveals cathepsin K to be overexpressed in glioblastoma. PLoS One *9*, e111819.

Verbovšek, U., Van Noorden, C.J., and Lah, T.T. (2015). Complexity of cancer protease biology: cathepsin K expression and function in cancer progression. Semin. Cancer Biol. *35*, 71–84.

Wang, Y.H., Dong, Y.Y., Wang, W.M., Xie, X.Y., Wang, Z.M., Chen, R.X., Chen, J., Gao, D.M., Cui, J.F., and Ren, Z.G. (2013). Vascular endothelial cells facilitated HCC invasion and metastasis through the Akt and NF-κB pathways induced by paracrine cytokines. J. Exp. Clin. Cancer Res. *32*, 51.

Wilkinson, R.D., Magorrian, S.M., Williams, R., Young, A., Small, D.M., Scott, C.J., and Burden, R.E. (2015). CCL2 is transcriptionally controlled by the lysosomal protease cathepsin S in a CD74-dependent manner. Oncotarget *6*, 29725–29739.

Wolf, M., Albrecht, S., and Märki, C. (2008). Proteolytic processing of chemokines: implications in physiological and pathological conditions. Int. J. Biochem. Cell Biol. *40*, 1185–1198.

Unauthenticated
Download Date | 6/13/17 3:10 PM

Xie, L., Moroi, Y., Hayashida, S., Tsuji, G., Takeuchi, S., Shan, B., Nakahara, T., Uchi, H., Takahara, M., and Furue, M. (2011). Cathepsin K-upregulation in fibroblasts promotes matrigel invasive ability of squamous cell carcinoma cells via tumor-derived IL-1α. J. Dermatol. Sci. *61*, 45–50.

Yamada, K., Maishi, N., Akiyama, K., Towfik Alam, M., Ohga, N., Kawamoto, T., Shindoh, M., Takahashi, N., Kamiyama, T., Hida, Y., et al. (2015). CXCL12-CXCR7 axis is important for tumor endothelial cell angiogenic property. Int. J. Cancer *137*, 2825–2836.

Yamamoto, K., Murphy, G., and Troeberg, L. (2015). Extracellular regulation of metalloproteinases. Matrix Biol. *44–46*, 255–263.

Yang, J., Lv, X., Chen, J., Xie, C., Xia, W., Jiang, C., Zeng, T., Ye, Y., Ke, L., Yu, Y., et al. (2016). CCL2-CCR2 axis promotes metastasis of nasopharyngeal carcinoma by activating ERK1/2-MMP2/9 pathway. Oncotarget *7*, 15632–15647.

Yin, M., Soikkeli, J., Jahkola, T., Virolainen, S., Saksela, O., and Höltta, E. (2012). TGF-β signaling, activated stromal fibroblasts, and cysteine cathepsins B and L drive the invasive growth of human melanoma cells. Am. J. Pathol. *181*, 2202–2216.

Zhang, B., Shi, L., Lu, S., Sun, X., Liu, Y., Li, H., Wang, X., Zhao, C., Zhang, H., and Wang, Y. (2015). Autocrine IL-8 promotes F-actin polymerization and mediate mesenchymal transition via ELMO1-NF-κB-Snail signaling in glioma. Cancer Biol. Ther. *16*, 898–911.

Unauthenticated
Download Date | 6/13/17 3:10 PM

2.2 Mesenchymal Stem Cells Differentially Affect the Invasion of Distinct Glioblastoma Cell Lines

Barbara Breznik, Helena Motaln, Miloš Vittori, Ana Rotter, Tamara Lah Turnšek

Oncotarget 2017; 8(15): 25482-25499. DOI: 10.18632/oncotarget.16041

www.impactjournals.com/oncotarget/ Oncotarget, Advance Publications 2017

Mesenchymal stem cells differentially affect the invasion of distinct glioblastoma cell lines

Barbara Breznik[1,2], Helena Motaln[1], Miloš Vittori[1], Ana Rotter[1], Tamara Lah Turnšek[1,2,3]

[1]Department of Genetic Toxicology and Cancer Biology, National Institute of Biology, 1000 Ljubljana, Slovenia

[2]International Postgraduate School Jozef Stefan, 1000 Ljubljana, Slovenia

[3]Department of Biochemistry, Faculty of Chemistry and Chemical Engineering, University of Ljubljana, 1000 Ljubljana, Slovenia

Correspondence to: Tamara Lah Turnšek, email: Tamara.Lah@nib.si

Keywords: glioblastoma multiforme, proteases, mesenchymal stem cells, tumor heterogeneity, zebrafish model

Received: November 25, 2016 Accepted: February 07, 2017 Published: March 09, 2017

ABSTRACT

Glioblastoma multiforme are an aggressive form of brain tumors that are characterized by distinct invasion of single glioblastoma cells, which infiltrate the brain parenchyma. This appears to be stimulated by the communication between cancer and stromal cells. Mesenchymal stem cells (MSCs) are part of the glioblastoma microenvironment, and their 'cross-talk' with glioblastoma cells is still poorly understood. Here, we examined the effects of bone marrow-derived MSCs on two different established glioblastoma cell lines U87 and U373. We focused on mutual effects of direct MSC/glioblastoma contact on cellular invasion in three-dimensional invasion assays *in vitro* and in a zebrafish embryo model *in vivo*. This is the first demonstration of glioblastoma cell-type-specific responses to MSCs in direct glioblastoma co-cultures, where MSCs inhibited the invasion of U87 cells and enhanced the invasion of U373. Inversely, direct cross-talk between MSCs and both of glioblastoma cell lines enhanced MSC motility. MSC-enhanced invasion of U373 cells was assisted by overexpression of proteases cathepsin B, calpain1, uPA/uPAR, MMP-2, -9 and -14, and increased activities of some of these proteases, as determined by the effects of their selective inhibitors on invasion. In contrast, these proteases had no effect on U87 cell invasion under MSC co-culturing. Finally, we identified differentially expressed genes, in U87 and U373 cells that could explain different response of these cell lines to MSCs. In conclusion, we demonstrated that MSC/glioblastoma cross-talk is different in the two glioblastoma cell phenotypes, which contributes to tumor heterogeneity.

INTRODUCTION

Tumor heterogeneity is recognized as one of the key reasons for ineffective radiotherapy, chemotherapy and recurrence in many cancers, as occurs in the most aggressive glioma stage WHO IV, glioblastoma multiforme (GBM). GBMs are classified according to their gene-expression patterns, as the proneural, neural, classical and mesenchymal subtypes [1, 2]. Clonal evolution *via* GBM stem-like cells gives rise to heterogeneous populations of differentiated, invasive GBM cells [3]. We demonstrated that the generally used GBM cell lines, U87 and U373, show distinct phenotypes and they differ in expression of genes associated with extracellular matrix (ECM) organization, developmental processes and cell differentiation [4]. Upon the *in vitro* co-culturing of U87 and U373 cells, we identified different clusters of de-regulated genes in these two GBM cell lines. The molecular 'cross-talk' between U87 and U373 cells strikingly increased the invasiveness of both cells types [4], reflecting the mutually induced phenotypic changes, as may occur in tumors *in vivo*, and as has been suggested recently by *Ricklefs et al.* [5].

Cell invasion is a crucial obstacle to overcome in glioma treatment, as GBM cells represent distinct moving targets, spreading into various sites in the brain. Many

studies have been focused on therapeutic targeting of various types of proteases involved in GBM cell invasion [6]. According to the MEROPS database (http://www.merops.ac.uk), the protease superfamily consists of 990 known and putative genes. Verbovšek *et al.* [7] used a transcriptomics approach that revealed 311 protease genes that were differentially expressed in both GBM tissues and in GBM U87 and U373 cell lines, when compared to normal brain and normal astrocytes, respectively. These proteases induce protease signaling [8] on their own, or in cascade-like reactions [9], which play important roles in GBM progression [6, 10, 11]. Most relevant players in pericellular invasion of GBM cells are distinct lysosomal cathepsins, such as cathepsins B and S [12–15], calpains [16], urokinase-type plasminogen activator and selected matrix metalloproteases [9–11], that enhance cell invasion [6, 9]. These proteases are considered as potential targets for anti-invasive therapy [10] and were selected in this GBM heterogeneity study.

Recent findings have suggested that cancer–stromal interactions contribute to a complex proteolytic network, that is regulated also *via* pro-inflammatory cytokines and a selection of growth factors [10, 17, 18]. Communication between stromal cells and GBM cells creates a tumor-promoting environment [19]. Stromal mesenchymal stem cells (MSCs) can induce the transition to a more invasive GBM cell phenotype [20] that shows similarities with epithelial to mesenchymal transition (EMT) or with the mesenchymal to amoeboid transition [21]. The key difference between these two cell migration modalities are proteases that are involved in cell invasion in co-culture models, as we showed in the present study.

MSCs are known as adult stem cells, and reside in many organs for the regeneration of damaged tissue. MSCs are increasingly used in cell therapies and tissue engineering because of their availability, multi-potency, and immunomodulatory activity [22]. Recruited bone marrow-derived MSCs can home neoplasia and become part of the tumor microenvironment [23–26], including GBM [27], but seem to have dual roles in tumors, which mainly depend on their immuno-activation status [28]. In glioma, both roles of MSCs in promotion [24, 26] and inhibition of tumor growth have been reported [26–30]. However, the molecular mechanisms of their interactions with GBM cells are not yet well defined.

To study tumor heterogeneity, we used a three-dimensional (3D) spheroid model, which included direct MSC/GBM cell contact, as well as paracrine signaling. As the critical step in translational oncology remains the bridge between *in vitro* cell cultures to *in vivo* animal models, as a preclinical phase I step, in this study we used a zebrafish model for that respect. The strongest benefit for their use as a tumor model is the transparency of the embryos that allows imaging of tumor progression at single-cell resolution in a real time [31–34].

The major aim of the present study was to determine how cross-talk between the phenotypically distinct GBM cell lines U87 and U373 and the bone marrow-derived MSCs mutually affects cell invasion. Using transcriptome analyses, we have identified the key upregulated proteases in GBM, and have revealed their differential expression in the two distinct GBM phenotypes, when in direct co-cultures with MSCs, which the protease expression was also altered. We have been also able to translate this *in-vitro* 3D model into the experimental *in vivo* zebrafish embryo model.

RESULTS

MSCs reduce invasion of U87 cells and enhance invasion of U373 cells *in vitro*

To determine the effects of MSCs and GBM cells on cellular invasion *in vitro*, we performed a 3D spheroid invasion assays, using various ECM components, such as laminin, collagen type I, and Matrigel. In monocultured spheroids, U87 cells were more invasive than U373 cells when embedded in collagen type I or Matrigel. In contrast, U373 cells were more invasive on laminin (Figure 1A). In the MSC/U87 spheroid co-cultures, U87 cells were significantly less invasive compared to U87 monospheroids, irrespective of the ECM component used (Figure 1A, left panel; Figure 1C). The strongest inhibition of U87 cellular invasion by MSCs was observed in collagen type I (up to 50% inhibition on day 1). In contrast, MSCs enhanced invasion of U373 cells compared to U373 monocultured spheroids by nearly 30% in collagen type I and by 45% in Matrigel (on day 4), whereas on laminin the highest increase in U373 cell invasion (50% on day 4) was observed (Figure 1A, right panel; Figure 1C). Both GBM cell lines enhanced the invasiveness of MSCs. This effects were dependent on the ECM component present, as U87 cells enhanced MSC invasion by 80% in Matrigel on day 4 (Figure 1B, left panel), whereas U373 enhanced invasion of MSCs by as much as 200% on laminin on day 3 and 4 (Figure 1B. right panel).

Transcriptome analyses of GBM reveals upregulated protease genes

As cross-talk between MSCs and GBM cells altered invasive behavior of the GBM cells, we searched for proteases involved in the interplay between these 2 cell types. In a related study [7], we have investigated the deregulated GBM transcriptome of protease genes, as compared to that of normal brain tissue. Among the upregulated genes, we searched for intersections with a list of human proteases obtained from the MEROPS database, which resulted in 78 upregulated proteases in GBM *versus* normal brain, including 25 serine, 23 cysteine, 20

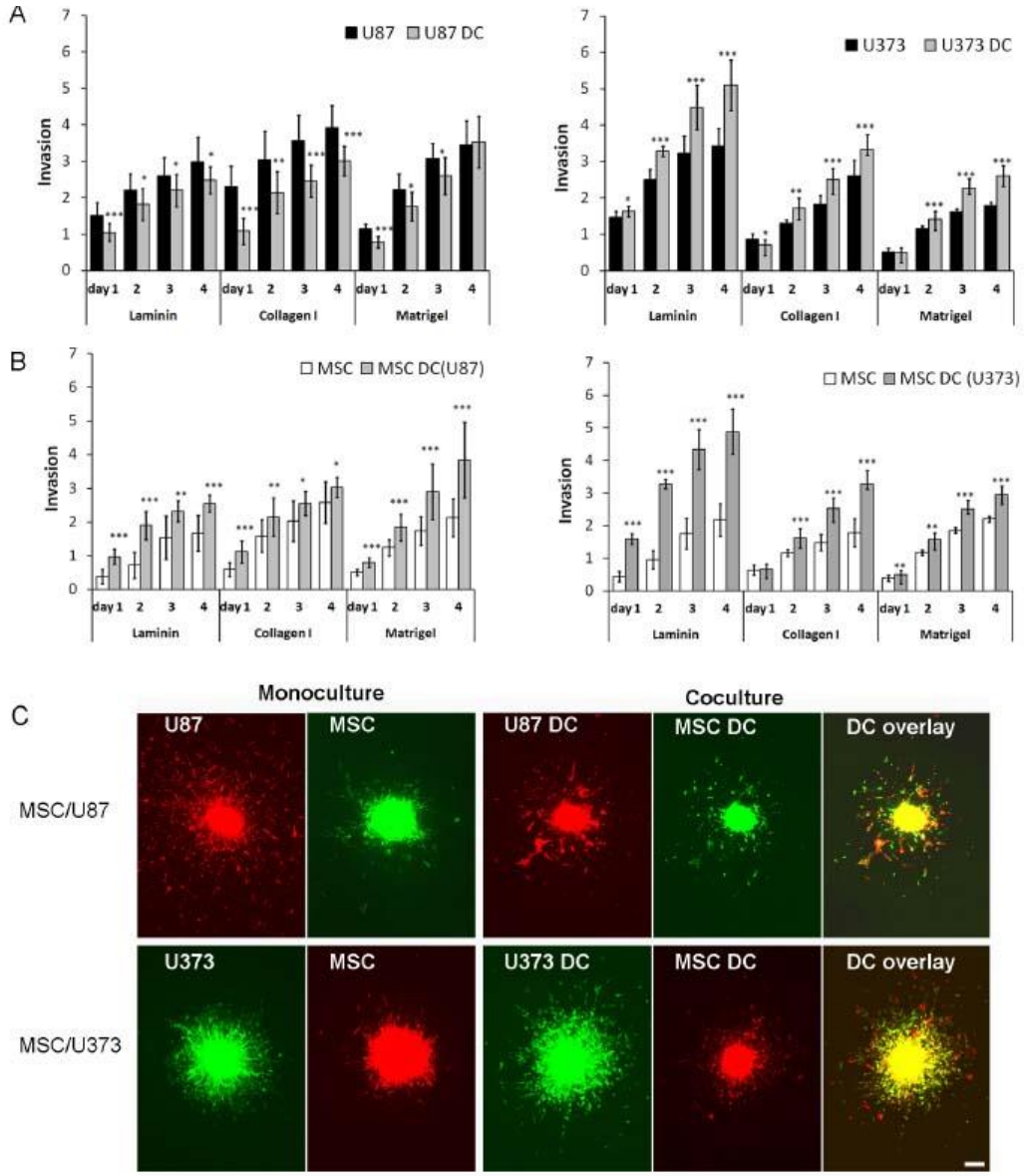


Figure 1: Invasion of DiO/DiI-labelled MSCs, U87dsRed and U373eGFP cells from spheroids. Spheroids of MSCs, GBM cells (monocultured) and MSC/GBM cells as direct co-cultures (DC) were prepared and embedded in laminin, collagen I and Matrigel. Invasion distance *versus* spheroid diameter (Invasion) was measured over a period of 4 days using a fluorescent inverted microscope. **(A)** Invasion of U87 cells (left) and U373 cells (right) from spheroids. **(B)** Invasion of MSCs from spheroids, as MSCs co-cultured with U87 cells (left) and U373 cells (right). **(C)** Representative images of MSCs and U87 and U373 cells invading from monocultures and MSC/GBM direct co-cultures (DC) after 2 days in collagen I (magnification, 40×). Scale bar = 200 μm. Data are means ± SD. * $P < 0.05$, ** $P < 0.01$, *** $P < 0.001$.

metallo-, 1 aspartic, and 3 mixed protease family genes (Supplementary Table 1). We selected seven proteases and one protease receptor for validation in the co-culture model, as this panel of proteases has been reported to be functionally associated with cellular invasion [6, 9].

Validation of selected cysteine, serine and metallo-proteases in MSC/GBM co-cultures

The canonical proteolytic cascade that leads to enhanced cancer cell invasion is considered to be initiated by (pro)cathepsin B, which translocates from lysosomes to plasma membranes, where it may activate uPA, which in turn activates MMP-14, followed by activation of gelatinases MMP-2 and MMP-9 [14]. We analyzed gene expression of these proteases using RT-PCR and protein levels by Western blotting and flow cytometry, in media and cells of monocultures and MSC/GBM co-cultures. To demonstrate the impact of MSC:GBM cell ratios on protease expression in these cells, we used 3 ratios of MSCs to GBM cells, i.e., 1:3, 1:1 and 3:1 (Figure 2A).

Changes in cathepsin B mRNA content was not observed in the MSC/U87 co-cultures, whereas cathepsin B mRNA was upregulated by 20-45% in MSC/U373 direct co-cultures in a cell-ratio-dependent manner when compared to the respective monocultures (Figure 2B). Increased cathepsin B protein secretion was observed only in the 3:1 ratio of MSC/U87 co-cultures (Figure 2C, left panel) and in all MSC:GBM ratios of MSC/U373 co-cultures (Figure 2C, right panel). Flow cytometry confirmed no alteration of cellular cathepsin B protein in co-cultured U87 cells, but upregulation of cathepsin B protein expression in co-cultured U373 cells at all MSC:GBM ratios by 20%. In contrast, both GBM cell types downregulated cathepsin B expression in MSCs by 15-30% (Figure 2D).

mRNA levels of calpain1 and calpain2 did not change in either of the MSC/GBM co-cultures (Figure 2B). Secreted calpain1 increased only slightly in MSC/U87 co-cultures with 3:1 ratio, and in all MSC/U373 co-cultures. Increased calpain1 in co-cultures was most likely secreted from GBM cells (Figure 2C), as MSCs upregulated protein expression of calpain1 only slightly in the co-cultured U87 cells with 3:1 ratio and by up to 80% in the co-cultured U373. In contrast, calpain1 was significantly downregulated in the co-cultured MSCs with U87 cells and not altered in co-cultured MSCs with U373 cells. Calpain2 protein levels were lower in both GBM cell, lines and not detected in the media, whereas in MSCs calapin2 was downregulated in MSCs in co-cultures with U87 cells, but not with U373 cells (Figure 2D).

mRNA levels of the serine protease uPA increased by 30-50% in both MSC/U87 and MSC/U373 co-cultures, as compared to monocultures (Figure 3A). The increased secretion of uPA from both of these co-cultures was confirmed by Western blotting (Figure 3B), and increased protein expression in the co-cultured GBM cells was confirmed by flow cytometry (Figure 3C). In at contrast, uPA protein expression decreased in MSCs co-cultured with either of these GBM cell lines subtype by more than 30% at 1:3 ratio (Figure 3C). mRNA levels of the urokinase receptor uPAR remained unchanged in MSC/U87 co-cultures, when compared to monocultures, but increased by more than 40% in MSC/U373 co-cultures (in DC 3:1), when compared with monocultures (Figure 3A). uPAR protein levels decreased in co-cultured U87 cells by 20%, but increased by 60-80% in co-cultured U373 cells. In contrast, MSCs when co-cultured with U87 cells, showed decrease in uPAR expression in a cell-ratio-dependent manner (30-70%), whereas when co-cultured with U373 cells uPAR expression remained unchanged (Figure 3C).

mRNA levels of metalloprotease MMP-2 in MSC/U87 co-cultures did not change (Figure 4A), and alteration in MMP-2 secretion was not detected in MSC/U87 co-cultures, as compared to U87 monocultures, except for decrease in the 3:1 co-cultures (Figure 4B, left panel). mRNA levels of MMP-2 increased in MSC/U373 co-cultures up to 50% in 3:1 co-cultures, as compared to U373 monocultures (Figure 4A). This was in line with increased secretion of MMP-2 protein from MSC/U373 co-cultured cells (Figure 4B, right panel). Flow cytometry revealed no changes in MMP-2 protein expression in either of the GBM cell types co-cultured with MSCs. In contrast, MSCs showed a cell-ratio-dependent decrease in MMP-2 expression in both types of co-cultures (Figure 4C).

MMP-9 mRNA levels were decreased in MSC/U87 co-cultures, but increased 2.5-fold in MSC/U373 co-cultures in 1:1 and 1:3 ratios, as compared to their respective monocultures (Figure 4A). This coincided with secreted MMP-9 protein, which was decreased in MSC/U87, but increased in MSC/U373 co-cultures (Figure 4B). This was in line with the unchanged protein expression of MMP-9 in co-cultured U87 cells, and increased MMP-9 expression up to 100% in co-cultured U373 cells in 1:3 and 3:1 ratio (Figure 4C). Although MMP-9 protein expression did not change in the co-cultured U87 cells, the decreased MMP-9 secretion by MSC/U87 co-cultures may have been the result of the downregulation of MMP-9 protein expression in the co-cultured MSCs by up to 85% in 1:3 co-cultures (Figure 4C).

Interestingly, MMP-14 mRNA increased by up to 30% in MSC/U87 co-cultures, and also by up to 110% in 3:1 MSC/U373 co-cultures (Figure 4A). However, MMP-14 protein expression was downregulated by up to 30% in co-cultured U87 cells, whereas it was upregulated in co-cultured U373 cells, by 40-55% in 1:3, 1:1 and 3:1 ratios, respectively (Figure 4C). In contrast, MMP-14 protein expression in MSCs was decreased by 25-60% in U87 co-cultures, and by 30-35% in U373 cell co-cultures.

Taken together, cathepsin B, calpain1, and MMP-2, -9, and -14 were upregulated at the mRNA and/or

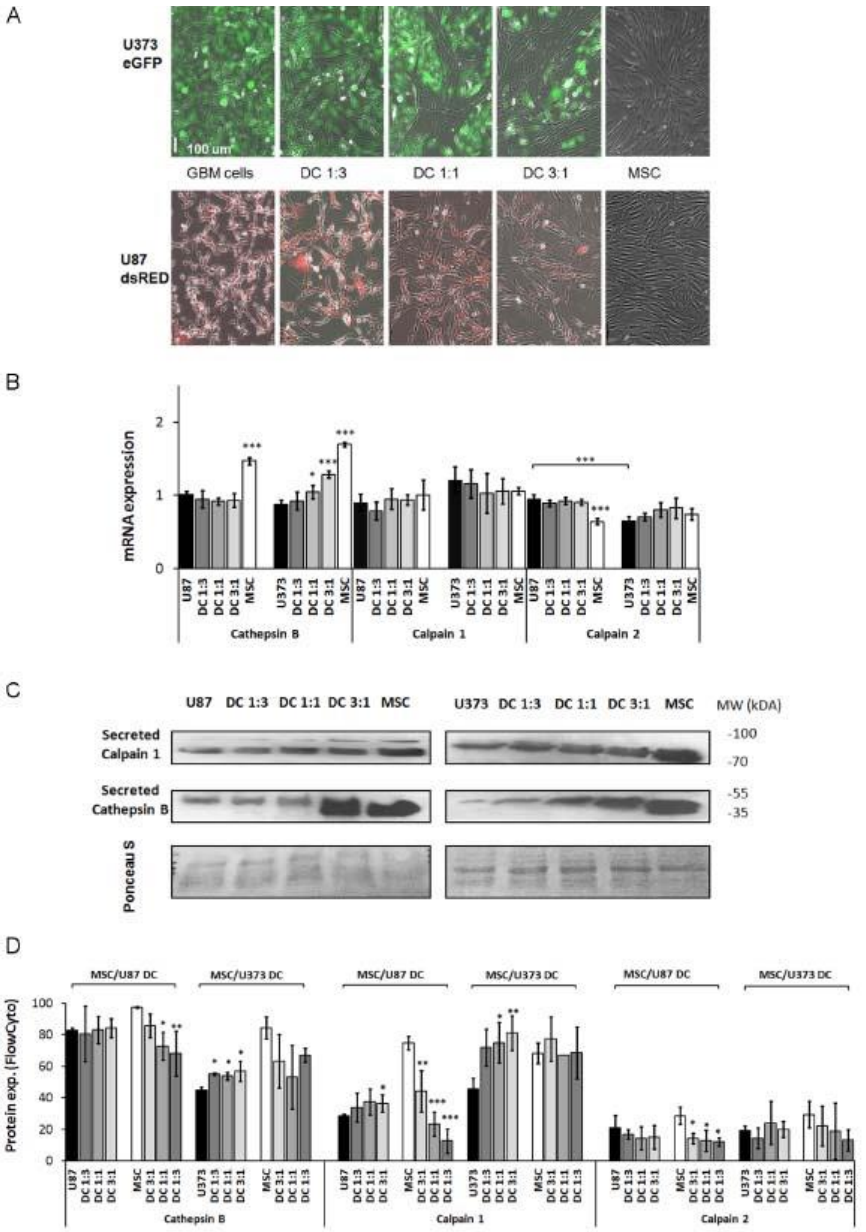


Figure 2: Expression of the cysteine proteases cathepsin B, calpain1 and calpain2 in GBM cells, MSCs and their direct co-cultures. (A) MSCs and GBM cells (U87, U373) monocultured or in direct co-cultures (DC) at 3 different ratios, were grown for 72 h as monolayers and analyzed. **(B)** Cathepsin B, calpain1 and calpain 2 mRNA levels in U87 cells, U373 cells, MSCs, and in their direct co-cultures (DC) as determined by qPCR. **(C)** Detection of secreted cathepsin B and calpain1 in culture medium of MSCs, U87 cells (left), U373 cells (right) and their co-cultures (DC) at different ratios, using Western blotting. Western blots were stained with Ponceau S to confirm equal protein loading. **(D)** Cathepsin B, calpain1 and calpain2 protein expression in MSCs and GBM cells grown as monocultures and direct co-cultures at different ratios, analyzed by flow cytometry. Data are means ± SD. * P <0.05, ** P <0.01, *** P <0.001.

protein levels in U373 cells, co-cultured with MSCs that showed enhanced invasion. However, among tested proteases only the protein expression of MMP-14, which was downregulated in co-cultured U87 cells, correlated with decreased invasion of U87 cells upon co-culturing with MSCs. uPA was upregulated in both of these cell lines, although its receptor was upregulated in U373 and downregulated in U87 cells in co-cultures. In MSCs, both types of GBM cells downregulated most of the above described proteases (Figure 5).

Invasion of GBM cells from MSC/GBM co-cultures is differentially affected by protease inhibitors

We performed spheroid invasion assays in the presence and absence of selective synthetic inhibitors of cathepsin B, MMP-9 and MMP-14: CA-074Me, MMP-9 inhibitor I, and NSC405020, respectively, at non-toxic concentrations (Supplementary Figure 1). In U87 monocultured spheroids, cell invasion was

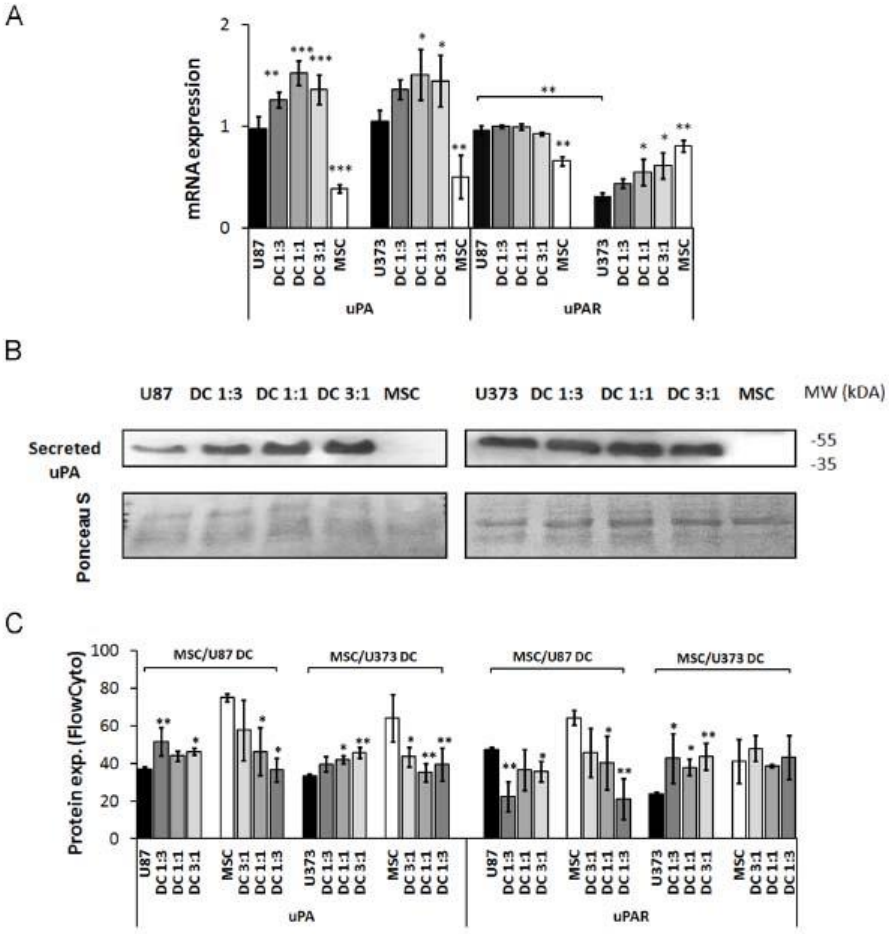


Figure 3: Expression of serine protease urokinase-type plasminogen activator (uPA) and its receptor (uPAR) in GBM cells, MSCs and their co-cultures (DC). MSCs and GBM cells were mixed in different ratios, grown for 72 h as monolayers and analyzed. **(A)** uPA and uPAR mRNA levels in U87 cells, U373 cells, MSCs and their direct co-cultures at different ratios, as determined by qPCR. **(B)** Detection of uPA secreted into the cell medium of MSCs, U87 cells (left), U373 cells (right) and their co-cultures (DC) at different ratios, as analyzed by Western blotting. The Western blots were stained with Ponceau S to confirm equal protein loading. **(C)** uPA and uPAR expression analyzed in GBM cells and MSCs grown as monocultures and co-cultures at different ratios, as analyzed by flow cytometry. Data are means ± SD. * P <0.05, ** P <0.01, *** P <0.001.

inhibited by 20% by the cathepsin B inhibitor, by 40% by the MMP-9 inhibitor, and by 42% by the MMP-14 inhibitor (Figure 6A). Invasion of U87 cells from the MSC/U87 co-cultured spheroids was already inhibited, and no further changes were observed upon addition of any of the inhibitors. The protease inhibitors had no effects on invasion of MSCs from MSC/U87 spheroids (Figure 6A). In contrast, only CA-074Me reduced invasion of U373 cells from monospheroids by 20%, whereas both the cathepsin B and MMP-9 inhibitors reduced U373 cell invasion from spheroid co-cultures, as compared with control U373 in co-cultures by 50% and 40%, respectively (Figure 6B). The MMP-14 inhibitor reduced U373 cell invasion from co-cultured spheroids by approximately 35% below that of the U373 monospheroids. CA-074Me, MMP-9I and NSC405020 inhibitors reduced the invasion of MSCs from MSC/U373 co-cultured spheroids by 35%, 25% and 40%, respectively, but the inhibitors were not effective in MSC monospheroids (Figure 6B).

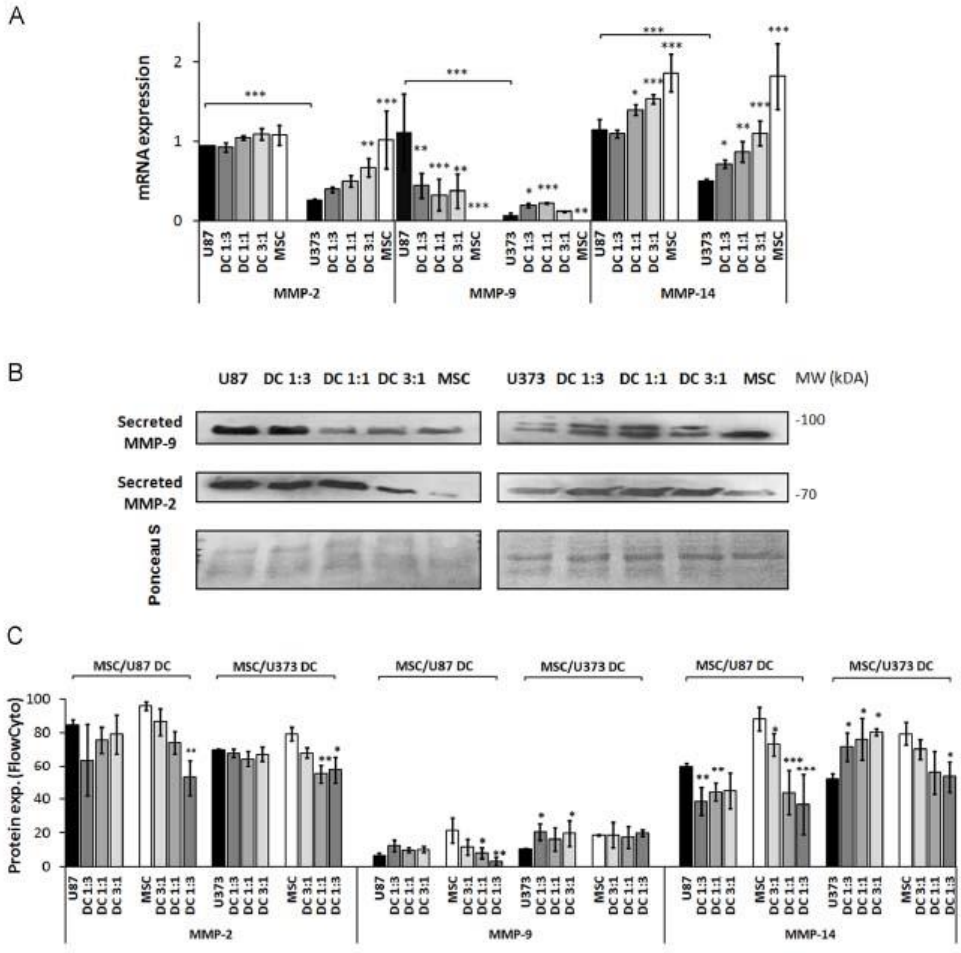


Figure 4: MMP-2, MMP-9 and MMP-14 expression in GBM cells, MSCs and their co-cultures. MSCs and GBM cells were monocultured or direct co-cultured (DC) at different ratios, grown for 72 h as monolayers and analyzed. **(A)** MMP-2, -9 and -14 mRNA level, as determined by qPCR. **(B)** Secreted MMP-2 and MMP-9 in culture medium of MSCs, U87 cells (left), U373 cells (right) and their co-cultures, by Western blotting. The western blots were stained with Ponceau S to confirm equal protein loading. **(C)** MMP-2, -9 and -14 expression, analyzed by flow cytometry. Data are means ± SD. * P <0.05, ** P <0.01, *** P <0.001.

A

Altered in MSC/GBM co-cultures vs monocultures	Cell line U87	Cell line U373
Cell Invasion	↓	↑
Protease expression		
Cathepsin B	not changed	↑
Calpain1	↑	↑
Calpain2	not changed	not changed
uPA	↑	↑
uPAR	↓	↑
MMP-2	not changed	↑
MMP-9	↓	↑
MMP-14	↓	↑

B

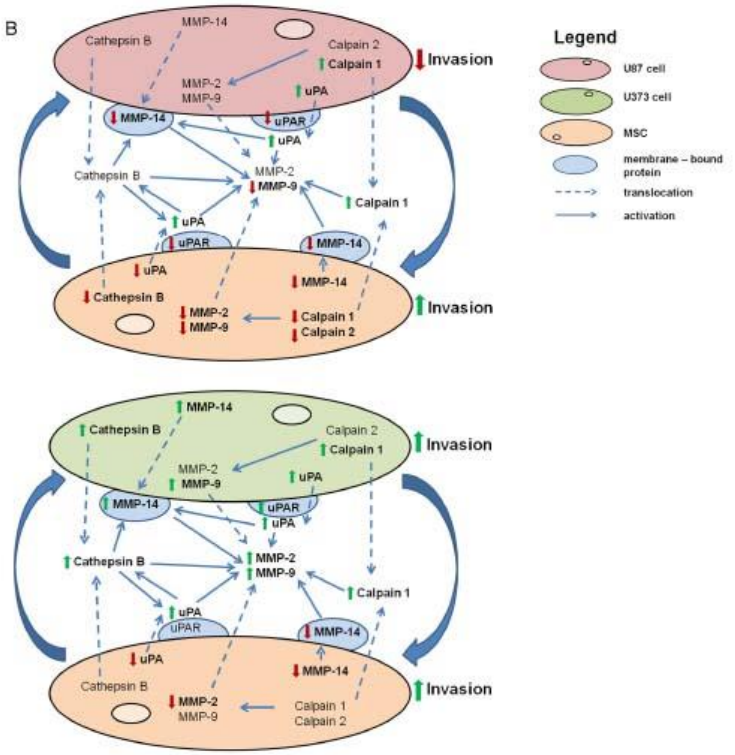


Figure 5: Alterations in invasion and the protease expression in GBM cells and MSCs upon co-culturing. **(A)** Changes in invasiveness and the candidate protease expression in GBM cells after co-culturing with MSCs are presented in the table. Red and green arrows indicate lower and higher invasion of GBM cells from MSC/GBM co-cultures, respectively, compared with monocultures. Similarly, red and green arrows indicate decreased and increased expression, respectively, at any of the levels of the candidate proteases, compared with monocultures. **(B)** The scheme shows the presentation of the effects of MSC/GBM co-culturing on the protease expression, involved in invasion-associated proteolytic cascade, in the respective cells and their co-culture media. The upper part of the scheme represents direct cross-talk of U87 cells with MSCs, resulting in decreased invasion of U87 cells, correlating with decreased expression of uPAR and MMP-14 and secretion of MMP-9. Simultaneously, MSC invasion was increased in spite of decreased expression of all the proteases. The lower part of the scheme shows that enhanced U373 invasion was associated with increased levels of all proteases, except calpain2. This shows that MSCs trigger opposite response of two types of GBM cells with respect to invasion, which is associated with different pattern of proteases expression. The lowest part of the scheme shows that MSC/U373 cell cross-talk also results in increased MSC invasion, downregulation of uPA, MMP-9 and -14 and not altered expression of other tested proteases. Alterations of invasion and proteases are shown as bold red arrows (down-regulation) and green arrows (up-regulated).

Xenotransplantation of MSC/GBM cell mixtures into zebrafish embryo brain confirms differential behavior of U87 and U373 cells

To confirm these results from *in vitro* assays *in vivo*, we injected GBM cells alone or together with MSCs into the brains of zebrafish embryos. Both U87 and U373 cells proliferated in zebrafish embryo brains (Figure 7A). However, after 72 h, fluorescence intensity of U87 cell xenografts was approximately 2-fold stronger compared to that of U373 cell xenografts, which implied more rapid proliferation of U87 cells in the zebrafish embryo brain (Figure 7B). Moreover, U87 cells invaded from the xenograft mass within the zebrafish embryo brain more readily than U373 cells. U87 cells showed 30% more relative invasion as compared to U373 cells (Figure 7C), which is in line with the *in vitro* observations. Co-injection of GBM

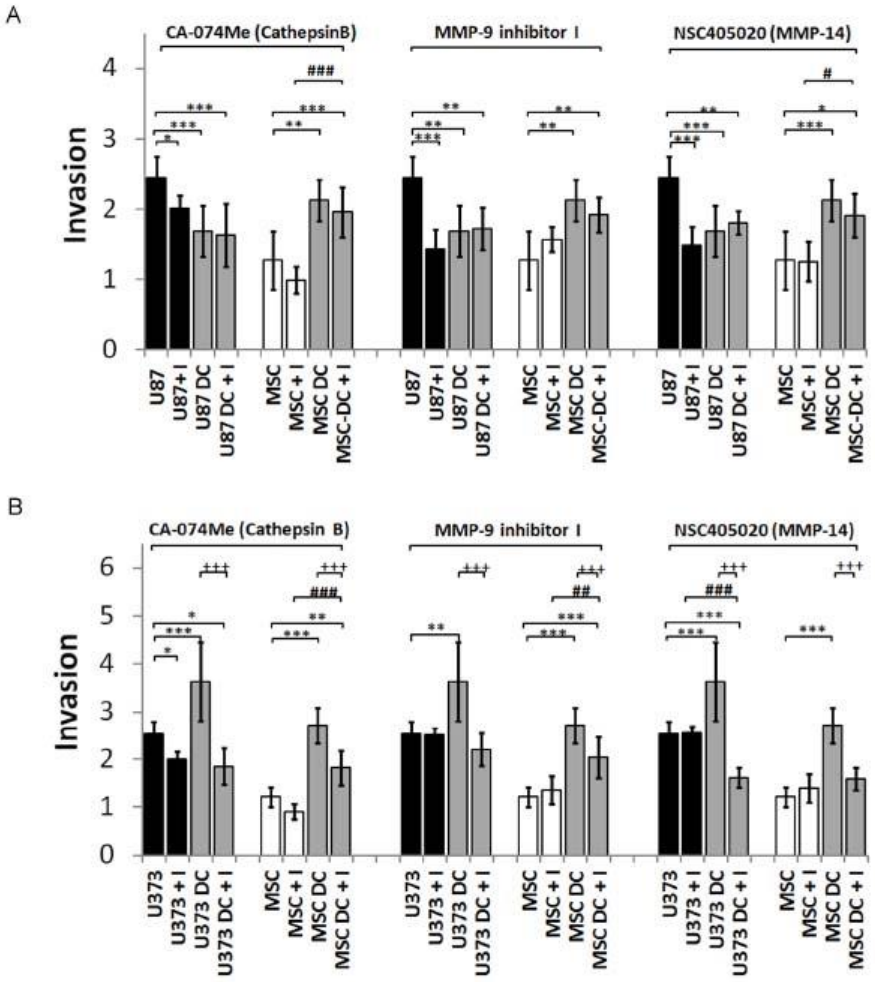


Figure 6: Invasion of DiO/DiI-labelled MSCs and GBM (U87 dsRED, U373 eGFP) cells from spheroids upon treatment with selective inhibitors of cathepsin B (2 µM), MMP-9 (100 nM) and MMP-14 (10 µM). Generated monospheroids (MSCs, U87, U373) and mixed spheroids were incubated in laminin-coated wells and treated with protease inhibitors or control (0.1% DMSO). **(A)** Invasion (invasion distance/ spheroid diameter) of MSCs and U87 cells from spheroids in the presence of protease inhibitors or control medium, measured after 72 h. **(B)** Invasion of MSCs and U373 cells from spheroids in the presence of protease inhibitors or control medium after 72 h. Data are means ± SD. * P <0.05, ** (++, ##) P <0.01, *** (+++, ###) P <0.001.

cells and MSCs mixtures into the brain of zebrafish embryos resulted in reduced proliferation of both GBM cell types, in U87 cells by 20%, and in U373 cells by 15% (Figure 7B). Direct contact between MSCs and GBM cells enhanced the invasion of U373 cells by 35%, but inhibited invasion of U87 cells by 30% (Figure 7A, 7C), again similar to the findings *in vitro*.

U87 and U373 cells differ in expression of genes involved in the cellular response to growth factor TGF-β

As U87 and U373 cells are both highly differentiated GBM cells lines, expressing low levels of GBM stem cells marker CD133, but phenotypically distinct [4] and

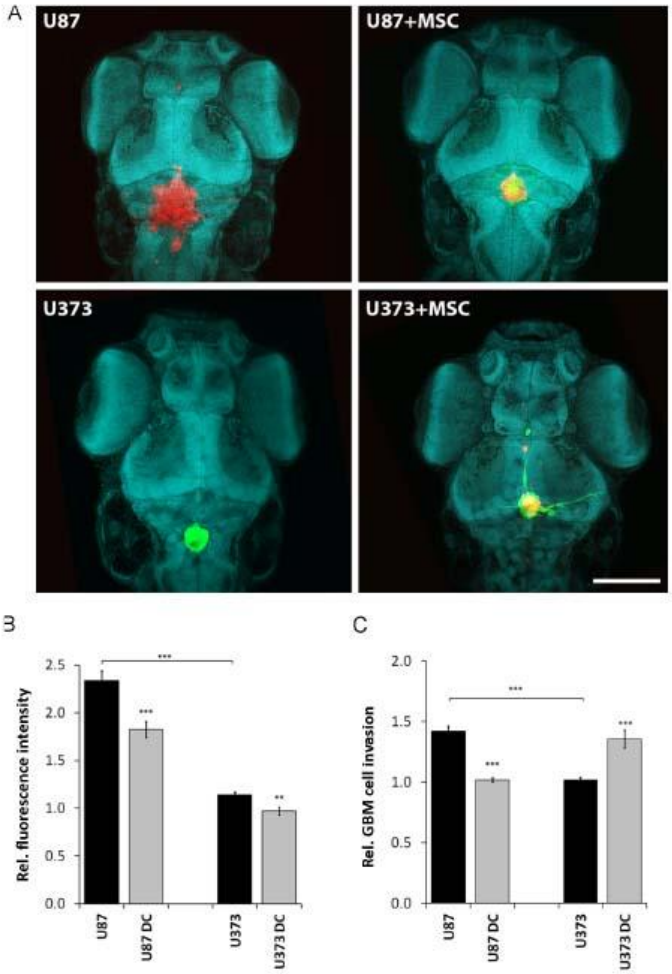


Figure 7: Proliferation and invasion of U87 dsRED and U373 eGFP cells in the zebrafish embryo brain upon co-injection with DiO/DiI- labelled MSCs. **(A)** Two days after zebrafish embryo fertilisation, U87 and U373 cells alone (left upper and lower panels) or mixed with fluorescently stained MSCs with DiO (green) in the case of U87 (right upper panel), and with DiI (red) in the case of U373 (right lower panel), were injected into the brains of the zebrafish embryos. Cell nuclei were stained with methyl green (magnification, 10×, green blue shapes; scale bar = 250 μm). **(B)** GBM cell proliferation was determined 24 h and 72 after the injections by confocal microscopy and quantified as relative fluorescence intensity of U373eGFP and U87dsRed labelled cells injected alone or with MSCs (DC). **(C)** Relative invasion of U87dsRed and U373eGFP cells injected alone, or with fluorescently stained MSCs (DC) was determined as described in Material and Methods, clearly showing increased U373eGFP invasiveness and reduced U87 invasiveness from co-culture xenografts. Thirty zebrafish embryos were used per group. Data are means ± SD. ** P <0.01, *** P <0.001.

A

Gene	Group	U87_1_2	U87_2_2	U87_3_2	U87_1_3	U87_2_3	U87_3_3	U373_1_2	U373_2_2	U373_3_2
COL1A2	MES	2.7730106	2.931963	2.235503	3.144119	2.675755	2.515198	4.817913	5.207645	5.195738
COL1A1	MES	[illegible]	[illegible]	[illegible]	[illegible]	[illegible]	[illegible]	5.135492	5.411082	5.576324
TGFBI	MES	5.4914958	5.700163	4.981562	5.827401	5.732577	5.518999	6.443684	6.53557	6.731468
THBS1	MES	-1.858874	-2.137366	-3.0777	-1.620586	-1.683385	-1.953995	5.464228	4.56507	5.585223
DAB2	MES	1.5154363	1.154463	1.182776	1.376875	1.966162	1.181875	2.456955	1.459063	2.334402
S100A4	MES	-1.378393	-1.305218	-1.31586	[illegible]	-1.302563	-1.272414	3.20045	3.154989	2.624954
P2RX7	PN	-0.889432	-1.036825	-0.79928	-1.13355	-1.180884	-0.802929	-1	-1.06211	-1.1855
STMN4	PN	NA	NA	NA	NA	NA	NA	NA	NA	NA
SOX10	PN	NA	NA	NA	NA	NA	NA	NA	NA	NA
ERBB3	PN	-4.134054	-3.961418	-4.03833	-3.920147	NA	-3.448192	-3.81463	NA	NA
ACSBG1	CL	-3.911662	-3.337793	-3.52931	NA	NA	-3.886881	-3.53678	NA	-4.051
KCNF1	CL	NA	NA	NA	NA	NA	NA	NA	NA	NA

-2 2

B

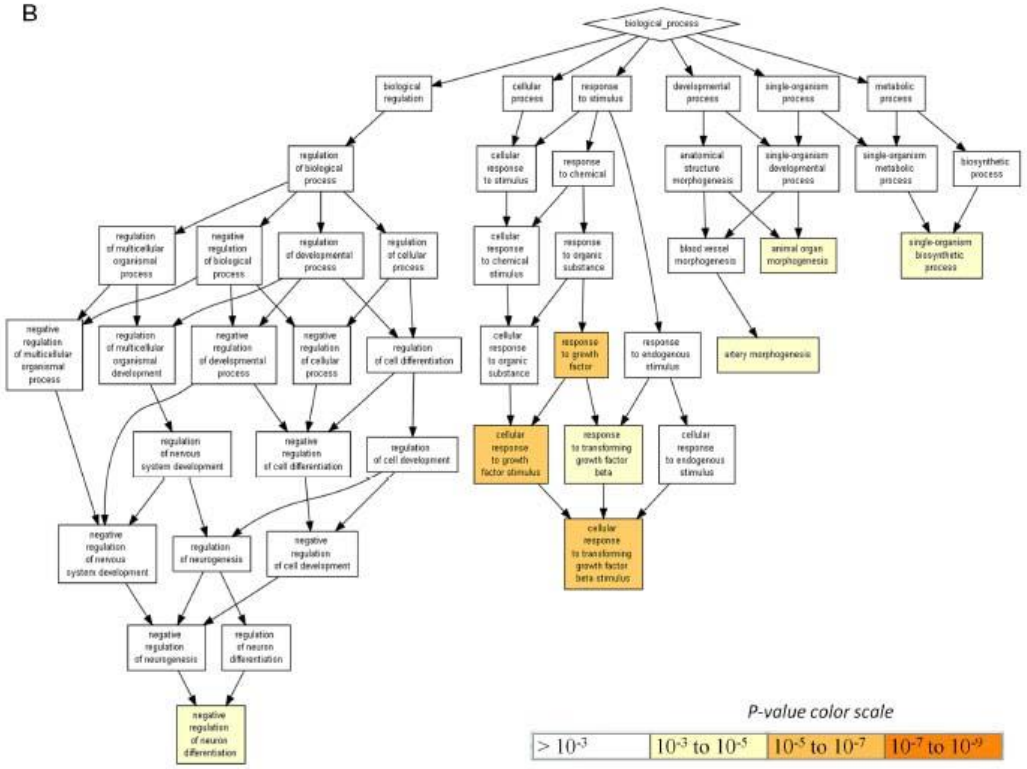


Figure 8: U87 and U373 cells differ in expression of mesenchymal genes and genes involved in response to growth factors, neuron differentiation, developmental and metabolic processes. (A) Expression of 12 Behnan's genes [35] in U87 and U373 cells. These 12 genes (COL1A2, COL1A, TGFBI, THBS1, DAB2, S100A4, P2RX7, STMN4, SOX10, ERBB3, ACSBG1 and KCNF1) alone can subtype the GBM into 3 main subtypes: mesenchymal (MES), proneural (PN) and classical (CL). Genes with the expression that was filtered out during quality control are denoted with NA. **(B)** Differentially expressed genes between U87 and U373 cells were functionally analyzed using Gene Ontology enRIchment anaLysis and visuaLizAtion tool (GOrilla) [36]. 294 genes with a significantly different standardized expression values between the two cell lines were inserted into GOrilla in order to determine the enriched pathways.

showed differential response to MSCs, we were interested to investigate if these two cell lines show different GBM subtype according to *Verhaak and co-workers* [1]. Based on transcriptome analysis of 840 Verhaak's signature genes (210 genes per group) we observed that both, U87 and U373 cells, show mesenchymal signature (Supplementary Table 2). *Behnan et al.* [35] recently identified 12 genes, which could replace the 840 genes used for GBM genotyping and these genes also originate from Verhaak's classification. The analysis of these 12 genes revealed that U373 cells have stronger mesenchymal feature than U87 cells, as all the mesenchymal genes COL1A1, COL1A2, TGFBI, THBS1, DAB2 and S100A4 are highly expressed in U373 cells, but only some of these genes are also expressed in U87 cells (Figure 8A). Moreover, analysis using Gene Ontology enRIchment anaLysis and visuaLizAtion tool (GORILLA) [36] with differentially expressed Verhaak's genes in U87 compared to U373 cells showed that these two cell lines differ in the genes, which are associated with negative regulation of neuron differentiation, artery morphogenesis, animal organ morphogenesis and single-organism biosynthetic process. The most significant difference between these two cell lines was observed in the expression of genes involved in cellular response to growth factors and in particular in response to transforming growth factor beta (TGF-β) (Figure 8B). All the genes involved in response to TGF-β, such as COL1A1, ABL1, SOX9 and COL4A2 (Supplementary Table 3), were expressed more in U373 compared to U87 cells (Supplementary Table 2).

DISCUSSION

Glioblastoma (GBM) cell heterogeneity is a consequence of the presence of different tumor and infiltrating stromal cells, among which the mesenchymal stem cells (MSCs) have not been studied to a great extent, compared to various types of immune cells. In addition to this non-cell-autonomous driver of (e.g., stromal) heterogeneity, the cell autonomous source of (e.g., genetic and epigenetic) heterogeneity [37], which relates to heterogeneous populations of GBM cells, may be present in a single tumor. The present study clearly demonstrates the intertwined relations of both kinds of heterogeneity *in vitro* and *in vivo*, showing opposite effects on invasiveness of two types of GBM cells by co-culturing them with bone marrow-derived MSCs.

Besides being part of the GBM microenvironment [28], MSCs have been suggested as therapeutic vectors for cellular therapy of GBM [23–30], but such treatment is still not approved due to observed opposite effects of MSCs on the same type of tumors *in vivo* and *in vitro* [28, 38]. However, here we show for the first time that the reason for the opposite effect is also the heterogeneity of GBM cells, highly relevant for an overall response of infiltrated and/or exogenously applied MSCs into the tumor. GBM U87 and U373 cells are frequently used in studies of various processes of GBM progression, but we only recently revealed that these cells show different GBM phenotype [4]. We also reported that bone marrow MSCs inhibited the invasion of indirectly co-cultured U87 cells [39], but increased invasion of U373 cells upon direct contact [24], and ascribed this obstacle to different co-culture conditions. Here, we used the same 3D spheroid assay of MSC/U87 and MSC/U373 co-cultures to study their invasiveness.

Invasion is defined as a three-step process: adhesion, induction of proteases, and migration via the loosened ECM [40]. This was later redefined by Friedl and Alexander [21], who dissected out the molecular processes that underlie various modalities of cell movement, showing that these are strongly depended on the tissue origin of the cells. MSCs strongly enhanced invasion of U373 cells, but not that of U87, on laminin, the main constituent of basal lamina in humans. Laminin is distributed around blood vessels and the pial surface (*glia limitans*), which have been reported as the preferential GBM migration pathways [10]. In contrast, MSCs strongly decreased U87 cell invasion in collagen I, which is the substrate most preferably invaded by these cells [12]. In spite of these matrix component preferences *in vitro*, differential invasion responses to MSCs was clearly cell-type-dependent. Diverse effects have been described for stromal fibroblasts that promoted invasiveness of breast cancer cells of the basal type, but not of the luminal type [41].

To confirm this differential effect of MSCs on GBM cells invasion in more physiological matrix, e.g. brain parenchyma *in vivo*, we used a novel animal model of zebrafish (*Danio rerio*) embryos. It is well known that most zebrafish organ systems are functionally similar to that of humans, and 82% of disease-causing human proteins have orthologues in zebrafish [31]. These zebrafish models have already contributed to a better understanding of a number of pathologies, including cardiovascular, neuronal and metabolic disorders [31], with respect to understanding their pathobiology and to study efficacy of therapy. As zebrafish embryos, do not develop adaptive immunity up to 3-4 weeks of age [32], they are replacing the NOD/SCID mice models of cancer progression, including for studying glioblastoma progression [34]. By using this animal system, we overcome the interfering effects of well recognized MSC immunomodulatory activity [22, 28, 42]. The zebrafish embryos' brains mimic well the human GBM microenvironment with the presence of neuronal tracts and laminin at the early stages [43, 44], which justifies their use as a proper model for studying GBM invasion. Invasive GBM cells in the zebrafish embryonic central nervous system follow similar anatomical pathways as in human brains; *e.g.*, along blood vessels [45] and axons [33, 34]. After their co-injection, we observed tight associations of MSCs and GBM cells

in the growing mixed tumors in the brains of the zebrafish embryos, which suggested strong intercellular interactions. We demonstrated the same differential invasion responses of U87 and U373 cells to MSCs in zebrafish embryos as seen *in vitro*, confirming that the invasion pattern is indeed cell-type-specific, also within the more complex brain parenchyma matrix and microenvironment.

With respect of proteases, we show here that in MSC co-cultures of U373 cells, but not of U87 cells, the U373 invasion depended on the overexpression and activation of cathepsin B, which is a known as a potential initiator of the proteolytic cascade [14, 46]. Herein, the cathepsin B expression correlated with cell invasion, which was inhibited by its selective inhibitor CA-074. Cathepsin B is associated in the invasion process in many types of cancer [6] and these data confirmed the essential role of this cathepsin, in contrast to cathepsin L [47] and cathepsin K [7, 48] in GBM invasion. Interestingly, in the *in vivo* spheroid invasion assay of established GBM cell lines and primary GBM cultures from patients cathepsin B was highly expressed and only cathepsin B silencing and cathepsin B inhibitor, but not those of cathepsin L and S, inhibited GBM cell invasion in the collagen I embedded spheroids [49]. In NOD/SCID mice, cathepsin B was consistently located at the invasive edges of the GBM tumor [12]. Cathepsin B when translocated to newly formed invadopodia [12] anchors to the plasma membrane through the annexin II tetramer and may associates with uPAR [15] and α3β1 integrin to enhance invasion via FAK/Src kinase signaling [46]. Cathepsin B also activates uPA precursor, when this is bound to its membrane receptor uPAR [14].

Indeed, the MSC-enhanced invasion of U373 cells correlated well with increased levels of uPA/uPAR at the mRNA and protein levels. In contrast, the downregulated uPAR protein expression in co-cultured U87 cells correlated with their decreased invasion, in spite of increased expression of uPA. This confirmed that uPA activates an invasion cascade only upon binding to its receptor, as has been suggested previously [14, 50]. The uPA/uPAR complex is crucial in GBM invasion, as it is involved in ECM protein degradation, directly or indirectly via activation of plasminogen and pro-MMPs [50, 51]. Here we found increased amounts of MMP-2 and MMP-9 in the MSC/U373 co-culture medium that paralleled uPA/uPAR expression. Similar to U373 cells, activation of the uPA/uPAR-MMP axis was observed in direct co-cultures of fibroblasts with pancreatic carcinoma cells [52]. Moreover, calpains increase MMP expression and activity *via* glutamate-activated AMPA receptors and Ca^{2+} influx [16]. As we observed simultaneously increased secretion of calpain1 in MSC/U373 co-cultures, it is possible that calpain1 contributed to enhanced MMP-2/-9 levels and invasion. We functionally confirmed cathepsin B, MMP-9 and MMP-14 activation by the effects of their selective inhibitors, which completely abolished the effects of MSCs on enhanced U373 cell invasion, while having no effects on the co-cultured U87 cells. Taken together, we confirmed simultaneous activation of distinct proteases that may degrade ECM components and enhance U373 cell invasion.

In contrast, both GBM cell types enhanced invasiveness of MSCs out of the mixed spheroids, confirming our earlier results on U373 cell line [24]. However, this paralleled with a decrease of most protease levels in MSCs upon their direct contact with both types of GBM cells. It is possible that MSC invasion involves other proteolytic pathway(s), as the ones measured here, or proceeds by a protease-independent movement, possibly adopting a migratory phenotype, similar to an amoeboid movement [21].

Our last aim was to explore whether different response of U87 and U373 cells to MSCs is due to different GBM molecular subtype of these two established cell lines. When using the GBM molecular subtype classification according to *Verhaak et al.* [1] both, U87 and U373 cells belong to the mesenchymal subtype, although they significantly differ in expression of proteases and some other mesenchymal subtype-associated genes [35] as well as the genes, associated with cellular response to TGF-β. As observed, the identification of GBM subtype based on 4 Verhaak's gene expression fingerprints [1] is not sufficient to predict the response of GBM cells to stromal cells such as MSCs. Despite the fact that both, U87 and U373 cells have a predominant feature of mesenchymal GBM tumors, they react differently to MSCs. The reason may be due to fact that Verhaak's classification is based on heterogeneous GBM tissues, with respect to stromal and cancer cell components. Thus, this kind of classification is not enough adequate to characterize established cell lines that have been grown in serum conditions *in vitro* as single cell population.

Paracrine signaling between MSCs and GBM cells is mediated through growth factors and cytokines which are released from MSCs [22, 39]. Out of this, the most relevant with respect to invasion is TGF-β, which plays an important role in epithelial to mesenchymal transition [53] and shifts the expression of mesenchymal cell type-related genes in favor of more migratory/invasive GBM cell type [53, 54]. Additionally, TGF-β causes activation of invasion-related proteases, such as cathepsin B [55], MMP-2 and -9 [53]. We may speculate that exogenous TGF-β, released from MSCs, was triggering the proteases expression, increasing U373 invasion, but that was not the case in U87 cells. This may be due to TGF-β triggering alternative signaling pathways [56], in the two phenotypically different GBM cell lines. The reason for differential U87 and U373 cells' response in the same (MSC mediated) microenvironment may also/in addition dwell in their diverse cytokines' expression [4], as for instance, compared to U87 cells, the U373 express and secrete more CCL2/MCP-1 [4], which is a known

activator of gelatinases MMP-2 and MMP-9 *via* ERK 1/2 signaling [57].

Taken together, we have demonstrated specific responses of these two GBM cell phenotypes to MSCs both *in vitro* and *in vivo*. We have shown that MSCs reduce the invasion of U87 cells, but enhance the invasion of U373 cells, which is mediated by upregulated cathepsin B, calpain1, uPA/uPAR, as well as MMP-2, -9 and -14 in this cell line. Moreover, we showed that differentially expressed genes, associated with cellular response to TGF-β, in U87 and U373 cells may be responsible for differential behavior of these two cell lines in co-cultures. By monitoring GBM cell invasion upon their co-injection with MSCs into the brains of zebrafish embryo, we confirmed these GBM cell-type-dependent responses to MSCs also *in vivo*. We demonstrated that zebrafish embryos are an excellent model for addressing GBM intra-tumoral heterogeneity, which opens new avenues for studying GBM microenvironment. However, the relevance of these data *in vivo*, e.g. in the presence of various GBM infiltrating cells of immune system, such as T-cells and natural killer cells, is questionable. Multilateral interactions, such as for example between GBM/T-cells/NK cells [58] and MSC/NK cells, may namely put the presented data in rather different perspective.

MATERIALS AND METHODS

Cell culture

Human bone marrow-derived MSCs were obtained from Lonza Bioscience (Lot. 6F4393, USA) and were cultured according to the manufacturer recommendations [30]. Human GBM cell lines (U87, U373 cells) were obtained from American Type Culture Collection (USA), and all cell types were cultured in the same growth medium. Authentication of the cell lines was performed as described previously [7]. U373 cells stably expressing enhanced green fluorescent protein (U373 eGFP cells) [24] and U87 cells expressing red fluorescent protein (dsRED) were prepared as described previously [59].

Preparation of monolayer and spheroid co-cultures

Monolayer co-cultures of MSCs and GBM cells (U87 or U373) were prepared by mixing the cells in three different ratios (MSC/GBM cells) of 1:3, 1:1 and 3:1, that were seeded into monolayer culture plates with formats, corresponding to each particular experiment. The cells were analyzed after 72 h of direct co-culturing.

For monitoring of invasion of MSCs and GBM cells in MSC/GBM spheroid co-cultures, MSCs were labeled prior to spheroid formation with the fluorescent dyes Vybrant DiO/ DiI (Molecular Probes, USA), according to the manufacturer instructions. For mixed spheroid formation, Vybrant-labelled MSCs and U87 dsRED or U373 eGFP cells were mixed in a 1:1 ratio and seeded in medium containing 4% methylcellulose in U-bottomed 96-well plates (2.5 $\times 10^3$ cells/well; BD Biosciences, USA), which were then centrifuged at 850×*g* for 90 min, and then incubated overnight.

Three-dimensional spheroid invasion assays

For the assessment of cellular invasion, fluorescent MSCs and GBM cells and mixed spheroids were transferred into 24-well plates (Corning, Life Sciences, USA) and embedded in collagen type I (1 mg/mL; BD Biosciences) or Matrigel (6.35 mg/mL; BD Biosciences). To assess cellular invasion on laminin, the 96-well plates were coated with laminin (2 μg/cm^2; Sigma-Aldrich). The spheroids were then placed in the middle of each well in the growth medium. Cell invasion was monitored using a fluorescence inverted microscope with the NIS-Elements software (Eclipse Ti-E; Nikon, Japan). Invasiveness was defined as the distance measured from the edge of the spheroids to the most distant cell population, divided by the spheroid diameter.

Transcriptome analysis

To select candidate proteases for *in vitro* analysis the transcriptome analysis of GBM tissue and normal brain tissue was performed as described previously [7]. Briefly, raw data of gene expression for GBM tissue and normal brain were taken from The Cancer Genome Atlas data portal (July 2011; https://tcga-data.nci.nih.gov/tcga/) as Batch 8 (24 GBM samples, 10 unmatched control brain samples). As these data were merged from different experimental sources, a Bioconductor package of RankProd was used for the detection of differentially expressed genes. Differentially expressed genes with their percentage of false predictions <0.05 that have been recently identified for GBM tissue *versus* normal brain tissue were published recently [7]. Among the upregulated genes, we used unique Entrez IDs to search for the intersections with a list of human proteases (653) obtained from the MEROPS database that were selected in October 2013.

The transcriptome analysis of U87 and U373 cell lines was performed as described previously [39]. Briefly, six biological replicates of U87 cells and three biological replicates of U373 cells were used. Samples were hybridized to Illumina HumanWG-6 v3 Expression BeadChip (Illumina BeadChip; Illumina, San Diego, CA, USA). After scanning, image acquisition was carried out by applying BeadStudio version 3.3.7 software (Illumina). Data is deposited in NCBI's Gene Expression Omnibus (GEO, http://www.ncbi.nlm.nih.gov/geo/) – series GSE26283 (samples GSM645515, GSM645519 and GSM645523) for U87-MG cells and

series GSE59634 (samples GSM1440969, GSM1440973 and GSM1440977) for U373 cells. Data preprocessing was done as described in *Verhaak et al.* [1]. Data were log-transformed and median centered. The 840 genes that were defined as marker genes for classification of GBM samples into one of the four groups (MES – mesenchymal, PN – proneural, N – neural and CL – classical) by Verhaak were then filtered out and sorted (see Supplementary Table 2). Only genes that passed the quality control were taken into consideration (517 genes overall). The genes with the high standardized gene expressions were color-coded in red, while genes with low standardized gene expressions were colored in green. The highest number of highly expressed genes for both U373 and U87 cell lines corresponded to the MES subtype (as determined by *Verhaak et al.* and shown in the column B on Supplementary Table 2). Finally, we used t-test in order to determine the genes with a significantly different expression values between the two cell lines (U373 and U87). The resulting 294 genes were then uploaded to GOrilla (http://cbl-gorilla.cs.technion.ac.il/) [36] to identify and visualize the enriched pathways, i.e. the pathways that differ between the both cell lines in terms of gene ontology.

qRT-PCR

Total RNA was isolated from MSCs, GBM cells and their direct co-cultures (as monolayers) using Trizol reagent (Invitrogen, UK). cDNA was generated from 1 µg total RNA using High Capacity cDNA Reverse Transcription kits (Applied Biosystems, USA). The expression of candidate protease genes (Supplementary Table 4) was quantified using real-time quantitative PCR (ABI 7900 HT Sequence Detection System). Real-time PCR reactions were performed using 1:5 dilutions of each cDNA, added to TaqMan Universal PCR Master Mix and TaqMan Gene Expression assays (Applied Biosystems). The analyses were performed with the SDS v2.2 software (Applied Biosystems, USA), and the mRNA levels relative to the housekeeping gene GAPDH mRNA are presented.

Flow cytometry

After 72h of co-culturing the mono and direct co-cultures of MSCs and GBM cells (U87 dsRED and U373 eGFP) were collected and pelleted. Cell pellets were washed by 1x PBS, resuspended and fixed in 0.5% gluteraldehyde. Permeabilization was performed with 0.1% Triton X-100. Cells were incubated for 30 min with the primary antibodies. Primary antibodies and their dilutions are listed in Supplementary Table 5. After washing with 1x PBS the secondary anti-mouse or anti-rabbit antibodies were used (1:300; conjugated with Alexa Fluor 488 for U87 dsRED co-cultures, or Alexa Fluor 647 for U373 eGFP co-cultures; Life Technologies, UK) and incubated for 30 min. After final PBS wash, the cells were re-suspended in 300 µl of 1x PBS and analyzed by flow cytometer (BD FACSCalibur, BD Biosciences) using the CellQuest software (BD Biosciences). To distinguish between proteases expressed in MSCs and fluorescent GBM cells and to show expression of protease in different cell populations, cell gating based on fluorescence was performed. Protein expression of candidate protein in each cell type was determined as percentage of cells stained positive for candidate protein out of total (stained and unstained) cells (see Supplementary Method).

Western blotting

Western blots were performed with conditioned medium from monocultures and direct MSC/GBM co-cultures grown as monolayers. After 72 h of co-culturing, the culture media were replaced by serum-free medium. The conditioned media was centrifuged at 300×*g* for 10 min, and concentrated 100-fold using an Amicon Ultra-4 centrifugal filter device with a 10-kDa cut off (Merck Millipore, Germany), according to the manufacturer's instructions. Concentrated media (15 µg total protein) were subjected to Western blotting [7] using the indicated antibodies (Supplementary Table 5).

Cytotoxicity assay

To determine cellular toxicity of synthetic protease inhibitors and the final non-toxic concentrations for use in further experiments, MTT assays were performed. MSCs, U87 and U373 cells were plated into 96-well plates and left to grow for 24 h before addition of the following cell-permeable protease inhibitors (dissolved in dimethylsulphoxide [DMSO]), and with 0.1% DMSO as control: CA-074Me, a cathepsin B inhibitor (Peptide Institute, Japan), MMP-9 inhibitor I (Calbiochem, USA), and NSC405020, a MMP-14 inhibitor (Tocris Bioscience, UK). After 72 h incubation, the MTT reagent (Sigma-Aldrich) was added to the cells, and the formazan crystals formed were dissolved in DMSO. Absorbance was measured at 570/690 nm with a plate reader (Synergy MX; BioTek, USA).

Effects of protease inhibitors

Spheroid invasion assays were set up with fluorescent MSCs, GBM cells, and mixed co-culture spheroids on laminin-coated 96-well plates, as described above. The selective synthetic protease inhibitors were used at their non-cytotoxic final concentrations: 2 µM CA-074Me, 100 nM MMP-9 inhibitor I, and 10 µM NSC405020, all diluted in 0.1% DMSO. Cell invasion was assessed after 72 h, as described above.

Zebrafish embryo model

Wild-type AB zebrafish (*Danio rerio*) embryos were collected and incubated at 26°C in dilution water (ISO

7346-3:1996). After 36 h of age 0.005% phenylthiourea was added to the water to inhibit pigment formation. Zebrafish embryo xenotransplantation experiments were performed as described previously [34]. Prior to implantation, MSCs were labeled with Vybrant DiI or DiO (Molecular Probes, USA) for co-implantation with the U373 and U87 cells, respectively. Mixtures of GBM cells with labeled MSCs were prepared in a 1:1 ratio. Xenotransplantation of 50 to 100 GBM cells or 100 to 200 cells of the MSC/GBM mixture (containing 50-100 GBM cells) was performed by injecting 5 nl of cell suspension into the brain of embryos at 52 h after fertilization with the MICROINJECTOR system (Tritech Research, USA). Embryos with implanted cells were incubated at 31°C. For quantification of GBM cell invasion, fluorescence images of GBM cells in the embryos in lateral orientation were obtained at 1 day and 3 days after cell implantation, using an inverted fluorescence microscope (Eclipse T300; Nikon, Japan). The largest diameter and the diameter perpendicular to the largest of each xenograft were measured in images, and these two diameters were then averaged to obtain a parameter of xenograft size as a measure of cell invasion. Relative GBM cell invasion was compared between GBM cells alone and the MSC/GBM mixed xenografts, using the Welch's t-test. To determine differences in proliferation rates of GBM cells in MSC/GBM mixed xenografts, relative changes in fluorescence intensity of GBM cells between 1 day and 3 days after cell implantation were quantified using ImageJ (http://rsbweb.nih.gov/ij/; National Institutes of Health, USA). For confocal imaging, the embryos were fixed at 72 h after cell injection using 4% paraformaldehyde in phosphate-buffered saline for 2 h, and cleared in Sca/e U2, which was modified to enable visualization of carbocyanine-dye-labelled cells [60]. Imaging was performed with a TCS SPE confocal microscope (Leica) as described previously [34].

Statistical analysis

Unless stated otherwise, statistical analysis was performed with one-way ANOVA, followed by the Bonferroni tests for pair-wise comparisons, in GraphPad Prism. $P < 0.05$ was considered to indicate statistically significant differences. Data are expressed as means ± standard deviation (SD) of 3 independent experiments, with each performed at least in duplicate.

ACKNOWLEDGMENTS AND FUNDING

We would like to thank Miss Mateja Burjek and Miss Monika Golob for technical assistance. Furthermore, we thank Prof. Cornelis J.F. van Noorden for critical reading of the manuscript.

This work was supported by the Operational Program for Italy-Slovenia, 2007–2013 (the INTERREG project) CB134-GLIOMA, the ARRS project J1-4274, and ARRS Program P10245 (all to TTL), and the ARRS Young Researcher grant to BB.

CONFLICTS OF INTEREST

No potential conflicts of interest were disclosed.

Author contributions

This research project was conceived by TTL, the experiments were designed by TTL, HM, BB, MV, AR; and performed by BB and MV. The data were analyzed by TTL, HM, AR, BB and MV, written by BB, AR and TTL and reviewed by HM, AR and MV.

REFERENCES

1. Verhaak RG, Hoadley KA, Purdom E, Wang V, Qi Y, Wilkerson MD, Miller CR, Ding L, Golub T, Mesirov JP, Alexe G, Lawrence M, O'Kelly M, et al. Integrated genomic analysis identifies clinically relevant subtypes of glioblastoma characterized by abnormalities in PDGFRA, IDH1, EGFR, and NF1. Cancer Cell. 2010; 17:98-110.
2. Van Meir EG, Hadjipanayis CG, Norden AD, Shu HK, Wen PY, Olson JJ. Exciting new advances in neuro-oncology: the avenue to a cure for malignant glioma. CA Cancer J Clin. 2010; 60:166-93.
3. Sottoriva A, Spiteri I, Piccirillo SG, Touloumis A, Collins VP, Marioni JC, Curtis C, Watts C, Tavaré S. Intratumor heterogeneity in human glioblastoma reflects cancer evolutionary dynamics. Proc Natl Acad Sci U S A. 2013; 110:4009-14.
4. Motaln H, Koren A, Gruden K, Ramšak Ž, Schichor C, Lah TT. Heterogeneous glioblastoma cell cross-talk promotes phenotype alterations and enhanced drug resistance. Oncotarget. 2015; 6:40998-1017.
5. Ricklefs F, Mineo M, Rooj AK, Nakano I, Charest A, Weissleder R, Breakefield XO, Chiocca EA, Godlewski J, Bronisz A. Extracellular Vesicles from High-Grade Glioma Exchange Diverse Pro-oncogenic Signals That Maintain Intratumoral Heterogeneity. Cancer Res. 2016; 76:2876-81.
6. Lah TT, Durán Alonso MB, Van Noorden CJ. Antiprotease therapy in cancer: hot or not? Expert Opin Biol Ther. 2006; 6:257-79.
7. Verbovšek U, Motaln H, Rotter A, Atai NA, Gruden K, Van Noorden CJ, Lah TT. Expression analysis of all protease genes reveals cathepsin K to be overexpressed in glioblastoma. PLoS One. 2014; 9:e111819.
8. Turk B, Turk D, Turk V. Protease signalling: the cutting edge. EMBO J. 2012; 31:1630-43.
9. Schmitt M, Jänicke F, Moniwa N, Chucholowski N, Pache L, Graeff H. Tumor-associated urokinase-type plasminogen activator: biological and clinical significance. Biol Chem Hoppe Seyler. 1992; 373:611-22.

10. Mentlein R, Hattermann K, Held-Feindt J. Lost in disruption: role of proteases in glioma invasion and progression. Biochim Biophys Acta. 2012; 1825:178-85.
11. Paw I, Carpenter RC, Watabe K, Debinski W, Lo HW. Mechanisms regulating glioma invasion. Cancer Lett. 2015; 362:1-7.
12. Gole B, Huszthy PC, Popović M, Jeruc J, Ardebili YS, Bjerkvig R, Lah TT. The regulation of cysteine cathepsins and cystatins in human gliomas. Int J Cancer. 2012; 131:1779-89.
13. Fonović M, Turk B. Cysteine cathepsins and extracellular matrix degradation. Biochim Biophys Acta. 2014; 1840:2560-70.
14. Mohamed MM, Sloane BF. Cysteine cathepsins: multifunctional enzymes in cancer. Nat Rev Cancer. 2006; 6:764-75.
15. Gondi CS, Rao JS. Cathepsin B as a cancer target. Expert Opin Ther Targets. 2013; 17:281-91.
16. Jang HS, Lal S, Greenwood JA. Calpain 2 is required for glioblastoma cell invasion: regulation of matrix metalloproteinase 2. Neurochem Res. 2010; 35:1796-804.
17. Sevenich L, Joyce JA. Pericellular proteolysis in cancer. Genes Dev. 2014; 28:2331-47.
18. Osuala KO, Sameni M, Shah S, Aggarwal N, Simonait ML, Franco OE, Hong Y, Hayward SW, Behbod F, Mattingly RR, Sloane BF. Il-6 signaling between ductal carcinoma *in situ* cells and carcinoma-associated fibroblasts mediates tumor cell growth and migration. BMC Cancer. 2015; 15:584.
19. Bougnaud S, Golebiewska A, Oudin A, Keunen O, Harter PN, Mäder L, Azuaje F, Fritah S, Stieber D, Kaoma T, Vallar L, Brons NH, Daubon T, et al. Molecular crosstalk between tumour and brain parenchyma instructs histopathological features in glioblastoma. Oncotarget. 2016; 7:31955-71.
20. Iser IC, Ceschini SM, Onzi GR, Bertoni AP, Lenz G, Wink MR. Conditioned Medium from Adipose-Derived Stem Cells (ADSCs) Promotes Epithelial-to-Mesenchymal-Like Transition (EMT-Like) in Glioma Cells *In vitro*. Mol Neurobiol. 2016; 53:7184-7199.
21. Friedl P, Alexander S. Cancer invasion and the microenvironment: plasticity and reciprocity. Cell. 2011; 147:992-1009.
22. Motaln H., Turnse TL. Cytokines play a key role in communication between mesenchymal stem cells and brain cancer cells. Protein Pept Lett. 2015; 22:322–331.
23. Jeong KY, Lee EJ, Kim SJ, Yang SH, Sung YC, Seong J. Irradiation-induced localization of IL-12-expressing mesenchymal stem cells to enhance the curative effect in murine metastatic hepatoma. Int J Cancer. 2015; 137:721-30.
24. Schichor C, Albrecht V, Korte B, Buchner A, Riesenberg R, Mysliwietz J, Paron I, Motaln H, Turnsek TL, Jürchott K, Selbig J, Tonn JC. Mesenchymal stem cells and glioma cells form a structural as well as a functional syncytium *in vitro*. Exp Neurol. 2012; 234:208-19.
25. Kim SM, Kang SG, Park NR, Mok HS, Huh YM, Lee SJ, Jeun SS, Hong YK, Park CK, Lang FF. Presence of glioma stroma mesenchymal stem cells in a murine orthotopic glioma model. Childs Nerv Syst. 2011; 27:911-22.
26. Torsvik A, Bjerkvig R. Mesenchymal stem cell signaling in cancer progression. Cancer Treat Rev. 2013; 39:180-8.
27. Nakamizo A, Marini F, Amano T, Khan A, Studeny M, Gumin J, Chen J, Hentschel S, Vecil G, Dembinski J, Andreeff M, Lang FF. Human bone marrow-derived mesenchymal stem cells in the treatment of gliomas. Cancer Res. 2005; 65:3307-18.
28. Barcellos-de-Souza P, Gori V, Bambi F, Chiarugi P. Tumor microenvironment: bone marrow-mesenchymal stem cells as key players. Biochim Biophys Acta. 2013; 1836:321-35.
29. Dasari VR, Kaur K, Velpula KK, Gujrati M, Fassett D, Klopfenstein JD, Dinh DH, Rao JS. Upregulation of PTEN in glioma cells by cord blood mesenchymal stem cells inhibits migration via downregulation of the PI3K/Akt pathway. PLoS One. 2010; 5:e10350.
30. Kološa K, Motaln H, Herold-Mende C, Koršič M, Lah TT. Paracrine effects of mesenchymal stem cells induce senescence and differentiation of glioblastoma stem-like cells. Cell Transplant. 2015; 24:631-44.
31. MacRae CA, Peterson RT. Zebrafish as tools for drug discovery. Nat Rev Drug Discov. 2015; 14:721-31.
32. White R, Rose K, Zon L. Zebrafish cancer: the state of the art and the path forward. Nat Rev Cancer. 2013; 13:624-36.
33. Vittori M, Motaln H, Turnsek TL. The study of glioma by xenotransplantation in zebrafish early life stages. J Histochem Cytochem. 2015; 63:749-61.
34. Vittori M, Breznik B, Gredar T, Hrovat K, Bizjak Mali L, Lah TT. Imaging of human glioblastoma cells and their interactions with mesenchymal stem cells in the zebrafish (Danio rerio) embryonic brain. Radiol Oncol. 2016; 50:159-67.
35. Behnan J, Stangeland B, Hosainey SA, Joel M, Olsen TK, Micci F, Glover JC, Isakson P, Brinchmann JE. Differential propagation of stroma and cancer stem cells dictates tumorigenesis and multipotency. Oncogene. 2016 - Epub ahead of print
36. Eden E, Navon R, Steinfeld I, Lipson D, Yakhini Z. GOrilla: a tool for discovery and visualization of enriched GO terms in ranked gene lists. BMC Bioinformatics. 2009; 10:48.
37. Cassidy JW, Caldas C, Bruna A. Maintaining Tumor Heterogeneity in Patient-Derived Tumor Xenografts. Cancer Res. 2015; 75:2963-8.
38. Klopp AH, Gupta A, Spaeth E, Andreeff M, Marini F 3rd. Concise review: Dissecting a discrepancy in the literature: do mesenchymal stem cells support or suppress tumor growth? Stem Cells. 2011; 29:11-9.

39. Motaln H, Gruden K, Hren M, Schichor C, Primon M, Rotter A, Lah TT. Human mesenchymal stem cells exploit the immune response mediating chemokines to impact the phenotype of glioblastoma. Cell Transplant. 2012; 21:1529-45.
40. Liotta LA, Stetler-Stevenson WG. Tumor invasion and metastasis: an imbalance of positive and negative regulation. Cancer Res. 1991; 51:5054s-5059s.
41. Dang TT, Prechtl AM, Pearson GW. Breast cancer subtype-specific interactions with the microenvironment dictate mechanisms of invasion. Cancer Res. 2011; 71:6857-66.
42. Zhang L, Su XS, Ye JS, Wang YY, Guan Z, Yin YF. Bone marrow mesenchymal stem cells suppress metastatic tumor development in mouse by modulating immune system. Stem Cell Res Ther. 2015; 6:45.
43. Gutzman JH, Graeden EG, Lowery LA, Holley HS, Sive H. Formation of the zebrafish midbrain-hindbrain boundary constriction requires laminin-dependent basal constriction. Mech Dev. 2008; 125:974-83.
44. Burrill JD, Easter SS Jr. The first retinal axons and their microenvironment in zebrafish: cryptic pioneers and the pretract. J Neurosci. 1995; 15:2935-47.
45. Lal S, La Du J, Tanguay RL, Greenwood JA. Calpain 2 is required for the invasion of glioblastoma cells in the zebrafish brain microenvironment. J Neurosci Res. 2012; 90:769-81.
46. Rao Malla R, Gopinath S, Alapati K, Gorantla B, Gondi CS, Rao JS. Knockdown of cathepsin B and uPAR inhibits CD151 and α3β1 integrin-mediated cell adhesion and invasion in glioma. Mol Carcinog. 2013; 52:777-90.
47. Strojnik T, Kavalar R, Trinkaus M, Lah TT. Cathepsin L in glioma progression: comparison with cathepsin B. Cancer Detect Prev. 2005; 29:448-55.
48. Verbovšek U, Van Noorden CJ, Lah TT. Complexity of cancer protease biology: Cathepsin K expression and function in cancer progression. Semin Cancer Biol. 2015; 35:71-84.
49. Gole B, Durán Alonso MB, Dolenc V, Lah T. Post-translational regulation of cathepsin B, but not of other cysteine cathepsins, contributes to increased glioblastoma cell invasiveness *in vitro*. Pathol Oncol Res. 2009; 15:711-23.
50. Veeravalli KK, Rao JS. MMP-9 and uPAR regulated glioma cell migration. Cell Adh Migr. 2012; 6:509-12.
51. Li Q, Chen B, Cai J, Sun Y, Wang G, Li Y, Li R, Feng Y, Han B, Li J, Tian Y, Yi L, Jiang C. Comparative Analysis of Matrix Metalloproteinase Family Members Reveals That MMP9 Predicts Survival and Response to Temozolomide in Patients with Primary Glioblastoma. PLoS One. 2016; 11:e0151815.
52. He Y, Liu XD, Chen ZY, Zhu J, Xiong Y, Li K, Dong JH, Li X. Interaction between cancer cells and stromal fibroblasts is required for activation of the uPAR-uPA-MMP-2 cascade in pancreatic cancer metastasis. Clin Cancer Res. 2007; 13:3115-24.
53. Pickup M, Novitskiy S, Moses HL. The roles of TGFβ in the tumour microenvironment. Nat Rev Cancer. 2013; 13:788-99.
54. Singh SK, Fiorelli R, Kupp R, Rajan S, Szeto E, Lo Cascio C, Maire CL, Sun Y, Alberta JA, Eschbacher JM, Ligon KL, Berens ME, Sanai N, at al. Post-translational Modifications of OLIG2 Regulate Glioma Invasion through the TGF-β Pathway. Cell Rep. 2016; 16:950-66.
55. Aggarwal N, Sloane BF. Cathepsin B: multiple roles in cancer. Proteomics Clin Appl. 2014; 8:427-37.
56. Piek E, Westermark U, Kastemar M, Heldin CH, van Zoelen EJ, Nistér M, Ten Dijke P. Expression of transforming-growth-factor (TGF)-beta receptors and Smad proteins in glioblastoma cell lines with distinct responses to TGF-beta1. Int J Cancer. 1999; 80:756-63.
57. Yang J, Lv X, Chen J, Xie C, Xia W, Jiang C, Zeng T, Ye Y, Ke L, Yu Y, Liang H, Guan XY, Guo X, et al. CCL2-CCR2 axis promotes metastasis of nasopharyngeal carcinoma by activating ERK1/2-MMP2/9 pathway. Oncotarget. 2016; 7:15632-47.
58. Tseng HC, Inagaki A, Bui VT, Cacalano N, Kasahara N, Man YG, Jewett A. Differential Targeting of Stem Cells and Differentiated Glioblastomas by NK Cells. J Cancer. 2015; 6:866-76.
59. Pillat MM, Oliveira MN, Motaln H, Breznik B, Glaser T, Lah TT, Ulrich H. Glioblastoma-mesenchymal stem cell communication modulates expression patterns of kinin receptors: Possible involvement of bradykinin in information flow. Cytometry A. 2016; 89:365-75.
60. Azaripour A, Lagerweij T, Scharfbillig C, Jadczak AE, Willershausen B, Van Noorden CJ. A survey of clearing techniques for 3D imaging of tissues with special reference to connective tissue. Prog Histochem Cytochem. 2016; 51:9-23.

2.3 Imaging of Human Glioblastoma Cells and Their Interactions with Mesenchymal Stem Cells in the Zebrafish *(Danio rerio)* Embryonic Brain

Miloš Vittori, Barbara Breznik, Tajda Gredar, Katja Hrovat, Lilijana Bizjak Mali, Tamara Lah Turnšek

Radiology and Oncology 2016; 50(2): 159-67. DOI: 10.1515/raon-2016-0017

DE GRUYTER OPEN Radiology and Oncology | Ljubljana | Slovenia | www.radioloncol.com RADIOLOGY AND ONCOLOGY 1

research article

Imaging of human glioblastoma cells and their interactions with mesenchymal stem cells in the zebrafish *(Danio rerio)* embryonic brain

Milos Vittori[1], Barbara Breznik[1,2], Tajda Gredar[3], Katja Hrovat[1,3], Lilijana Bizjak Mali[3], Tamara T. Lah[1,4]

[1] Department of Genetic Toxicology and Cancer Biology, National Institute of Biology, Ljubljana, Slovenia
[2] Jozef Stefan International Postgraduate School, Ljubljana, Slovenia
[3] Department of Biology, Biotechnical Faculty, University of Ljubljana, Ljubljana, Slovenia
[4] Department of Chemistry and Biochemistry, Faculty of Chemistry and Chemical Technology, University of Ljubljana, Ljubljana, Slovenia

Radiol Oncol 2016

Received 3 December 2015
Accepted 7 February 2016

Correspondence to: Miloš Vittori, Department of Genetic Toxicology and Cancer Biology, National Institute of Biology, Večna pot 111, SI-1000 Ljubljana, Slovenia. Phone: +386 59 232 884; Fax: +386 59 232 715; E-mail: milos.vittori@gmail.com

Disclosure: No potential conflicts of interest were disclosed.

Background. An attractive approach in the study of human cancers is the use of transparent zebrafish (*Danio rerio*) embryos, which enable the visualization of cancer progression in a living animal.

Materials and methods. We implanted mixtures of fluorescently labeled glioblastoma (GBM) cells and bone-marrow-derived mesenchymal stem cells (MSCs) into zebrafish embryos to study the cellular pathways of their invasion and the interactions between these cells *in vivo*.

Results. By developing and applying a carbocyanine-dye-compatible clearing protocol for observation of cells in deep tissues, we showed that U87 and U373 GBM cells rapidly aggregated into tumor masses in the ventricles and midbrain hemispheres of the zebrafish embryo brain, and invaded the central nervous system, often using the ventricular system and the central canal of the spinal cord. However, the GBM cells did not leave the central nervous system. With co-injection of differentially labeled cultured GBM cells and MSCs, the implanted cells formed mixed tumor masses in the brain. We observed tight associations between GBM cells and MSCs, and possible cell-fusion events. GBM cells and MSCs used similar invasion routes in the central nervous system.

Conclusions. This simple model can be used to study the molecular pathways of cellular processes in GBM cell invasion, and their interactions with various types of stromal cells in double or triple cell co-cultures, to design anti-GBM cell therapies that use MSCs as vectors.

Key words: brain tumors; tumor microenvironment; animal models; xenotransplantation

Introduction

Glioblastoma multiformae (GBM) is the most aggressive type of glioma and also the most frequent and fatal among brain tumors.[1] An essential hallmark of GBM is its diffuse invasion into the brain parenchyma, which prevents successful surgical removal.[2] Understanding the mechanisms and the pathways of GBM cell invasion is therefore of crucial importance for the treatment of the aggressive spread of GBM.[1-3] The process of GBM cell infiltration into the brain parenchyma[4] differs from carcinoma cells invading the more compact extracellular matrix and the basal membranes of blood vessels.[5,6] The recently recognized important role of the tumor microenvironment in cancer cell invasion[7] has become an important topic and the subject of intensive research.[8-10] The effects of the microenvironment also include the impact of the different types of cells comprising the stroma

 Unauthenticated Download Date | 4/20/16 10:53 AM doi:10.1515/raon-2016-0017

within a tumor mass. Infiltrating and tumor-associated mesenchymal stem cells (MSCs) may significantly affect tumor progression and resistance to treatment, as reviewed in.[8,11] MSCs are known to be recruited by tumor-secreted signaling molecules *via* the blood circulation, and to become part of the tumor-supporting stroma, where they have a role that remains poorly understood.[10,12] Several studies have addressed this issue *in vitro* and *in vivo*, also by using genetically modified MSCs.[13,14] Previously, we studied the molecular mechanisms that support the observed phenotype changes in GBM cells and MSCs upon co-culture *in vitro*, including decreased U87 GBM cell proliferation and invasion, and increased U373 GBM cell invasion *in vitro*.[15,16] By investigating the GBM-MSC interactions in a mouse model, Behnan *et al*.[17] recently showed that cells with an MSC-like phenotype can infiltrate the stroma of the mouse GBM and have important roles in tumor cell growth. Moreover, their data demonstrated an alteration in GBM cell marker expression upon the encounter with MSCs *in vivo*. In the present study, we aimed to use an alternative and simpler *in vivo* GBM xenotransplantation model in zebrafish embryos[18], to study human GBM cell invasion and their interactions with MSCs at the cellular level.

The zebrafish (*Danio rerio*) is the major vertebrate model in developmental biology and genetics.[19] There are several technologies available in the zebrafish that have made it a unique model in cancer research.[20] In particular, cancers can be studied throughout the life cycle of zebrafish, with each zebrafish developmental stage offering its own experimental advantages. This makes zebrafish a powerful complement to other more traditional model systems.[21] As well as their high fecundity and ease of maintenance, the major advantage of zebrafish is the transparency of their embryos and larvae, which allows *in vivo* visualization of cellular processes related to cancer growth and progression at single-cell resolution.[20,22,23] Xenotransplantation of either dye-labeled or fluorescent-protein-expressing human cells in zebrafish embryos is becoming an increasingly used tool to study cancers of the central nervous system (CNS).[18,24-26]

The aim of the present study was to investigate the interactions of GBM cells with the brain matrix components and MSCs in the zebrafish embryonic brain by co-implantation of fluorescently labeled GBM cells and MSCs. To deepen our understanding of GBM cell behavior within the brain of zebrafish embryos, we combined *in vivo* imaging of GBM progression with imaging of fluorescently counterstained whole-mount preparations that allowed the visualization of the anatomical context of the implanted cells. As chemical fixation leads to loss of transparency of the embryonic tissues, it necessitated the clearing of the embryos, which was achieved with the use of clearing agents.[27-39] To this end, we optimized and applied protocols to clear fixed tissues while preserving the fluorescent protein signal over a period of several weeks.

Materials and methods

Ethical statement

The experimental procedures were approved by the Republic of Slovenia National Medical Ethics Committee, approval No. 92/06/12. All of the procedures were performed according to the relevant regulations.

Zebrafish husbandry

Wild-type AB zebrafish (*Danio rerio*) were maintained under conditions according to the Organisation for Economic Cooperation and Development guidelines.[40] The zebrafish embryos were collected and incubated in dilution water (ISO 7346-3:1996) with 0.005% phenylthiourea, to inhibit pigment formation after 36 h of age.

Human cells

The U373 and U87-MG human GBM cell lines were from American Type Culture Collection (USA), and the BM-MSC2 human bone-marrow-derived MSC cell line was from Lonza Bioscience (USA). The cells were cultured in Dulbecco's modified Eagle's medium (Sigma-Aldrich, USA) supplemented with 10% fetal bovine serum (Gibco, USA), 100 U/mL penicillin (Sigma-Aldrich), 100 mg/mL streptomycin (Sigma-Aldrich), 2 mM L-glutamine (Sigma-Aldrich), 1 mM Na-pyruvate (Gibco), and non-essential amino acids (Sigma-Aldrich).

Xenotransplantation procedures

The U373 GBM cells were transfected with the pEGFP-N1 plasmid to stably express enhanced green fluorescent protein (GFP). The U87 GBM cells were transfected for the expression of the red fluorescent protein DsRed, as described previously.[16] Cells were transfected using the Superfect Transfection Reagent (Qiagen, Germany) by 3 h pre-incubation at 37°C, 5% CO_2. The transfection

Unauthenticated
Download Date | 4/20/16 10:53 AM

TABLE 1. Compositions of the selected optical clearing agents

Optical clearing agent	Composition	Reference
SeeDB	80% (w/w) fructose, 0.5% (w/w) α-thioglycerol in water	Ke *et al.*[34]
sRIMS	70% (w/v) sorbitol, 0.01% (w/v) sodium azide, 0.1% (w/v) Tween 20 in 0.02 M phosphate buffer (pH 7.5)	Yang *et al.*[39]
ScaleA2	4 M urea, 0.1% (w/v) Triton X-100, 10% (w/w) glycerol in water	Hama *et al.*[33]
ScaleU2	4 M urea, 0.1% (w/v) Triton X-100, 30% (w/w) glycerol in water	Hama *et al.*[33]

mix was then removed and upon washing with phosphate-buffered saline (PBS), fresh culture medium was added to the cells. Transfected cells were selected for by adding 0.8 mg/ml Geneticin (G418, Gibco, USA) to the medium. The uniformity of emitted fluorescence was confirmed with flow cytometry. The stability of fluorescent protein expression was verified with repeated flow cytometry analyses after 10 and 20 passages and proved to be stable (>99% of fluorescent protein-expressing cells). Prior to implantation, MSCs were labeled with Vybrant DiI or DiO (Molecular Probes, USA) for co-implantation with the U373 and U87 cells, respectively, according to the manufacturer instructions. For injection into the embryos, suspensions of GBM cells prepared in PBS were mixed with labeled MSCs in a 1:1 ratio. Embryos at 52 h after fertilization were injected either with 50 to 100 GBM cells or 100 to 200 cells of the GBM/MSC mixture (*i.e.*, maintaining 50-100 GBM cells), using a borosilicate glass capillary and a MICROINJECTOR system (Tritech Research, USA). After cell implantation, the embryos were incubated at 31°C in 48-well plates for 3 days.

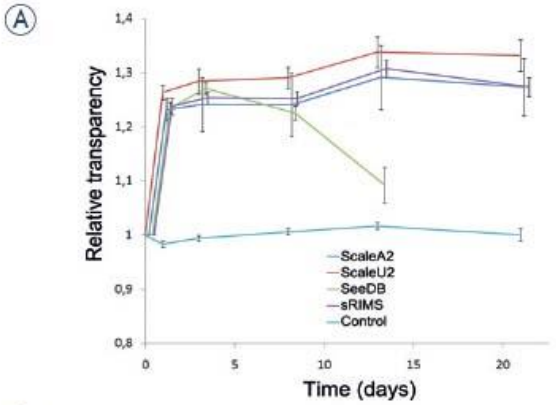
Clearing agents

The clearing agents used were SeeDB, a near-saturated solution of fructose with α-thioglycerol[34], sRIMS, a buffered solution of sorbitol[39], and two aqueous solutions of urea and glycerol known as Sca*l*eA2 and Sca*l*eU2.[33] An overview of the compositions of these clearing agents is shown in Table 1.

Analysis of clearing efficiency and fluorescence preservation

At 3 days after fertilization (for measurements of transparency and size) and 5 days after fertilization (for fluorescence imaging of implanted cells), the zebrafish embryos were fixed in 4% paraformaldehyde at 4°C overnight, after which time the fixative was washed off with PBS. The fixed embryos were then embedded in 2% low-melting-point agarose in PBS in 50-mm Petri dishes. For the optical clearing agent SeeDB, the embryos were transferred to SeeDB through a graded series of sucrose, as described by Ke *et al.*[34], and maintained at room temperature. For sRIMS and Sca*l*e, the embryos were immersed in the clearing agents and kept at 4°C in the dark. In all cases, the clearing agents were replaced every 3 days. The control embryos were incubated in parallel in PBS. For analysis of the whole-embryo clearing, transmitted light images were obtained at constant (maximum) illumination at 32× magnification. For imaging and quantification of GFP fluorescence, the images were captured at 80× magnification using the GFP filter set. Micrographs were obtained using a fluorescence stereomicroscope (Leica MZ FLIII). The imaging was carried out over a period of 21 days. The analysis of fluorescence preservation was performed on embryos with implanted U373 cells. Fluorescence intensity, embryo transparency, and embryo size were quantified with the image analysis software ImageJ.[41] For determination of embryo transmittance, the parameter 'Integrated density' was measured. The relative integrated densities and areas were determined by dividing the values of these parameters at the given time points with their values at the beginning of the observation on day 0. As integrated density represents the product of pixel intensities and area, the changes in embryo size that were caused by some of the clearing agents were accounted for by dividing the integrated density of the structure analyzed with its area, thus obtaining the relative embryo transparency. Fluorescence intensity was analyzed by thresholding the fluorescent images with a constant threshold and measuring the integrated density of the selection. For the analysis of changes in embryo size and transparency, 8 embryos per treatment were measured. For the analysis of GFP fluorescence intensity changes, 24 embryos per treatment were measured. Measurements were compared with ANOVA in GraphPad Prism.

Unauthenticated
Download Date | 4/20/16 10:53 AM



Confocal microscopy

The nuclei of the embryos that had been fixed, embedded in agarose, and cleared as described above were counterstained by addition of 0.004% methyl green to the individual clearing agent.[42] Confocal z-stacks of the embryos were obtained using a spectral confocal laser scanning microscope (Leica TCS SPE) at 10× magnification after 7 days of treatment.

Results

Clearing efficiencies of the different clearing agents

To evaluate the applicability of the different optical clearing agents (Table 1) to zebrafish embryo imaging, we treated embryos fixed at 3 days after fertilization with SeeDB, sRIMS, Scale*A2*, and Scale*U2* for 3 weeks, with regular imaging. The tissues were cleared best by Scale*U2* and Scale*A2* with no statistically significant difference between them at any time point. These agents performed significantly better than SeeDB on all treatment days. The least effective agent was sRIMS (Figure 1A). After approximately 1 week of incubation, fructose began to crystallize from the SeeDB solution, preventing further analyses. With regard to the preservation of GFP fluorescence, Scale*U2* was the optimal clear-

FIGURE 1. **(A)** Clearing of zebrafish embryos. Embryos were fixed 3 days after fertilization, exposed to the different clearing agents SeeDB, sRIMS, Scale*A2*, and Scale*U2* for 21 days, and imaged regularly. Time courses of changes in relative transparency are shown, which represents the value of integrated density relative to day 0 divided by the embryo area relative to day 0. Differences between treatments are statistically significant in all cases except between Scale*A2* and Scale B2 (on all days) and between Scale*A2* and sRIMS on day 21. Green, SeeDB; purple, sRIMS; dark blue, Scale*A2*; red, Scale*U2*; light blue, PBS control. Data for the different clearing agents are displaced horizontally for improved clarity. Means ± SE of eight embryos per treatment are shown. **(B)** Preservation of GFP fluorescence during clearing. Changes in the detected GFP fluorescence intensity of glioblastoma cells implanted in the brain of zebrafish embryos during treatment with different clearing agents of SeeDB, sRIMS, Scale*A2*, and Scale*U2*, measured over 21 days of the treatment. The integrated density of GFP-expressing cells relative to day 0 was measured. Fluorescence intensity was significantly increased compared to control in the case of Scale*U2* on all days except on day 3, but not in the case of other clearing agents. Means ±SE of 24 embryos per treatment are shown. **(C)** Fluorescence of U373-GFP cells in the brain of zebrafish embryos. Representative images show embryos treated with the different clearing agents obtained at the beginning of observation (Day 0, left) and after 3 days of clearing (Day 3, right). The appearance of autofluorescence of the yolk (arrow) is evident in the case of SeeDB. Scale bar: 400 μm.

Unauthenticated
Download Date | 4/20/16 10:53 AM

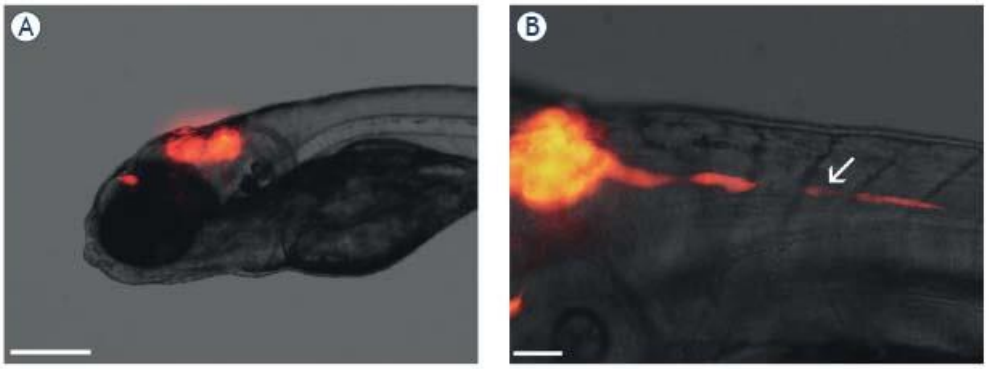


FIGURE 2. *In vivo* imaging of glioblastoma cells in the brain of zebrafish embryos. **(A)** Embryo 3 days after the implantation of U87-DsRed cells in the brain (visible as red fluorescence). Compact tumors have formed in the midbrain and forbrain. **(B)** An embryo with implanted U87-DsRed cells 2 days after implantation, with a string of U87-DsRed cells rapidly invading from the tumor in the brain in the posterior direction (arrow). Scale bars: 300 μm **(A)**; 50 μm **(B)**.

ing agent, resulting in a several-fold increase in fluorescence intensity during the first 3 days of incubation and no demonstrable reduction in its intensity during 3 weeks of observation (Figure 1B). These changes were statistically significant when compared with the control. Complete loss of fluorescence occurred in the case of SeeDB within a week and no statistically significant increases in intensity compared to the control were demonstrated in the cases of Sca*l*eA2 and sRIMS. The loss of GFP fluorescence in SeeDB was accompanied by the appearance of strong autofluorescence of the yolk and eye (Figure 1C).

Localization of implanted glioblastoma cells and pathways of GBM cell invasion in the zebrafish embryonic brain

After selecting Sca*l*eU2 as the optimal clearing agent for the visualization of the fluorescent-protein-labeled cells, it was applied to visualize tumor progression in the whole-mount preparations of the zebrafish embryos. We implanted U373-GFP cells into the brain of embryos 2 days after fertilization, and monitored these over the following 3 days.

By imaging the GBM cells in zebrafish embryos *in vivo*, we demonstrated that implanted cells aggregated and formed tumors in the zebrafish brain (Figure 2A). In some embryos, individual cells moved posteriorly in the embryo at great speed, as they progressed at several hundreds of micrometers per day (Figure 2B). This rapid invasion outside of the brain in the posterior direction was observed more frequently for the U87 cells (35 ± 5% of the embryos, as 3 experimental repeats, and 20 embryos per repeat) than for the U373 cells (20 ± 5% of the embryos, as 3 experimental repeats, and 20 embryos per repeat).

Tumors were seen to form predominantly in the midbrain hemispheres and in the ventricles of the midbrain and hindbrain (Figure 3A–C). Individual cells, or small strands of cells, invaded the ventricular system and the brain tissue using pseudopodal movement (Figure 3A,B). In particular, cells present in the midbrain hemispheres formed elongated pseudopodia and invaded the neighboring brain areas dorsally, most likely along axonal tracts that connect the hemispheres (Figure 3A). Whole-mount imaging of embryos with cells invading posteriorly in the body revealed that the rapidly invading cells invaded the spinal cord *via* the central canal (Figure 3D,E). We did not observe GBM cells outside of the brain and spinal cord, indicating that GBM cell invasion in zebrafish embryos was limited to the CNS, and that the cells did not spread *via* the circulatory system.

Imaging of xenotransplanted GBM and MSC co-cultures

To study the interactions between the GBM cells and MSCs *in vivo*, we implanted co-cultures of U373-GFP cells and carbocyanine-dye-labeled human MSCs into the brain of zebrafish embryos 2 days after fertilization. As labeling with carbocyanine dyes relies on the hydrophobic nature of these dyes, they can be washed out with organic sol-

Unauthenticated
Download Date | 4/20/16 10:53 AM

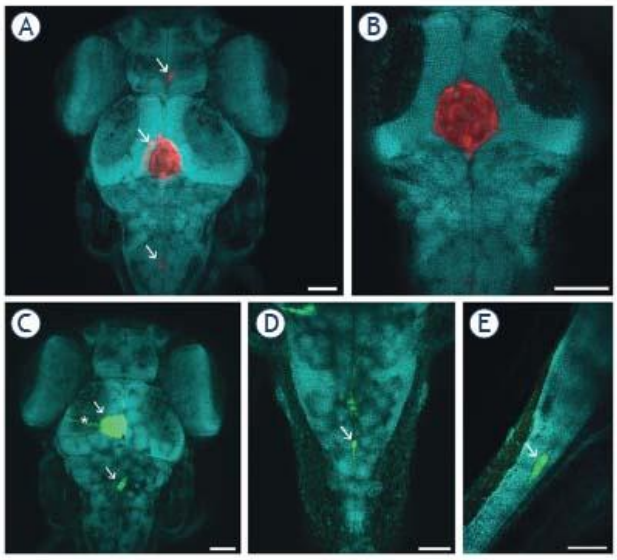


FIGURE 3. Visualization of GBM cells in cleared zebrafish embryos, counterstained with methyl green (presented in blue). Embryos with U373-GFP and U87-DsRed cells implanted in the brain were cleared with ScaleU2, counterstained with methyl green, and imaged with confocal microscopy. **(A)** U87-DsRed cells (arrows) in the brain of a zebrafish embryo 3 days after implantation. **(B)** An optical section through the tumor in **(A)**, demonstrating that the tumor is a compact mass of U87 cells in the midbrain ventricle. **(C)** U373-GFP cells (arrows) in the brain of a zebrafish embryo 3 days after implantation. Elongated U373-GFP cells are visible invading from the tumor (asterisk). **(D)** A U373-GFP cell invading along the central canal of the spinal cord (arrow), in dorsal view. **(E)** A U373-GFP cell invading along the central canal of the spinal cord (arrow), in lateral view. Scale bars: 70 μm **(A, B, C)**; 50 μm **(D, E)**.

vents and detergents. Thus, we prepared Scale*U2* without Triton X-100, with which we successfully visualized dye-labeled cells in whole-mount preparations. In implanted mixtures of GBM cells and MSCs, the MSCs preferentially associated with the implanted GBM cells instead of being interspersed individually or as separate clusters in the brain (Figure 4A–C). The MSCs often used similar invasion routes as the GBM cells, as they moved along the ventricles and the central canal of the spinal cord (Figure 4B,C).

Confocal imaging of U373 and MSC co-cultures *in situ* revealed that the GBM cells and MSCs formed mixed tumor masses that consisted of both of these cell types in similar locations as for the GBM cells alone; *i.e.*, in the ventricles and midbrain hemispheres (Figure 4A,B). These two cell types were interspersed in these tumors, and interacted closely with each other (Figure 4D). In some cases, cells simultaneously emitting the fluorescence of proteins and the carbocyanine dye were observed, which indicated possible cell fusion between the GBM cells and MSCs (Figure 5).

Discussion

The major advantage of the zebrafish model is the transparency of their embryos and larvae, which allows *in vivo* visualization of cellular processes related to cancer progression at single-cell resolution. We identified Scale*U2* as the optimal clearing agent for zebrafish embryos among the agents tested. Furthermore, we were able to modify it to be compatible with the labeling of cells with carbocyanine dyes. The superiority of Scale*U2* in fluorescence preservation appears to result from its high glycerol concentration, and thus might be linked to the protein-stabilizing effects of glycerol in aqueous solution.[43,44]

The proposed protocols were used to study the invasion of the U87 and U373 human GBM cell lines alone and in co-cultures with bone-marrow-derived MSCs in the zebrafish embryo. By combining the *in vivo* imaging with confocal microscopy of fluorescently counterstained whole-mount preparations, we demonstrated that GBM cells aggregate in the brain of zebrafish embryos and form tumors predominantly in the ventricles. This indicates that GBM cells have tropism towards each other upon implantation to form tumors, which are preferentially formed in the ventricles and dorsal areas of the midbrain. The tendency of the GBM cells to aggregate in these areas might be linked to the ease of dislodging the embryonic brain tissues in anatomical structures such as the ventricles, which are fluid-filled spaces where the brain cells are not in direct contact. The localization of GBM cells to the ventricular system has previously not been reported. Eden *et al.*[45] recently reported that mouse xenografts in the brain of juvenile (30-day-old) zebrafish reproduced the histology and gene expression profiles of the murine tumors of their origin within the tissues of the brain. Thus, the observed localization of the GBM cells to the ventricular system might be limited to embryos and larval stages.

We were able to identify the central canal of the spinal cord as the major route of GBM invasion in zebrafish embryos that has not been reported before. Furthermore, GBM cells did not leave the central nervous system, which is similar to their behavior in humans.[46] In a previous study on murine tumor xenografts in the zebrafish brain, tumor masses developed 1 day to 2 days after the im-

Unauthenticated
Download Date | 4/20/16 10:53 AM

plantation in the spinal cord. Histological analysis confirmed that these masses were independent, distant tumors, rather than direct extensions of the main tumor mass, thus demonstrating that the implanted GBM cells disseminated in the CNS of the zebrafish.[45] This is in agreement with our observations of single-cell invasion along the central canal of the spinal cord, which may result in separate tumor formation within the spinal cord. The underlying molecular mechanisms of this rapid invasion remain to be established. The process might be facilitated by the low resistance of the central canal to cell invasion, as the GBM cells are believed to generally invade through structures that have low resistance to cell movement.[5,6,46]

One of the preferential pathways of GBM invasion in the human brain is the white matter, where GBM cells invade along axons.[46] It is likely that this preference is recapitulated in zebrafish embryos, as we observed pseudopodal invasion in the midbrain area that is rich in axonal connections between the two hemispheres (Figure 3C). This is reminiscent of tumor invasion via the *corpus callosum* in human patients.[2]

Pseudopodia and cell elongation characterize the mesenchymal type of cell invasion, which is typical for gliomas and depends on cell-matrix adhesion.[5,6] The observed strand migration in the spinal cord as well as the midbrain (Figure 2B,4B) is linked to proteolytic matrix remodeling and is characteristic of cancer cells belonging to the mesenchymal type.[5] A mesenchymal molecular fingerprint has recently been established for U373 GBM cells.[47] This invasion pattern has also previously been observed for U87 cells in mouse models, together with elevated cathepsin B expression at the tumor periphery.[48] In a study on zebrafish larvae, invasion of U87 GBM cells along the abluminal surface of blood vessels has also been demonstrated.[25] As the basal lamina of blood vessels is a known invasion pathway in the human brain[46], this further strengthens the view that the invasion of GBM cells in the zebrafish model resembles this process in mammals.

Confocal imaging of GBM and MSC co-cultures *in situ* revealed that both of these types of cells form mixed tumor masses at similar locations as for the GBM cells alone; *i.e.*, in the ventricles and midbrain hemisphere. The GBM and MSC cells used similar invasion routes along the ventricles and the central canal of the spinal cord, but did not invade other tissues. The association of GBM cells and MSCs into such mixed tumors in the brain of these zebrafish embryos suggests a strong intercellular interaction between them, which would appear to also have a role in the human GBM microenvironment. Indeed, MSC tropism towards GBM cells has previously been described[10], and a set of cytokines has been shown to mediate the interactions between these cells *in vitro*.[49,50] Among these, the monocyte chemoattractant protein (MCP-1) has been suggested as the major trigger of various molecular pathways that can enhance MSC proliferation and invasion, whereas a different set of genes has been shown to impair U87 cell invasion and proliferation, and to even induce their senescence.[49] When mixtures of U87 or U373 GBM cells and MSCs were implanted

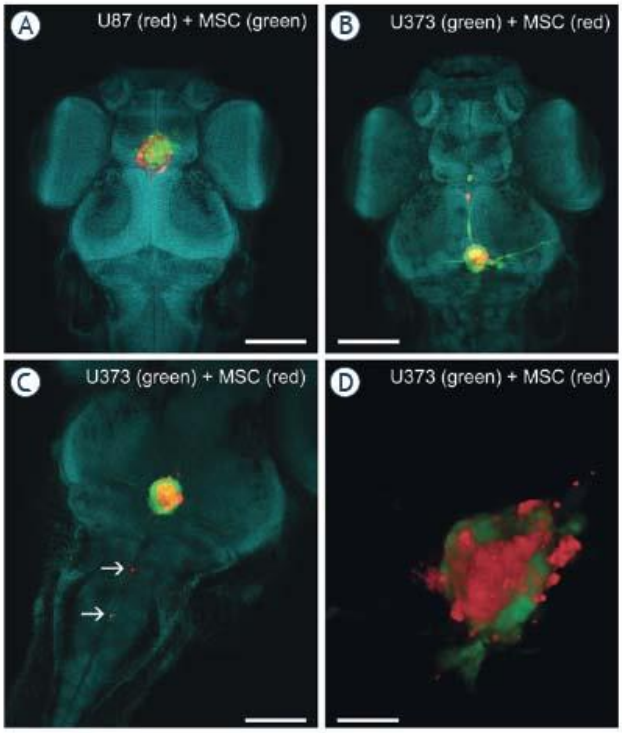


FIGURE 4. Imaging of co-cultures of GBM cells and MSCs in the brain of zebrafish embryos. A mixture of fluorescent-protein-expressing GBM cells and carbocyanine-dye-labeled MSCs was implanted into the brain of the zebrafish embryos. Three days after implantation, the embryos were fixed, cleared in ScaleU2 without the addition of Triton X-100, and imaged with confocal microscopy. **(A)** The head of a zebrafish embryo with a co-culture of U87-DsRed cells (red) and DiO-labeled MSCs (green) implanted in the brain. **(B)** The head of a zebrafish embryo with a co-culture of U373-GFP cells (green) and DiI-labeled MSCs (red) implanted in the brain. **(C)** Invasion of DiI-labeled MSCs (red) along the central canal of the spinal cord. **(D)** Three-dimensional rendering of a mixed mass of U373 cells (green) and MSCs (red) in a brain obtained from a cleared embryo. Nuclei are stained with methyl green (presented in blue). Scale bars: 250 μm (A, B); 100 μm **(C)**; 50 μm **(D)**.

Unauthenticated
Download Date | 4/20/16 10:53 AM

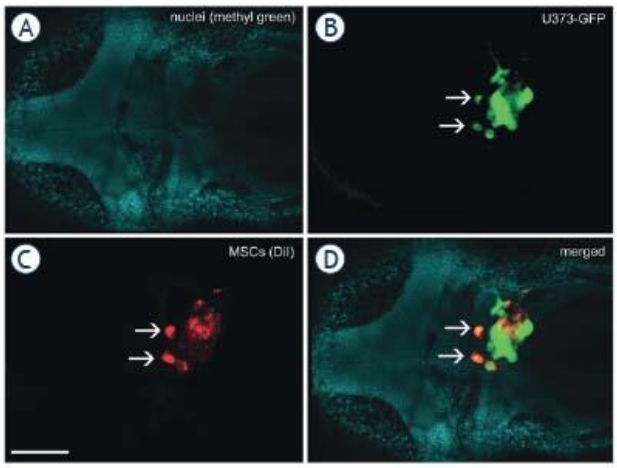


FIGURE 5. Fusion between GBM cells and MSCs in the zebrafish brain. A mixture of U373-GFP cells and DiI-labeled MSCs was implanted in the brain of the embryos, which were fixed, cleared and imaged 3 days after implantation of the cells. Two cells (arrows) emit green GFP fluorescence as well as red DiI fluorescence, which strongly indicates that the U373-GFP cells and MSCs have fused after implantation. **(A)** Nuclei of embryonic tissues labeled with methyl green. **(B)** Green fluorescent protein fluorescence of U373 cells. **(C)** Red fluorescence of DiI, used to label the MSCs. **(D)** Merged image of all of the fluorescent channels. Scale bar: 200 µm.

into the zebrafish embryos, these established very close contacts and apparently also formed a structural syncytium *in vivo*. This finding confirms our previous *in-vitro* studies of direct co-cultures using U373 GBM cells and MSCs. These studies showed the formation of gap junctions between these cell types (*i.e.*, formation of a functional syncytium), as demonstrated by fluorescein transmission and connexin 43 expression. Furthermore, there was membrane fusion between these cells (*i.e.*, formation of a structural syncytium), as demonstrated by the co-localization of different carbocyanine dyes.[15] Direct membrane fusion between the GBM cells and MSCs affects gene expression and the cell phenotype, which might lead to enhanced invasion of hybrid cells, which is of relevance to tumor progression.[15]

Taken together, our enhanced clearing methodology has enabled us to study GBM cell localization in the brain of zebrafish embryos and to observe their interaction with MSCs at single-cell resolution. This allowed us to identify the invasion patterns of GBM cells in the zebrafish brain and identify the central canal of the spinal cord as a major invasion route. As the frequency of this single-cell invasion of the spinal cord is also quantifiable, the observation of this process in high-throughput screening can now be developed as a fast and objective methodology. Thus it can not only to be used to study basic mechanisms in terms of the differences among heterogeneous GBM populations, but also for diagnostic purposes with patient biopsies. This study is also the first to address co-culture implantation in the zebrafish brain model in order to define the interactions between GBM cells and MSCs. We demonstrated that these two cell types invade the surrounding brain tissue along similar invasion roots as the GBM cells alone, whereby they often moved along the central canal of the spinal cord, but did not leave the CNS.

In perspective, the zebrafish xenotransplantation model of GBM has many benefits in terms of cost, simplicity, possibility for single-cell visualization *in vivo*, and high throughput.[18] As demonstrated by the present study, this simple model can be used to study cell processes involved in GBM cell invasion and the interactions of GBM cells with many other cells of the stroma in double or triple cell co-cultures.

Acknowledgments

The authors wish to thank Prof. Dr. Cornelis J.F. van Noorden (Academic Medical Centre, Amsterdam) for his introduction to the CLARITY technique. We also thank Dr. David Dobnik (National Institute of Biology, Ljubljana) for his help with confocal microscopy. This work was funded by the INTERREG EC Project 2011, Ref. No. 42 (GLIOMA) and the Reserch Programme P1-0245, awarded by the Slovenian Research Agency.

References

1. Ohgaki H, Kleihues P. The definition of primary and secondary glioblastoma. *Clin Cancer Res* 2013; **19:** 764-72.
2. Claes A, Idema A, Wesseling P. Diffuse glioma growth: a guerilla war. *Acta Neuropathol* 2007; **114:** 443-58.
3. Gupta MK, Jayaram S, Reddy DN, Polisetty RV, Sirdeshmukh R. Transcriptomic and proteomic data integration and two-dimensional molecular maps with regulatory and functional linkages: application to cell proliferation and invasion networks in glioblastoma. *J Proteome Res* 2015; **14:** 5017-27.
4. Klekner Á, Hutóczki G, Virga J, Reményi-Puskár J, Tóth J, Scholtz B, et al. Expression pattern of invasion-related molecules in the peritumoral brain. *Clin Neurol Neurosurg* 2015; **139:** 138-43.
5. Friedl P, Wolf K. Tumour-cell invasion and migration: diversity and escape mechanisms. *Nat Rev Cancer* 2003; **3:** 362-74.
6. Friedl P, Wolf K. Plasticity of cell migration: a multiscale tuning model. *J Cell Biol* 2010; **188:** 11-9.
7. Hanahan D, Weinberg RA. Hallmarks of cancer: the next generation. *Cell* 2011; **144:** 646-74.

Unauthenticated
Download Date | 4/20/16 10:53 AM

8. Grisendi G, Bussolari R, Veronesi E, Piccinno S, Burns JS, De Santis G, et al. Understanding tumor-stroma interplays for targeted therapies by armed mesenchymal stromal progenitors: the Mesenkillers. *Am J Cancer Res* 2011; **1:** 787-805.

9. Kološa K, Motaln H, Herold-Mende C, Koršič M, Lah TT. Paracrine effects of mesenchymal stem cells induce senescence and differentiation of glioblastoma stem-like cells. *Cell Transplant* 2015; **24:** 631-44.

10. Motaln H, Lah TT. Cytokines play a key role in communication between mesenchymal stem cells and brain cancer cells. *Protein Pept Lett* 2015; **22:** 322-31.

11. Barcellos-de-Souza P, Gori V, Bambi F, Chiarugi P. Tumor microenvironment: bone marrow-mesenchymal stem cells as key players. *Biochim Biophys Acta* 2013; **1836:** 321-35.

12. Arango-Rodriguez ML, Ezquer F, Ezquer M, Conget P. Could cancer and infection be adverse effects of mesenchymal stromal cell therapy? *World J Stem Cells* 2015; **7:** 408-17.

13. Fei S, Qi X, Kedong S, Guangchun J, Jian L, Wei Q. The antitumor effect of mesenchymal stem cells transduced with a lentiviral vector expressing cytosine deaminase in a rat glioma model. *J Cancer Res Clin Oncol* 2012; **138:** 347-57.

14. Kim SM, Woo JS, Jeong CH, Ryu CH, Lim JY, Jeun SS. Effective combination therapy for malignant glioma with TRAIL-secreting mesenchymal stem cells and lipoxygenase inhibitor MK886. *Cancer Res* 2012; **72:** 4807-17.

15. Schichor C, Albrecht V, Korte B, Buchner A, Riesenberg R, Mysliwietz J, et al. Mesenchymal stem cells and glioma cells form a structural as well as a functional syncytium in vitro. *Exp Neurol* 2012; **234:** 208-19.

16. Pilat MM, Oliveira M, Motaln H, Breznik B, Glaser T, Lah TT, et al. Glioblastoma-mesenchymal stem cell communication modulates expression and activities of kinin receptors: possible involvement of bradykinin on information flow. *Cytometry A* 2016; DOI: 10.1002/cyto.a.22800

17. Behnan J, Isakson P, Joel M, Cilio C, Langmoen I, Vik-Mo EO, et al. Recruited brain tumor-derived mesenchymal stem cells contribute to brain tumor progression. *Stem Cells* 2014; **32:** 1110-23.

18. Vittori M, Motaln H, Lah TT. The study of glioma by xenotransplantation in zebrafish early life stages. *J Histochem Cytochem* 2015; **63:** 749-61.

19. Grunwald DJ, Eisen JS. Headwaters of the zebrafish – emergence of a new model vertebrate. *Nat Rev Genet* 2002; **3:** 717-24.

20. Feng Y, Martin P. Imaging innate immune responses at tumour initiation: new insights from fish and flies. *Nat Rev Cancer* 2015; **15:** 556-62.

21. White R, Rose K, Zon L. Zebrafish cancer: the state of the art and the path forward. *Nat Rev Cancer* 2013; **13:** 624-36.

22. Zon LI, Peterson RT. *In vivo* drug discovery in the zebrafish. *Nat Rev Drug Discov* 2005; **4:** 35-44.

23. Keller PJ, Schmidt AD, Wittbrodt J, Stelzer EH. Reconstruction of zebrafish early embryonic development by scanned light sheet microscopy. *Science* 2008; **322:** 1065-9.

24. Geiger GA, Fu W, Kao GD. Temozolomide-mediated radiosensitization of human glioma cells in a zebrafish embryonic system. *Cancer Res* 2008; **68:** 3396-404.

25. Lal S, La Du J, Tanguay RL, Greenwood JA. Calpain 2 is required for the invasion of glioblastoma cells in the zebrafish brain microenvironment. *J Neurosci Res* 2012; **90:** 769-81.

26. Konantz M, Balci TB, Hartwig UF, Dellaire G, André MC, Berman JN, et al. Zebrafish xenografts as a tool for *in vivo* studies on human cancer. *Ann N Y Acad Sci* 2012; **1266:** 124-37.

27. Sakhalkar HS, Dewhirst M, Oliver T, Cao Y, Oldham M. Functional imaging in bulk tissue specimens using optical emission tomography: fluorescence preservation during optical clearing. *Phys Med Biol* 2007; **52:** 2035-54.

28. Dodt HU, Leischner U, Schierloh A, Jährling N, Mauch CP, Deininger K, et al. Ultramicroscopy: three-dimensional visualization of neuronal networks in the whole mouse brain. *Nat Methods* 2007; **4:** 331-6.

29. Zukor KA, Kent DT, Odelberg SJ. Fluorescent whole-mount method for visualizing three-dimensional relationships in intact and regenerating adult newt spinal cords. *Dev Dyn* 2010; **239:** 3048-57.

30. Oldham M, Sakhalkar H, Oliver T, Allan Johnson G, Dewhirst M. Optical clearing of unsectioned specimens for three-dimensional imaging via optical transmission and emission tomography. *J Biomed Opt* 2008; **13:** 021113.

31. Ertürk A, Becker K, Jährling N, Mauch CP, Hojer CD, Egen JG, et al. Three-dimensional imaging of solvent-cleared organs using 3DISCO. *Nat Protoc* 2012; **7:** 1983-95.

32. Becker K, Jährling N, Saghafi S, Weiler R, Dodt H-U. Chemical clearing and dehydration of GFP expressing mouse brains. *PLoS ONE* 2012; **7:** e33916.

33. Hama H, Kurokawa H, Kawano H, Ando R, Shimogori T, Noda H, et al. Scale: a chemical approach for fluorescence imaging and reconstruction of transparent mouse brain. *Nat Neurosci* 2011; **14:** 1481-8.

34. Ke MT, Fujimoto S, Imai T. SeeDB: a simple and morphology-preserving optical clearing agent for neuronal circuit reconstruction. *Nat Neurosci* 2013; **16:** 1154-61.

35. Susaki EA, Tainaka K, Perrin D, Kishino F, Tawara T, Watanabe TM, et al. Whole-brain imaging with single-cell resolution using chemical cocktails and computational analysis. *Cell* 2014; **157:** 726-39.

36. Tainaka K, Kubota SI, Suyama TQ, Susaki EA, Perrin D, Ukai-Tadenuma M, et al. Whole-body imaging with single-cell resolution by tissue decolorization. *Cell* 2014; **159:** 911-24.

37. Kuwajima T, Sitko AA, Bhansali P, Jurgens C, Guido W, Mason C. *Clear*^{T}: a detergent- and solvent-free clearing method for neuronal and non-neuronal tissue. *Development* 2013; **140:** 1364-8.

38. Chung K, Wallace J, Kim SY, Kalyanasundaram S, Andalman AS, Davidson TJ, et al. Structural and molecular interrogation of intact biological systems. *Nature* 2013; **497:** 332-7.

39. Yang B, Treweek JB, Kulkarni RP, Deverman BE, Chen CK, Lubeck E, et al. Single-cell phenotyping within transparent intact tissue through whole-body clearing. *Cell* 2014; **158:** 945-58.

40. Organisation for Economic Cooperation and Development. *OECD Guidelines For Testing of Chemicals*. Test No. 236. Fish Embryo Acute Toxicity (FET) Test. Paris: OECD Publishing; 2013.

41. Abramoff MD, Magalhães PJ, Ram SJ. Image processing with ImageJ. *Biophotonics Intern* 2004; **11:** 36-42.

42. Prieto D, Aparicio G, Morande PE, Zolessi FR. A fast, low-cost, and highly efficient fluorescent DNA labeling method using methyl green. *Histochem Cell Biol* 2014; **142:** 335-45.

43. Gekko, K, Timasheff SN. Mechanism of protein stabilization by glycerol: preferential hydration in glycerol-water mixtures. *Biochemistry* 1981; **20:** 4667-76.

44. Street TO, Bolen DW, Rose GD. A molecular mechanism for osmolyte-induced protein stability. *Proc Natl Acad Sci U S A* 2006; **103:** 13997-4002.

45. Eden C, Ju B, Murugesan M, Phoenix T, Nimmervoll B, Tong Y, et al. Orthotopic models of pediatric brain tumors in zebrafish. *Oncogene* 2015; **34:** 1736-42.

46. Gritsenko PG, Ilina O, Friedl P. Interstitial guidance of cancer invasion. *J Pathol* 2012; **226:** 185-99.

47. Motaln H, Koren A, Gruden K, Ramšak Ž, Schichor C, Lah TT. Heterogeneous glioblastoma cell cross-talk promotes phenotype alterations and enhanced drug resistance. *Oncotarget* 2015; **38:** 40998-1017.

48. Gole B, Huszthy PC, Popović M, Jeruc J, Ardebili YS, Bjerkvig R, Lah TT. The regulation of cysteine cathepsins and cystatins in human gliomas. *Int J Cancer* 2012; **131:** 1779-89.

49. Motaln H, Gruden K, Hren M, Schichor C, Primon M, Rotter A, et al. Human mesenchymal stem cells exploit the immune response mediating chemokines to impact the phenotype of glioblastoma. *Cell Transplant* 2012; **21:** 1529-45.

50. Tajnšek U, Motaln H, Levičar N, Rotter A, Lah TT. The duality of stem cell: double edged sword in tumour evolution and treatment. In: Resende RR, Ulrich H, editor. *Trends in Stem Cell Proliferation and Cancer Research*. Dordrecht: Springer Netherlands; 2013. p. 391-434.

Unauthenticated
Download Date | 4/20/16 10:53 AM

2.4 Addition of 2-(Ethylamino)Acetonitrile Group to Nitroxoline Results in Significantly Improved Anti-Tumor Activity *in vitro* and *in vivo*

Ana Mitrović, Izidor Sosič, Špela Kos, Urša Lampreht Tratar, Barbara Breznik, Simona Kranjc, Bojana Mirković, Stanislav Gobec, Tamara Lah, Maja Čemažar, Gregor Serša and Janko Kos

Oncotarget 2017; 8(35): 59136-59147. DOI: 10.18632/oncotarget.19296

www.impactjournals.com/oncotarget/ Oncotarget, Advance Publications 2017

Addition of 2-(ethylamino)acetonitrile group to nitroxoline results in significantly improved anti-tumor activity *in vitro* and *in vivo*

Ana Mitrović[1], Izidor Sosič[1], Špela Kos[2], Urša Lampreht Tratar[2], Barbara Breznik[3,4], Simona Kranjc[2], Bojana Mirković[1], Stanislav Gobec[1], Tamara Lah[3], Maja Čemažar[2], Gregor Serša[2] and Janko Kos[1,5]

[1]Faculty of Pharmacy, University of Ljubljana, 1000 Ljubljana, Slovenia,

[2]Department of Experimental Oncology, Institute of Oncology Ljubljana, 1000 Ljubljana, Slovenia

[3]Department of Genetic Toxicology and Cancer Biology, National Institute of Biology, 1000 Ljubljana, Slovenia

[4]International Postgraduate School Jožef Stefan, 1000 Ljubljana, Slovenia

[5]Department of Biotechnology, Jožef Stefan Institute, 1000 Ljubljana, Slovenia

Correspondence to: *Janko Kos,* ***email:*** *janko.kos@ffa.uni-lj.si*

Keywords: *nitroxoline derivative, cathepsin B, inhibition, tumor invasion, cell migration*

Received: *April 03, 2017* ***Accepted:*** *June 10, 2017* ***Published:*** *July 17, 2017*

Copyright: Mitrović et al. This is an open-access article distributed under the terms of the Creative Commons Attribution License 3.0 (CC BY 3.0), which permits unrestricted use, distribution, and reproduction in any medium, provided the original author and source are credited.

ABSTRACT

Lysosomal cysteine peptidase cathepsin B, involved in multiple processes associated with tumor progression, is validated as a target for anti-cancer therapy. Nitroxoline, a known antimicrobial agent, is a potent and selective inhibitor of cathepsin B, hence reducing tumor progression *in vitro* and *in vivo*. In order to further improve its anti-cancer properties we developed a number of derivatives using structure-based chemical synthesis. Of these, the 7-aminomethylated derivative (compound 17) exhibited significantly improved kinetic properties over nitroxoline, inhibiting cathepsin B endopeptidase activity selectively. In the present study, we have evaluated its anti-cancer properties. It was more effective than nitroxoline in reducing tumor cell invasion and migration, as determined *in vitro* on two-dimensional cell models and tumor spheroids, under either endpoint or real time conditions. Moreover, it exhibited improved action over nitroxoline in impairing tumor growth *in vivo* in LPB mouse fibrosarcoma tumors in C57Bl/6 mice. Taken together, the addition of a 2-(ethylamino)acetonitrile group to nitroxoline at position 7 significantly improves its pharmacological characteristics and its potential for use as an anti-cancer drug.

INTRODUCTION

The proteolytic potential of lysosomal cysteine peptidases is highly relevant for cancer progression, initiating and assisting invasion related proteolytic cascades at the invasive edges of tumors. Of these, cathepsin B (EC 3.4.22.1) has been identified as an important tumor promoting factor [1–3], involved in extracellular matrix (ECM) degradation, a process enabling tumor migration, invasion, metastasis and angiogenesis [1, 4]. Cathepsin B can modulate the ECM, either directly by proteolytic degradation of its components, such as laminin, fibronectin, collagen type I and IV and proteoglycans, or indirectly with the activation of other proteases downstream in a proteolytic cascade [5–9]. Additionally, cathepsin B enhances tumor progression by proteolytic degradation of the metalloprotease inhibitors, TIMP-1 and TIMP-2, and by release of growth factors VEGF and TGF-β1 bound to the ECM proteins [10–12].

Cathepsin B is unique among cysteine cathepsins because it acts as both an endopeptidase and an exopeptidase [13]. Its dual activity is due to the presence of an extra structural element termed the occluding loop [14]. This ~20 amino acid long occluding loop blocks binding of longer endopeptidase substrates, as it covers the S2' and S3' subsites of the active site cleft [15]. In the acidic milieu two salt bridges (Asp22-His110 and Asp224-Arg116) bind the loop to the body of the enzyme, limiting access of extended substrates to primed sites of the active site cleft, thereby favoring its dipeptidyl carboxypeptidase activity [14–17]. When the pH increases the salt bridges are disrupted and the resulting conformational change increases the enzyme's endopeptidase activity, with an optimum at neutral pH values [16, 18]. It has been proposed that the endopeptidase activity is involved predominantly in ECM degradation and tumor progression, although recent results suggest also the contribution of exopeptidase activity in tumor progression [19].

Cathepsin B has been validated as a promising target in the treatment of cancer, using a range of research tools, including cathepsin B-specific inhibitors, siRNAs and cathepsin B knock-down or overexpression mouse models [4, 20]. Several groups of cathepsin B inhibitors have been identified. The majority are covalent inhibitors that contain a peptidyl backbone with an electrophilic warhead that reacts with the active site cysteine residue, either reversibly or irreversibly [2, 21, 22]. However, due to their low bioavailability and off-target side effects, none of these compounds can be translated into clinical practice [2]. However, a number of non-covalent, reversible, small molecule inhibitors of cathepsin B have recently been reported [20, 23–27]. We identified nitroxoline (5-nitro-8-hydroxyquinoline), a well-established antimicrobial agent for the treatment of urinary tract infections, as a potent, reversible and selective non-covalent inhibitor of cathepsin B endopeptidase activity [27]. It was shown to reduce significantly ECM degradation, cell proliferation, tumor invasion and endothelial tube formation and induce cell cycle arrest *in vitro* in a number of cell lines. Moreover, it significantly abrogated tumor growth, angiogenesis and metastasis *in vivo* in various mouse models [20, 28–32]. In order to further improve the anti-cancer properties of nitroxoline we designed and synthesized a number of its derivatives [27, 33]. Among them, 2-{[(8-hydroxy-5-nitroquinoline-7-yl)methyl]amino}-acetonitrile (compound 17) showed significantly improved kinetic properties for inhibition of cathepsin B endopeptidase activity [19, 33].

In the present study, we have further evaluated its effect on tumor growth, invasion and migration *in vitro* and *in vivo*. Compound 17 impairs tumor cell invasion and migration more effectively than nitroxoline, as monitored *in vitro* on two- and three-dimensional (2D and 3D) models, in both endpoint and real time conditions. Moreover, it also delayed the growth of LPB fibrosarcoma tumors in C57Bl/6 mice more strongly than nitroxoline, thus designating compound 17 as a promising candidate for evaluation of its potential in anti-cancer therapy.

RESULTS

Compound 17 impairs tumor cell invasion

The ability of compound 17 to reduce tumor cell invasion was evaluated on the human glioma cell line U-87 MG and on the mouse fibrosarcoma cell line LPB-1. Invasion was monitored in real time using the xCELLigence system [34]. This system measures invasion of cells through Matrigel, a model of ECM, by monitoring the impedance, expressed as cell index (CI) (Figure 1A), across microelectrodes integrated in the membrane between top and bottom compartments of the CIM (cell invasion and migration)-plate 16. This was carried out over the entire course of the experiment. Compound 17 significantly reduced invasion of tumor cell lines, at 2.5 μM concentration for U-87 MG cells by 21 ± 5% and at 5 μM concentration by 61 ± 3% and 74 ± 4% for U-87 MG and LPB-1 cells (Figure 1B). Furthermore, it shows improved inhibition of tumor invasion on U-87 MG cells compared to nitroxoline.

To exclude the possibility that the reduction of tumor cell invasion was due to compound 17-induced cytotoxicity, its effect on cell viability was evaluated by MTS cell viability assay. After treatment with compound 17 at concentrations up to 5 μM for 24 or 72 h, the viability of neither cell line was reduced (Figure 2). On the other hand, nitroxoline did not affect cell viability of U-87 MG cells at concentrations up to only 2.5 μM (Figure 2), however it did not affect cell viability of LPB-1 cells in concentration up to 5 μM [20].

Compound 17 reduces tumor cell invasion in a three-dimensional assay

Compound 17 was further evaluated for its ability to impair tumor cell invasion using a 3D *in vitro* tumor cell invasion model. This model is based on implantation of tumor spheroids into ECM-mimicking matrices and, as such, mimics early, avascular stages of tumor growth. It is therefore a more representative model of tumor cell invasion than are classic models involving cell monolayers. Spheroids from U-87 MG cells were prepared using the hanging drop method [35] following their implantation in Matrigel. Growth of spheroids was monitored for three days by measuring their dimensions under a light microscope with an ocular micrometer (Figure 3A). Representative images of U-87 MG spheroids were recorded on day three after implantation. U-87 MG spheroids displayed steady growth and formed invasive stands in a sunburst pattern around the original spheroid during the entire course of the experiment (Figure 3B).

Incubation of U-87 MG spheroids in the presence of compound 17 (2.5 and 5 μM) and of nitroxoline (2.5 μM) significantly reduced the growth of spheroids, the effect being more pronounced at the higher concentration of compound 17 (51 ± 9%).

Compound 17 inhibits cell migration in a three-dimensional assay

Compound 17 was evaluated for its ability to inhibit migration of two glioblastoma cell lines, U-87 MG and U373 cells out of spheroids. Relative migration, calculated as the ratio between migration distance and spheroid diameter, was assessed on day three after the generation of spheroids. Compound 17 (2.5 and 5 μM) and nitroxoline (2.5 μM) both significantly decreased migration of cells out of U-87 MG spheroids, by 24 ± 3% and 61 ± 6% at 2.5 and 5 μM concentrations of compound 17, and by 52 ± 8% for nitroxoline (2.5 μM; Figure 4A and 4B). However, only compound 17 inhibited migration of cells out of U373 spheroids by 14 ± 3 % at both concentrations used (Figure 4C and 4D). Its effect on the migration of U-87

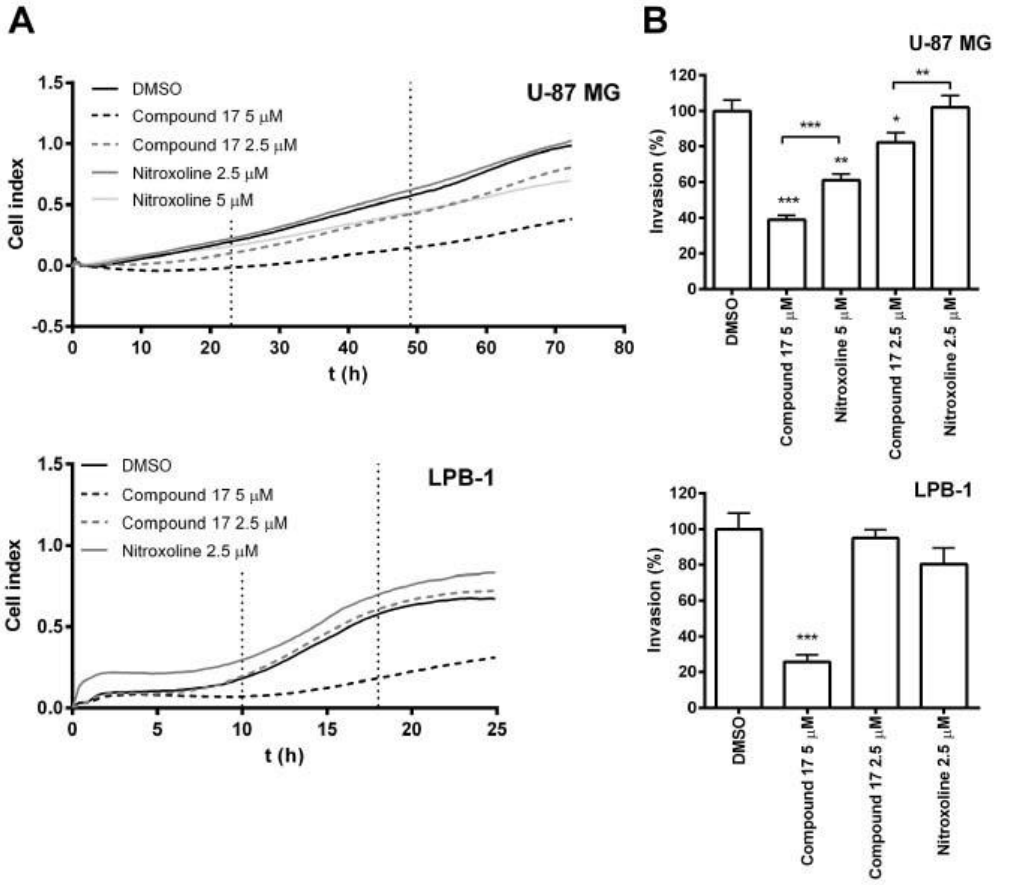


Figure 1: Compound 17 impairs the invasion of tumor cells. **(A)** Tumor cell invasion monitored in real time. Upper compartments of CIM-plate 16 were coated with Matrigel (2 mg/mL and 1 mg/ml for U-87 MG and LPB-1 cells, respectively). U-87 MG (7.5×10^4) or LPB-1 (5×10^4) cells were then seeded on top of it. The growth medium in the upper and lower compartments of the CIM-plate 16 was supplemented with compound 17 (2.5 μM or 5 μM), nitroxoline (2.5 μM or 5 μM) or DMSO (0.05%) as a control. Tumor cell invasion was then monitored continuously for 72 h by measuring impedance (reported as CI) using the xCELLigence system. **(B)** The ability of the cells to invade correlated to the slopes (1/h) in the time interval between 23 and 49 h for U-87 MG cells and between 10 and 18 h for LPB-1 cells and was used to calculate the percentage of invasion (%), presented as means ± SEM. The experiments were performed in quadruplicate and repeated three times. * $P < 0.05$, ** $P < 0.01$*** $P < 0.001$.

MG or U373 cells and mesenchymal stem cells (MSCs) out of co-cultured spheroids was also monitored. Co-cultured spheroids constitute a more complex model that takes into account interactions of tumor cells with stromal cells derived from the tumor microenvironment. In U-87 MG/MSC co-cultured spheroids, the migration of U-87 MG cells decreased compared to U-87 MG monoculture spheroids, while the migration of MSCs increased (Figure 4B). Neither compound 17 (2.5 and 5 μM) nor nitroxoline (2.5 μM) had any effect on cell migration out of U-87 MG/MSC co-cultured spheroids (Figure 4A). Interactions between MSCs and U373 cells, on the other hand, increased migration out of U373/MSC co-cultured spheroids of both cell lines, U373 and MSCs, (Figure 4C). Interestingly, after treatment with compound 17 or nitroxoline a significant decrease in cell migration out of U373/MSC co-cultured spheroids was observed for both cell lines compared to that for control cells treated with DMSO. Compound 17 decreased migration of U373 cells by 42 ± 4% and 42 ± 5% at 2.5 and 5 μM concentrations respectively, and nitroxoline by 33 ± 3%. Simultaneously, MSC cell migration was decreased by 28 ± 5% and 30 ± 5% at 2.5 and 5 μM concentrations of compound 17, and by 12 ± 5% for nitroxoline (2.5 μM; Figure 4C).

Compound 17 did not induce cytotoxicity of U-87 MG, U373 cells or MSC in concentrations up to 5 μM, as evaluated by MTS assay, while nitroxoline was not cytotoxic at concentrations up to only 2.5 μM (Figure 2).

Compound 17 delayed tumor growth *in vivo*

Administration of compound 17 *per os* delayed LPB fibrosarcoma tumor growth *in vivo* in C57Bl/6 mice. Compound 17 (20 mg/kg) and nitroxoline (20 mg/kg) were administered in drinking water for the entire duration of the experiment. Tumor volumes in mice receiving compound 17 or nitroxoline were both smaller in mice receiving drinking water only (Figure 5A). The

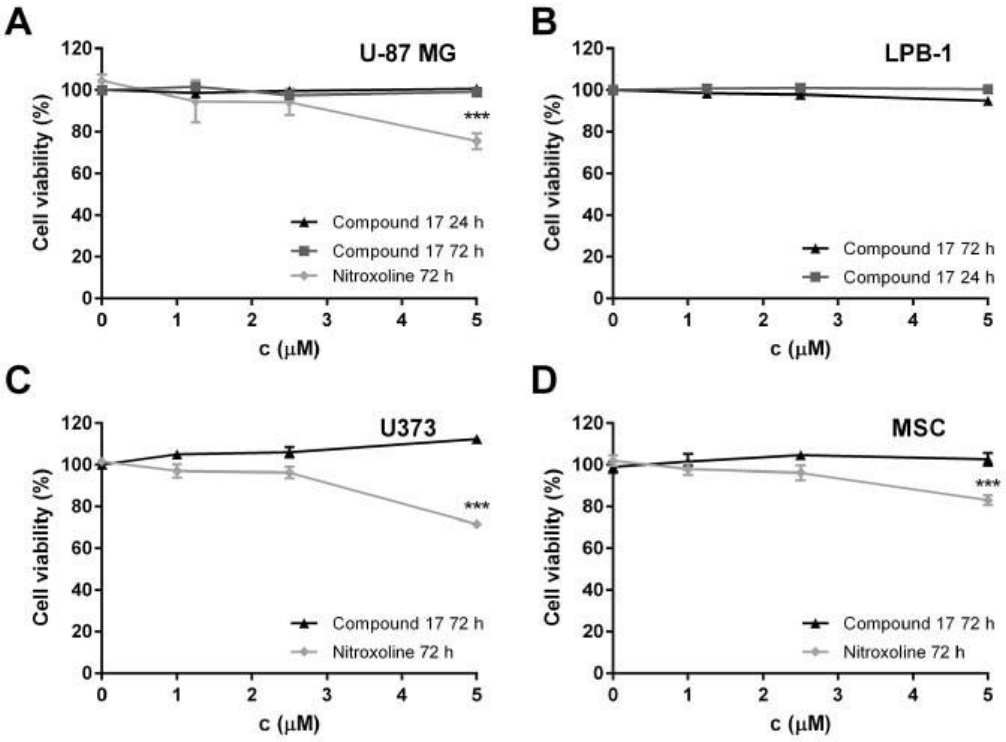


Figure 2: The cytotoxicity of compound 17 on U-87 MG, U373 and LPB-1 cells and mesenchymal stem cells (MCS) as determined by MTS assay. (A) U-87 MG cells (3×10^4 and 5×10^3 for 24 and 72 h, respectively), **(B)** LPB-1 cells (1×10^5 and 2.5×10^3 for 24 and 72 h, respectively), **(C)** U373 cells (3×10^4) and **(D)** MSCs (3×10^4) treated with increasing concentrations of compound 17 and nitroxoline for 24 or 72 h, following addition of MTS reagent. Results are presented as the percentage of viable cells from two independent experiments (mean ± SEM) in the presence of the inhibitor compared to DMSO used as a control. The experiments were performed in quadruplicate. ***$P < 0.001$.

time tumors needed to reach 40 mm^3 was significantly increased by compound 17, but only moderately by nitroxoline treatment (Figure 5B). Similar results were observed for delay of tumor growth, where compound 17 was more effective than nitroxoline (Figure 5B).

Neither compound 17 nor nitroxoline induced any systemic toxicity, as judged by monitoring body weight, behavior and appearance of the mice over the entire course of the experiment.

DISCUSSION

Compound 17 is a product of focused chemical synthesis of nitroxoline derivatives that are based on the crystal structure of nitroxoline-cathepsin B complex [27, 33]. It is nitrile inhibitor that combines nitroxoline scaffold with nitrile fragment connected through amine spacer on position 7 (Figure 6) structure element described as suitable for cysteine cathepsin inhibitors [36]. Due to its potent but reversible inhibition of cathepsin B endopeptidase activity, together with the improved selectivity for cathepsin B with regard to related peptidases cathepsins H and L [33], compound 17 was chosen for further evaluation of its anti-tumor activity *in vitro* and *in vivo*. Compound 17 was shown to reduce tumor cell migration and invasion and tumor growth significantly better than the parent compound nitroxoline.

Cathepsin B is an important tumor promoting enzyme. Its increased expression and activity are associated with various cancer types [37, 38]. Accordingly, to study the effect of compound 17 on tumor cell migration and invasion *in vitro*, we selected cell lines of different origins, all expressing high levels of cathepsin B [20, 39]. Compound 17 was effective in inhibiting tumor cell invasion of the human glioblastoma cells U-87 MG and mouse fibrosarcoma LPB-1 cells (Figure 1). The effect, observed by monitoring tumor invasion in real time on an xCELLigence system, was very pronounced and more reliable than using the end-point approach. Next, compound 17 was evaluated in a 3D invasion assay *in vitro* which, more accurately than the 2D model, reproduces the tumor microenvironment and captures the complexity of tumors [35]. In this assay, both compound 17 and nitroxoline reduced the growth of U-87 MG spheroids in Matrigel (Figure 3). The reason that the effect of both compounds is stronger in a 3D than in a 2D invasion

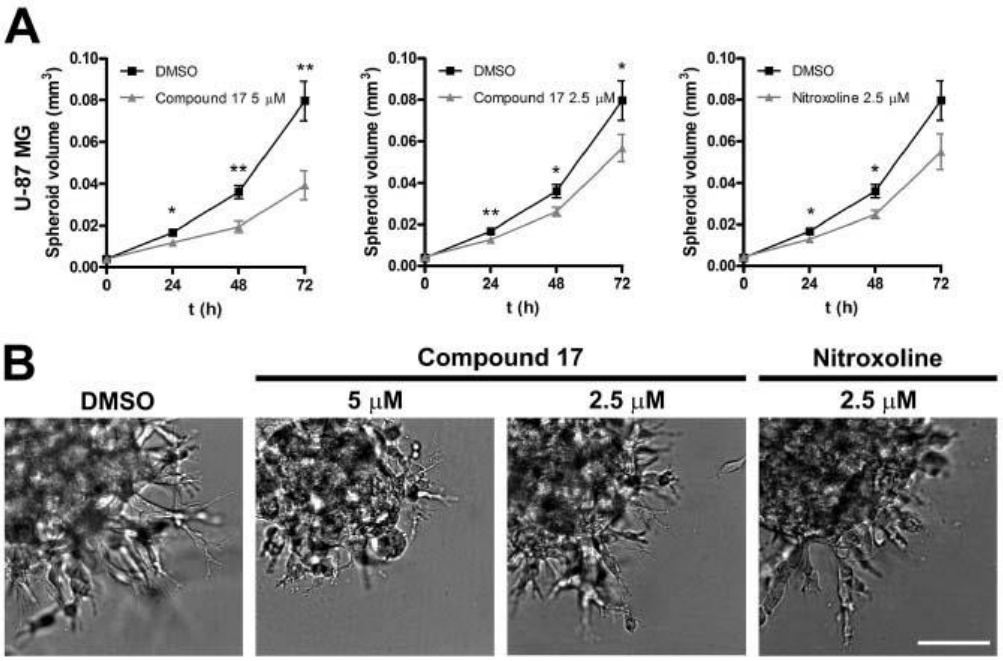


Figure 3: Compound 17 impairs invasion of U-87 MG cells in a 3D *in vitro* model of tumor invasion. **(A)** U-87 MG spheroids were implanted in Matrigel (5 mg/mL) and covered with growth medium. Compound 17 (2.5 μM or 5 μM), nitroxoline (2.5 μM) or DMSO (0.05%) as a control were added to the growth medium and to Matrigel. The spheroid volume was monitored for up to three days by measuring the spheroid dimensions. Data are presented as means ± SEM (n = 3). **(B)** Representative images of U-87 MG spheroids obtained at day three after implantation. Scale bar, 100 μm. * $P < 0.05$, ** $P < 0.01$

model is that the former is more complex and better resembles the *in vivo* situation. The function of cathepsin B is thus more significant, since it could also participate in the degradation of ECM in cell adhesion and signaling [40], these processes being important for cell organization within the spheroids. Taken together, the presented data from independent models of tumor cell invasion show that compound 17, by inhibiting cathepsin B endopeptidase activity, acts as a potent inhibitor of tumor cell invasion *in vitro*.

Another process that is enhanced during tumor progression is cell migration [38]. Therefore, in addition

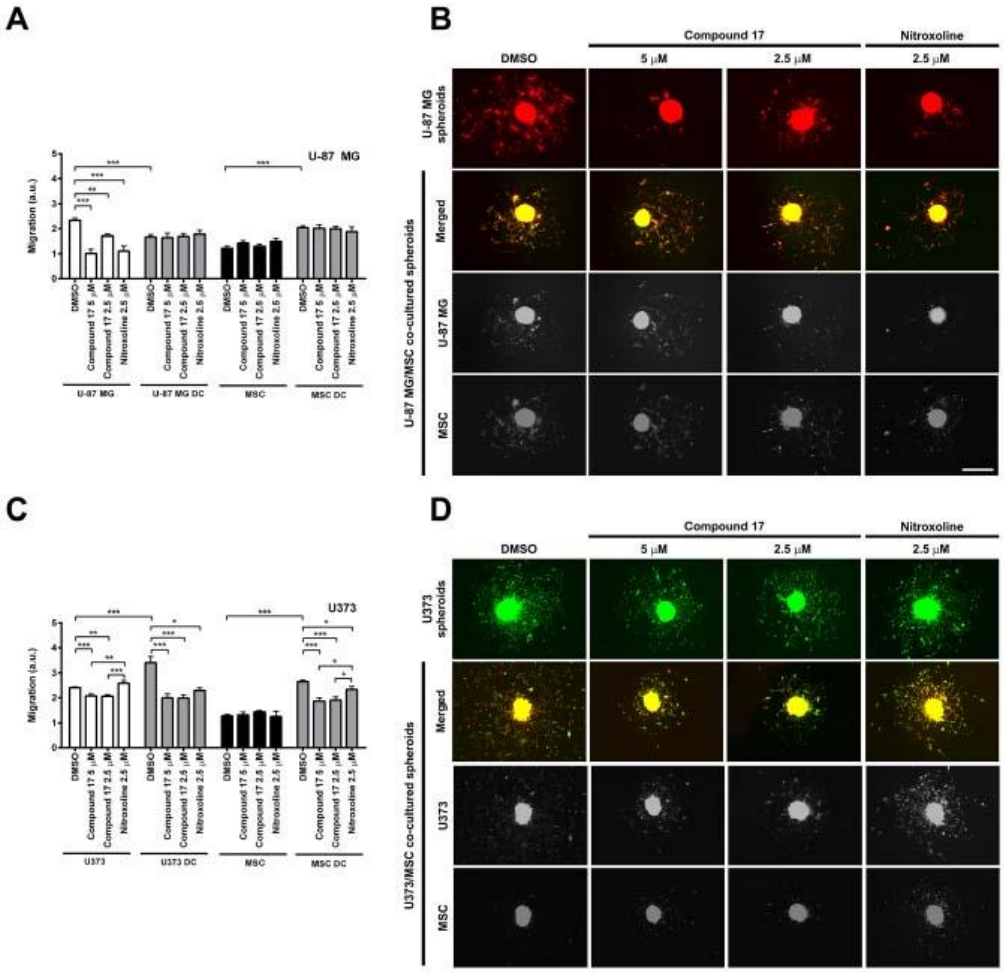


Figure 4: Effects of compound 17 and nitroxoline on the migration of cells out of co-cultured spheroids. (A and C) U-87 MG, U373 or MSC spheroids or MSC/glioblastoma direct co-cultured (DC) spheroids were, after generation, placed in the middle of laminin-coated wells of 96-well plates in medium containing compound 17 (2.5 μM or 5 μM), nitroxoline (2.5 μM) or DMSO (0.1%) as a suitable control. Migration of cells was expressed as relative migration and was assessed on day three. Relative migration was calculated as the ratio of migration distance to spheroid diameter, of MSCs and U-87 MG or U373 cells, respectively, out of monoculture and co-cultured spheroids in presence of compound 17 (2.5 μM or 5 μM), nitroxoline (2.5 μM) or control after 72 h on laminin. Experiments were performed in triplicate and are presented as means ± SEM. **(B and D)** Representative images of cell migration out of spheroids, obtained after 72 h on laminin. U-87 MG cells are red; U373 cells are green. MSCs in U-87 MG/MSC spheroids are green and in U373/MSC spheroids are red. Single-channel images from co-cultured spheroids are displayed in grayscale. Scale bar, 500 μm. Statistical analysis was performed with one-way ANOVA, followed by the Bonferroni post-hoc test. $*P < 0.05$, $**P < 0.01$, $***P < 0.001$

to the growth of spheroids and formation of their invading stands in Matrigel, we evaluated the effects of compound 17 and of nitroxoline on the migration of cells out of spheroids, using two human glioblastoma cell lines, U-87 MG and U373. Both compound 17 and nitroxoline significantly decreased migration of cells out of U-87 MG spheroids, while only compound 17 impaired cell migration out of U373 spheroids (Figure 4). In addition to tumor cells, stromal cells, including mesenchymal stem cells (MSCs), also form a tumor microenvironment and their interactions with tumor cells play a crucial role in tumor progression [41–45]. In the presence of glioblastoma cells, MSCs enhance tumor cell invasion through multiple distant processes, among them peptidase activity regulation [46]. We therefore evaluated the effect of cathepsin B inhibitors, compound 17 and nitroxoline

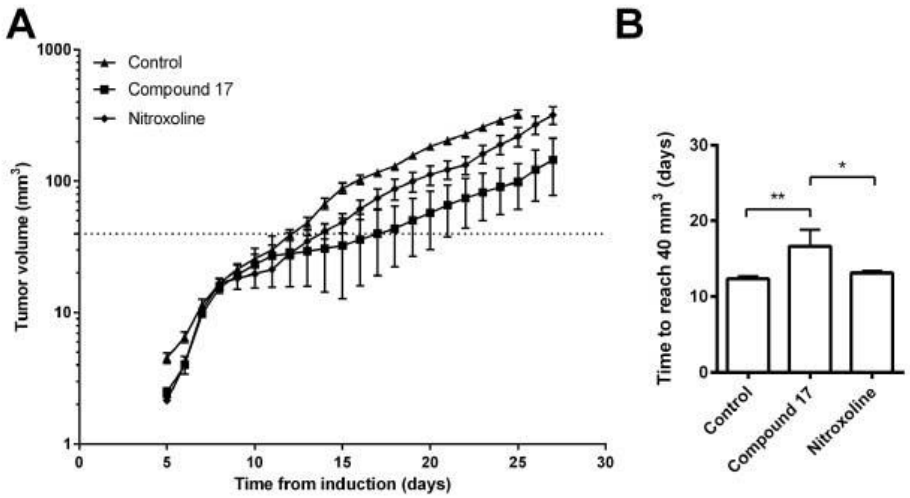
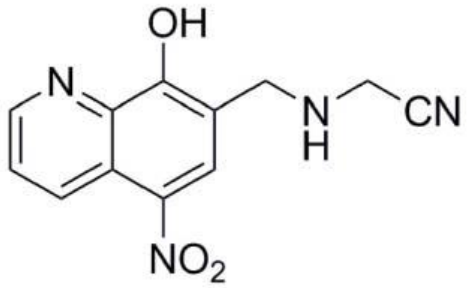


Figure 5: Compound 17 reduces tumor growth in an LPB mouse tumor model. **(A)** LPB cells (1.8×10^6) were injected into the right flank of C57BI/6 mice following treatment with compound 17 or nitroxoline at 20 mg/kg, with drinking water *ad libitum* or, in the case of the control group, with drinking water only for the entire duration of the experiment. The size of LPB-induced tumors was measured every second day. The line indicates a tumor volume of 40 mm^3. **(B)** The time required for tumors to reach a volume of 40 mm^3 representing the tumor growth delay between the experimental and control group, was calculated from the growth curves. Data are presented as means ± SEM. $*P < 0.05$, $**P < 0.01$ as determined with one-way ANOVA.



Compound 17

Figure 6: Chemical structure of 2-{[(8-hydroxy-5-nitroquinoline-7-yl)methyl]amino}-acetonitrile (compound 17).

on the migration of tumor cells out of co-cultured glioblastoma-MSCs spheroids. In U-87 MG/MSC co-cultured spheroids we observed decreased migration of U-87 MG cells out of spheroids and increased MSC migration. However, the addition of either compound 17 or nitroxoline had no effect on the migration of either U-87 MG cells or MSCs out of co-cultured spheroids. On the other hand, when U373/MSC co-cultured spheroids were prepared and studied, the migration of all cells increased and was significantly impaired by compound 17 as well as by nitroxoline. As in U373 monoculture spheroids, compound 17 exhibited a more pronounced inhibition of cell migration than nitroxoline (Figure 4). Our results are in line with the upregulated cathepsin B levels in glioblastoma U373 cells on direct cell-to-cell interactions with MSCs [45, 47]. Besides expression, cathepsin B secretion was also increased in U373/MSC

co-cultured spheroids. Moreover, MSC-mediated invasion of U373 cells decreased after treatment by CA-074Me, a cell permeable analogue of the irreversible cathepsin B inhibitor, CA-074. In contrast, the expression of cathepsin B was not altered in co-cultures of MSCs and other glioblastoma cell line U-87 MG, when compared to U-87 MG monocultures [47].

The anti-cancer properties of compound 17 were further evaluated *in vivo* in an LPB mouse fibrosarcoma tumor model. *Per os* administration of compound 17 reduced the tumor volume and delayed tumor growth (Figure 5). Again, it displayed higher anti-tumor activity than that induced by nitroxoline, since its administration resulted in a significantly greater reduction of tumor volume with prolonged growth delay. Nevertheless, for better assessment of the impact of compound 17 on tumor growth, the concentration of nitroxoline used in this study was just half that used previously [20]. At a higher concentration therefore, it would result in a reduction of tumor growth similar to that in our previous study [20].

Compound 17 is thus shown to be a potent and selective inhibitor of cathepsin B endopeptidase activity and to impair tumor invasion and migration in *in vitro* models, as well as delaying tumor growth in an *in vivo* mouse model. Using focused chemical synthesis, therefore, we have increased the anti-tumor potential of nitroxoline and a novel inhibitor prepared showing more appropriate pharmacological characteristics, making it a promising candidate for further evaluation as an anti-cancer drug.

MATERIALS AND METHODS

Compounds

Compound 17 was synthesized as described [33]. Its purity was determined by ^{1}H NMR and ^{13}C NMR spectroscopy and by CHN elemental analysis. Nitroxoline was obtained from Sigma-Aldrich (St. Louis, MO, USA).

Cell culture

The human glioblastoma cell lines U-87 MG and U373 were obtained from American Type Culture Collection (ATCC, Manassas, VA, USA). The cell lines were authenticated by ATCC and thawed from early passage stocks. The LPB-1 fibrosarcoma cell line [48], a clonal derivative of the methylcholanthrene-induced C57Bl/6 mouse sarcoma tumor, was provided by Jean Jr. Belehradek (Institut Gustave Roussy, Villejuif, France). Human bone marrow-derived MSCs were obtained from Lonza Bioscience (Lot. 6F4393, Walkersville, MD, USA). All cell lines were passaged for fewer than 6 months after thawing. No authentication was done by the authors. U-87 MG cells were cultured in Advanced Dulbecco's Modified Eagle's Medium (DMEM; Gibco, Carlsbad, CA, USA) supplemented with 10% fetal bovine serum (FBS; Gibco), 2 mM glutamine (Sigma-Aldrich) and antibiotics. U373 cells and MSCs were cultured in DMEM supplemented with 10% FBS, 2 mM glutamine, antibiotics, 1 mM Na-pyruvate (Gibco) and non-essential amino acids (Sigma-Aldrich). LPB-1 cells were cultured in Minimum Essential Medium (MEM; Sigma-Aldrich) supplemented with 10% FBS, 2 mM glutamine and antibiotics. U373 cells stably expressing enhanced green fluorescent protein (U373 eGFP cells) and U87 cells expressing red fluorescent protein (dsRED) were prepared as described [45, 49]. The cells were maintained at 37 °C in a humidified atmosphere containing 5% CO_2 until 80% confluent. Prior to their use in the assay, cells were detached from the culture flask using 0.05% trypsin (Gibco) and 0.02% EDTA in phosphate buffered saline (PBS), pH = 7.4.

Cell viability assay

The possible cytotoxic effects of compound 17 and nitroxoline in the cell lines used were determined by MTS [3-(4,5-dimethylthiazol-2-yl)-5-(3-carboxymetoxyphenyl)-2-(4-sulfophenyl)-2H-tetrazolium] colorimetric assay. U-87 MG (3×10^4 and 5×10^3 for 24 and 72 hours respectively), LPB-1 (1×10^5 and 2.5×10^3 for 24 and 72 h, respectively), U373 (3×10^4 cells for 72 h) cells and MSCs (3×10^4 for 72 h) were seeded into wells of a 96-well microplate and allowed to attach overnight. They were then treated with 100 µl of medium containing 1.25, 2.5 or 5 µM of inhibitor or DMSO (0.05%) and incubated for 24 or 72 h. 10 µl of MTS (Promega, Madison, WI, USA) was then added to the walls of a 96-well microplate and, after incubation, absorbance of formazan was measured at 490 nm on a Tecan Safire²™ (Tecan, Mannedorf, Switzerland). Cell viability (%) was expressed as the ratio of absorbance obtained in the presence of compounds to that in DMSO alone. All assays were performed in quadruplicate and repeated twice.

Real-time invasion assay

Tumor cell invasion in real time of U-87 MG and LPB-1 cells was monitored using an xCELLigence RTCA instrument (ACEA Biosciences Inc., San Diego, CA, USA). Before the experiment, the cells were starved of serum for 24 h. First, the bottoms of the wells of a CIM-plate 16 (ACEA Biosciences Inc.) were coated for 30 min with 0.3 µg of fibronectin from bovine plasma (Calbiochem, Darmstadt, Germany). Following coating of the upper compartments of a CIM-plate 16 with 20 µl of Matrigel (2 mg/ml and 1 mg/ml for U-87 MG and LPB-1 cells (BD Biosciences, Franklin Lakes, NJ, USA)) in serum-free medium (SFM). Matrigel was allowed to gel for 20 min at 37 °C. 180 µl of medium containing respective compound (2.5 or 5 µM) or DMSO (0.05 %) as control

was added to the lower compartments and the top and the bottom parts of the CIM-plate 16 were assembled together. Next, 60 µl of SFM, together with the compounds to be tested, were added to the upper compartments. After 1 h incubation at 37°C, 80 µl of U-87 MG or LPB-1 cells (7.5×10^4 or 5×10^4 cells/well for U-87 MG or LPB-1 cells) were seeded in the top chambers of a CIM-plate 16 and placed into the xCELLigence system. The system measures impedance data, reported as cell index (CI), in real time every 15 min during the 72 h course of the experiment. The data were analyzed with the RTCA Software (Roche). The relative invasion (%) was expressed as a percentage of that of control cells treated with DMSO.

Three-dimensional invasion assay

The 3D invasion model is based on implantation of tumor spheroids into Matrigel, representing a model of the ECM (tumor microenvironment). Spheroids were prepared according to the hanging-drop method [35]. Drops (20 µl) of U-87 MG cell suspension (150 cells/drop) were placed on the lids of 100 mm tissue-culture dishes which were then inverted over 10 ml of water. After 5 days, the aggregates formed were transferred to wells of a Lab-Tek™ Chambered Coverglass coated with 70 µl of Matrigel (5 mg/ml) in SFM. Next, a further 70 µl of Matrigel was added to cover the spheroids and, after 20 min incubation at 37°C, 400 µl of complete medium was added. Compounds (2.5 or 5 µM) or DMSO (0.05 %) were added to the Matrigel and the medium. The growth of spheroids was monitored daily for up to three days by measuring the spheroid dimensions under a light microscope, using an ocular micrometer. Spheroid volume was calculated according to the equation: $V = (\pi \times (\text{spheroid length}) \times (\text{spheroid width})^2)/6$. Images of tumor spheroids were obtained using an Olympus IX 81 motorized inverted microscope and Cell^R software (Olympus, Tokyo, Japan).

Migration assay

Cell migration was monitored using fluorescent glioblastoma cells U-87 MG dsRED and U373 eGFP, and MSCs. For separate monitoring of MSCs and glioblastoma cell migration in co-cultured MSC/U-87 MG and MSC/U373 cell spheroids, MSCs were labelled, prior to spheroid formation, with the non-toxic fluorescent dyes Vybrant DiO and Vybrant DiI (Molecular Probes, Eugene, OR, USA) according to the manufacturer's instructions. For co-cultured spheroid formation fluorescent glioblastoma cells and Vybrant-labelled MSCs were mixed together in a 1:1 ratio and seeded, at a density of 2.5×10^3 cells/100 µl in complete growth medium containing 4% methylcellulose, into BD Falcon U-bottom 96-well cell culture plates (BD Biosciences, Franklin Lakes, NJ, USA). They were then centrifuged at 850 x g and 31°C for 90 min and then incubated overnight. For the migration assay, 96-well plates (Corning, Corning, NY, USA) were coated with laminin (2 µg/cm², Sigma-Aldrich) for 2 h at 37°C and washed twice with PBS. U-87 MG, U373 and MSC spheroids from monoculture and co-cultured spheroids were then placed in the middle of each well in 100 µL of growth medium. Compounds (2.5 or 5 µM) or DMSO (0.1%) were added to the culture medium. The cell migration was monitored for up to 3 days under a Nikon Eclipse Ti-E fluorescence inverted microscope (40× magnification, Nikon, Tokyo, Japan). The migration ability of the cells (relative migration) was assessed on day 3 and defined as the distance measured from the edge of the spheroid to the most distant cell population divided by the spheroid diameter.

Mouse tumor models

Ethics statement

Animal studies were carried out in accordance with EU guidelines and with permission from the Veterinary Administration of the Ministry of Agriculture, Forestry and Food of the Republic of Slovenia (permission number: U34401-14/2014/4). Mice were housed in a specific-pathogen-free animal colony at controlled temperature and humidity with a 12 h light/dark cycle. Food and water were provided *ad libitum*.

LPB mouse fibrosarcoma tumor model

The effect of compounds on tumor growth *in vivo* was observed in C57Bl/6 female mice, 8 to 12 weeks old. 1.8×10^6 LPB fibrosarcoma cells, in 100 µL of 0.9% NaCl, were injected subcutaneously into the right flank of each mouse. In the experimental group, mice were given a solution of compound 17 (n = 7, 20 mg/kg) or nitroxoline (n = 12, 20 mg/kg – half the dose used in the previous study [20]) in their drinking water *ad libitum* for the entire duration of the study (27 days). The bottle with fresh solution of the compounds was provided every fourth day. The control group (n = 11) received drinking water only. The dose of inhibitor received was calculated from the volume of the consumed solution per mouse provided prior the beginning of the study (2.8 ± 0.1 ml). Tumor growth was determined every 2 to 3 days from the fifth day after the induction of tumors, using a digital Vernier caliper. The tumors were measured in three perpendicular directions (a, b, c) and tumor volume was calculated as $V = a \times b \times c \times \Pi/6$. The tumor growth curves were used to determine the time required to reach a volume of 40 mm³. Tumor growth delay was determined as the difference between the time required for tumors to reach a volume of 40 mm³ in the experimental and in the control groups. The weight, behavior and appearance of the mice, using a scoring system, were followed as a general indicator of systemic toxicity.

Statistical analysis

The GraphPad Prism 6.0 software package was used for data analysis. Data are presented as means ± SEM unless stated otherwise. The statistical significance of the differences between groups of data was evaluated using nonparametric, two-tailed Student's t test, unless stated otherwise. Differences were considered significant at $P \leq 0.05$.

Abbreviations

CI: cell index; DMSO: dimethyl sulfoxide; ECM: extracellular matrix; MSC: mesenchymal stem cell; MTS: [3-(4,5-dimethylthiazol-2-yl)-5-(3-carboxymetoxyphenyl)-2-(4-sulfophenyl)-2H-tetrazolium]; 2D: two-dimensional; 3D: three-dimensional.

Author contributions

A.M., Š.K., U.L.T., B.B., S.K., B.M., T.L., M.Č., G.S. and J.K. conceived and designed the experiments. A.M., Š.K., U.L.T., B.B. and S.K. performed the experiments and analyzed the data. I.S. and S.G. synthetized the inhibitor. A.M. and J.K. prepared the manuscript. All authors reviewed the manuscript.

ACKNOWLEDGMENTS

The authors thank prof. Roger Pain for critical reading of the manuscript.

CONFLICTS OF INTEREST

The authors declare no potential conflicts of interest.

FINANCIAL SUPPORT

This work was supported by the Slovenian Research Agency (grant numbers J4-5529 and P4-0127 to J.K. and Z1-7181 to I.S.).

REFERENCES

1. Mohamed MM, Sloane BF. Cysteine cathepsins: multifunctional enzymes in cancer. Nat Rev Cancer. 2006; 6: 764–75. https://doi.org/ 10.1038/nrc1949.
2. Kos J, Mitrović A, Mirković B. The current stage of cathepsin B inhibitors as potential anticancer agents. Future Med Chem. 2014; 6: 1355–71. https://doi.org/ 10.4155/fmc.14.73.
3. Vasiljeva O, Reinheckel T, Peters C, Turk D, Turk V, Turk B. Emerging roles of cysteine cathepsins in disease and their potential as drug targets. Curr Pharm Des. 2007; 13: 387–403.
4. Joyce JA, Hanahan D. Multiple roles for cysteine cathepsins in cancer. Cell Cycle. 2004. p. 1516–9. https://doi.org/ 10.4161/cc.3.12.1289.
5. Skrzydlewska E, Sulkowska M, Koda M, Sulkowski S. Proteolytic-antiproteolytic balance and its regulation in carcinogenesis. World Journal of Gastroenterology Mar 7, 2005 p. 1251–66.
6. Roshy S, Sloane BF, Moin K. Pericellular cathepsin B and malignant progression. Cancer Metastasis Rev. 2003; 22: 271–86.
7. Buck MR, Karustis DG, Day NA, Honn K V, Sloane BF. Degradation of extracellular-matrix proteins by human cathepsin B from normal and tumour tissues. Biochem J. 1992; 282: 273–8.
8. Premzl A, Zavašnik-Bergant V, Turk V, Kos J. Intracellular and extracellular cathepsin B facilitate invasion of MCF-10A neoT cells through reconstituted extracellular matrix *in vitro*. Exp Cell Res. 2003; 283: 206–14. https://doi.org/ 10.1016/S0014-4827(02)00055-1.
9. Mirković B, Premzl A, Hodnik V, Doljak B, Jevnikar Z, Anderluh G, Kos J. Regulation of cathepsin B activity by 2A2 monoclonal antibody. FEBS J. 2009; 276: 4739–51. https://doi.org/ 10.1111/j.1742-4658.2009.07171.
10. Kostoulas G, Lang A, Nagase H, Baici A. Stimulation of angiogenesis through cathepsin B inactivation of the tissue inhibitors of matrix metalloproteinases. FEBS Lett. 1999; 455: 286–90. https://doi.org/ 10.1016/S0014-5793(99)00897-2.
11. Premzl A, Turk V, Kos J. Intracellular proteolytic activity of cathepsin B is associated with capillary-like tube formation by endothelial cells *in vitro*. J Cell Biochem. 2006; 97: 1230–40. https://doi.org/ 10.1002/jcb.20720.
12. Cavallo-Medved D, Rudy D, Blum G, Bogyo M, Caglic D, Sloane BF. Live-cell imaging demonstrates extracellular matrix degradation in association with active cathepsin B in caveolae of endothelial cells during tube formation. Exp Cell Res. 2009; 315: 1234–46. https://doi.org/ 10.1016/j.yexcr.2009.01.021.
13. Barrett AJ, Kirschke H. Cathepsin B, Cathepsin H, and Cathepsin L. Methods Enzymol. 1981; 80 Pt C: 535–61. https://doi.org/ 10.1016/S0076-6879(81)80043-2.
14. Illy C, Quraishi O, Wang J, Purisima E, Vernet T, Mort JS. Role of the occluding loop in cathepsin B activity. J Biol Chem. 1997; 272: 1197–202. https://doi.org/ 10.1074/jbc.272.2.1197.
15. Musil D, Zucic D, Turk D, Engh RA, Mayr I, Huber R, Popovic T, Turk V, Towatari T, Katunuma N. The refined 2.15 A X-ray crystal structure of human liver cathepsin B: the structural basis for its specificity. EMBO J. 1991; 10: 2321–30.
16. Nägler DK, Storer AC, Portaro FC V., Carmona E, Juliano L, Ménard R. Major increase in endopeptidase activity of human cathepsin B upon removal of occluding loop contacts. Biochemistry. American Chemical Society; 1997; 36: 12608–15. https://doi.org/ 10.1021/bi971264+.
17. Krupa JC, Hasnain S, Nägler DK, Ménard R, Mort JS. S2' substrate specificity and the role of His110 and His111 in the exopeptidase activity of human cathepsin B. Biochem J. 2002; 361: 613–9. https://doi.org/ 10.1042/0264-6021:3610613.

18. Almeida PC, Nantes IL, Chagas JR, Rizzi CC, Faljoni-Alario a, Carmona E, Juliano L, Nader HB, Tersariol IL. Cathepsin B activity regulation. Heparin-like glycosaminogylcans protect human cathepsin B from alkaline pH-induced inactivation. J Biol Chem. 2001; 276: 944–51. https://doi.org/ 10.1074/jbc.M003820200.
19. Mitrović A, Mirković B, Sosič I, Gobec S, Kos J. Inhibition of endopeptidase and exopeptidase activity of cathepsin B impairs extracellular matrix degradation and tumour invasion. Biol Chem. 2016; 397: 165–74. https://doi.org/ 10.1515/hsz-2015-0236.
20. Mirković B, Markelc B, Butinar M, Mitrović A, Sosič I, Gobec S, Vasiljeva O, Turk B, Čemažar M, Serša G, Kos J. Nitroxoline impairs tumor progression *in vitro* and *in vivo* by regulating cathepsin B activity. Oncotarget. 2015; 6: 19027–42.
21. Schmitz J, Beckmann A-M, Dudic A, Li T, Sellier R, Bartz U, Gütschow M. 3-Cyano-3-aza-β-amino Acid Derivatives as Inhibitors of Human Cysteine Cathepsins. ACS Med Chem Lett. American Chemical Society; 2014; 5: 1076–81. https://doi.org/ 10.1021/ml500238q.
22. Schmitz J, Li T, Bartz U, Gütschow M. Cathepsin B Inhibitors: Combining Dipeptide Nitriles with an Occluding Loop Recognition Element by Click Chemistry. ACS Med Chem Lett. 2016; 7: 211–6. https://doi.org/ 10.1021/acsmedchemlett.5b00474.
23. Pan X, Tan N, Zeng G, Zhang Y, Jia R. Amentoflavone and its derivatives as novel natural inhibitors of human Cathepsin B. Bioorg Med Chem. 2005; 13: 5819–25. https://doi.org/ 10.1016/j.bmc.2005.05.071.
24. Zeng GZ, Pan XL, Tan NH, Xiong J, Zhang YM. Natural biflavones as novel inhibitors of cathepsin B and K. Eur J Med Chem. 2006; 41: 1247–52. https://doi.org/ 10.1016/j.ejmech.2006.06.002.
25. Schenker P, Alfarano P, Kolb P, Caflisch A, Baici A. A double-headed cathepsin B inhibitor devoid of warhead. Protein Sci. 2008; 17: 2145–55. https://doi.org/ 10.1110/ps.037341.108.
26. Sosič I, Mirković B, Turk S, Štefane B, Kos J, Gobec S. Discovery and kinetic evaluation of 6-substituted 4-benzylthio-1,3,5-triazin-2(1H)-ones as inhibitors of cathepsin B. Eur J Med Chem. 2011; 46: 4648–56. https://doi.org/ 10.1016/j.ejmech.2011.08.005.
27. Mirković B, Renko M, Turk S, Sosič I, Jevnikar Z, Obermajer N, Turk D, Gobec S, Kos J. Novel mechanism of cathepsin B inhibition by antibiotic nitroxoline and related compounds. ChemMedChem. 2011; 6: 1351–6. https://doi.org/ 10.1002/cmdc.201100098.
28. Shim JS, Matsui Y, Bhat S, Nacev BA, Xu J, Bhang HEC, Dhara S, Han KC, Chong CR, Pomper MG, So A, Liu JO. Effect of nitroxoline on angiogenesis and growth of human bladder cancer. J Natl Cancer Inst. 2010; 102: 1855–73. https://doi.org/ 10.1093/jnci/djq457.
29. Lazovic J, Guo L, Nakashima J, Mirsadraei L, Yong W, Kim HJ, Ellingson B, Wu H, Pope WB. Nitroxoline induces apoptosis and slows glioma growth *in vivo*. Neuro Oncol. 2015; 17: 53–62. https://doi.org/ 10.1093/neuonc/nou139.
30. Zhang QI, Wang S, Yang D, Pan K, Li L, Yuan S. Preclinical pharmacodynamic evaluation of antibiotic nitroxoline for anticancer drug repurposing. Oncol Lett. 2016; 11: 3265–72. https://doi.org/ 10.3892/ol.2016.4380.
31. Chang W-L, Hsu L-C, Leu W-J, Chen C-S, Guh J-H. Repurposing of nitroxoline as a potential anticancer agent against human prostate cancer: a crucial role on AMPK/mTOR signaling pathway and the interplay with Chk2 activation. Oncotarget. 2015; 6: 39806–20. https://doi.org/ 10.18632/oncotarget.5655.
32. Mao H, Du Y, Zhang Z, Cao B, Zhao J, Zhou H, Mao X. Nitroxoline shows antimyeloma activity by targeting the TRIM25/p53 axle. Anticancer Drugs. 2017; 28: 376–83. https://doi.org/ 10.1097/CAD.0000000000000466.
33. Sosič I, Mirković B, Arenz K, Štefane B, Kos J, Gobec S. Development of new cathepsin B inhibitors: Combining bioisosteric replacements and structure-based design to explore the structure-activity relationships of nitroxoline derivatives. J Med Chem. 2013; 56: 521–33. https://doi.org/ 10.1021/jm301544x.
34. Eisenberg MC, Kim Y, Li R, Ackerman WE, Kniss DA, Friedman A. Mechanistic modeling of the effects of myoferlin on tumor cell invasion. Proceedings of the National Academy of Sciences. 2011. p. 20078–83. https://doi.org/ 10.1073/pnas.1116327108.
35. Kelm JM, Timmins NE, Brown CJ, Fussenegger M, Nielsen LK. Method for generation of homogeneous multicellular tumor spheroids applicable to a wide variety of cell types. Biotechnol Bioeng. 2003; 83: 173–80. https://doi.org/ 10.1002/bit.10655.
36. Frizler M, Lohr F, Lülsdorff M, Gütschow M. Facing the gem-dialkyl effect in enzyme inhibitor design: preparation of homocycloleucine-based azadipeptide nitriles. Chemistry. 2011; 17: 11419–23. https://doi.org/ 10.1002/chem.201101350.
37. Kos J, Lah TT. Cysteine proteinases and their endogenous inhibitors: Target proteins for prognosis, diagnosis and therapy in cancer (review). Oncology Reports. 1998. p. 1349–61.
38. Aggarwal N, Sloane BF. Cathepsin B: Multiple roles in cancer. Proteomics - Clin Appl. 2014; 8: 427–37. https://doi.org/ 10.1002/prca.201300105.
39. Gole B, Huszthy PC, Popović M, Jeruc J, Ardebili YS, Bjerkvig R, Lah TT. The regulation of cysteine cathepsins and cystatins in human gliomas. Int J cancer. 2012; 131: 1779–89. https://doi.org/ 10.1002/ijc.27453.
40. Pišlar A, Perišić Nanut M, Kos J. Lysosomal cysteine peptidases – molecules signaling tumor cell death and survival. Semin Cancer Biol. 2015;. https://doi.org/ 10.1016/j.semcancer.2015.08.001.
41. Hanahan D, Weinberg RA. Hallmarks of cancer: The next generation. Cell. Elsevier Inc.; 2011. p. 646–74. https://doi.org/ 10.1016/j.cell.2011.02.013.

42. Motaln H, Turnsek TL. Cytokines play a key role in communication between mesenchymal stem cells and brain cancer cells. Protein Pept Lett. 2015; 22: 322–31.

43. Sloane BF, Yan S, Podgorski I, Linebaugh BE, Cher ML, Mai J, Cavallo-Medved D, Sameni M, Dosescu J, Moin K. Cathepsin B and tumor proteolysis: Contribution of the tumor microenvironment. Semin Cancer Biol. 2005; 15: 149–57. https://doi.org/ 10.1016/j.semcancer.2004.08.001.

44. Joyce JA, Pollard JW. Microenvironmental regulation of metastasis. Nat Rev Cancer. 2009; 9: 239–52. https://doi.org/ 10.1038/nrc2618.

45. Schichor C, Albrecht V, Korte B, Buchner A, Riesenberg R, Mysliwietz J, Paron I, Motaln H, Turnšek TL, Jürchott K, Selbig J, Tonn J-C. Mesenchymal stem cells and glioma cells form a structural as well as a functional syncytium *in vitro*. Exp Neurol. 2012; 234: 208–19. https://doi.org/ 10.1016/j.expneurol.2011.12.033.

46. Swamydas M, Ricci K, Rego SL, Dréau D. Mesenchymal stem cell-derived CCL-9 and CCL-5 promote mammary tumor cell invasion and the activation of matrix metalloproteinases. Cell Adh Migr. 2013; 7: 315–24. https://doi.org/ 10.4161/cam.25138.

47. Breznik B, Motaln H, Vittori M, Rotter A, Lah Turnšek T, Breznik B, Motaln H, Vittori M, Rotter A, Lah Turnšek T. Mesenchymal stem cells differentially affect the invasion of distinct glioblastoma cell lines. Oncotarget. Impact Journals; 2017; 5. https://doi.org/ 10.18632/oncotarget.16041.

48. Belehradek J, Barski G, Thonier M. Evolution of cell-mediated antitumor immunity in mice bearing a syngeneic chemically induced tumor. Influence of tumor growth, surgical removal and treatment with irradiated tumor cells. Int J cancer. 1972; 9: 461–9.

49. Pillat MM, Oliveira MN, Motaln H, Breznik B, Glaser T, Lah TT, Ulrich H. Glioblastoma-mesenchymal stem cell communication modulates expression patterns of kinin receptors: Possible involvement of bradykinin in information flow. Cytometry A. 2016; 89: 365–75. https://doi.org/ 10.1002/cyto.a.22800.

2.5 Cathepsins K and X in Glioblastoma Progression and Survival (in Revision)

Barbara Breznik, Clara Limback, Andrej Porčnik, Andrej Blejec, Miha Koprivnikar Krajnc, Roman Bošnjak, Janko Kos, Cornelis J.F. Van Noorden, Tamara Lah Turnšek

In revision in International Journal of Molecular Sciences (Glioma invasion special issue)

International Journal of *Molecular Sciences*

MDPI

Research Article

Cathepsins K and X in glioblastoma progression and survival

Barbara Breznik [1,*], Clara Limback [2], Andrej Porčnik [3], Andrej Blejec [4], Miha Koprivnikar Krajnc [5], Roman Bošnjak [6], Janko Kos [7], Cornelis J.F. Van Noorden [8] and Tamara Lah Turnšek [9,*]

[1] *Department of Genetic Toxicology and Cancer Biology, National Institute of Biology, Ljubljana, Slovenia, and International Postgraduate School Jozef Stefan, Ljubljana, Slovenia; barbara.breznik@nib.si*
[2] *Faculty of Medicine, Imperial College London, UK, and Department of Histopathology, Charing Cross Hospital, London, UK; clara.limback-stanic@nhs.net*
[3] *Department of Neurosurgery, University Clinical Centre Ljubljana, Slovenia; andrej.porcnik@ukclj.si*
[4] *Department of Organisms and Ecosystems Research, National Institute of Biology, Ljubljana, Slovenia; andrej.blejec@nib.si*
[5] *Department of Genetic Toxicology and Cancer Biology, National Institute of Biology, Ljubljana; mkoprivnikarkrajnc@gmail.com*
[6] *Department of Neurosurgery, University Clinical Centre Ljubljana, Slovenia; roman.bosnjak@kclj.si*
[7] *Department of Pharmaceutical Biology, Faculty of Pharmacy, University of Ljubljana, Slovenia, and Department of Biotechnology, Jozef Stefan Institute, Ljubljana, Slovenia; janko.kos@ffa.uni-lj.si*
[8] *Cancer Center Amsterdam, Department of Medical Biology at the Academic Medical Center, Amsterdam, The Netherlands; c.j.vannoorden@amc.uva.nl*
[9] *Department of Genetic Toxicology and Cancer Biology, National Institute of Biology, Ljubljana, Slovenia, and International Postgraduate School Jozef Stefan, Ljubljana, Slovenia; tamara.lah@nib.si*
* Correspondence: barbara.breznik@nib.si, tamara.lah@nib.si; Tel.: +386 59 232 870, +386 59 232 703

Academic Editor: name
Received: date; Accepted: date; Published: date

Abstract: The spread of glioblastoma is characterized by early invasion of cancer cells into the brain parenchyma, preventing complete tumor eradication. Cysteine cathepsins B, S and L have been found to be overexpressed in glioblastoma, but until recently cathepsin K and in particular cathepsin X have not been associated with glioma malignancy. In this study using public transcriptomic datasets of glioblastoma, gene expression of both cathepsins K and X tissue were found to increase with tumor progression, in particular in the mesenchymal glioblastoma subtype, as compared to normal brain. We also demonstrated that cathepsins K and X proteins were highly and heterogeneously expressed in serial sections of 21 human glioblastoma samples. With respect to the survival prediction, high cathepsin X mRNA expression correlated with poorer survival, but its high protein expression did not. No association was found between cathepsin K mRNA expression and glioblastoma patient's survival, with the exception of high cathepsin K mRNA expression in the proneural glioblastoma subtype, which was significantly related with lower survival. High cathepsins K and X immunolocalization was observed in CD133-, SDF-1α- and CD68-positive glioblastoma stem cell niche regions around arterioles and cathepsins K and X mRNA expression correlated with mRNA expression of niche markers, indicating a specific role in glioblastoma stem cell regulation.

Keywords: cathepsins; glioblastoma; immunohistochemistry; survival; stem cell niches

1. Introduction

Glioblastoma (GBM, WHO grade IV) is the most aggressive and also most common primary brain tumor [1]. Despite modern treatment strategies, such as surgical removal of the tumor and radio- and chemotherapy, GBM is characterized by a 5-year survival rate of 5 % and a mean survival

after diagnosis of approximately 1.4 years [2]. The poor survival rates are due to extensive tumoral heterogeneity as well as due to the single GBM cell invasion into the surrounding brain parenchyma, both being responsible for the recurrence of the disease [3,4]. Thus, numerous research groups are focusing on finding new biomarkers to target and develop better biological treatment approaches to improve the patients' survival.

The invasive intracranial spread of GBM cells is tightly associated with production and secretion of proteolytic enzymes [5], including lysosomal cysteine cathepsins, belonging to the C1A family of papain-like proteases [6,7]. The cysteine cathepsin family comprises of 11 proteases, that are active by the same proteolytic mechanism and share several structural elements (Figure S1), although these proteases have distinct conformations and catalytic activity (Figure S1) and are different with respect to their distribution and physiological roles. Cathepsins also play distinct roles in cancer progression, including invasion, the development of therapeutic resistance [8] and apoptosis [9]. Besides the hydrolysis of selective proteins, cysteine cathepsins participate in proteolytic cascades, where one protease activates one or several others in sequences that finally regulate hydrolysis of peptide and protein substrates, which may affect pathobiological functions, what we call protease signaling [10]. For example, serine proteases play dominant roles in invasion cascades. Meanwhile, cathepsin B primarily contributes to induction of migration of GBM cells into the loose extracellular matrix (ECM) in the brain. In addition, extracellular cathepsins modify the GBM microenvironment by shedding cell-cell adhesion molecules and processing relevant cytokines and growth factors to enhance tumor progression [8, 10,11]. In contrast, cathepsins may also possess tumor-suppressive roles [12]. These conflicting roles depend on the context, which emphasizes the importance of *in vivo* analyses to understand functions of the cathepsins in GBM pathobiology [13]. We have extensively investigated expression of cathepsins B, L an S at gene and protein levels [14,15] and found considerable differences in the correlation between expression of these three cathepsins and specific end-points of glioma progression. For example, cathepsin B is undoubtedly involved in GBM cell invasion [7], whereas the nuclear fraction of cathepsin L plays a role in apoptotic threshold regulation in GBM cells [9]. Cathepsin S has also been proven to contribute to glioma progression *in vitro* [16], although its inhibition did not impair GBM cell invasion [7]. Very little is known about the expression and the role of other cathepsins, such as K and X, in GBM progression.

Cathepsin K has been recently identified as one of the highest differentially-expressed proteases in GBM tissue/cell lines as compared to normal counterparts [17]. Cathepsin K belongs to the cathepsin L-like cluster of the C1A family. Highly-positive charged basic residues in its structure allow allosteric accommodation of negatively-charged resident glycosaminoglycans (GAGs), enabling formation of complexes with unique collagenolytical activity, and unwinding of triple helical collagens [18], thereby participating in ECM destruction, in particular in bone metastasis [19]. Cathepsin K as a monomer also degrades growth factors and chemokines, such as SDF-1α [20,21], thereby indirectly affecting signaling pathways and migration.

The structure and activity of cathepsin X (also called cathepsin Z) show several unique features that distinguish it from other cysteine cathepsins [22]. Cathepsin X exhibits solely carboxypeptidase activity and is activated by other lysosomal endopeptidases. Cathepsin X expression seems to be restricted to cells of immune system, regulating their proliferation, maturation, migration, adhesion, phagocytosis and signal transduction [23]. Various molecular targets of cathepsin X exopeptidase activity have been identified, including the β-chain of integrin receptors, y-enolase, profilin-1, chemokine SDF-1α and others. However, cathepsin X has been detected in the brain, localized in neurons, glial cells and ependymal cells [22, 24]. Increased cathepsin X expression has been associated with various types of cancer, such as lung, colorectal and gastric cancers [25-27].

Some studies have reported that cathepsins are involved in migration and self-renewal of tumor-initiating and therapy-resistant subpopulation of GBM stem cells (GSCs) [28,29]. The GSC stemness and malignancy is maintained in specific microenvironments, so-called GSC niches, where these cells are protected from the immune system and therapy [4,30,31]. The final goal of GSC niche targeting as a new anti-GBM approach is to disintegrate the GSC niches and by that to increase GBM therapeutic sensitivity. Since cathepsins are potent modifiers of tumor microenvironment, we

speculate that they exert specific functions in GSC niche regions by modifying ECM and processing of cytokines/growth factors.

Our aim was to explore the expression patterns of two tumor stroma remodeling cathepsins, K and X, in GBM tissue at the gene and protein levels. At the transcriptome level, the data were obtained from publicly available databases. To explore cathepsins' protein levels, immunohistochemistry was performed on serial sections of 21 human GBM patients. We were also interested whether the expression of cathepsins K and X is associated with survival of GBM patients. At the end, we selected several known GSC markers and those associated with peri-ateriolar GSC niche [21,32] to localize cathepsins K and X in these specific tumor tissue regions and to correlate cathepsins expression with GSC niche markers expression in GBM samples. This would give a hint to explain one of the possible roles of these two cathepsins in GBM malignancy.

2. Results

2.1. mRNA expression of cathepsins K and X is up-regulated in GBM, as compared to gliomas of lower grades and normal brain tissue

To explore the mRNA level of cathepsins K and X in gliomas of different grades, we compared the expression of both cathepsins in GBM vs. lower grade gliomas II and III, as well as in GBM vs. normal brain tissue in public transcriptomic datasets (The Cancer Genom Atlas –TCGA) using the GlioVis data portal [33]. We found higher cathepsins mRNA expression in grade IV glioma than in lower-grade gliomas II and III (Figure 1A, D) and higher cathepsin K and X mRNA expression in GBM compared to normal brain (Figure 1B, E). Furthermore, we observed overexpression of both cathepsins in the mesenchymal subtype (Figure 1C, F), which has been reported as therapy resistant and more aggressive subtype of GBM [34]. In contrast, the mRNA expression of cathepsins K and X was the lowest in the classical and proneural GBM subtype (Figure 1C, F).

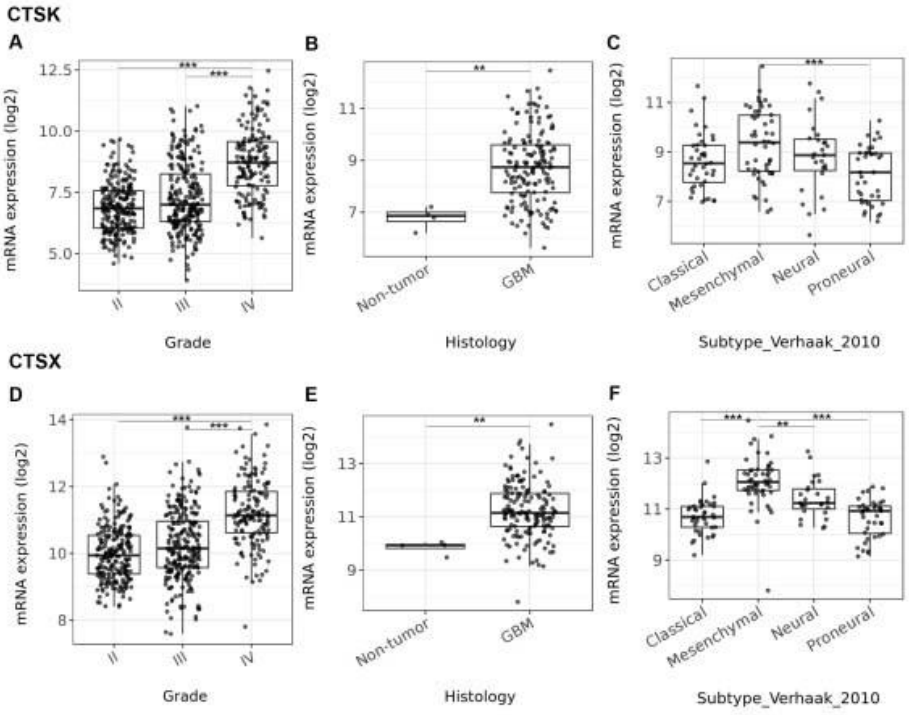
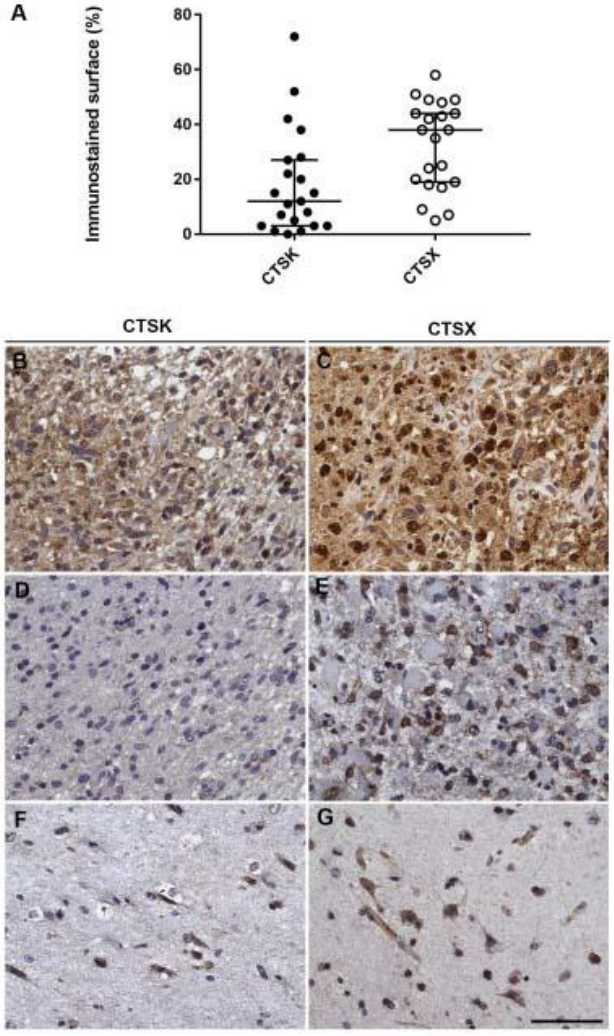


Figure 1. mRNA expression of cathepsins K and X in gliomas of different grades and GBM subtypes. Public transcriptomic datasets were used as described in Materials and Methods. Higher cathepsin K mRNA expression was found in grade IV glioma vs. grade II and III glioma (A), in GBM vs. normal brain

126 (B), and in the mesenchymal subtype of GBM vs. classical, proneural and neural subtypes, classified
127 according to Verhaak et al. [35] (C). Higer cathepsin X expression was found in grade IV glioma vs. grade
128 II and III glioma (D), in GBM vs. normal brain (E), and in the mesenchymal subtype of GBM (F). Boxplots
129 show the distribution of mRNA expression (log2) in different glioma grades and GBM. Data were retrieved
130 from GlioVis portal [33]. The significance was set at $p < 0.01$ (**), $p < 0.001$ (***).

131 *2.2. Inter- and intratumoral heterogeneity of cathepsins K and X expression in GBM tissues*

132 In order to determine protein expression of cathepsins K and X in GBM, we performed
133 immunohistochemistry on serial paraffin-embedded sections in a cohort of 21 GBM samples. The
134 quantification was carried out as described in Materials and Methods. We observed that the
135 expression of cathepsin X in GBM tissue was higher (38.0 % of immunostained areas), compared to
136 that of cathepsin K (11.6 % of immunostained areas) (Figure 2A). Moreover, the expression of both
137 cathepsins was highly heterogeneous among the tumors as well as within the same tumor (Figure
138 2B-E). Cathepsins K and X protein expression was detected in cancer cells and non-cancer cells of
139 the tumor microenvironment. Moreover, protein expression of both cathepsins was observed in the
140 cells of normal tissue around the GBM tumors (Figure 2F, G).



141

Figure 2. Cathepsin K and X immunohistochemical staining in serial paraffin-embedded GBM sections. The expression of cathepsins K and X in 21 GBM samples, quantified as percentage (%) of immunostained areas (A). Box plots show the distribution of cathepsins expression in GBMs. Heterogeneous imunohistochemical signal in different parts of the same GBM section for cathepsin K (panels B, D) and for cathepsin X (C, E). Cathepsin K (F) and cathepsin X (G) expression was present in specific cells in normal brain tissue of GBM patients. These cells were not further identified. Immunohistochemical labelling of cathepsins was performed with DAB as substrate (brown color). Cell nuclei were stained using hematoxylin (purple), as described in Materials and Methods. Scale bar = 50 μm.

2.3. *Predictive value of cathepsins K and X mRNA expression is GBM subtype dependent*

To evaluate the predictive value of cathepsins K and X at the mRNA level in GBM, we performed Kaplan-Maier survival analysis, using public GBM cDNA microarray datasets. Cathepsin K mRNA expression did not correlate with survival of all GBM patients. When the GBMs were stratified into different subtypes, we still did not find a correlation of cathepsin K mRNA expression and the patinet survival in classical and mesenchymal subtypes. However, in the proneural subtype, cathepsin K expression had a potential predictive value (median survival being 8.9 months for CTSK high-expressing tumors and 21.9 months for CTSK low-expressing tumors, p = 0.062 by log-rank and P = 0.011 by Wilcoxons' analysis) (Figure S2). In contrast, significant differences in survival were found for GBMs expressing different mRNA levels of cathepsin X, with Kaplan-Meier estimates of median survival being 11.8 months for high cathepsin X tumors and 14.9 months for low cathepsin X tumors (log-rank p = 0.027) (Figure 3B). This correlation was dependent on GBM subtype (Figure 3C), as high mRNA level of cathepsin X correlated with the shorter survival of GBM patients of the classical subtype (median survival being 10.8 months for CTSX high-expressing tumors and 15.8 months for CTSX low-expressing tumors, log-rank p = 0.049). In mesenchymal and proneural GBM subtypes, the cathepsin X mRNA expression did not have predictive value (Figure 3C).

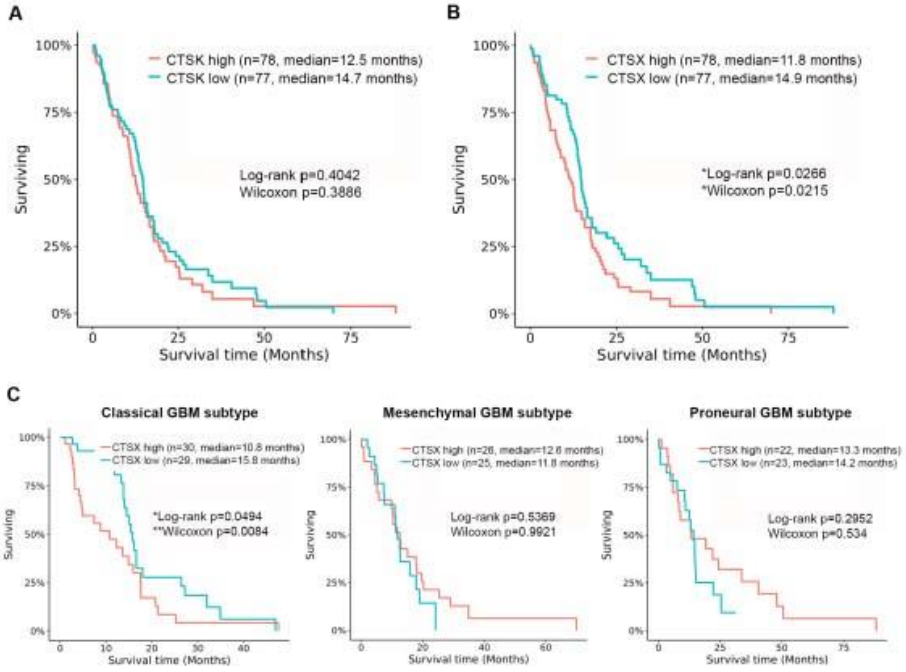


Figure 3. Kaplan-Meier survival curves of overall survival time in relation to cathepsins K and X mRNA expression. Cathepsin K mRNA expression (A) did not correlate with survival of all GBM patients. In contrast, patients with tumors expressing high cathepsin X mRNA levels (B) exhibited poorer survival than the patients with low cathepsin X mRNA expression. When we stratified GBMs in different subtypes (C), only in the classical GBM subtype, cathepsin X mRNA expression had predictive value ($p = 0.049$ by log-rank and $p = 0.0084$ by Wilcoxons' test). Kaplan-Maier survival curves were obtained from GlioVis data portal [33]. GBM tumors were stratified into two groups, tumors with high and with low cathepsin K/X expression, using median values as a cutoff.

2.4. Protein expression of cathepsins K and X is not associated with the survival of GBM patients

We were interested whether cathepsin K and X protein expression had an impact on the survival of GBM patients. We stratified GBM patients based on percentage (%) of cathepsins K and X protein expression into 2 groups, tumors with low and high cathepsin expression, and then performed Kaplan-Meier survival analysis. As already observed at the mRNA level, cathepsin K protein expression in all GBMs did not correlate with the survival of GBM patients (Figure 4A). Similarly, cathepsin X protein expression was not associated with GBM survival (Figure 4B). These results were confirmed with Cox proportional hazard models (Table S1).

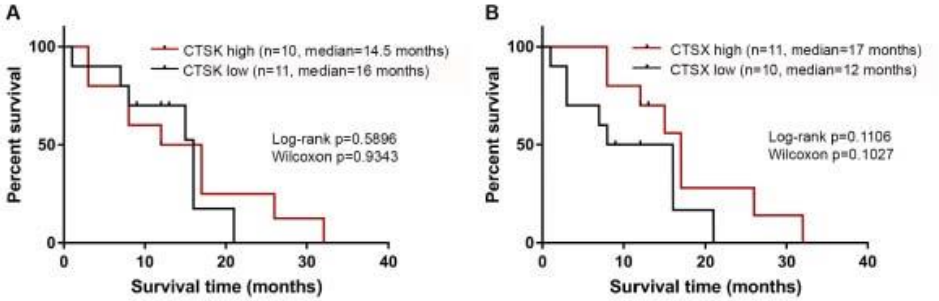


Figure 4. Kaplan-Meier survival curves: overall survival time in relation to cathepsin K and X protein expression in 21 GBM samples. Cathepsins K (A) and X (B) protein expression did not correlate with the survival of GBM patients. GBM were stratified into two groups, tumors with high and low cathepsins expression, using median value as cutoff.

2.5. The GSC niches around arterioles express cathepsins K and X

Besides being present in GBM cells, we observed cathepsins' K and X expression in stromal cells, such as endothelial cells of tumor vasculature. Furthermore, the expression of both cathepsins was demonstrated in special regions of GBM tumors, in so-called peri-arteriolar GSC niches as identified by immunohistochemical localization of the most-widley used GSC marker CD133/Prominin1, α-smooth muscle actin (SMA) as smooth muscle cell marker, and stromal-derived factor 1α (SDF-1α/CXCL12), which have been all proved to be part of GSC niches [21,32]. Briefly, CD133 is localized on GSC plasma membranes [36], SMA is specifically localized in smooth muscle cells of arteriolar and venular walls, whereas SDF-1α, a chemotactic cytokine, is produced by endothelial cells and is involved in angiogenesis [37] and in the retention of GSCs within their niches [21, 38]. Using the macrophage and microglia marker CD68, we also found that macrophages/microglia are infiltrating in the regions of GSC niches around arterioles (Figure 5A-D).

Cathepsins K and X were localized in CD133-, SDF-1α- an CD68-positive regions around arterioles, defined by a thick layer of tunica media of SMA-positive smooth muscle cells (Figure 5A-F). Cathepsins were present in astrocyte-like cells and in endothelial cells, localized within the region

of GSC niches as well as extracellularly, presumably secreted. Overlap of CD133, cathepsin K and X immunostaining in GSC niches was observed (Figure 5B, D, E). Images of GSC niche taken under higher magnification are shown in Supplemtary material (Figures S3 and S4). Taken together, GSC marker CD133, cytokine SDF-1α- and the macrophage marker CD68 are localized around arterioles expressing cathepsins K and X.

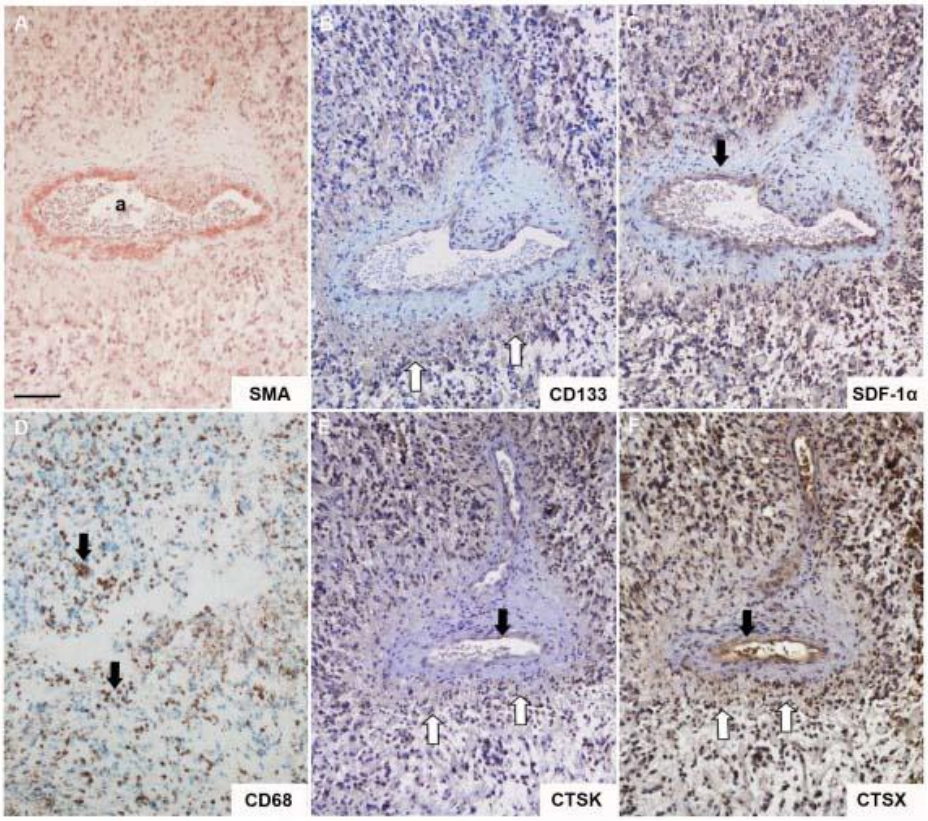


Figure 5. Serial GBM sections immunohistochemically stained for peri-arteriolar GSC niche markers, a macrophage/microglia marker and cathepsins K and X. Cathepsins K (E) and X (F) were highly expressed within CD133-, SDF-1α- and CD68- positive GSC niches around SMA-positive arterioles (A-D) and their expression was co-localised with CD133-positive cells (B, E, F), as indicated by white arrows. Cathepsins and SDF-1α were also present in the endothelial cells of arterioles (C, E, F), as indicated by black arrows. CD68-positive macrophages and macroglia were also expressed in peri-arteriolar GSC niches (D) as indicated by black arrows. Immunohistochemical labelling of SMA (A) was performed with AEC as substrate (red colour) and of the other proteins (B-E) with DAB as substrate (brown colour). Cell nuclei were stained using hematoxylin (blue/purple). a, arteriole. Scale bar = 100 μm.

2.6. In silico correlation of cathepsins expression with the expression of selected GSC markers and peiri-arteriolar GSC niche markers

Finally, to test the association of cathepsins K and X and GSC stem cell niches, we correlated gene expression levels of these two cathepsins with GSC niche markers using public microarray datasets [33]. We searched for GSC markers CD133/PROM1 and SOX2, endothelial marker CD31/PECAM1, α-smooth muscle actin marker SMA/ACTA2, chemotactic cytokine SDF-1α /CXCL12 and its receptor CXCR4 and macrophage/microglia markers CD68 and Iba1/AIF1. Cathepsin K mRNA expression negatively correlated with GSC marker SOX2 (Pearson's $r = -0.38$, *** $p < 0.001$) and

positively with several GSC niche markers: PECAM1 (Pearson's r = 0.40, *** p < 0.001), ACTA2 (Pearson's r = 0.23, *** p < 0.001), CXCL12 (Pearson's r = 0.35, ** p < 0.01), CXCR4 (Pearson's r = 0.23, *** p < 0.001), CD68 (Pearson's r = 0.22, *** p < 0.001) and AIF1 (Pearson's r = 0.29, *** p < 0.001) (Figure S5). On the other hand, cathepsin X negatively correlated with GSC markers PROM1(Pearson's r = -0.18, * p < 0.05) and SOX2 (Pearson's r = -0.23, *** p < 0.001) (Figure 6A, B). A strong positive correlation was observed between cathepsin X and the endothelial cell markers PECAM1 (Pearson's r = 0.49, *** p < 0.001) and ACTA2 (Pearson's r = 0.45, *** p < 0.001), CXCL12 (Pearson's r = 0.45, *** p < 0.001), CXCR4 (Pearson's r = 0.46, *** p < 0.001) (Figure 6C-F). The strongest positive correlation was found for cathepsin X and the macrophage and microglia markers CD68 (Pearson's r = 0.80, *** p < 0.001) and AIF1 (Pearson's r = 0.65, *** p < 0.001) (Figure 6G-H). Taken together, cathepsins K and X expression negatively correlated with GSC markers and positively correlated with other several markers of GSC niches. However, the positive correlation of cathepsin X and GSC niche markers was much stronger than that of cathepsin.K.

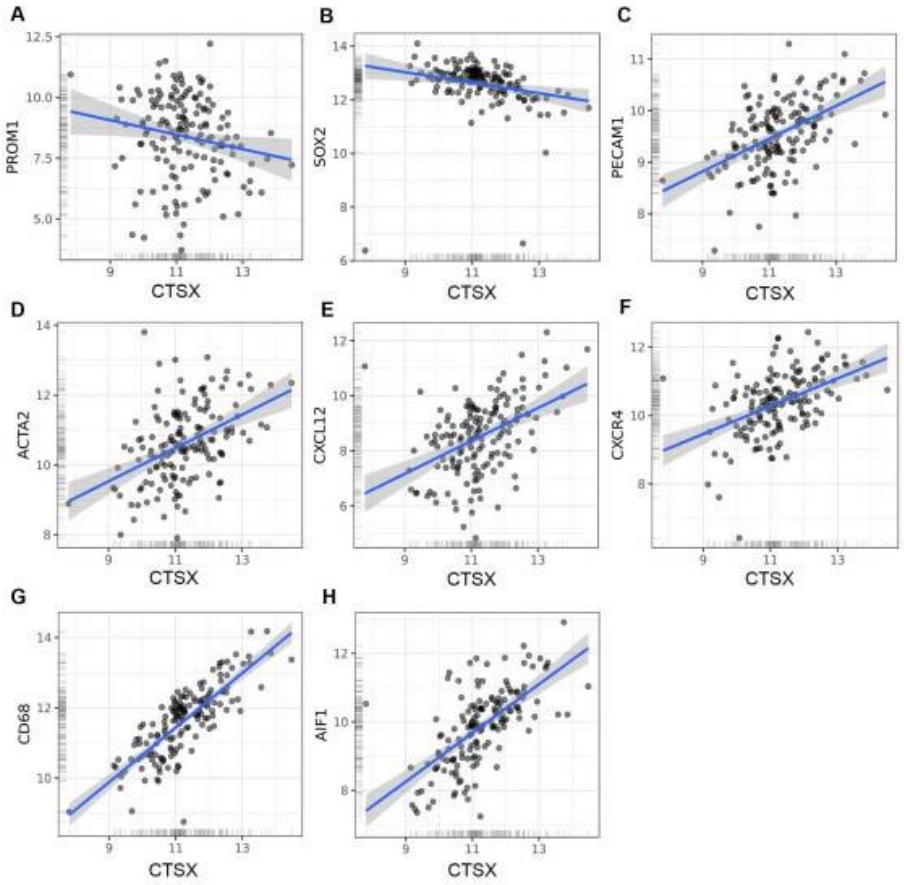


Figure 6. Correlation of microarray-based gene expression levels of cathepsin X and GSC stem cell niche markers. Cathepsin X negatively correlated with GSC markers CD133/PROM1 (A) and SOX2 (B) and positevely correlated with the other GSC niche markers: endothelial marker CD31/PECAM1 (C), α-smooth muscle actin marker SMA/ACTA2 (D), chemotactic cytokine SDF-1α/CXCL12 (E) and its receptor CXCR4 (F), as well as with macrophage/microglia markers CD68 (G) and Iba1/AIF1 (H). Trend lines indicate linear regression estimates. Log2-transformed mRNA expression data were obtained via GlioVis portal.

3. Discussion

Despite intensive research and anti-cancer therapy using radiation and chemotherapy, the most lethal brain tumor GBM remains incurable. A better understanding of GBM pathobiology and a discovery of molecules with predictive impact are thus crucial for the improvement of novel treatment approaches. Such markers may become targets for therapy with personalized potential. In the search for new biomarkers "omics" analyses, followed by molecular validation is the usual approach. Immunohistochemistry is the most common type of analysis in oncology, due to its relative simplicity in determination of biomarkers for diagnosis, prognosis and to predict response to therapy.

Therefore, we attempted here to assess the predictive value of two potential new biomarkers, cysteine cathepsins K and X. The selection of these cathepsins was based on the fact that a related protease, cathepsin B, has been consistently found to be predictive, not only among grade IV glioma (GBM) [6], but also among all gliomas [39]. Moreover, in patients with lower rates of survival, cathepsin B expression in the endothelial cells within the tumor was significantly higher. This enabled the detection of patients at higher risk of death and follow them more carefully or treat them more aggressively. However, cathepsin B, that may initiate the proteolytic cascade needed for cancer cells' invasion [14], is widely distributed in normal cells as well, and it is thus not recommended as a selective tumor cell target for cancer treatment.

High cathepsin K expression confirmed our initial findings on cathepsin K mRNA upregulation in glioblastoma cells and tissues vs. their normal counterparts [17]. However, we did not find any association of cathepsin K mRNA and protein expression with survival of GBM patients, as was proven for several other types of cancers, such as pulmonary adenocarcinomas and squamous cell carcinomas [18]. Similar results have been reported for cysteine cathepsin L, by Strojnik and co-workers [40], showing high cathepsin L expression in astrocytomas and GBM, which was not predictive. However, when GBM were stratified according to the subtype, high cathepsin K in proneural GBM subtypes showed a borderline predictive potential for poor survival.

We have also shown, that cathepsin K is expressed in normal brain cells as have been reported for all brain regions of wild type mice [41] to be linked to neurobehavioral disorders such as schizophrenia [42]. At the protein level, cathepsin K was detected in vesicles of neuronal and non-neuronal cells throughout the mouse brain and its deficiency was associated with a marked decrease in differentiated astrocytes, indicating a specific role of cathepsin K in stem cell differentiation.

Cathepsin X has been also linked to cancer progression as its up-regulation has been detected in several types of cancer [22,27]. Previously, high cathepsin X levels in the serum and cancer tissue of patients with colorectal cancer and hepatocellular carcinoma, respectively, have been shown to be associated with shorter overall survival [27,43]. In this study, we confirmed the same trend for cathepsin X mRNA levels in 156 GBM patients, although its predictive impact was dependent on GBM subtypes and was not confirmed in mesenchymal and proneural subtypes. In contrast, we observed no association between cathepsin X protein expression and survival of 21 GBM patients, which were not stratified by their subtypes. The discrepancy between the two studies is most likely due to very different sizes and characteristics of GBM patients' cohorts.

Cathepsin X promotes tumor processes by enhancing epithelial-to-mesenchymal transition (EMT), compensating for cathepsin B proteolytic activity and by cleaving integrin receptors and profilin 1 [22,44,45]. Moreover, invasion-promoting functions of cancer cell- and stromal cell-derived cathepsin X are mediated *via* RGD motifs in the protease prodomain, binding to integrins and ECM [46]. This is also the first report that in GBM cathepsin X gene expression is significantly higher than in lower-grade gliomas with better clinical outcome and in the normal brain, which is in line with studies in other types of cancer, such as hepatocellular carcinoma and melanoma, revealing the correlation between cathepsin X overexpression in cancer tissue and advanced tumor stage [43]. In addition to the presence of cathepsin X in the glioblastoma cells within GBM tissues, its high levels were detected also in endothelial cells of the tumor vasculature, which implies the involvement of cathepsin X in GBM angiogenesis, similarly as for cathepsin B [39]. Interestingly, highest cathepsin X expression was observed in the mesenchymal subtype of GBM, which represents the most aggressive and therapy-resistant GBM subtype [34,35], what needs to be explored further.

As already mentioned, GBM is a heterogeneous disease, both at molecular and cellular levels. Cathepsins K and X expression exhibited high inter- and intratumoral heterogeneity, which may be explained by differential infiltration of stromal cells, including macrophages, endothelial cells, fibroblasts and lymphocytes, which are important source of proteases [10]. For example, it is known that GBMs of the mesenchymal subtype possess a higher immune cell infiltration than all other subtypes [35,47]. However, the only organized structures where cathepsins K and X have been found clustered were the peri-arterioral regions, which function as GSC niches [21, 32]. In niches, GSCs are surrounded by ECM and stromal cells, predominantly endothelial cells, pericytes and macrophages [4,48]. Cross-talk between endothelial cells and cancer cells is crucial for GSC propagation within the niches [48,49]. Furthermore, the SDF-1α/CXCR4/CXCR7 axis is important for the retention and maintenance of GSC in their niches as well as radiotherapy resistance [38,50]. We confirmed cathepsins K and X co-localization with the widely-used GSC marker CD133, SMA as smooth muscle cell marker present in arteriolar and venular walls, chemotactic cytokine SDF-1α and macrophage marker CD68. Thus, we confirmed our previous observations that cathepsins are present in GSC niche regions, where they may be involved in GSC trafficking in/out of niches, including by processing SDF-1α [21]. Interestingly, we found a reversed correlation between cathepsins K and X mRNA expression with mRNA expression of GSC markers CD133 and SOX2 in GBM tissues, which is in line with our previous results [51], showing a reverse correlation between CD133 mRNA levels and mRNA and activity of cathepsins B, L and S in isolated primary CD133-positive vs. CD133-negative GBM cells. On the other hand, a positive correlation between the expression of cathepsins K and X and other GSC niche markers, as listed above, was observed. Based on these results and the fact, that the cathepsin K cleavage of SDF-1α inhibits its chemotactic activity towards GSCs [21], we speculate that cathepsins K and X may be responsible for GSC release out of their niches, thus causing GSC differentiation and enhanced GSC migration. This is a similar mechanism that was reported by Kollet et al. [52] for mobilization of hematopoietic progenitor cells from bone marrow niches and we may speculate that similar mechanisms occur for neural/astrocyte differentiation in normal brain.

In conclusion, our data support the notion that cathepsins K and X are associated with glioma progression, as both are progressively upregulated from low grade to high grade glioma GBM, as we demonstrated by their significantly increased mRNA and protein expression. On the basis of their distinct structural confirmation and specific activity, the pathobiological role of two cathepsins K and X must be different, as reflected as well by their prognostic impact, in particular when different GBM subtypes are considered. Further, we have shown that cathepsins K and X proteins clustered in the regions of peri-arteriolar GSC niches, and even their mRNA expression correlated with the niche markers, implying a distinct role of these two cathepsins in maintaining/trafficking of GSCs in or out of niches.

4. Materials and Methods

4.1. mRNA expression and survival analyses of glioma patients using public transcriptomic datasets

Cathepsins' mRNA expression analysis in the glioma tissue and its association with survival of patients was performed using publically available GlioVis data portal (http://gliovis.bioinfo.cnio.es/) [33]. Briefly, two datasets (RNA-seq) were used: TCGA_LGGGBM (RNA-seq platform) for comparing cathepsins expression in different glioma grades and TCGA_GBM (RNA-seq platform) for all the other analyses. Two hundred twenty-six (226) patients with grade II, 244 patients with grade III, 156 patients with GBM (grade IV) and 4 non-tumor patients were included in the query. All statistical analyses were performed in GlioVis data portal using pairwise comparisons between group levels with corrections for multiple testing (p-values with Bonferroni correction), and the log-rank test for Kaplan-Meier survival curve analysis. Correlation analyses (Pearson correlation coefficient, r) were performed between cathepsins' mRNA expression and the mRNA expression of GSC niche markers.

4.2. Patients and brain tumor samples

Paraffin-embedded tissue sections were obtained from biopsies of GBM patients, which were operated at the Department of Neurosurgery, University Clinical Centre of Ljubljana, Slovenia from 2013 to 2016. The study was approved by the National Medical Ethics Committee of the Republic of Slovenia (Approval no. 92/06/13). Altogether, 21 patients with glioblastoma (glioma WHO grade IV) were included. Tumor diagnoses were established by standard histopathology protocols at the Institute of Pathology of the Medical Faculty, University of Ljubljana. Complete patient's diagnosis and tumor sample data are shown in the Supporting Information section (Table S2). The samples used for immunohistochemical analysis were obtained during surgery of newly-diagnosed GBM patients before radio- or/and chemotherapy.

4.3. Immunohistochemistry

Immunohistochemistry was performed on serial GBM paraffin sections. Five µm-thick paraffin sections of GBM biopsy samples were prepared according to routine procedures of the Institute of Pathology, University of Ljubljana. The paraffin GBM sections were dewaxed in 100 % xylene (3 min) and then rehydrated in 100 %, 96 %, 50 % and 0 % ethanol (in each ethanol dilution for 3 min). Heat-mediated antigen retrieval was achieved with sodium citrate buffer (pH 6.0). Blockage of endogenous peroxidase activity in the tissue was performed by incubation with 3% H_2O_2 in 100% methanol for 30 min at room temperature. To reduce non-specific background staining, the sections were incubated with 10 % goat or rabbit normal serum (Sigma) in PBS containing 0.1 % BSA. After tapping off the serum-containing buffer, sections were incubated overnight at 4°C with primary antibodies: rabbit anti-SMA (1:200; Abcam, ab5694), mouse anti-CD133 (1:10; Miltenyi Biotec, W6B3C1), rabbit anti-SDF-1α (1:200; Abcam, ab9797), mouse anti-CD68 (1:50; Dako, EBM 11), rabbit anti-cathepsin K (1:200; Abcam, ab19027) and goat anti-cathepsin X (1:200; R&D systems, AF934). These incubations were followed by incubation with the anti-mouse, anti-rabbit or anti-goat secondary horse-radish-peroxidase–conjugated antibodies (1:200; Dako) for 1 h. Protein expression was detected using DAB (Abcam) or AEC (Vector Laboratories), and hematoxylin was used for counterstaining. The negative-control staining was performed in the absence of primary antibodies (Figure S6). All sections were analyzed by light microscopy and images were taken using a Ti Elclipse inverted microscope (Nikon) and NIS elements software (Nikon). Expression of cathepsins was presented as percentage (%) of immunostained areas of tumor sections. Twenty visual fields per tumor section (20x magnification) in non-necrotic areas were quantified using ImageJ software (https://imagej.nih.gov/ij/) and Immunohistochemistry Image Analysis Toolbox [6,53,54].

4.4. Statistical analyses

All statistical analyses were performed using R and GraphPad Prims 7. Overall survival of GBM patients was calculated from the date of surgery to date of death or last follow-up. Survival analyses were estimated by Kaplan-Meier survival curves and these curves were compared with log-rank test. The correlations between prognostic factors and survival were evaluated with COX proportional hazards model. A p value of less than 0.05 was considered statistically significant.

Supplementary Materials: Figure S1: Relationship between catalytic activities and the structures of cathepsins B, K, L, S and X, Figure S2: Kaplan-Meier survival curves for overall survival time with respect to cathepsin's K mRNA levels, Table S1: Comparison of prognostic significance of measured variables by COX proportional hazard model in 21 GBM patients, Figure S3: High-magnification images of serial paraffin-embedded GBM sections labelled for GSC niche markers SMA, CD133 and SDF-1α, macrophage marker CD68 and cathepsins K and X, Figure S4: High-magnification images of serial paraffin-embedded GBM sections labelled for GSC niche markers CD133 and SDF-1α and cathepsins K and X, Figure S5: Correlation of microarray-based gene expression level of cathepsin K and GSC stem cell niche markers, Table S2: Characteristics of the 21 globlastoma (GBM) patients, operated at the Department of Neurosurgery of the University of Ljubljana, Figure S6: Control incubations of paraffin-embedded GBM sections for IHC. Supplementary materials can be found at www.mdpi.com/link.

Acknowledgments: This work was supported by the Slovenian Research Agency (ARRS), Program P1-0245 (TTL) and ARRS young researcher grant (BB).

Author Contributions: All authors revised the manuscript and approved the final version of the manuscript. Specifically, B.B. designed the study, performed experiments, analyzed and interpreted the data and wrote the manuscript; C.L, provided GBM sections and optimized the immunohistochemical experiments; M.K.K. performed experiments and analyzed the data; A.B. contributed to statistical analyses and interpretation of the data; A.P., J.K., R.B. provide GBM samples/patients data/sections/antibodies, analyzed and interpreted the data; T.T.L., C.J.F.V.N. conceived and designed the study, analyzed and interpreted the data and wrote the final version of the manuscript.

Conflicts of Interest: No potential conflicts of interest were disclosed.

Abbreviations

CTSK	Cathepsin K
CTSX	Cathepsin X

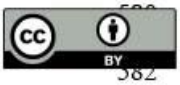
References

1. Louis, D.N.; Perry, A.; Reifenberger, G.; von Deimling, A.; Figarella-Branger, D.; Cavenee, W.K.; Ohgaki, H.; Wiestler, O.D.; Kleihues, P.; Ellison, D.W. The 2016 World Health Organization Classification of Tumors of the Central Nervous System: a summary. Acta Neuropathol. 2016, 131, 803-20, DOI: 10.1007/s00401-016-1545-1.
2. Czarnek, N.; Clark, K.; Peters, K.B. Mazurowski MA. Algorithmic three-dimensional analysis of tumor shape in MRI improves prognosis of survival in glioblastoma: a multi-institutional study. J Neurooncol. 2017, 132, 55-62, DOI: 10.1007/s11060-016-2359-7
3. Cuddapah, V.A.; Robel, S.; Watkins, S.; Sontheimer, H. A neurocentric perspective on glioma invasion. Nat Rev Neurosci. 2014. 15, 455-65, DOI: 10.1038/nrn3765.
4. Roos, A.; Ding, Z.; Loftus, J.C.; Tran, N.L. Molecular and Microenvironmental Determinants of Glioma Stem-Like Cell Survival and Invasion. Front Oncol. 2017, 7, 120, DOI: 10.3389/fonc.2017.00120.
5. Mentlein, R.; Hattermann, K.; Held-Feindt, J. Lost in disruption: role of proteases in glioma invasion and progression. Biochim Biophys Acta 2012, 1825, 178-85, DOI: 10.1016/j.bbcan.2011.12.001.
6. Colin, C.; Voutsinos-Porche, B.; Nanni, I.; Fina, F.; Metellus, P.; Intagliata, D.; Baeza, N.; Bouvier, C.; Delfino, C.; Loundou, A.; Chinot, O.; Lah, T.; Kos, J.; Martin, P.M.; Ouafik, L.; Figarella-Branger, D. High expression of cathepsin B and plasminogen activator inhibitor type-1 are strong predictors of survival in glioblastomas. Acta Neuropathol. 2009, 118, 745-54, DOI: 10.1007/s00401-009-0592-2.
7. Gole, B.; Huszthy, P.C.; Popović, M.; Jeruc, J.; Ardebili, Y.S.; Bjerkvig, R.; Lah, T.T. The regulation of cysteine cathepsins and cystatins in human gliomas. Int J Cancer. 2012, 131, 1779-89, DOI: 10.1002/ijc.27453.
8. Olson, O.C.; Joyce, J.A. Cysteine cathepsin proteases: regulators of cancer progression and therapeutic response. Nat Rev Cancer 2015, 15, 712-29, DOI: 10.1038/nrc4027.
9. Kenig, S.; Frangež, R.; Pucer, A.; Lah, T. Inhibition of cathepsin L lowers the apoptotic threshold of glioblastoma cells by up-regulating p53 and transcription of caspases 3 and 7. Apoptosis 2011, 16, 671-82, DOI: 10.1007/s10495-011-0600-6.
10. Breznik, B.; Motaln, H.; Turnšek, T.L. Proteases and cytokines as mediators of interactions between cancer and stromal cells in tumours. Biol Chem. 2017, 398, 709-719, DOI: 10.1515/hsz-2016-0283.
11. Kramer, L.; Turk, D.; Turk, B. The Future of Cysteine Cathepsins in Disease Management. Trends Pharmacol Sci. 2017, 38, 873-898, DOI: 10.1016/j.tips.2017.06.003.
12. López-Otín, C.; Matrisian, L.M. Emerging roles of proteases in tumour suppression. Nat Rev Cancer. 2007, 7, 800-8, DOI: 10.1038/nrc2228.
13. Quail, D.F.; Joyce, J.A. The Microenvironmental Landscape of Brain Tumors. Cancer Cell 2017, 31, 326-341, DOI: 10.1016/j.ccell.2017.02.009.
14. Lah, T.T.; Duran Alonso, M.B.; Van Noorden, C.J.F. Antiprotease therapy in cancer: hot or not? Expert Opin Biol Ther. 2006, 6, 257-79, DOI: 10.1517/14712598.6.3.257.
15. Lah T.T.; Obermajer, N.; Duran Alonso, M.B.; Kos, J. Cysteine cathepsins and cystatins as cancer biomarkers. In: The Cancer Degradome: Proteases and Cancer Biology; Edwards, D.; Hoyer-Hansen, G.; Blasi, F.; Sloane, B.F., Eds.; Springer: New York, USA, 2008; pp. 575–613; ISBN 978-0-387-69056-8.

16. Flannery, T.; McQuaid, S.; McGoohan, C.; McConnell, R.S.; McGregor, G.; Mirakhur, M.; Hamilton, P.; Diamond, J.; Cran, G.; Walker, B.; Scott, C.; Martin, L.; Ellison, D.; Patel, C.; Nicholson, C.; Mendelow, D.; McCormick, D.; Johnston, P.G. Cathepsin S expression: An independent prognostic factor in glioblastoma tumours--A pilot study. Int J Cancer 2006, 119, 854–60, DOI: 10.1002/ijc.21911.
17. Verbovšek, U.; Motaln, H.; Rotter, A.; Atai, N.A.; Gruden, K.; Van Noorden, C.J.; Lah, T.T. Expression analysis of all protease genes reveals cathepsin K to be overexpressed in glioblastoma. PLoS One 2014, 9, e111819, DOI: 10.1371/journal.pone.0111819.
18. Verbovšek, U.; Van Noorden, C.J.; Lah, T.T. Complexity of cancer protease biology: Cathepsin K expression and function in cancer progression. Semin Cancer Biol. 2015, 35, 71-84, DOI: 10.1016/j.semcancer.2015.08.010.
19. Novinec, M.; Lenarčič, B. Cathepsin K: a unique collagenolytic cysteine peptidase. Biol Chem. 2013, 394, 1163-79, DOI: 10.1515/hsz-2013-0134.
20. Staudt, N.D.; Maurer, A.; Spring, B.; Kalbacher, H.; Aicher, W.K.; Klein G. Processing of CXCL12 by different osteoblast-secreted cathepsins. Stem Cells Dev. 2012, 21, 1924-35, DOI: 10.1089/scd.2011.0307.
21. Hira, V.V.; Verbovšek, U.; Breznik, B.; Srdič, M.; Novinec, M.; Kakar, H.; Wormer, J.; der Swaan, B.V.; Lenarčič, B.; Juliano, L.; Mehta, S.; Van Noorden, C.J.; Lah, T.T. Cathepsin K cleavage of SDF-1α inhibits its chemotactic activity towards glioblastoma stem-like cells. Biochim Biophys Acta 2017, 1864, 594-603, DOI: 10.1016/j.bbamcr.2016.12.021.
22. Kos, J.; Vižin, T.; Fonović, U.P.; Pišlar, A. Intracellular signaling by cathepsin X: molecular mechanisms and diagnostic and therapeutic opportunities in cancer. Semin Cancer Biol. 2015, 31, 76-83, DOI: 10.1016/j.semcancer.2014.05.001.
23. Kos, J.; Jevnikar, Z.; Obermajer, N. The role of cathepsin X in cell signaling. Cell Adh Migr. 2009, 3, :164-6, PMC2679876.
24. Wendt, W.; Zhu, X.R.; Lübbert, H.; Stichel, C.C. Differential expression of cathepsin X in aging and pathological central nervous system of mice. Exp Neurol. 2007, 204, 525-40, DOI: 10.1016/j.expneurol.2007.01.007.
25. Nägler, D.K.; Krüger, S.; Kellner, A.; Ziomek, E.; Menard, R.; Buhtz, P.; Krams, M.; Roessner, A.; Kellner, U. Up-regulation of cathepsin X in prostate cancer and prostatic intraepithelial neoplasia. Prostate 2004, 60, 109-19, DOI: 10.1002/pros.20046.
26. Krueger, S.; Kalinski, T.; Hundertmark, T.; Wex, T.; Küster, D.; Peitz, U.; Ebert, M.; Nägler, D.K.; Kellner, U.; Malfertheiner, P.; Naumann, M.; Röcken, C.; Roessner, A. Up-regulation of cathepsin X in Helicobacter pylori gastritis and gastric cancer. J Pathol. 2005, 207, 32-42, DOI: 10.1002/path.1820.
27. Vizin, T.; Christensen, I.J., Nielsen, H.J.; Kos, J. Cathepsin X in serum from patients with colorectal cancer: relation to prognosis. Radiol Oncol. 2012, 46, 207-12, DOI: 10.2478/v10019-012-0040-0.
28. Gopinath, S.; Malla, R.; Alapati, K.; Gorantla, B.; Gujrati, M.; Dinh, D.H.; Rao, J.S. Cathepsin B and uPAR regulate self-renewal of glioma-initiating cells through GLI-regulated Sox2 and Bmi1 expression. Carcinogenesis 2013, 34, 550-9, DOI: 10.1093/carcin/bgs375.
29. Alapati, K.; Kesanakurti, D.; Rao, J.S.; Dasari VR. uPAR and cathepsin B-mediated compartmentalization of JNK regulates the migration of glioma-initiating cells. Stem Cell Res. 2014, 12, 716-29, DOI: 10.1016/j.scr.2014.02.008.
30. Lathia, J.D.; Mack, S.C.; Mulkearns-Hubert, E.E.; Valentim, C.L.; Rich, J.N. Cancer stem cells in glioblastoma. Genes Dev. 2015, 29, 1203-17, DOI: 10.1101/gad.261982.115.
31. Godlewski, J.; Ferrer-Luna, R.; Rooj, A.K.; Mineo, M.; Ricklefs, F.; Takeda, Y.S.; Nowicki, M.O.; Salińska, E.; Nakano, I.; Lee, H.; Weissleder, R.; Beroukhim, R.; Chiocca, E.A.; Bronisz, A. MicroRNA Signatures and Molecular Subtypes of Glioblastoma: The Role of Extracellular Transfer. Stem Cell Reports 2017, 8, 1497-1505, DOI: 10.1016/j.stemcr.2017.04.024.
32. Hira, V.V.; Ploegmakers, K.J.; Grevers, F.; Verbovšek, U.; Silvestre-Roig, C.; Aronica, E.; Tigchelaar, W.; Turnšek, T.L.; Molenaar, R.J.; Van Noorden C.J. CD133+ and Nestin+ Glioma Stem-Like Cells Reside Around CD31+ Arterioles in Niches that Express SDF-1α, CXCR4, Osteopontin and Cathepsin K. J Histochem Cytochem. 2015, 63, 481-93, DOI: 10.1369/0022155415581689.
33. Bowman, R.L.; Wang, Q.; Carro, A.; Verhaak, R.G.; Squatrito, M. GlioVis data portal for visualization and analysis of brain tumor expression datasets. Neuro Oncol. 2017, 19, 139-141, DOI: 10.1093/neuonc/now247.
34. Segerman, A.; Niklasson, M.; Haglund, C.; Bergström, T.; Jarvius, M.; Xie, Y.; Westermark, A.; Sönmez, D.; Hermansson, A.; Kastemar, M.; Naimaie-Ali, Z.; Nyberg, F.; Berglund, M.; Sundström, M.; Hesselager, G.; Uhrbom, L.; Gustafsson, M.; Larsson, R.; Fryknäs, M.; Segerman, B.; Westermark,

505 B. Clonal Variation in Drug and Radiation Response among Glioma-Initiating Cells Is Linked to
506 Proneural-Mesenchymal Transition. Cell Rep 2016, 17, 2994-3009, doi: 10.1016/j.celrep.2016.11.056.
507 35. Verhaak, R.G.; Hoadley, K.A.; Purdom, E.; Wang, V.; Qi, Y.; Wilkerson, M.D.; Miller, C.R.; Ding, L.;
508 Golub, T.; Mesirov, J.P.; Alexe, G.; Lawrence, M.; O'Kelly, M.; Tamayo, P.; Weir, B.A.; Gabriel, S.;
509 Winckler, W.; Gupta, S.; Jakkula, L.; Feiler, H.S.; Hodgson, J.G.; James, C.D.; Sarkaria, J.N.; Brennan,
510 C.; Kahn, A.; Spellman, P.T.; Wilson, R.K.; Speed, T.P.; Gray, J.W.; Meyerson, M.; Getz, G.; Perou,
511 C.M.; Hayes, D.N.; Cancer Genome Atlas Research Network. Integrated genomic analysis identifies
512 clinically relevant subtypes of glioblastoma characterized by abnormalities in PDGFRA, IDH1,
513 EGFR, and NF1. Cancer Cell 2010, 17, 98-110, DOI: 10.1016/j.ccr.2009.12.020.
514 36. Zeppernick, F.; Ahmadi, R.; Campos, B.; Dictus, C.; Helmke, B.M.; Becker, N.; Lichter, P.; Unterberg,
515 A.; Radlwimmer, B.; Herold-Mende, C.C. Stem cell marker CD133 affects clinical outcome in glioma
516 patients. Clin Cancer Res. 2008, 14, 123-9, doi: 10.1158/1078-0432.CCR-07-0932.
517 37. Kenig, S.; Alonso, M.B.; Mueller, M.M.; Lah, T.T. Glioblastoma and endothelial cells cross-talk,
518 mediated by SDF-1, enhances tumour invasion and endothelial proliferation by increasing
519 expression of cathepsins B, S, and MMP-9. Cancer Lett. 2010, 289: 53-61, DOI:
520 10.1016/j.canlet.2009.07.014.
521 38. Plaks, V.; Kong, N.; Werb, Z. The cancer stem cell niche: how essential is the niche in regulating
522 stemness of tumor cells? Cell Stem Cell 2015, 16, 225-38, doi: 10.1016/j.stem.2015.02.015.
523 39. Strojnik, T.; Kos, J.; Zidanik, B.; Golouh, R.; Lah, T. Cathepsin B immunohistochemical staining in
524 tumor and endothelial cells is a new prognostic factor for survival in patients with brain tumors. Clin
525 Cancer Res 1999, 5, 559-67, PMID: 10100707.
526 40. Strojnik, T.; Kavalar, R.; Trinkaus, M.; Lah, T.T. Cathepsin L in glioma progression: comparison with
527 cathepsin B. Cancer Detect Prev 2005, 29, 448-55, DOI: 10.1016/j.cdp.2005.07.006.
528 41. Dauth, S.; Schmidt, M.M.; Rehders, M.; Dietz, F.; Kelm, S.; Dringen, R.; Brix, K. Characterisation and
529 metabolism of astroglia-rich primary cultures from cathepsin K-deficient mice. Biol Chem. 2012, 393,
530 959–70, DOI: 10.1515/hsz-2012-0145.
531 42. Dauth, S.; Sîrbulescu, R.F.; Jordans, S.; Rehders, M.; Avena, L.; Oswald, J.; Lerchl A.; Brix, K.
532 Cathepsin K deficiency in mice induces structural and metabolic changes in the central nervous
533 system that are associated with learning and memory deficits. BMC Neurosci. 2011, 12, 74, DOI:
534 10.1186/1471-2202-12-74.
535 43. Wang, J.; Chen, L.; Li, Y.; Guan, X.Y. Overexpression of cathepsin Z contributes to tumor metastasis
536 by inducing epithelial-mesenchymal transition in hepatocellular carcinoma. PLoS One 2011, 6,
537 e24967, DOI: 10.1371/journal.pone.0024967.
538 44. Sevenich, L.; Schurigt, U.; Sachse, K.; Gajda, M.; Werner, F.; Müller, S.; Vasiljeva, O.; Schwinde, A.;
539 Klemm, N.; Deussing, J.; Peters, C.; Reinheckel T. Synergistic antitumor effects of combined
540 cathepsin B and cathepsin Z deficiencies on breast cancer progression and metastasis in mice. Proc
541 Natl Acad Sci U S A 2010, 107, 2497-502, DOI: 10.1073/pnas.0907240107.
542 45. Mitrović, A.; Pečar Fonović, U.; Kos, J. Cysteine cathepsins B and X promote epithelial-mesenchymal
543 transition of tumor cells. Eur J Cell Biol. 2017, 96, 622-631, DOI: 10.1016/j.ejcb.2017.04.003.
544 46. Akkari, L.; Gocheva, V.; Kester, J.C.; Hunter, K.E.; Quick, M.L.; Sevenich, L.; Wang, H.W.; Peters, C.;
545 Tang, L.H.; Klimstra, D.S.; Reinheckel, T.; Joyce, J.A. Distinct functions of macrophage-derived and
546 cancer cell-derived cathepsin Z combine to promote tumor malignancy via interactions with the
547 extracellular matrix. Genes Dev. 2014, 28, 2134-50, DOI: 10.1101/gad.249599.114.
548 47. Euskirchen, P.; Radke, J.; Schmidt, M.S.; Schulze Heuling, E.; Kadikowski, E.; Maricos, M.; Knab, F.;
549 Grittner, U.; Zerbe, N.; Czabanka, M.; Dieterich, C.; Miletic, H.; Mørk, S.; Koch, A.; Endres, M.;
550 Harms C. Cellular heterogeneity contributes to subtype-specific expression of ZEB1 in human
551 glioblastoma. PLoS One 2017, 12, e0185376, DOI: 10.1371/journal.pone.0185376.
552 48. Calabrese, C.; Poppleton, H.; Kocak, M.; Hogg, T.L.; Fuller, C.; Hamner, B.; Oh, E.Y.; Gaber, M.W.;
553 Finklestein, D.; Allen, M.; Frank, A.; Bayazitov, I.T.; Zakharenko, S.S.; Gajjar, A.; Davidoff, A.;
554 Gilbertson, R.J. A perivascular niche for brain tumor stem cells. Cancer Cell 2007, 11, 69-82, DOI:
555 10.1016/j.ccr.2006.11.020.
556 49. Zhu, T.S.; Costello, M.A.; Talsma, C.E.; Flack, C.G.; Crowley, J.G.; Hamm, L.L.; He, X.; Hervey-
557 Jumper, S.L.; Heth, J.A.; Muraszko, K.M.; DiMeco, F.; Vescovi, A.L.; Fan, X. Endothelial cells create a
558 stem cell niche in glioblastoma by providing NOTCH ligands that nurture self-renewal of cancer
559 stem-like cells. Cancer Res. 2011, 71, 6061-72, DOI: 10.1158/0008-5472.CAN-10-4269.
560 50. Goffart, N.; Lombard, A.; Lallemand, F.; Kroonen, J.; Nassen, J.; Di Valentin, E.; Berendsen, S.;
561 Dedobbeleer, M.; Willems, E.; Robe, P.; Bours, V.; Martin, D.; Martinive, P.; Maquet P.; Rogister, B.

562 CXCL12 mediates glioblastoma resistance to radiotherapy in the subventricular zone. Neuro Oncol.
563 2017, 19, 66-77, DOI: 10.1093/neuonc/now136.
564 51. Ardebili, S.Y.; Zajc, I.; Gole, B.; Campos, B.; Herold-Mende, C.; Drmota, S.; Lah, T.T.
565 CD133/prominin1 is prognostic for GBM patient's survival, but inversely correlated with cysteine
566 cathepsins' expression in glioblastoma derived spheroids. Radiol Oncol. 2011, 45, 102-15, DOI:
567 10.2478/v10019-011-0015-6.
568 52. Kollet, O.; Dar, A.; Shivtiel, S.; Kalinkovich, A.; Lapid, K.; Sztainberg, Y.; Tesio, M.; Samstein, R.M.;
569 Goichberg, P.; Spiegel, A.; Elson, A.; Lapidot, T. Osteoclasts degrade endosteal components and
570 promote mobilization of hematopoietic progenitor cells. Nat Med. 2006, 12, 657–64, DOI:
571 10.1038/nm1417.
572 53. Završnik, J.; Butinar, M.; Trstenjak Prebanda, M.; Krajnc, A.; Vidmar, R.; Fonović, M.; Grubb, A.;
573 Turk, V.; Turk, B.; Vasiljeva, O. Cystatin C deficiency suppresses tumor growth in a breast cancer
574 model through decreased proliferation of tumor cells. Oncotarget 2017, 8, 73793-73809,
575 https://doi.org/10.18632/oncotarget.17379.
576 54. Chieco, P.; Jonker, A.; De Boer, B.A.; Ruijter, J.M.; Van Noorden, C.J. Image cytometry: protocols for
577 2D and 3D quantification in microscopic images. Prog Histochem Cytochem. 2013, 47, 211-333, DOI:
578 10.1016/j.proghi.2012.09.001.
579



© 2017 by the authors. Submitted for possible open access publication under the terms and conditions of the Creative Commons Attribution (CC BY) license (http://creativecommons.org/licenses/by/4.0/).

2.6 Cysteine Cathepsins B, X and K Expression in Peri-Arteriolar Glioblastoma Stem Cell Niches (in Revision)

Barbara Breznik, Clara Limbaeck Stokin, Janko Kos, Mohammed Khurshed, Roman Bošnjak, Tamara Lah Turnšek, Cornelis J.F. Van Noorden

In revision in Journal of Histochemistry and Cytochemistry

Original article

Full title: Cysteine cathepsins B, X and K expression in peri-arteriolar glioblastoma stem cell niches

Short title: Cathepsins B, X and K expression in GSC niches

Barbara Breznik *[1,2], Clara Limbaeck Stokin [3], Janko Kos [4], Mohammed Khurshed [5], Roman Bošnjak [6], Tamara Lah Turnšek [1,2], Cornelis J.F. Van Noorden [5]

[1] *Department of Genetic Toxicology and Cancer Biology, National Institute of Biology, Večna pot 111, 1000 Ljubljana, Slovenia*

[2] *International Postgraduate School Jozef Stefan, Jamova 39, 1000 Ljubljana, Slovenia*

[3] *Institute of Pathology, Faculty of Medicine, University of Ljubljana, Ljubljana, Slovenia*

[4] *Department of Pharmaceutical Biology, Faculty of Pharmacy, University of Ljubljana, Slovenia*

[5] *Cancer Center Amsterdam, Department of Medical Biology at the Academic Medical Center, Meibergdreef 15, 1105 AZ Amsterdam, The Netherlands*

[6] *Department of Neurosurgery, University Clinical Centre Ljubljana, Slovenia*

***Corresponding author:**

* Barbara Breznik

Department of Genetic Toxicology and Cancer Biology

National Institute of Biology

Večna Pot 111

1000 Ljubljana, Slovenia

Phone: + 386 (0)59 232 870

Fax: + 386 (0)59 232 715

E-mail: barbara.breznik@nib.si

Total number of words: 4181

Abstract: 198 words

Number of figures: 5

Number of tables: 1

Number of references: 55

Abstract

Glioblastoma (GBM) is the most lethal brain tumour mainly due to malignant and therapy-resistant GBM stem cells (GSCs) that are localized in protecting hypoxic peri-arteriolar GSC niches. Cysteine cathepsin proteases have been found to be upregulated in GBM. Here, we investigated whether cathepsins B and X are localized in GSC niches like cathepsin K. Therefore, we determined expression of cathepsins B, X and K in serial sections of 16 human GBM samples using immunohistochemistry and metabolic mapping of cathepsin activity using selective fluorogenic substrates. Cathepsins B, X and K were expressed by stromal cells and cancer cells in GBM tissues. Moreover, we detected cathepsins B, X and K presence in GSC niches, which were defined by the expression of GSC markers CD133 and nestin, and peri-arteriolar GSC niche markers SDF-1α and SMA. Metabolic mapping showed that cathepsin B but not cathepsin K is active in the GSC niche. An interesting finding was the high levels of cathepsin X in erythrocytes in all samples investigated. On the basis of these findings, it is concluded that cathepsin B, X and K have distinct functions in GBM and that cathepisn K is the most likely GSC niche-related cathepsin of the three.

Keywords: cysteine cathepsins, glioblastoma stem cells, niches, stroma, proteolytic activity

51 **Introduction**

52 Glioblastoma (GBM) remains the most lethal and most frequently-occurring primary brain
53 tumour (1). GBM is characterized by extensive cancer cell proliferation, vascularization,
54 necrosis as well as invasion of GBM cells into surrounding brain parenchyma (2, 3).
55 Infiltration deep into normal brain prevents complete surgical resection (4) and this has been
56 found to be tightly associated with expression and activity of proteolytic enzymes (5, 6), such
57 as lysosomal cysteine cathepsins (7), urokinase (8) and metalloproteases (9). Extracellular
58 matrix (ECM) of GBM is mainly composed of chondroitin sulfate proteoglycan, tenascin C
59 and collagen type IV (10, 11), that can be degraded by proteolytic activity to enable
60 intracranial GBM cell trafficking.
61 Cysteine cathepsins, a group of lysosomal proteases belonging to the C1A family of papain–
62 like proteases (https://www.ebi.ac.uk/merops/) (12), have been shown to be associated with
63 growth and invasive spread of GBM (4, 8, 13, 14). Cysteine cathepsins B, X and K are
64 involved in various processes in cancer progression, including therapeutic resistance (15) and
65 apoptosis (16). On the other hand, cathepsins also play a role in tumour suppression (7, 17).
66 These seemingly conflicting roles depend on the context, which emphasizes the importance of
67 *in vivo* analyses to understand functions of cathepsins, in a particular in the GBM landscape
68 (10). Whereas intracellular cathepsins are crucial players in signal transduction pathways that
69 drive GBM and GSC growth and migration, secreted cathepsins in the extracellular space
70 have emerged as potent modifiers of the GBM microenvironment by activating cascade of
71 proteases, inhibiting their inhibitors, processing or regulation of activity of growth factors and
72 cytokines (13) in addition to modifications of the ECM. Cathepsins can also shed cell-cell
73 adhesion molecules and thereby contribute to brain tissue-specific invasion (15).
74 Cathepsin B is recognised as the most pro-invasive lysosomal cathepsin (14) and its
75 expression is highly prognostic in various types of cancers, including GBM (18). The
76 expression of cathepsin B correlates with brain tumour malignancy and it has been found to
77 be an independent predictor of survival of GBM patients (19, 20). Cathepsin B is both an
78 endo- and exopeptidase and the cathepsins B conformation defines its intralysosomal activity
79 at low pH. Its activity is also found extracellular. In addition, by activating other proteases
80 such as matrix metalloproteases (MMPs) and urokinase (uPA), cathepsin B initiates
81 proteolytic cascades on cell membranes (7, 15). By proteolytic processing and release of
82 cytokines and growth factors, such as transforming growth factor beta (TGF-β), cathepsin B
83 affect invasive behaviour of cells (13, 21).

Structure and activity of cathepsin X, formerly named cathepsin Z, show several unique features that distinguish it from other cysteine cathepsins, as has been reviewed by Kos et al. (22). Cathepsin X exhibits solely carboxypeptidase activity and is activated by other lysosomal endopeptidases. So far, cathepsin X expression has been found to be restricted to the cells of the immune system, regulating their proliferation, maturation, migration, adhesion, phagocytosis and signal transduction (23). Various molecular targets of cathepsin X exopeptidase activity have been identified, including the β-chain of integrin receptors, γ-enolase, chemokine SDF-1α, profilin-1 and others. Cathepsin X expression has been detected in the brain, localized in neurons, glial cells and ependymal cells (22, 24). Increased cathepsin X expression has been associated with various types of cancer (25-27), but until now, its expression in GBM has not been explored.

Cathepsin K belongs to the cathepsin L-like cluster of the C1A family. Its tetrameric form allows allosteric accommodation of negatively-charged glycosaminoglycans (GAGs), enabling formation of complexes with unique collagenolytic activity (28). However, cathepsin K degrades also smaller proteins, including growth factors and chemokines, such as SDF-1α (29, 30) thereby indirectly affecting signalling pathways.

A major cause of GBM recurrence is the presence of highly tumorigenic and therapy-resistant subpopulation of GBM cells in GBM tumours with characteristic expression of stem cell-related genes, the GBM stem cells (GSCs) (31-34). GSC stemness is tightly regulated by the GSC microenvironment, that are specific micro-anatomical regions within the tumour, named GSC niches (35). Recently, Hira et al. (32, 33, 36) reported that GSC niches are exclusively localized in hypoxic peri-arteriolar niches at the edge of the lamina adventitia of the arterioles. These niches were found to be a replica of hematopoietic stem cell niches in bone marrow (33, 36, 37). In these regions, maintenance and protection of GSCs is achieved by remodelling by GSCs of their own microenvironment (34) and by interactions with cells that are present the niches (38, 39). However, it is still poorly understood which molecular programs and proteins exert specific functions in the GSC niche. Identification of proteins and signalling pathways within GSC niches may have therapeutic value, because niche-residing GSCs are therapy resistant, and targeting/disintegrating the niche stroma (cells and ECM) may reduce affinity of GSC to niches and may thus increase GBM sensitivity to anti-cancer therapy (29). For example, Lathia and co-workers (40) reported that the ECM proteins laminins are localized in perivascular GBM niches and that high expression of laminin α2 is associated with poor patient prognosis. Laminin α chains were mostly expressed and produced by non-GSCs and tumour-associated endothelial cells. This highlights the contribution of juxtacrine

signalling and suggests that the brain vascular ECM promotes tumour malignancy through maintenance of the GSC compartment. As cathepsin B has been previously demonstrated to be expressed in GBM-associated vasculature (20) and degrades extracellular laminin (41), it is likely that it plays a role in the cellular cross-talk within the GSC niche. In addition, since cathepsin B has been previously associated with GSCs (42) and cathepsin K with its niche in GBM (32, 33), they are potential proteases that are involved in regulation of GSC homing and/or migration out of their niches. Therefore, we aimed to reveal their localization and activities in a cohort of serial sections of 16 GBM tumours and showing their differential expression pattern.

Materials and Methods

Patients and brain tumour samples

For cryostat sections, GBM samples from 5 patients were obtained from the Brain Tumour Bank maintained by the Department of Neuropathology at the Academic Medical Centre (AMC, Amsterdam, The Netherlands). Research was performed on "waste" material that was stored in a coded fashion. Consent for this project was reviewed and waivered, and the project was approved by the Medical Ethics Review Committee of the Academic Medical Center and University of Amsterdam (reference number W14_224 # 14.17.0286). Consent for removal of the tissue and its storage in the tumour bank for research purposes was obtained and documented in the patients' medical charts. Tissue samples were snap-frozen in liquid nitrogen in the operating room and stored at -80°C until use. Cryostat sections (7-µm thick) were cut at -25°C on an HM560 cryostat (MICROM, Walldorf, Germany), picked up on glass slides, and stored at -80°C until use. All staining procedures, including those for controls, were performed on serial sections of each GBM sample.

For paraffin-embedded tissue sections, GBM tumour biopsies were obtained from GBM patients, that were operated at the Department of Neurosurgery, University Medical Centre of Ljubljana, Slovenia. The study was approved by the National Medical Ethics Committee of the Republic of Slovenia (Approval no. 92/06/13). Altogether, 21 patients with GBM (glioma grade IV) were included. Tumour diagnoses were established by standard histopathology protocols at the Institute of Pathology of the Medical Faculty, University of Ljubljana. Complete patient diagnosis and tumour sample data are shown in the Supporting Information (Supplementary Table 1).

Immunohistochemistry

152 Immunohistochemistry (IHC) was performed on serial cryostat sections (8 µm thick) of 2
153 GBM samples and paraffin-embedded sections (5 µm thick) of 14 GBM tumours. Five series
154 of sections were excluded from the study because of poor morphology and loss of sections
155 during staining procedures.
156 Cryostat sections were air-dried at room temperature for 15 min before staining. Sections
157 were then fixed in acetone (-20°C) for 10 min and air-dried afterwards for 15 min. Sections
158 were encircled with a PAP pen (Dako, Glostrup, Denmark), followed by 3 washing steps of 5
159 min with 1x phosphate-buffered saline (PBS). The sections were treated with 100% methanol
160 containing 0.5% H_2O_2 for 15 min to block endogenous peroxidase activity and to prevent non-
161 specific background staining, followed by 3 washing steps of 5 min each using PBS. Then,
162 sections were incubated in PBS containing 10% normal goat or rat serum (Dako) and 0.1%
163 bovine serum albumin (BSA; Sigma-Adrich) for 45 min to further reduce nonspecific
164 background staining. After tapping off the serum-containing buffer, sections were incubated
165 overnight at 4°C with primary antibodies listed in Table 1. After incubation with primary
166 antibodies, sections were washed 3 times for 5 min in PBS containing 0.1% BSA. Sections
167 incubated with antibodies against Cathepsin K, nestin, SMA and SDF-1α were incubated with
168 polyclonal goat-anti-rabbit secondary antibody conjugated with horse-radish peroxidase
169 (HRP) (Dako) in a 1:200 dilution in PBS containing 0.1% BSA for 1 h. Sections incubated
170 with antibodies against cathepsin B and CD133 were incubated with polyclonal rabbit-anti-
171 mouse secondary antibody conjugated with HRP in a 1:200 dilution in PBS containing 0.1%
172 BSA for 1 h. Sections incubated with anti-cathepsin X antibody were incubated with
173 polyclonal rabbit-anti-goat secondary antibody conjugated with HRP (1:200 dilution; Abcam,
174 UK). Incubation with secondary antibodies was followed by 3 washing steps of 5 min with
175 PBS. Afterwards, sections were incubated with DAB for 10 min, followed by one washing
176 step of 5 min using PBS. Sections were placed in running tap water for 10 min and then in
177 distilled water followed by incubation for 1 min in hematoxylin (Thermo Fisher Scientific,
178 Waltham, MA) to stain nuclei. Sections were again placed in running tap water for 15 min
179 and then in distilled water. All incubation steps were performed at room temperature, except
180 for the overnight incubations with primary antibodies that were performed at 4°C. Finally,
181 sections were covered with glycerin/gelatin mounting medium (Sigma-Aldrich). Control
182 incubations were performed in the absence of primary antibody.
183 Paraffin sections of GBM samples were prepared according to routine procedures of the
184 Institute of Pathology at the University of Ljubljana, Slovenia. Paraffin sections were firstly
185 de-waxed in 100 % xylene (3 min) and then rehydrated in 100%, 96%, 50% and 0% ethanol

(in each ethanol dilution for 3 min). Heat-mediated antigen retrieval was achieved with sodium citrate buffer (pH 6.0). The blockage of endogenous peroxidase activity in the tissue was performed by incubation in the presence of 3% H_2O_2 in 100% methanol for 30 min at room temperature. To reduce non-specific background staining, sections were incubated in a solution of 10 % goat or rabbit normal serum (Dako) in PBS containing 0.1 % BSA. After tapping off the serum-containing buffer, sections were incubated overnight at 4°C with primary antibodies listed in Table 1. Afterwards, sections were incubatied with the secondary horse-radish-peroxidase–conjugated antibodies (1:200; Dako) for 1 h at room temperature as described for the staining of cryostat sections. Protein expression was detected using DAB (Dako) or AEC (Vector Laboratories, Burlingame, CA), and haematoxylin was used for counterstaining. The negative-control staining was performed without the addition of primary antibodies.

All sections were analysed by light microscopy and images were taken using Leica DMLB microscope (Leica, Wetzlar, Germany) and QWin software.

Determination of cathepsin B and K activity by fluorescence metabolic mapping

The activities of cathepsins B and K in GBM serial sections were detected using fluorescence metabolic mapping as described by Van Noorden et al. (43) and Hazen et al. (44). This method is based on the detection of protease activity by coupling 2-hydroxy-5-nitrobenzaldehyde (NSA) with cleaved 4-methoxy-β-naphthylamide (4MβNA), resulting in green fluorescent coupling products. NSA binds also non-specifically to $–NH_2$ groups in proteins, giving rise to a green fluorescent background (for details see Supplementary Fig. 1). Moreover, by imaging sections while they are incubated in medium containing specific substrate and NSA, the formation of green fluorescent final reaction product can be followed in time. Unfixed GBM cryostat sections were air-dried for 10 min and incubated with the drop of incubation medium containing dithiotreitol (final concentration 1 mM; Amresco), EDTA (final concentration 1.3 mM; Sigma), L-cysteine (final concentration 2.7 mM; Merck), 2-hydroxy-5-nitrobenzaldehyde (final concentration 1 mM; Sigma-Aldrich) and specific substrate of the cathepsins (final concentration 1 mg/mL), all dissolved in 100 mM phosphate buffer (pH 6.0). For determination of cathepsin B and K activity, the substrates Z-Ala-Arg-Arg-4MβNA acetate and Z-Gly-Pro-Arg-4MβNA acetate (both Bachem, Switzerland) were used, respectively. After covering the medium on the top of the section by a coverslip, formation of green fluorescence dots was monitored in time in the sections using the fluorescence microscope Leica DMF6 B and FITC filter (excitation filter 440-500 nm;

emission filter 515 nm) for time intervals up to 90 min. The images were taken using the Leica Application Suite X software and Leica DFC 9000 GT camera. The control incubations were carried out in the presence of the cathepsin inhibitor leupeptin (final concentration 5 µM; Sigma) and in the absence of the specific substrate.

Results

Cysteine cathepsins B, X and K are expressed in glioblastoma cells and stromal cells within specific GBM areas

We examined the expression of cathepsins in GBM tissues from 16 patients by performing IHC on GBM sections. Cathepsins B was expressed in macrophages/microglia cells in all 16 samples, in endothelial cells in 4 out of 16 samples, in fibroblast-like cells in 2 out of 16 samples and in GBM cells (Fig. 1A-C). Cathepsin X was expressed in macrophages/microglia cells in all 16 samples, in erythrocytes in all 16 samples, in endothelial cells in 15 out of 16 samples, and in GBM cells in 10/16 samples (Fig. 1D-F). Cathepsin K was expressed in macrophages/microglia cells in all 16 samples, in endothelial cells in 4 out of 16 samples, in fibroblast-like cells in 3 out of 16 samples, and in GBM cells in 7/16 samples (Fig. 1G-I). IHC-stained sections exhibited ubiquitous and granular staining of cathepsins B and X (Fig. 1A, D). The presence of cathepsins in macrophages was demonstrated by comparing the immunostaining pattern of cathepsins and macrophage marker CD68 in consecutive sections of the same GBM sample (Fig. 1C, F, I, J). In contrast to cathepsins B and X, cathepsin K protein expression was not found in all GBM samples and also its immunostaining signal was weaker as compared to that of cathepsins B and X (Fig. 1G). Co-localization of cathepsin K and CD68 was not very strong (Fig. 1I, J). In addition, the immunostaining of all 3 cathepsins was detected in normal brain tissue around the tumour, in microglia cells (data not shown), as also was demonstrated previously by Verbovšek et al. *(45)*.

Expression of cathepsins B, X and K around arterioles

We observed that cathepsins B, X and K were localized around the tunica adventitia of arterioles, cathespin B in 5 out of 166 arterioles, cathepsin X in 49 out of 166 and cathepsin K in 45 out of 166 arterioles. The localization of cathepsin K was distinctly present in specific cells, whereas cathepsin B and X were present in all cancer cells surrounding the arteriole. Moreover, cathepsin B was found in macrophages around arterioles.

Peri-arteriolar GSC niches in GBM samples

We identified peri-arteriolar GSC niches in GBM samples based on immunohistochemical localization of cancer stem cell markers CD133 and nestin, smooth muscle actin (SMA) as smooth muscle cell marker and cytokine SDF-1α, which have been proved to be associated with GSC niches (32, 33). Briefly, CD133 and nestin are the most widely-used GSC-associated markers (46), SMA is localized in smooth muscle cells of arteriolar and venular walls, whereas SDF-1α, a chemotactic cytokine, is produced by endothelial cells and is involved in the retention and maintenance of GSCs within their niches (29, 47). We observed that stem cell marker CD133 was expressed only within a few areas of GBM sections, mostly in the cells adjacent to arterioles, which showed a thicker layer of smooth muscle cells (SMA-positive cells), than the venules (Fig. 2A, B, D, E, G, H). In addition, strong intensity of SDF-1α staining was found around the same arterioles, which were positive for CD133 and SMA, in paraffin-embedded serial sections (Fig. 2C). In cryostat sections, weak staining of SDF-1α was found in CD133- and SMA-positive areas around arterioles, in arteriolar walls and in the endothelial cells. Staining of SDF-1α was observed as well in other parts of GBM sections, which were not related to SMA- and CD133-positive areas (Fig. 2 C, F, I). Nestin, a GSC-associated marker, showed no specificity for GSCs, since nestin staining occurred also in GBM cells outside niches (Fig. 3, 4). Control staining was performed in the absence of primary antibodies and appeared to be negative (Supplementary Fig. 2).

Cathepsins B, X and K are localized in peri-arteriolar GSC niches

Cathepsins B, X and K were expressed in CD133- and nestin-positive cells, as well as in SDF-1α-positive endothelial cells of SMA-positive arterioles in paraffin-embedded (Figs. 3, Supplementary Fig.3) and cryostat serial GBM sections (Fig. 4). In contrast to cathepsin K, cathepsins B and X exhibited similar localization patterns in CD133- and SDF-1α-positive cells and in macrophages/microglia cells (Figs. 3, Supplementary Fig.3). Furthermore, cathepsins were present extracellularly, in astrocyte-like cells and in endothelial cells. Overlap of CD133, cathepsin B, X and K immunostaining in GSC niches was observed (Figs. 3A, D-F, 4A, D-F).

Cathepsin B is proteolytically active in peri-arteriolar GSC niches

In addition to protein expression of cathepsins, we examined the proteolytic activity of cathepsins B and K in serial cryostat sections of GBM using fluorogenic metabolic mapping. This method enabled us to localize and image proteolytically-active proteases in specific regions of the tumours such as GSC niches. Similarly to the protein expression of cathepsin B,

high cathepsin B activity was detected in GBM cryostat sections. The green dots, representing reaction product, started to appear after 5 min incubation in the substrate and NSA-containing medium. After 45 min, green fluorescent dots were observed in cells in the tissue sections, localized near the nuclei (probably lysosomes) and in the peripheral parts of the cells (Fig. 5A, B). After 50 min, recrystallization of the final fluorescent reaction product started to occur, resulting in the formation of needle-like crystals (Supp. Fig. 1C). We detected the activity of cathepsin B in cells within peri-arteriolar GSC niches (Fig. 4 and 5D, E). When we tested the activity of cathepsin K, green fluorescence dots of coupling product started to appear after 20-30 min of incubation. We observed that cathepsin K was proteolytically active only in a few regions of GBM sections and we only found its activity in a few GBM samples (Fig. 5C). After 50-60 min, recrystallization of the final fluorescent reaction product started, resulting in the formation of needle-like crystals. We did not detect cathepsin K activity in areas of GSC niches. Incubations with an inhibitor of serine and cysteine proteases, leupeptin, and the incubations in the absence of the specific substrate, did not produce green fluorescent reaction product (Supplementary Fig. 4). We were not able to demonstrate the activity of cathepsin X because a selective fluorogenic substrate is not available.

Discussion

Five types of GSC niches have been described, perivascular, peri-immune, extracellular matrix, hypoxic and peri-arterioral niches, where GSCs are surrounded by ECM and stromal cells, predominantly endothelial cells and pericytes comprising the vessels and stromal fibroblasts and possibly other brain stroma cell components (35, 48, 49). Juxtacrine signalling between endothelial cells and GBM cells is crucial to keep the stem cell phenotype of GSCs (35, 48, 50, 51) Recently, the 5 types of niches were ingrated unto one concept, the hypoxic peri-arteriolar GSC niche (36), which is a copy of the hematopoietic stem cell niche in the bone marrow (33). In the present study, we analysed immunohistochemically localization patterns of the proteases cathepsins B, X and K in relation to arteriolar walls and in particular GSC niches to determine whether cathepsins B and X are also functionally involved in GSC niche like cathepsin K.

We have recently identified cathepsin K as one of the highest differentially-expressed proteases in GBM tissue and GBM cell lines as compared to normal brain and astrocytes, respectively (45). Cathepsin K protein was found to be localized in GBM tissue in macrophages/microglia cells, in GBM cells, in endothelial cells, in fibroblast-like cells, and in

the tissue layer adjacent to the tunica adventitia. This tissue layer adjacent to the tunica adventitia is considered as the place to be for GSCs, the GSC niche (33, 36). Activity of cathepsin K was detected in low levels in GBM tissues using a highly sensitive fluorogenic method (43, 44). However, cathepsin K activity was not associated with arteriolar walls. In a previous study, we were also not able to detect the activity of cathepsin K in GBM (45), probably due to the tight regulation of cathepsin K activity by ECM components and by the extracellular microenvironment (pH, redox potential) (52).

Cathepsin B protein expression was found to be associated with GBM cells, macrophages/microglia cells, endothelial cells and fibroblast-like cells, confirming our initial (20) and all subsequent studies on its presence in GBM (14, 18). Moreover, cathepsin B was present in GSCs/GBM cells and macrophages/microglia cells around arterioles. Metabolic mapping revealed that cathepin B was active in GSC niches.

Cathepsin X is involved in cancer cell adhesion, migration and invasion via interactions with integrins receptors, either by binding via the RGD motif or by proteolytic cleavage of integrin receptors (22, 53). As integrins are enriched in GSC populations and are participating in GSC self-renewal and therapy resistance (40, 54), cathepsin X modulation of integrins' function may affect GSC fate in GSC niches. In another study, the unfolded pro-cathepsin X was able to reduce the adhesion of hematopoietic stem cells (HSCs) to osteoblasts, implicating that the pro-domain of cathepsin X is directly involved in stem cell trafficking within the niche via modulation of the cell adhesion properties as well as in modulation of chemokines, as discussed below (30). We demonstrated the abundance of cathepsin X in GBM. We localized high levels of cathepsin X in the samples of 16 GBM patients. Cathepsin X was expressed in GBM cells, in macrophages/microglia and in endothelial cells. Cathepsin X appeared to be expressed in high levels in erythrocytes. This novel finding has to be investigated further, but it may well be that cathepsin X is expressed by all types of blood cells and not only erythrocytes (22, 23). Cathepsin X expression was found in a layer adjacent to the tunica adventitia. Its localization gave the impression that cathepsin X, together with B, were not specifically expressed in niches-like regions around arterioles like cathepsin K. However, we cannot rule out that cathepsins B and X have a functional role in the GSC niches.

The 3 cathepsins are structurally and functionally diverse, but were found in the same GSC niche microenvironment in GBM tissues and share the ability to proteolytically degrade the

chemokine SDF-1α, that is present in niches. Previously, we have demonstrated that CXCR4/CXCR7-positive GSCs migrate towards a gradient of SDF-1α and retains the GSCs in peri-arteriolar niches (29, 32). Moreover, the chemoattraction of SDF-1α towards GBM cells was inhibited in the presence of CXCR4 inhibitor plerixafor. Staudt et al. (30) clearly showed that all 3 cathepsins B, X, and K are able to cleave SDF-1α, although with different efficacy, and cleavage sites. This chemokine is also known to be important for retaining haematopoietic stem cells (HSCs) in their niches and only the cleavage of SDF-1α by cathepsin B caused reduction in chemotaxis of HSCs (30). On the other hand, only cathepsin X was able to reduce binding of HSCs to osteoblasts. Interestingly, non-activated pro-cathepsin X and mature cathepsin X did not interfere with HSC–osteoblast interactions. When pro-cathepsin X was treated with dithiothreitol, which unfolds but does not lead to full maturation of cathepsin X, this significantly reduced HSC adhesion to osteoblasts. These observations argue for a role of the accessible cathepsin X prodomain in diminishing cell binding in GSC niches as well. Furthermore, cathepsin K has been proven to act as regulator of GSC migration by specific cleavages of the SDF-1α N-terminal site, inhibiting its chemotactic activity towards GSCs (29). Activation of cathepsin K may thus be a promising target to block the GSC homing in niches and consequently sensitize GSC to therapy. It has also shown that SDF-1α mediates GBM resistance to radiotherapy (55). We may speculate that this is due to keeping the GSC in the protective niches. Altogether, since SDF-1α- and migration-affecting cathepsins B, X and K are all present in all GSC niches, it is possible that cooperation between tuimorall three cathepsins in regulation of SDF-1α chemotactic activity occurs *in vivo*.

In conclusion, we localized the cysteine cathepsins B, X and K in association with SMA-positive arterioles and CD133 and nestin stem cell markers and the GSC niche marker SDF-1α. Moreover, we detected the protease activity of cathepsins B in high levels and that of cathepsin K in low levels in the GBM sections. The localization of cathepsin K is in agreement with a functional role in GSC niches in peri-arteriolar regions. The presence of cathepsins B and X was abundant in the GBM samples and its localization was not specifically associated with the peri-arteriolar GSC niches. Finally, the high cathepsin X expression in erythrocytes is a novel finding and should be investigated further.

Conflicts of interest

No potential conflicts of interest were disclosed.

389

390 **Author contributions**

391 BB: designed the study, performed experiments, analysed and interpreted the data, wrote,
392 revised and approved the final version of the manuscript.
393 CL: provide GBM sections, performed experiments, analysed and interpreted the data,
394 revised the manuscript, approved the final version of the manuscript.
395 MK, TTL, CJFN: designed the study, analysed and interpreted the data, wrote, revised and
396 approved the final version of the manuscript.
397 CJFN: performed the microscopical analysis of the immunolocalization of SMA, and
398 cathepsins B, X and K in the GBM sections.
399 JK, RB: provide GBM samples/sections/antibodies, analysed and interpreted the data, revised
400 the manuscript, approved the final version of the manuscript.

401

402 **Acknowledgements and funding**

403 We would like to thank Mr. Miha Koprivnikar Krajnc (Faculty of Chemistry and Chemical
404 Engineering, University of Ljubljana), Mrs. Daisy Picavet, Mr. Rens van der Waal and Mrs.
405 Karoline Kielbassa (all AMC Amsterdam) for technical assistance. This work was supported
406 by the Slovenian Research Agency (ARRS) of the Republic of Slovenia, Programme P10245
407 (TTL), ARRS young researcher grant (BB) and by the Dutch Cancer Society, grant UVA
408 2014-6839 (MK, CJFN).

409 **References**

410 1. Louis DN, Perry A, Reifenberger G, von Deimling A, Figarella-Branger D, Cavenee WK,
411 Ohgaki H, Wiestler OD, Kleihues P, Ellison DW. The 2016 World Health Organization
412 Classification of Tumors of the Central Nervous System: a summary. Acta Neuropathol.
413 2016;131(6):803-20. doi: 10.1007/s00401-016-1545-1. PubMed PMID: 27157931.
414 2. Cuddapah VA, Robel S, Watkins S, Sontheimer H. A neurocentric perspective on glioma
415 invasion. Nat Rev Neurosci. 2014;15(7):455-65. doi:10.1038/nrn3765. PubMed PMID:
416 24946761; PubMed Central PMCID: PMC5304245.
417 3. Ohgaki H, Kleihues P. The definition of primary and secondary glioblastoma. Clin Cancer
418 Res. 2013;19(4):764-72. doi: 10.1158/1078-0432.CCR-12-3002. PubMed PMID:
419 23209033.
420 4. Claes A, Idema AJ, Wesseling P. Diffuse glioma growth: a guerilla war. Acta
421 Neuropathol. 2007;114(5):443-58. doi:10.1007/s00401-007-0293-7. PubMed PMID:
422 17805551; PubMed Central PMCID: PMC2039798.
423 5. Mentlein R, Hattermann K, Held-Feindt J. Lost in disruption: role of proteases in glioma
424 invasion and progression. Biochim Biophys Acta. 2012;1825(2):178-85. doi:
425 10.1016/j.bbcan.2011.12.001. PubMed PMID: 22209868.
426 6. Paw I, Carpenter RC, Watabe K, Debinski W, Lo HW. Mechanisms regulating glioma
427 invasion. Cancer Lett. 2015;362(1):1-7. doi: 10.1016/j.canlet.2015.03.015. PubMed
428 PMID: 25796440; PubMed Central PMCID: PMC4435977.
429 7. Lah TT, Durán Alonso MB, Van Noorden CJ. Antiprotease therapy in cancer: hot or not?
430 Expert Opin Biol Ther. 2006;6(3):257-279. doi: 10.1517/14712598.6.3.257. PubMed
431 PMID: 16503735.
432 8. Gondi CS, Lakka SS, Yanamandra N, Olivero WC, Dinh DH, Gujrati M, Tung CH,
433 Weissleder R, Rao JS. Adenovirus-mediated expression of antisense urokinase
434 plasminogen activator receptor and antisense cathepsin B inhibits tumor growth, invasion,
435 and angiogenesis in gliomas. Cancer Res. 2004;64(12):4069-77. doi:10.1158/0008-
436 5472.CAN-04-1243. PubMed PMID: 15205313.
437 9. Li Q, Chen B, Cai J, Sun Y, Wang G, Li Y, Li R, Feng Y, Han B, Li J, Tian Y, Yi L,
438 Jiang C. Comparative Analysis of Matrix Metalloproteinase Family Members Reveals
439 That MMP9 Predicts Survival and Response to Temozolomide in Patients with Primary
440 Glioblastoma. PLoS One. 2016;11(3):e0151815. doi: 10.1371/journal.pone.0151815.
441 PubMed PMID: 27022952; PubMed Central PMCID: PMC4811585.

442 10. Quail DF, Joyce JA. The Microenvironmental Landscape of Brain Tumors. Cancer Cell.
443 2017;31(3):326-341. doi: 10.1016/j.ccell.2017.02.009. PubMed PMID: 28292436;
444 PubMed Central PMCID: PMC5424263.
445 11. Song G, Luo T, Dong L, Liu Q. Extracellular diffusion quantified by magnetic resonance
446 imaging during rat C6 glioma cell progression. Braz J Med Biol Res. 2017;50(7):e5403.
447 doi: 10.1590/1414-431X20175403. PubMed PMID: 28678913; PubMed Central PMCID:
448 PMC5496150.
449 12. Kramer L, Turk D, Turk B. The Future of Cysteine Cathepsins in Disease Management.
450 Trends Pharmacol Sci. 2017;38(10):873-898. doi: 10.1016/j.tips.2017.06.003. PubMed
451 PMID: 28668224.
452 13. Breznik B, Motaln H, Turnšek TL. Proteases and cytokines as mediators of interactions
453 between cancer and stromal cells in tumours. Biol Chem. 2017;398(7):709-719. doi:
454 10.1515/hsz-2016-0283. PubMed PMID: 28002021.
455 14. Gole B, Huszthy PC, Popović M, Jeruc J, Ardebili YS, Bjerkvig R, Lah TT. The
456 regulation of cysteine cathepsins and cystatins in human gliomas. Int J Cancer.
457 2012;131(8):1779-89. doi:10.1002/ijc.27453. PubMed PMID:22287159.
458 15. Olson OC, Joyce JA. Cysteine cathepsin proteases: regulators of cancer progression and
459 therapeutic response. Nat Rev Cancer. 2015;15(12):712-29. doi: 10.1038/nrc4027.
460 PubMed PMID: 26597527.
461 16. Kenig S, Frangež R, Pucer A, Lah T. Inhibition of cathepsin L lowers the apoptotic
462 threshold of glioblastoma cells by up-regulating p53 and transcription of caspases 3 and 7.
463 Apoptosis. 2011;16(7):671-82. doi: 10.1007/s10495-011-0600-6. PubMed PMID:
464 21484410.
465 17. López-Otín C, Matrisian LM. Emerging roles of proteases in tumour suppression. Nat Rev
466 Cancer. 2007;7(10):800-8. doi: 10.1038/nrc2228. PubMed PMID: 17851543.
467 18. Strojnik T, Kavalar R, Trinkaus M, Lah TT. Cathepsin L in glioma progression:
468 comparison with cathepsin B. Cancer Detect Prev. 2005;29(5):448-55. doi:
469 10.1016/j.cdp.2005.07.006. PubMed PMID: 16183211.
470 19. Colin C, Voutsinos-Porche B, Nanni I, Fina F, Metellus P, Intagliata D, Baeza N, Bouvier
471 C, Delfino C, Loundou A, Chinot O, Lah T, Kos J, Martin PM, Ouafik L, Figarella-
472 Branger D. High expression of cathepsin B and plasminogen activator inhibitor type-1 are
473 strong predictors of survival in glioblastomas. Acta Neuropathol. 2009;118(6):745-54.
474 doi:10.1007/s00401-009-0592-2. PubMed PMID: 19774387.

475 20. Strojnik T, Kos J, Zidanik B, Golouh R, Lah T. Cathepsin B immunohistochemical
476 staining in tumor and endothelial cells is a new prognostic factor for survival in patients
477 with brain tumors. Clin Cancer Res. 1999;5(3):559-67. PubMed PMID: 10100707.
478 21. Mitrović A, Pečar Fonović U, Kos J. Cysteine cathepsins B and X promote epithelial-
479 mesenchymal transition of tumor cells. Eur J Cell Biol. 2017;96(6):622-631. doi:
480 10.1016/j.ejcb.2017.04.003. PubMed PMID: 28495172.
481 22. Kos J, Vižin T, Fonović UP, Pišlar A. Intracellular signaling by cathepsin X: molecular
482 mechanisms and diagnostic and therapeutic opportunities in cancer. Semin Cancer Biol.
483 2015;31:76-83. doi: 10.1016/j.semcancer.2014.05.001. PubMed PMID: 24835450.
484 23. Kos J, Jevnikar Z, Obermajer N. The role of cathepsin X in cell signaling. Cell Adh Migr.
485 2009;3(2):164-6. PubMed PMID: 19262176; PubMed Central PMCID: PMC2679876.
486 24. Wendt W, Zhu XR, Lübbert H, Stichel CC. Differential expression of cathepsin X in
487 aging and pathological central nervous system of mice. Exp Neurol. 2017;204(2):525-40.
488 doi: 10.1016/j.expneurol.2007.01.007. PubMed PMID: 17306794.
489 25. Krueger S, Kalinski T, Hundertmark T, Wex T, Küster D, Peitz U, Ebert M, Nägler DK,
490 Kellner U, Malfertheiner P, Naumann M, Röcken C, Roessner A. Up-regulation of
491 cathepsin X in Helicobacter pylori gastritis and gastric cancer. J Pathol. 2015;207(1):32-
492 42. doi: 10.1002/path.1820. PubMed PMID: 16025436.
493 26. Nägler DK, Krüger S, Kellner A, Ziomek E, Menard R, Buhtz P, Krams M, Roessner A,
494 Kellner U. Up-regulation of cathepsin X in prostate cancer and prostatic intraepithelial
495 neoplasia. Prostate. 2004;60(2):109-19. doi: 10.1002/pros.20046. PubMed PMID:
496 15162377.
497 27. Vižin T, Christensen IJ, Wilhelmsen M, Nielsen HJ, Kos J. Prognostic and predictive
498 value of cathepsin X in serum from colorectal cancer patients. BMC Cancer. 2014;14:259.
499 doi: 10.1186/1471-2407-14-259. PubMed PMID: 24725597; PubMed Central PMCID:
500 PMC4021260.
501 28. Verbovšek U, Van Noorden CJ, Lah TT. Complexity of cancer protease biology:
502 Cathepsin K expression and function in cancer progression. Semin Cancer Biol.
503 2015;35:71-84. doi: 10.1016/j.semcancer.2015.08.010. PubMed PMID: 26320409.
504 29. Hira VV, Verbovšek U, Breznik B, Srdič M, Novinec M, Kakar H, Wormer J, der Swaan
505 BV, Lenarčič B, Juliano L, Mehta S, Van Noorden CJ, Lah TT. Cathepsin K cleavage of
506 SDF-1α inhibits its chemotactic activity towards glioblastoma stem-like cells. Biochim
507 Biophys Acta. 2017;1864(3):594-603. doi: 10.1016/j.bbamcr.2016.12.021. PubMed
508 PMID: 28040478.

509 30. Staudt ND, Maurer A, Spring B, Kalbacher H, Aicher WK, Klein G. Processing of
510 CXCL12 by different osteoblast-secreted cathepsins. Stem Cells Dev. 2012;21(11):1924-
511 35. doi: 10.1089/scd.2011.0307. PubMed PMID: 22066471; PubMed Central PMCID:
512 PMC3396142.
513 31. Godlewski J, Ferrer-Luna R, Rooj AK, Mineo M, Ricklefs F, Takeda YS, Nowicki MO,
514 Salińska E, Nakano I, Lee H, Weissleder R, Beroukhim R, Chiocca EA, Bronisz A.
515 MicroRNA Signatures and Molecular Subtypes of Glioblastoma: The Role of
516 Extracellular Transfer. Stem Cell Reports. 2017;8(6):1497-1505.
517 doi:10.1016/j.stemcr.2017.04.024. PubMed PMID: 28528698; PubMed Central PMCID:
518 PMC5470095.
519 32. Hira VV, Ploegmakers KJ, Grevers F, Verbovšek U, Silvestre-Roig C, Aronica E,
520 Tigchelaar W, Turnšek TL, Molenaar RJ, Van Noorden CJ. CD133+ and Nestin+ Glioma
521 Stem-Like Cells Reside Around CD31+ Arterioles in Niches that Express SDF-1α,
522 CXCR4, Osteopontin and Cathepsin K. J Histochem Cytochem. 2015;63(7):481-93. doi:
523 10.1369/0022155415581689. PubMed PMID: 25809793.
524 33. Hira VVV, Wormer JR, Kakar H, Breznik B, van der Swaan B, Hulsbos R, Tigchelaar W,
525 Tonar Z, Khurshed M, Molenaar RJ, Van Noorden CJF. Periarteriolar Glioblastoma Stem
526 Cell Niches Express Bone Marrow Hematopoietic Stem Cell Niche Proteins. J Histochem
527 Cytochem. 2018:22155417749174. doi: 10.1369/0022155417749174. PubMed PMID:
528 29297738. –Epub ahead of print
529 34. Lathia JD, Mack SC, Mulkearns-Hubert EE, Valentim CL, Rich JN. Cancer stem cells in
530 glioblastoma. Genes Dev. 2015;29(12):1203-17. doi: 10.1101/gad.261982.115. PubMed
531 PMID: 26109046; PubMed Central PMCID: PMC4495393.
532 35. Roos A, Ding Z, Loftus JC, Tran NL. Molecular and Microenvironmental Determinants of
533 Glioma Stem-Like Cell Survival and Invasion. Front Oncol. 2017;7:120. doi:
534 10.3389/fonc.2017.00120. PubMed PMID: 28670569; PubMed Central PMCID:
535 PMC5472661.
536 36. Hira VVV, Aderetti DA, van Noorden CJF. Glioma Stem Cell Niches in Human
537 Glioblastoma Are Periarteriolar. J Histochem Cytochem. 2018:22155417752676. doi:
538 10.1369/0022155417752676. PubMed PMID: 29328867. -Epub ahead of print
539 37. Hira VVV, Van Noorden CJF, Carraway HE, Maciejewski JP, Molenaar RJ. Novel
540 therapeutic strategies to target leukemic cells that hijack compartmentalized continuous
541 hematopoietic stem cell niches. Biochim Biophys Acta. 2017;1868(1):183-198. doi:
542 10.1016/j.bbcan.2017.03.010. PubMed PMID: 28363872.

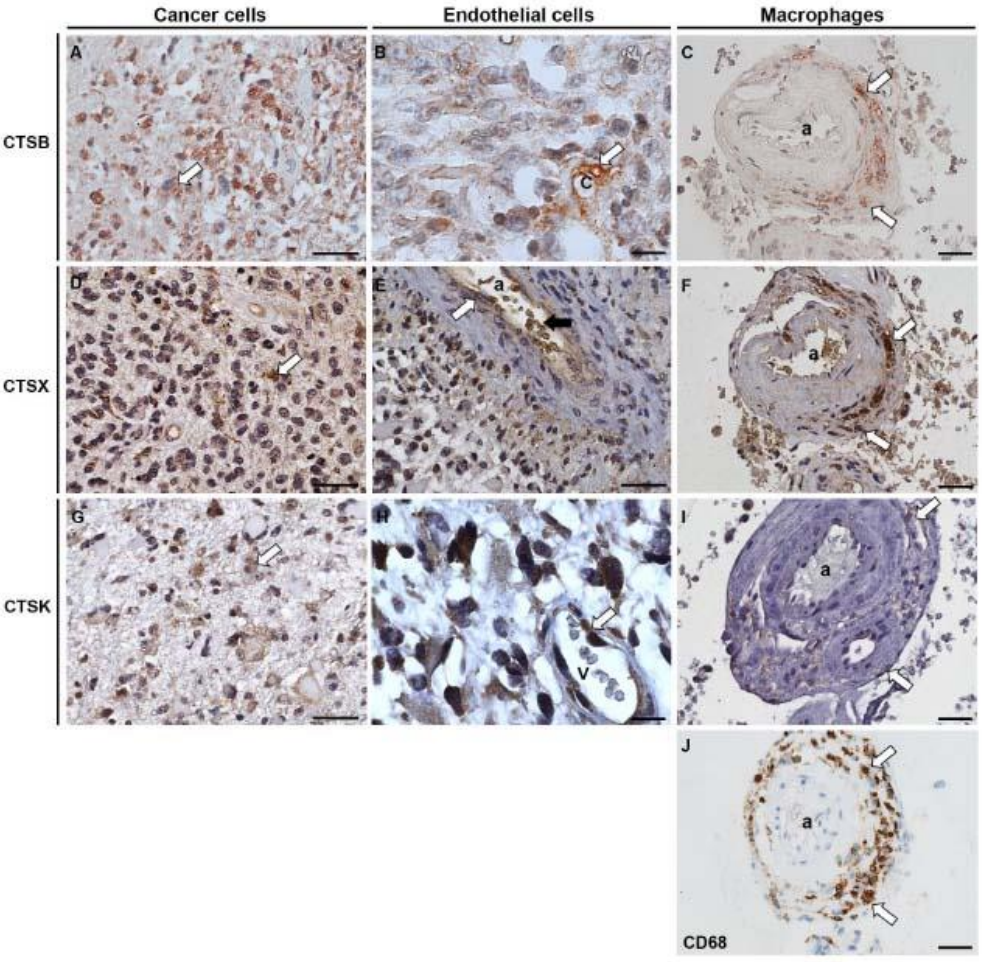
543 38. Hambardzumyan D, Bergers G. Glioblastoma: Defining Tumor Niches. Trends Cancer.
544 2015;1(4):252-265. doi:10.1016/j.trecan.2015.10.009. PubMed PMID: 27088132;
545 PubMed Central PMCID: PMC4831073.
546 39. Jackson M, Hassiotou F, Nowak A. Glioblastoma stem-like cells: at the root of tumor
547 recurrence and a therapeutic target. Carcinogenesis. 2015;36(2):177-85. doi:
548 10.1093/carcin/bgu243. PubMed PMID: 25504149.
549 40. Lathia JD, Li M, Hall PE, Gallagher J, Hale JS, Wu Q, Venere M, Levy E, Rani MR,
550 Huang P, Bae E, Selfridge J, Cheng L, Guvenc H, McLendon RE, Nakano I, Sloan AE,
551 Phillips HS, Lai A, Gladson CL, Bredel M, Bao S, Hjelmeland AB, Rich JN. Laminin
552 alpha 2 enables glioblastoma stem cell growth. Ann Neurol. 2012;72(5):766-78. doi:
553 10.1002/ana.23674. PubMed PMID: 23280793; PubMed Central PMCID: PMC3615417.
554 41. Lah TT, Buck MR, Honn KV, Crissman JD, Rao NC, Liotta LA, Sloane BF. Degradation
555 of laminin by human tumor cathepsin B. Clin Exp Metastasis. 1989;7(4):461-8. PubMed
556 PMID: 2785014.
557 42. Koh SP, Wickremesekera AC, Brasch HD, Marsh R, Tan ST, Itinteang T. Expression of
558 Cathepsins B, D, and G in Isocitrate Dehydrogenase-Wildtype Glioblastoma. Front Surg.
559 2017;4:28. doi: 10.3389/fsurg.2017.00028. PubMed PMID: 28611989; PubMed Central
560 PMCID: PMC5447023.
561 43. Van Noorden CJ, Vogels IM, Everts V, Beertsen W. Localization of cathepsin B activity
562 in fibroblasts and chondrocytes by continuous monitoring of the formation of a final
563 fluorescent reaction product using 5-nitrosalicylaldehyde. Histochem J. 1987;19(9):483-7.
564 PubMed PMID: 3440760.
565 44. Hazen LG, Bleeker FE, Lauritzen B, Bahns S, Song J, Jonker A, Van Driel BE, Lyon H,
566 Hansen U, Köhler A, Van Noorden CJ. Comparative localization of cathepsin B protein
567 and activity in colorectal cancer. J Histochem Cytochem. 2000;48(10):1421-30. doi:
568 10.1177/002215540004801012. PubMed PMID: 10990495.
569 45. Verbovšek U, Motaln H, Rotter A, Atai NA, Gruden K, Van Noorden CJ, Lah TT.
570 Expression analysis of all protease genes reveals cathepsin K to be overexpressed in
571 glioblastoma. PLoS One. 2014;9(10):e111819. doi: 10.1371/journal.pone.0111819.
572 PubMed PMID: 25356585; PubMed Central PMCID: PMC4214761.
573 46. Podergajs N, Motaln H, Rajčević U, Verbovšek U, Koršič M, Obad N, Espedal H, Vittori
574 M, Herold-Mende C, Miletic H, Bjerkvig R, Turnšek TL. Transmembrane protein CD9 is
575 glioblastoma biomarker, relevant for maintenance of glioblastoma stem cells. Oncotarget.

576 2016;7(1):593-609. doi: 10.18632/oncotarget.5477. PubMed PMID: 26573230; PubMed
577 Central PMCID: PMC4808020.
578 47. Plaks V, Kong N, Werb Z. The cancer stem cell niche: how essential is the niche in
579 regulating stemness of tumor cells? Cell Stem Cell. 2015;16(3):225-38. doi:
580 10.1016/j.stem.2015.02.015. PubMed PMID: 25748930; PubMed Central PMCID:
581 PMC4355577.
582 48. Calabrese C, Poppleton H, Kocak M, Hogg TL, Fuller C, Hamner B, Oh EY, Gaber MW,
583 Finklestein D, Allen M, Frank A, Bayazitov IT, Zakharenko SS, Gajjar A, Davidoff A,
584 Gilbertson RJ. A perivascular niche for brain tumor stem cells. Cancer Cell.
585 2007;11(1):69-82. doi:10.1016/j.ccr.2006.11.020. PubMed PMID:17222791.
586 49. Breznik B, Motaln H, Vittori M, Rotter A, Lah Turnšek T. Mesenchymal stem cells
587 differentially affect the invasion of distinct glioblastoma cell lines. Oncotarget.
588 2017;8(15):25482-25499. doi:10.18632/oncotarget.16041. PubMed PMID: 28424417;
589 PubMed Central PMCID: PMC5421945.
590 50. Schiffer D, Mellai M, Annovazzi L, Caldera V, Piazzi A, Denysenko T, Melcarne A. Stem
591 cell niches in glioblastoma: a neuropathological view. Biomed Res Int.
592 2014;2014:725921. doi: 10.1155/2014/725921. PubMed PMID: 24834433; PubMed
593 Central PMCID: PMC4009309.
594 51. Zhu TS, Costello MA, Talsma CE, Flack CG, Crowley JG, Hamm LL, He X, Hervey-
595 Jumper SL, Heth JA, Muraszko KM, DiMeco F, Vescovi AL, Fan X. Endothelial cells
596 create a stem cell niche in glioblastoma by providing NOTCH ligands that nurture self-
597 renewal of cancer stem-like cells. Cancer Res. 2011;71(18):6061-72. doi: 10.1158/0008-
598 5472.CAN-10-4269. PubMed PMID: 21788346; PubMed Central PMCID: PMC3355476.
599 52. Novinec M, Lenarčič B. Cathepsin K: a unique collagenolytic cysteine peptidase. Biol
600 Chem. 2013;394(9):1163-79. doi: 10.1515/hsz-2013-0134. PubMed PMID: 23629523.
601 53. Akkari L, Gocheva V, Kester JC, Hunter KE, Quick ML, Sevenich L, Wang HW, Peters
602 C, Tang LH, Klimstra DS, Reinheckel T, Joyce JA. Distinct functions of macrophage-
603 derived and cancer cell-derived cathepsin Z combine to promote tumor malignancy via
604 interactions with the extracellular matrix. Genes Dev. 2014;28(19):2134-50. doi:
605 10.1101/gad.249599.114. PubMed PMID: 25274726; PubMed Central PMCID:
606 PMC4180975.
607 54. Seguin L, Desgrosellier JS, Weis SM, Cheresh DA. Integrins and cancer: regulators of
608 cancer stemness, metastasis, and drug resistance. Trends Cell Biol. 2015;25(4):234-40.

609 doi: 10.1016/j.tcb.2014.12.006. PubMed PMID: 25572304; PubMed Central PMCID:
610 PMC4380531.
611 55. Goffart N, Lombard A, Lallemand F, Kroonen J, Nassen J, Di Valentin E, Berendsen S,
612 Dedobbeleer M, Willems E, Robe P, Bours V, Martin D, Martinive P, Maquet P, Rogister
613 B. CXCL12 mediates glioblastoma resistance to radiotherapy in the subventricular zone.
614 Neuro Oncol. 2017;19(1):66-77. doi:10.1093/neuonc/now136. PubMed PMID:
615 27370398; PubMed Central PMCID: PMC5193023.

616

617 **Figures**



618

619 **Figure 1. Immunohistochemical staining of cathepsins B, X and K in paraffin-embedded**
620 **sections of human GBM.**

All 3 cathepsins were present in GBM cells in sections of GBM tumour samples (A, D, G, indicated by arrows). Protein expression of cathepsins B (A-C), X (D-F) and K (G-I) was present in endothelial cells of blood vessels (B, E, H; indicated by white arrows), the most intensive endothelial cell labelling being that of cathepsin X. Cathepsin X expression was high in erythrocytes (E, indicated by black arrow). Macrophage marker CD68, detected in the wall of one arteriole (C, F, I, J; indicated by arrows) was co-localized with cathepsins B and X expression, and to a lesser degree with cathepsin K expression in serial GBM sections. Imunohistochemical labelling of cathepsin B (A-C) was detected using AEC substrate (red colour) and that of cathepsins X and K and CD68 (D-J) using DAB substrate (brown colour). Cell nuclei were counterstained using haematoxylin (blue/purple). a, arteriole; c, capillary; v, venule. **A, D, G, E**: scale bar = 30 μm; **B, H**: scale bar = 10 μm; **C, F, I, J**: scale bar = 20 μm.

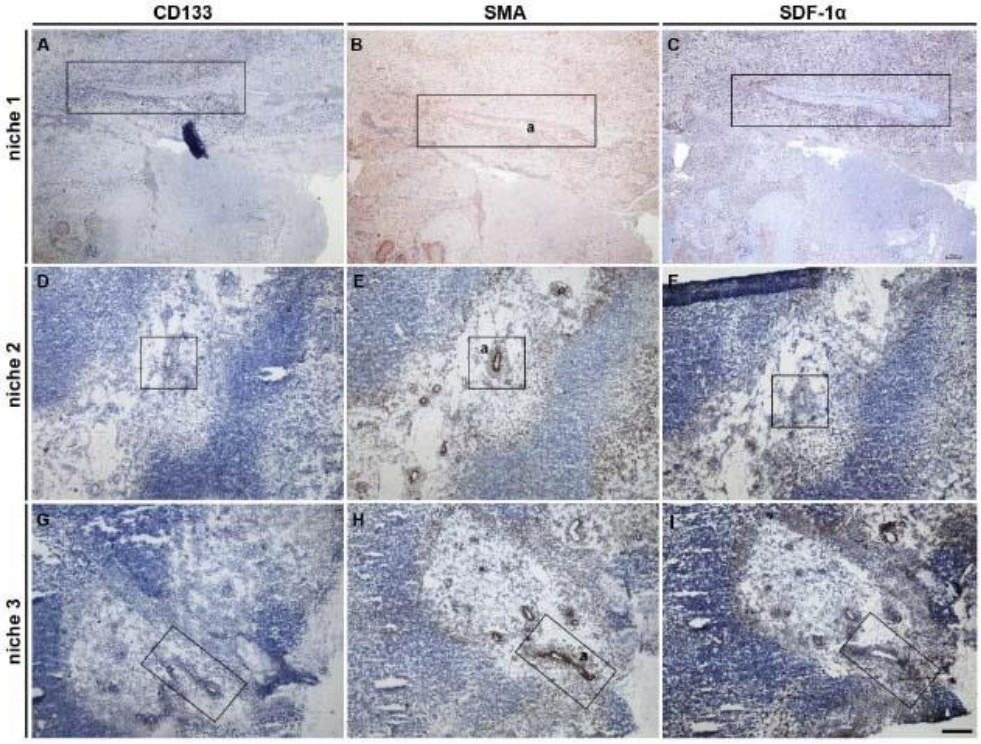
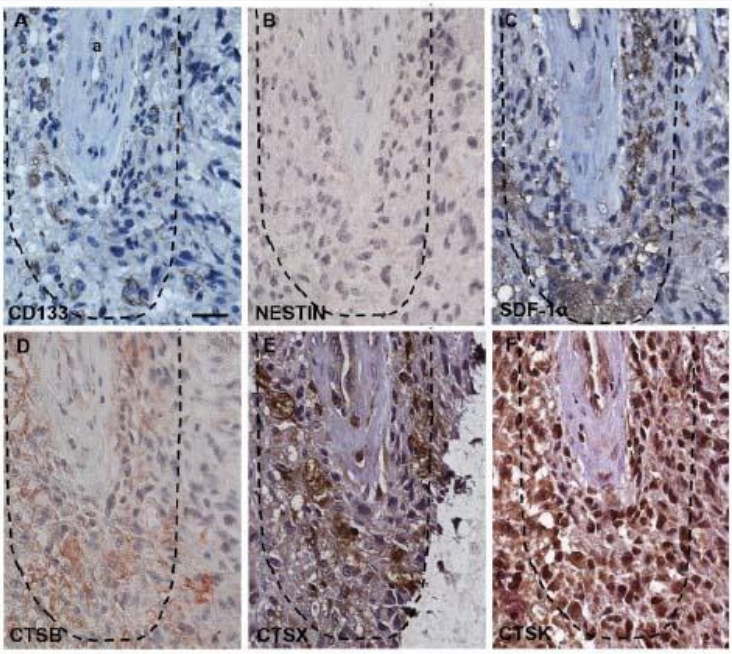


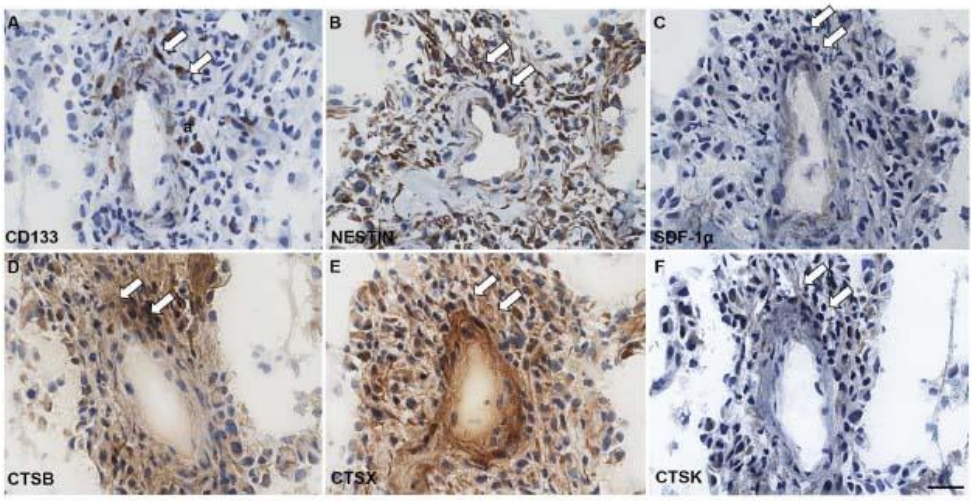
Figure 2. Low-magnification images of peri-arteriolar GSC niches, after immunohistochemical labelling of CD133, SMA and SDF-1α in paraffin-embedded sections and cryostat sections.

637 Serial sections of GBM were screened for GSC niche regions, stained for stem cell marker
638 CD133 (A, D, G) at low magnification (4x). GSC niches (marked by the rectangles) were also
639 immunolabelled for cytokine SDF-1α (C, F, I), using DAB substrate (brown colour) and
640 SMA-positive arterioles (B, E, H), as detected using AEC (B; red colour) or DAB substrate
641 (E, H; brown colour). Niche 1 (A-C) and niches 2 and 3 (D-I) were found in different GBM
642 patients. Cell nuclei were counterstained using haematoxylin (blue/purple). Niches are
643 marked by rectangles. a = arteriole. Scale bar = 200 μm.
644



645

646 **Figure 3. High-magnification images of serial paraffin-embedded GBM sections labelled**
647 **for GSC niche markers and cathepsins.**
648 Cathepsins B (D,), X (E,) and K (F,) are highly expressed within GSC niches (A-C) and their
649 expression was co-localised with CD133-positive cells (A, D-F). High-magnification images
650 of niche 1 of Figure 2 are presented. Immunohistochemical labelling of nestin (B) and
651 cathepsin B (D) was performed with AEC as substrate (red colour) and of the other proteins
652 (A, C, E, F) with DAB as substrate (brown colour). Cell nuclei were counterstained using
653 haematoxylin (blue/purple). a = arteriole. **A-F**: scale bar = 20 μm.
654



655

656 **Figure 4. Serial cryostat GBM sections immunohistochemically stained for GSC niche**
657 **markers and cathepsins.**
658 CD133 (A) was expressed in distinct GSC cells located around arterioles. Nestin (B)
659 extensively labelled some of the CD133-positive cells, endothelial cells of the arteriole and
660 GBM/GSC cells distant from arterioles. SDF-1α expression (C) was associated with CD133-
661 positive GSCs and endothelial cells of the arteriole. Cathepsin B expression (D) was present
662 in GSCs/GBM cells close to arterioles and also distant to the niche, where focal and diffuse
663 staining was observed, possibly indicating its extracellular localization. Cathepsin X (E) was
664 most intensely expressed in GSCs and endothelial cells in the niche, as well as in the more
665 distant GBM cells. Cathepsin K (F) was expressed less intensely in the GSC niche,
666 endothelial cells and in GBM cells distant to the niche. CD133-positive cells are indicated by
667 arrows. High-magnification images of niche 2 of Figure 2 are presented. a = arteriole. Scale
668 bar = 20 μm.
669

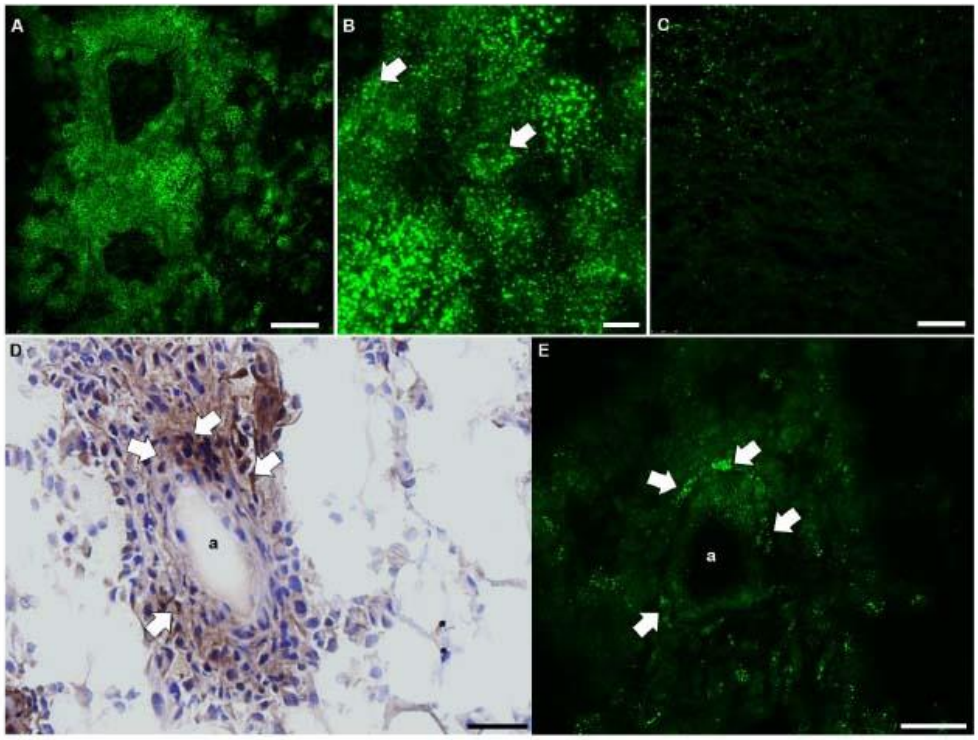


Figure 5. Activity of cathepsins B and K in GBM cryostat sections. Green fluorescent dots, representing cathepsin B (A, B, E) and K (C) proteolytic activity were detected in GBM sections. Higher magnification of GBM section with cathepsin B activity (B). Arrows indicate cathepsin B activity (green fluorescent coupling products) in the cells. Overlap of cathepsin B protein expression (D) and cathepsin B activity (E) in GSC niche as indicated by arrows. High-magnification images of niche 2 of Figure 2 are presented. a = arteriole. **A, D, E**: scale bar = 50 µm; **B**: scale bar = 10 µm; **C**: scale bar = 100 µm.

679 **Table 1. Primary antibodies and their dilutions used in immunohistochemical analyses**

Primary antibodies	Source	Dilution cryostat sections	Dilution paraffin sections	
Cathepsin B (mouse anti-human)	Faculty of Pharmacy, University of Ljubljana (3E1)	1:200	1:100	
Cathepsin K (rabbit anti-human)	Abcam (ab19027)	1:200	1:200	
Cathepsin X (goat anti-human)	R&D systems (AF934)	1:200	1:200	
CD133 (prominin-1) (mouse anti-human)	Miltenyi Biotech (W6B3C1)	1:50	1:10	
SDF-1α (stromal-derived factor 1α) (rabbit anti-human)	Abcam (ab9797)	1:200	1:200	
Nestin (rabbit anti-human)	Acris (R1555P)	1:200	1:200	
SMA (smooth muscle actin) (rabbit anti-human)	Abcam (ab5694)	1:200	1:200	
CD68 (mouse anti-human)	Dako (clone EBM 11)	/	1:50	

680

2.7 Cathepsin K Cleavage of SDF-1α Inhibits its Chemotactic Activity Towards Glioblastoma Stem-Like Cells

Vashendriya V.V. Hira, Urška Verbovšek, Barbara Breznik, Matic Srdič, Marko Novinec, Hala Kakar, JillWormer, Britt Van der Swaan, Brigita Lenarčič, Luiz Juliano, Shwetal Mehta, Cornelis J.F. Van Noorden, Tamara T. Lah

Biochimica et Biophysica Acta 2017; 1864(3): 594-603. DOI: 10.1016/j.bbamcr.2016.12.021

Biochimica et Biophysica Acta 1864 (2017) 594–603

Contents lists available at ScienceDirect

Biochimica et Biophysica Acta

journal homepage: www.elsevier.com/locate/bbamcr

Cathepsin K cleavage of SDF-1α inhibits its chemotactic activity towards glioblastoma stem-like cells

Vashendriya V.V. Hira [a,b,*,1], Urška Verbovšek [c,1], Barbara Breznik [c,d], Matic Srdič [e], Marko Novinec [e], Hala Kakar [a], Jill Wormer [a], Britt Van der Swaan [a], Brigita Lenarčič [e], Luiz Juliano [f], Shwetal Mehta [b], Cornelis J.F. Van Noorden [a], Tamara T. Lah [c,d,e]

[a] Department of Cell Biology and Histology, Academic Medical Center, University of Amsterdam, Meibergdreef 15, 1105 AZ Amsterdam, The Netherlands
[b] Division of Neurobiology, Barrow Brain Tumor Research Center, Barrow Neurological Institute, St. Joseph's Hospital and Medical Center, Phoenix, AZ 85013, USA
[c] Department of Genetic Toxicology and Cancer Biology, National Institute of Biology, Večna pot 111, 1000 Ljubljana, Slovenia
[d] Jozef Stefan International Postgraduate School, Jamova 39, 1000 Ljubljana, Slovenia
[e] Department of Biochemistry, Faculty of Chemistry and Chemical Engineering, University of Ljubljana, Večna pot 113, 1000 Ljubljana, Slovenia
[f] Department of Biophysics, Medical School, Federal University of Sao Paulo, Brazil

ARTICLE INFO

Article history:
Received 12 August 2016
Received in revised form 22 December 2016
Accepted 27 December 2016
Available online 28 December 2016

Keywords:
Glioma stem-like cells
Niche
Stromal-derived factor-1α
Cathepsin K

ABSTRACT

Glioblastoma (GBM) is the most aggressive primary brain tumor with poor patient survival that is at least partly caused by malignant and therapy-resistant glioma stem-like cells (GSLCs) that are protected in GSLC niches. Previously, we have shown that the chemo-attractant stromal-derived factor-1α (SDF-1α), its C-X-C receptor type 4 (CXCR4) and the cysteine protease cathepsin K (CatK) are localized in GSLC niches in glioblastoma. Here, we investigated whether SDF-1α is a niche factor that through its interactions with CXCR4 and/or its second receptor CXCR7 on GSLCs facilitates their homing to niches. Furthermore, we aimed to prove that SDF-1α cleavage by CatK inactivates SDF-1α and inhibits the invasion of GSLCs. We performed mass spectrometric analysis of cleavage products of SDF-1α after proteolysis by CatK. We demonstrated that CatK cleaves SDF-1α at 3 sites in the N-terminus, which is the region of SDF-1α that binds to its receptors. Confocal imaging of human GBM tissue sections confirmed co-localization of SDF-1α and CatK in GSLC niches. In accordance, 2D and 3D invasion experiments using CXCR4/CXCR7-expressing GSLCs and GBM cells showed that SDF-1α had chemotactic activity whereas CatK cleavage products of SDF-1α did not. Besides, CXCR4 inhibitor plerixafor inhibited invasion of CXCR4/CXCR7-expressing GSLCs.

In conclusion, CatK can cleave and inactivate SDF-1α. This implies that CatK activity facilitates migration of GSLCs out of niches. We propose that activation of CatK may be a promising strategy to prevent homing of GSLCs in niches and thus render these cells sensitive to chemotherapy and radiation.

© 2016 Elsevier B.V. All rights reserved.

1. Introduction

Glioblastoma (GBM) is the most malignant primary brain tumor with poor patient survival despite surgery, irradiation and chemotherapy. This is at least partly due to the existence of glioma stem-like cells (GSLCs) that are resistant to therapy [1–6]. Therefore, targeting GSLCs is the key to improve anti-GBM therapy [1–6]. GSLCs reside in protective niches, which are at least partly responsible for their resistance to therapy [1,7,8]. We have shown in a previous study in human GBM that GSLCs reside around the endothelium of arterioles in hypoxic niches, expressing the chemokine stromal-derived factor-1α (SDF-1α), its receptors C-X-C receptor type 4 (CXCR4) and the cysteine protease cathepsin K (CatK) [9]. These proteins are also functional in hematopoietic stem cell (HSC) niches in human bone marrow, where CXCR4-positive HSCs are retained in hypoxic niches by high levels of SDF-1α [10–13] (Hira et al., submitted). Bone-resorbing osteoclasts in bone marrow release several proteases during stress conditions, such as CatK that alone or collectively inactivate SDF-1α, resulting in migration of HSCs out of HSC niches into the circulation [12,14,15] (Hira et al., submitted).

The SDF-1α/CXCR4 signaling axis is overexpressed in many types of cancer, including GBM [7,16,17]. Another receptor for SDF-1α is CXCR7 that is like CXCR4 overexpressed in GBM cells and in particular in GSLCs [18–21]. This upregulation of SDF-1α, CXCR4 and CXCR7 in GBM is

Abbreviations: CatK, cathepsin K; CXCR4/7, C-X-C receptor type 4/7; GBM, glioblastoma; GSLC, glioma stem-like cell; HIF-1α, hypoxia-inducible factor-1α; HSC, hematopoietic stem cell; IHC, immunohistochemistry; SDF-1α, stromal-derived factor-1α; VEGF, vascular endothelial growth factor.

* Corresponding author at: Academic Medical Center, Department of Cell Biology and Histology, Meibergdreef 15, 1105 AZ Amsterdam, The Netherlands.
E-mail address: v.v.hira@amc.uva.nl (V.V.V. Hira).

[1] Authors contributed equally.

http://dx.doi.org/10.1016/j.bbamcr.2016.12.021
0167-4889/© 2016 Elsevier B.V. All rights reserved.

induced by hypoxia-inducible factor-1α (HIF-1α) and vascular endothelial growth factor (VEGF) [16,17], which are abundantly expressed in and around GSLC niches [9]. GSLCs are attracted by SDF-1α [22–27] and the SDF-1α/CXCR4 and SDF-1α/CXCR7 axes can facilitate homing of GSLCs into GSLC niches and protect GSLCs against chemo-irradiation [7]. Therefore, the development of novel strategies is in progress to prevent homing of GSLCs in niches and/or to enforce migration of GSLCs out of niches to render these cells sensitive to chemo-irradiation [7,8] (Hira et al., submitted).

CatK is an endolysosomal cysteine endopeptidase and is one of the highest differentially expressed proteases in GBM as compared to normal brain [28,29]. This was shown in an in silico study of gene expression in human GBM using publically-available data sets, in GBM tissue samples and in GBM cell lines. The overexpression of CatK was validated with RT-PCR, western blotting and immunohistochemistry [29]. However, activity of CatK has not been detected in extracts of GBM tissues and cells, in contrast to the high activity of CatB and CatS that is likely involved in invasion [30]. CatK activity may well not be detected because it is tightly regulated, which is needed to control its highly destructive proteolytic power [28,29,31]. Since CatK can cleave SDF-1α in human HSC niches [12,14,15] (Hira et al., submitted) and it is expressed in GSLC niches together with SDF-1α [9,28], we hypothesize that SDF-1α facilitates homing of CXCR4 and/or CXCR7-positive GSLCs in niches and that CatK regulates SDF-1α activity [9]. In the present study, we provide supporting evidence for this concept.

2. Materials and methods

2.1. Cell culture

NCH421k GSLCs [32,33] were a generous gift from Prof. Christel Herold-Mende (Heidelberg University, Heidelberg, Germany), and were cultured in Neurobasal medium (Gibco Life Technologies, Carlsbad, CA, USA) containing 1% penicillin/streptomycin (Sigma, St. Louis, MO, USA), 1% L-glutamine (Sigma), 2% B27, 0.08% bFGF (Gibco), 0.01% EGF (Gibco) and 0.01% heparin (Sigma) at 37 °C in a 5% CO_2 incubator. U87 GBM cells (ATTC, Teddington, Middlesex, UK) were cultured in DMEM medium (Sigma) containing 1% penicillin/streptomycin, 1% L-glutamine and 10% fetal bovine serum (Gibco) at 37 °C in a 5% CO_2 incubator. These cells were authenticated as described by Torsvik et al. [34]. Patient-derived cell line GB7 was established from resected primary GBM tumor tissue at the Barrow Neurological Institute, Phoenix, AZ, USA. These GSLCs were grown as neurospheres (Gibco) in DMEM and F12-Glutamax (Gibco) supplemented with B27 (Thermo Fisher Scientific; Waltham, MA, USA) and N2 (Thermo Fisher Scientific) in the presence of 20 ng/mL EGF (EMD Millipore; Billerica, MA, USA) and 20 ng/mL bFGF (EMD Millipore).

2.2. Quantitative real-time PCR

Quantitative real-time PCR (qRT-PCR) was performed to assess mRNA levels of CXCR4 and CXCR7. Total RNA was isolated from NCH421k and U87 cells using Trizol reagent (Invitrogen). cDNA was generated from 1 μg total RNA using a High Capacity cDNA Reverse Transcription Kit (Applied Biosystems; Carlsbad, CA, USA). Real-time PCR was performed with the ABI 7900 HT Sequence Detection System (Applied Biosystems) using Taqman gene expression assays (Applied Biosystems) for the detection of CXCR4 and CXCR7 mRNA expression. Glyceraldehyde 3-phosphate dehydrogenase (GAPDH) was used as internal control. The primers Hs00607978_s1 (Applied Biosystems), Hs00604567_m1 (Applied Biosystems) and No. 4310884E (Applied Biosystems) were used for CXCR4, CXCR7 and GAPDH, respectively. Analyses were performed with SDS v2.2 software (Applied Biosystems). The experiments were performed in triplicate.

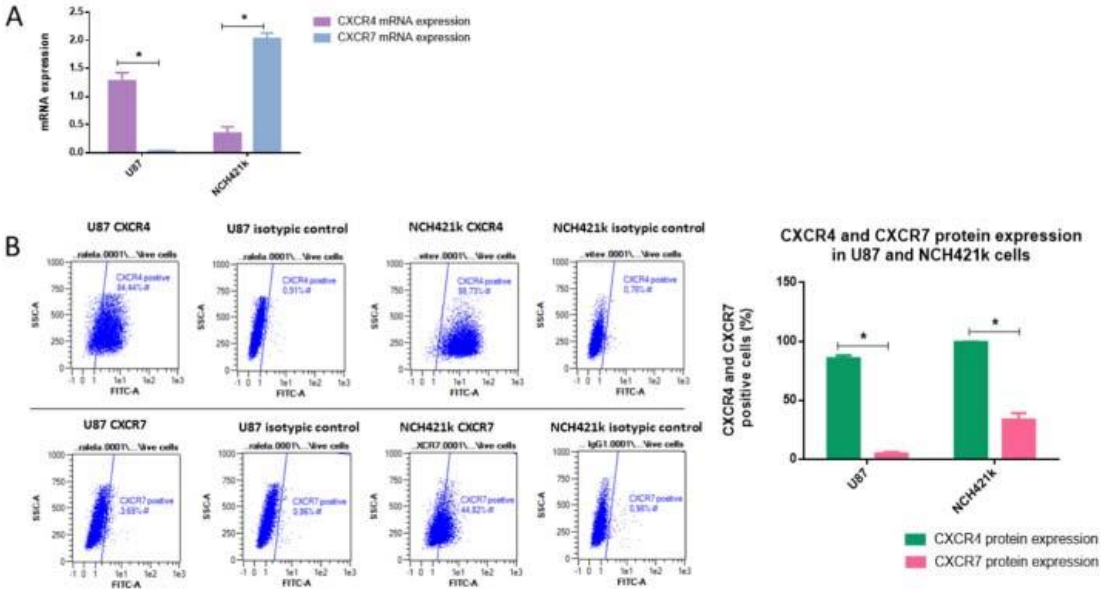


Fig. 1. mRNA and protein expression of CXCR4 and CXCR7 in U87 and NCH421k cells. (A) q-RT-PCR analysis of lysates of NCH421k GSLCs and U87 GBM cells was performed to determine their CXCR4 and/or CXCR7 mRNA expression. NCH421k GSLCs had a relatively low expression of CXCR4 and a high expression of CXCR7. U87 GBM cells had a relatively high expression of CXCR4 and virtually no expression of CXCR7. (B) Flow cytometry analysis was performed to determine CXCR4 and CXCR7 protein expression on U87 and NCH421k cells. The CXCR4 protein levels were equally high on both cell lines, whereas CXCR7 protein expression was higher on NCH421 k cells as compared to U87 cells. The error bars represent the standard error of the mean. *, $P < 0.05$.

2.3. Flow cytometry analysis

Flow cytometry analysis was performed to determine CXCR4 and CXCR7 expression on the cell surface of NCH421k and U87 cells. One million NCH421k and U87 cells were harvested and washed twice in buffer (2% BSA in 1 × PBS). Cells were incubated with primary antibodies against CXCR4 (1:500, R&D Systems, MAB42273; Minneapolis, MI, USA) and CXCR7 (1:50; R&D Systems, MAB172) for 30 min at 4 °C. After a washing step with buffer, cells were incubated with secondary antibody rabbit anti-mouse Alexa Fluor 488 (Life Technologies, Carlsbad, CA, USA) for 30 min at 4 °C, followed by another washing step with buffer and resuspension in 1 × PBS. Propidium iodide (1:100, Miltenyi Biotec; San Diego, CA, USA) was added to the cell suspensions to exclude dead cells. Analysis was performed using the flow cytometer MACSQuantify Analyzer 10 (Miltenyi Biotec) and MACSQuantify software (Miltenyi Biotec). Protein expression was observed in the FITC channel and isotypic controls (IgG2B and IgG1, Abcam) were used in the same concentrations as the primary antibodies to control for aspecific background staining.

2.4. Western blot analysis

Whole-cell lysates of GSLC line GB7 were generated using standard RIPA buffer (20 mM HEPES at pH 8.0, 1% NP40, 0.5% sodium deoxycholate, 0.1% SDS, 25 mM EDTA) containing complete phosphatase and protease inhibitors (Thermo Fisher Scientific), rotated at 4 °C for 30 min and then centrifuged at maximum speed to collect the supernatant. Protein concentrations were determined using the Bradford Assay (Thermo Fisher Scientific) and equal amounts of protein (30 μg) were loaded and transferred to PVDF membranes (EMD Millipore). Membranes were blocked in 5% BSA in TBST (Tris-buffered saline, 0.1% Tween 20) buffer for 1 h at RT, and incubated overnight with primary antibodies at 4 °C. Western blots were processed with fluorescent secondary antibodies (Pierce Dylight, Thermofisher Scientific) and developed with ClxLiCor Odyssey (Li-Cor; Lincoln, NE, USA). The following antibodies were used for western blotting: rabbit anti-human CXCR4 (Abcam, Cambridge, UK), rabbit anti-human CXCR7 (Santa Cruz Biotechnologies) and mouse anti-human vinculin (Abcam) as loading control.

2.5. Proteolytic processing of SDF-1α by CatK

Proteolytic cleavage of SDF-1α by CatK was performed in vitro to determine the cleavage sites of SDF-1α (Peprotech, Rocky Hill, NJ, USA) generated by CatK. Recombinant human procathepsin K was prepared as described previously [35]. Purified procathepsin K was activated in vitro at pH 4.0 and 37 °C. CatK activity was stopped by adjusting the pH of the activation mixture to ~5.5. The active enzyme concentration was determined by active site titration using the irreversible cystein cathepsin inhibitor E-64 (Bachem, Bubendorf, Switzerland). Hydrolysis was performed in 100 mM sodium acetate buffer pH 5.5 or in 50 mM HEPES buffer pH 7.4, each buffer containing 1 mM EDTA and 5 mM dithiothreitol (DTT). Reaction mixtures containing 20 μM SDF-1α and 0.4 μM CatK were incubated on a Thermomixer (Eppendorf, Hamburg, Germany) at 37 °C. The pH 5.5 reaction mixture was incubated for 30 min and the pH 7.4 reaction mixture was incubated for 15 min. Reactions were stopped either by the addition of E-64 in an amount equimolar to the CatK concentration or, alternatively, by selective removal of the produced small fragments by filtration through a 0.5 mL Ultra centrifugal filter (Amicon, Temecula, CA, USA) with a 3 kDa cut-off at 4 °C. The complete reaction mixtures, as well as mixtures of short cleavage products only, were used in further experiments. To determine the size and identity of the cleavage products, peptides generated by CatK were analyzed at the commercial proteomics facility at the Jožef Stefan Institute using matrix-assisted laser desorption/ionization time-of-flight (MALDI-TOF) mass spectrometry (Bruker, Bremen, Germany).

2.6. Two-dimensional invasion assays

Invasion assays were performed using the transwell chambers, inserts with 8.0 μm pores (Corning, Life Sciences, New York, NY, USA) and 2 cell lines: U87 cells (40.000 cells/insert) and NCH421k cells (80.000 cells/insert). The inserts were coated with 0.5 mg/mL Matrigel (Corning) and dried overnight. Cells were plated in serum-free medium in the upper chamber and normal medium containing SDF-1α or its derivatives were placed in the lower chamber: (1) SDF-1α (10 ng/mL); (2) PepC-C (3 ng/mL; sequence of 21 amino acids from the N-terminal end of SDF-1α, KPVSLSYRCPCRFFESHIARA, as described in [36]); (3) complete reaction mixture at pH 5.5 (10 ng/mL); (4) complete reaction mixture at pH 7.4 (10 ng/mL); (5) and (6) complete cleavage products of SDF-1α at pH 5.5 and 7.4 (10 ng/mL), respectively; (7) and 8) synthetic copies of peptides (10 ng/mL; KPVS and KPVSLS, respectively; GenicBio, Shanghai, China) that are cleavage products of SDF-1α generated by CatK, and (9) medium only as a control. After 48 h of incubation at 37 °C, tetrazolium salt MTT (Sigma) was added to the upper and lower chambers and

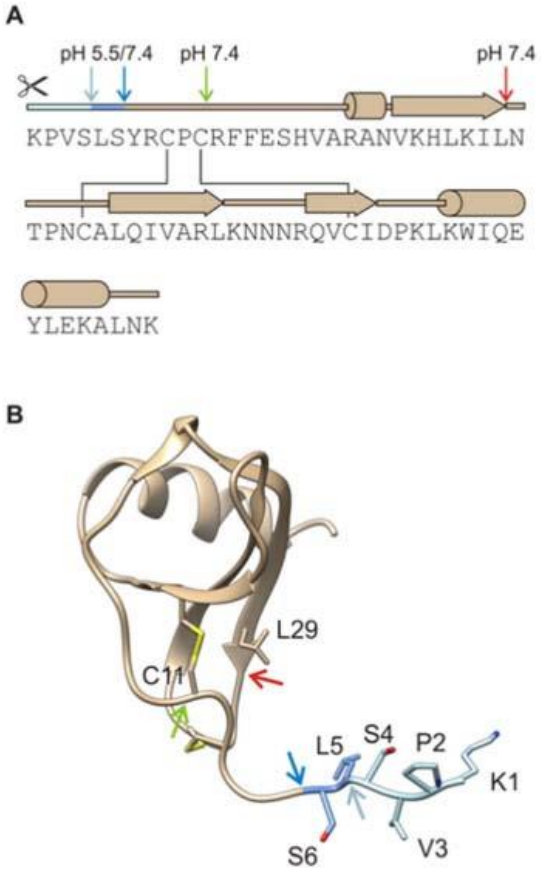


Fig. 2. CatK-induced cleavage products of SDF-1α. (A) Amino acid sequence of SDF-1α and the cleavage sites by CatK at pH 5.5 and/or pH 7.4. Cleavage sites are indicated by arrows and the secondary structure elements are shown above the amino acid sequence. (B) Three-dimensional (3D) molecular structure of SDF-1α with cleavage sites mapped onto the 3D structure of SDF-1α (PDB accession code 2N55). Residue numbering applies to the mature form of SDF-1α. The 2 disulfide bonds, the N-terminal 6 residues and Leu29 of SDF-1α are shown as sticks. The image was created with UCSF Chimera software (UCSF Chimera—a visualization system for exploratory research and analysis as described in [44]).

the incubation at 37 °C lasted for another 3 h. Then, formazan crystals were collected separately from each chamber, pelleted by centrifugation, dissolved in dimethylsulfoxide (DMSO) and the absorbance at 570 and 690 nm was measured using a plate reader (Synergy Mx, BioTek, Winooski, VT, USA). The relative invasion (%) was determined as the ratio of absorbance in the lower chamber and the sum of absorbance in both chambers. The experiments were performed in triplicate.

2.7. Three-dimensional invasion assays

NCH421k cells were seeded in complete Neurobasal medium (Gibco) containing 4% methylcellulose in U-bottomed 96-well plates with 3000 cells/well (BD Biosciences, San Diego, CA, USA) centrifuged at 850 × *g* and 31 °C for 90 min and incubated at 37 °C in a 5% CO_2 incubator for 3 days to form one spheroid in each well. Spheroids were transferred into 24-well plates (Corning) and embedded in 6.0 mg/mL Matrigel (Corning). After 30 min of incubation at 37 °C in a 5% CO_2 incubator, spheroids were covered with complete Neurobasal medium containing SDF-α (10 ng/mL), PepC-C (3 ng/mL) and deavage products of SDF-1α generated by CatK at pH 5.5 or pH 7.4 (10 ng/mL; after filtration and removal of peptides >3 kDa). As a control, only complete Neurobasal medium was used to cover the spheroids. Numbers of GSLCs that invaded from the spheroids into the Matrigel were determined using image analysis after day 3 and day 6 using an inverted fluorescence microscope (Nikon Eclipse Ti, Tokyo, Japan) at 4× magnification and NIS-Elements, Nikon software [37].

2.8. Cell viability assay

Fifty thousand GB7 cells were seeded on 6-well plates and were treated with 10, 25, 50, 100 and 500 nM of the CXCR4 inhibitor plerixafor (Selleck; Houston, TX, USA) for 24 h at 37 °C in a 5% CO_2 incubator. The number of viable cells was determined using a trypan blue exclusion assay to assess the toxicity of plerixafor.

2.9. Plerixafor-treated GSLCs in transwell invasion assays

The effect of plerixafor on invasion of GB7 GSLCs was determined using transwell assays and collagen-coated (Advanced BioMatrix; San Diego, CA, USA) inserts with a pore size of 8 μm (Becton Dickinson; Franklin Lakes, NJ, USA). Dissociated GB7 cells (50,000/insert) were resuspended in serum-free media with growth factors (20 ng/mL EGF and bFGF) and mixed with thawed Matrigel (BD Biosciences; San Jose, CA, USA). A total of 50 μL of Matrigel plus cell suspension was placed on the inserts in duplicates. Inserts were then placed in 24-well plates. After 24 h, invaded GB7 cells that accumulated on the bottom surface of the insert membrane were fixed with 4% paraformaldehyde for 20 min, washed with 1× PBS for 10 min and stained with DAPI (1:1000 in 1× PBS) for 10 min. The membranes were subsequently cut out and mounted on microscopic slides for quantification. Images of the membranes were taken using the fluorescence microscope (Zeiss; Jena, Germany) and the ZenPro software (Zeiss). The total number of cells in five individual fields per membrane was counted using Image J software [37,38]. Cells treated with 10, 25, 50, 100 and 500 nM plerixafor were compared with the control and in all transwells, SDF-1α (10 ng/mL) was used as chemo-attractant.

2.10. Brain tumor samples of patients

GBM samples from 10 patients were obtained from the Brain Tumor Bank maintained by the Department of Neuropathology at the Academic Medical Centre (AMC, Amsterdam, The Netherlands). Research was performed on "waste" material that was stored in a coded fashion. Consent for this project was reviewed and waivered, and the project was approved by the Medical Ethics Review Committee of the Academic Medical Center and University of Amsterdam (reference number W14_224 # 14.17.0286). Consent for removal of the tissue and its storage in the tumor bank for research purposes was obtained and documented in the patients' medical charts. Tissue samples were snap-frozen in liquid nitrogen in the operating room and stored at −80 °C until use. Cryostat sections (7-μm thick) were cut at −25 °C on an HM560 cryostat (MICROM, Walldorf, Germany), picked up on glass slides, and stored at −80 °C until use. All staining procedures, including those for controls, were performed on serial sections of each GBM sample [9].

2.11. Chromogenic immunohistochemistry

Immunohistochemistry (IHC) was performed on serial GBM cryostat sections. Sections were air-dried at room temp for 15 min before

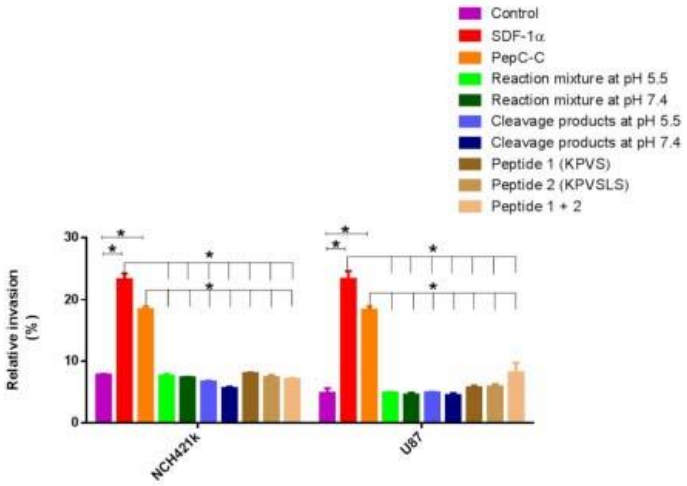


Fig. 3. Transwell invasion assays of NCH421k GSLCs and U87 GBM cells. Relative cell invasion percentages from the upper chamber to the lower chamber were determined after 48 h of incubation in transwells. The data shows that SDF-1α and PepC-C had a strong chemotactic effect on NCH421k GSLCs and U87 GBM cells as compared to control, complete reaction mixtures after incubation of SDF-1α and CatK and small cleavage products only after filtration (<3 kDa). The two small synthetic peptides (KPVS and KPVSLS) did not show any chemotactic effects in both cell lines either. The error bars represent the standard error of the mean. *, $P < 0.05$.

staining. Sections were fixed in acetone (−20 °C) for 10 min and air-dried afterwards for 15 min. Sections were encircled with a PAP pen (Dako, Glostrup, Denmark), followed by 3 washing steps of 5 min with PBS. The sections were treated with 100% methanol containing 0.3% H_2O_2 for 15 min to block endogenous peroxidase activity and to prevent non-specific background staining, followed by 3 washing steps of 5 min each using PBS. Then, sections were incubated with PBS containing 10% normal goat serum (Dako) and 0.1% bovine serum albumin (BSA) for 45 min to further reduce nonspecific background staining. After tapping off the goat serum-containing buffer, sections were incubated overnight at 4 °C with primary antibodies (rabbit-anti-human CatK, ab19027, dilution 1:200, Abcam, Cambridge, UK; rabbit-anti-human SDF-1α, MAB310, dilution 1:200, R&D Systems; mouse-anti-human smooth muscle actin (SMA), M0851 clone 1A4, dilution 1:500, Dako). After incubation with primary antibodies, sections were washed 3 times for 5 min in PBS containing 0.1% BSA. Sections incubated with antibodies against CatK and SDF-1α were incubated with polyclonal goat-anti-rabbit secondary antibody conjugated with horse-radish peroxidase (HRP) (Dako) in a 1:200 dilution in PBS containing 0.1% BSA for 1 h. Sections incubated with antibodies against SMA were incubated with polyclonal goat-anti-mouse secondary antibody conjugated with HRP (Dako) in a 1:200 dilution in PBS containing 0.1% BSA for 1 h. Incubation with secondary antibodies was followed by 3 washing steps of 5 min with PBS. After that, sections were incubated with AEC (peroxidase substrate kit; Vector Laboratories, Burlington, CA, USA) for 20 min, followed by one washing step of 5 min using PBS. Sections were placed in running tap water for 20 min and then in distilled water followed by incubation for 3 min in hematoxylin (Fluka Biochemica, Sigma-Aldrich) for nuclear staining. Sections were again placed in running tap water for 20 min and then in distilled water. All incubation steps were performed at room temp, except for the overnight incubations with primary antibodies that were performed at

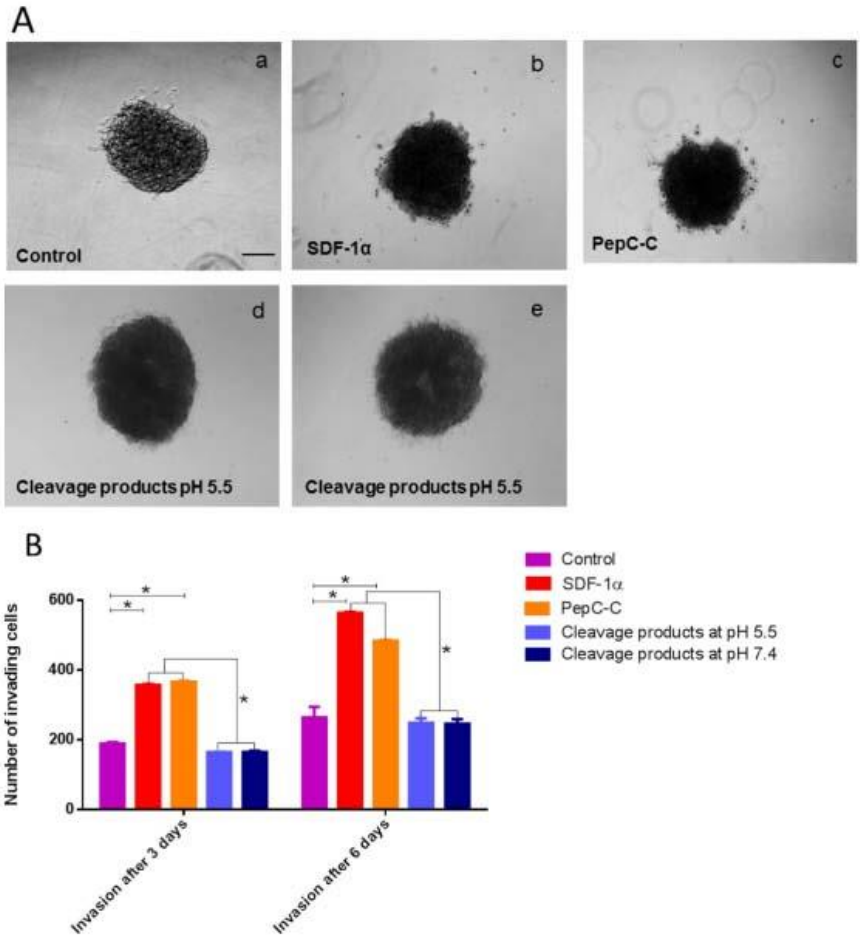


Fig. 4. Spheroid invasion assays using NCH421k GSLCs. (A) Images of spheroids surrounded by invading NCH421k GSLCs. Spheroids embedded in Matrigel were incubated for 6 days in the presence of SDF-1α (b), PepC-C (c), cleavage products of SDF-1α generated by CatK at pH 5.5 (d), cleavage products of SDF-1α generated by CatK at pH 7.4 (e) and control with medium only (a). Scale bar = 100 μm. Please note that images were captured of spheroids in the center and invading cells in the vicinity of the spheroids. However, cells invaded over larger distances away from the spheroids. (B) Numbers of GSLCs invading into Matrigel out of spheroids were determined using image analysis after treatment with SDF-1α, PepC-C, cleavage products of SDF-1α generated by CatK at pH 5.5 and 7.4 (<3 kDa) and medium only as control. All invaded cells, including the cells that invaded over larger distances than shown in Fig. 4A have been quantified. The data shows that treatment with SDF-1α and PepC-C significantly increased the numbers of GSLCs invading into the Matrigel out of spheroids as compared to the control and cleavage products of SDF-1α <3 kDa generated by CatK. The error bars represent the standard error of the mean. *, $P < 0.05$.

4 °C. Finally, sections were covered with glycerin/gelatin mounting medium (Sigma-Aldrich). Control incubations were performed in the absence of primary antibody. The second control panel was performed with rabbit serum or mouse serum in the same concentration as the primary antibody, to determine the effect of the serum on non-specific background staining.

2.12. Fluorescence immunohistochemistry

Sections were air-dried for 30 min at room temp, encircled using a PAP-pen (Daido Sangyo, Tokyo, Japan) and fixed for 10 min at room temp by using 4% paraformaldehyde (Acros Organics, Geel, Belgium) containing 3.7% methanol (Merck, Darmstadt, Germany) diluted in PBS. Sections were washed twice in PBS, followed by permeabilization using 0.1% Triton X (Sigma) in PBS and 2 washing steps in PBS. Blocking of non-specific staining was performed by incubation in PBS containing 0.5% BSA (Sigma). Afterwards, sections were incubated with primary antibodies at room temp (rabbit-anti-human CatK (isotype IgG), ab19027, dilution 1:500, Abcam; mouse-anti-human SDF-1α (isotype IgG1), MAB310, dilution 1:600, R&D Systems; rabbit-anti-human SMA, (isotype IgG2a), M0851 clone 1A4, dilution 1:500, Dako). Single, double or triple staining procedures were used for the 3 primary antibodies. After 60 min of incubation at room temp, sections were washed with PBS. Incubation with secondary antibodies was performed for 30 min at room temp (goat-anti-rabbit CatK (IgG) conjugated with Alexa 488, dilution 1:500, Invitrogen, Carlsbad, CA, USA; goat-anti-mouse SDF-1α (IgG1) conjugated with Alexa 647, dilution 1:500, Life Technologies, Carlsbad, CA, USA; goat-anti-mouse SMA (IgG2a) conjugated with Alexa 568, dilution 1:500, Life Technologies). Removal of fluorescent lipofuscin from sections was performed by incubation for 30 min in 30 mM ammonium acetate (Merck, Darmstadt, Germany), and 10 mM copper sulphate (Merck). Afterwards, sections were washed for 30 s using distilled water and 4 times 5 min using PBS. Sections were mounted in ProLong Gold containing DAPI (Life Technologies, Bleiswijk, The Netherlands) and coverslipped. Preparations were hardened overnight at room temp. Control incubations were performed in the absence of primary antibodies. Imaging was performed using a confocal microscope (SP8-X SMD; Leica, Amsterdam, The Netherlands). Images of 1024 × 1024 pixels were taken as optical sections and were analyzed using LAS X software (Amsterdam, The Netherlands).

2.13. Statistical analyses

Data were processed in Excel 2013 (Microsoft, Redmond, WA, USA) and GraphPad Prism 6 (La Jolla, CA, USA) for statistical analyses using *t*-tests for qRT-PCR data and one-way ANOVA tests for invasion assays. *P* values <0.05 were considered to indicate significant differences.

3. Results

3.1. Cellular expression of CXCR4 and CXCR7

Fig. 1A shows CXCR4 and CXCR7 mRNA expression levels in NCH421k GSLCs and U87 GBM cells. NCH421k cells had a relatively low expression of CXCR4 and a high expression of CXCR7, whereas U87 cells had a relatively high expression of CXCR4 and virtually no expression of CXCR7. However, flow cytometry analysis revealed that both U87 and NCH421k cells had a high and similar level of CXCR4 protein expression on the cell surface, whereas CXCR7 protein expression was higher on NCH421k cells as compared to U87 cells (Fig. 1B).

3.2. Proteolytic processing of SDF-1α by CatK

It has been shown in previous studies that CatK and other cysteine cathepsins can cleave SDF-1α [39]. To determine the effect of the CatK-induced cleavage on the chemotactic activity of SDF-1α, we analyzed the cleavage of SDF-1α in more detail, as presented in Fig. 2A. Since CatK is active in both the endolysosomal compartment as well as extracellularly, experiments were performed at two pH values, i.e. pH 5.5 to simulate endolysosomal conditions and pH 7.4 to mimic extracellular conditions. Optimal incubation periods for the cleavage reactions were determined to be 30 min at pH 5.5 and 15 min at pH 7.4 (data not shown). The mixtures of cleavage products were analyzed by MALDI-TOF mass spectrometry to identify the cleavage sites within

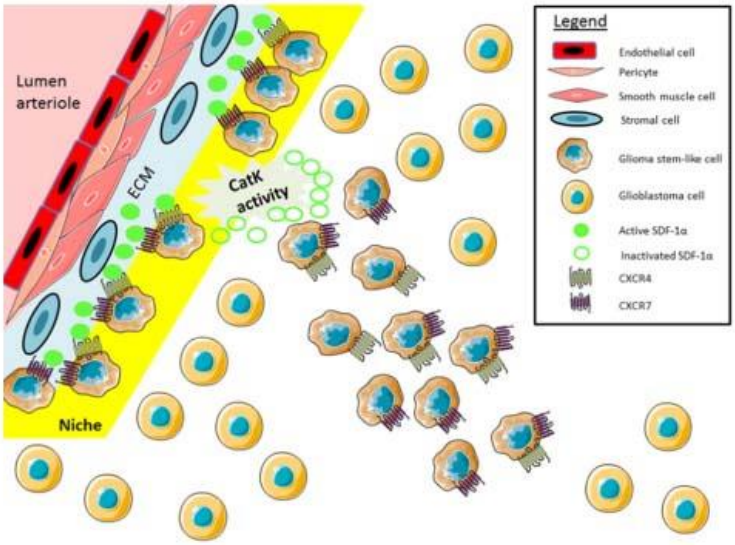


Fig. 5. Schematic representation of the GSLC niche. Our proposed model of GSLC niches around arterioles. The arteriolar wall consists of an endothelial cell layer surrounded by pericytes and smooth muscle cells and the adventitia (stroma) containing ECM and stromal cells. Endothelial cells and/or GBM cells secrete proteases, including CatK, that cleave SDF-1α in GSLC niches and loosen anchorage of GSLCs that express CXCR4 and/or CXCR7. CatK cleavage of SDF-1α enables mobilization of GSLCs out of niches.

SDF-1α. In both conditions, peaks with average molecular masses of 7964.375, 7552.878 and 7352.643 Da, respectively, were identified. These correspond to the singly protonated forms (MH^+) of full-length SDF-1α, and two N-terminally-cleaved fragments, the larger being cleaved after Ser4 and the smaller after Ser6. Two additional fragments were observed at pH 7.4 with molecular masses of 6729.879 and 4582.347 Da, respectively. These correspond to SDF-1α fragments produced by cleavage after Cys11 and Leu29. The kinetics of the reaction showed that larger numbers of fragments appeared after shorter incubation periods at pH 7.4 than at pH 5.5 (Fig. 2), indicating that CatK cleaves SDF-1α more readily at physiological extracellular pH. The positions of the cleavage sites in the three-dimensional (3D) structure of SDF-1α are shown in Fig. 2B. Chemokines are known to interact with two sites on their receptors, where the globular part of the chemokine interacts with the N-terminal extension of the receptor, and the N-terminus of the chemokine binds to the functional site of the receptor

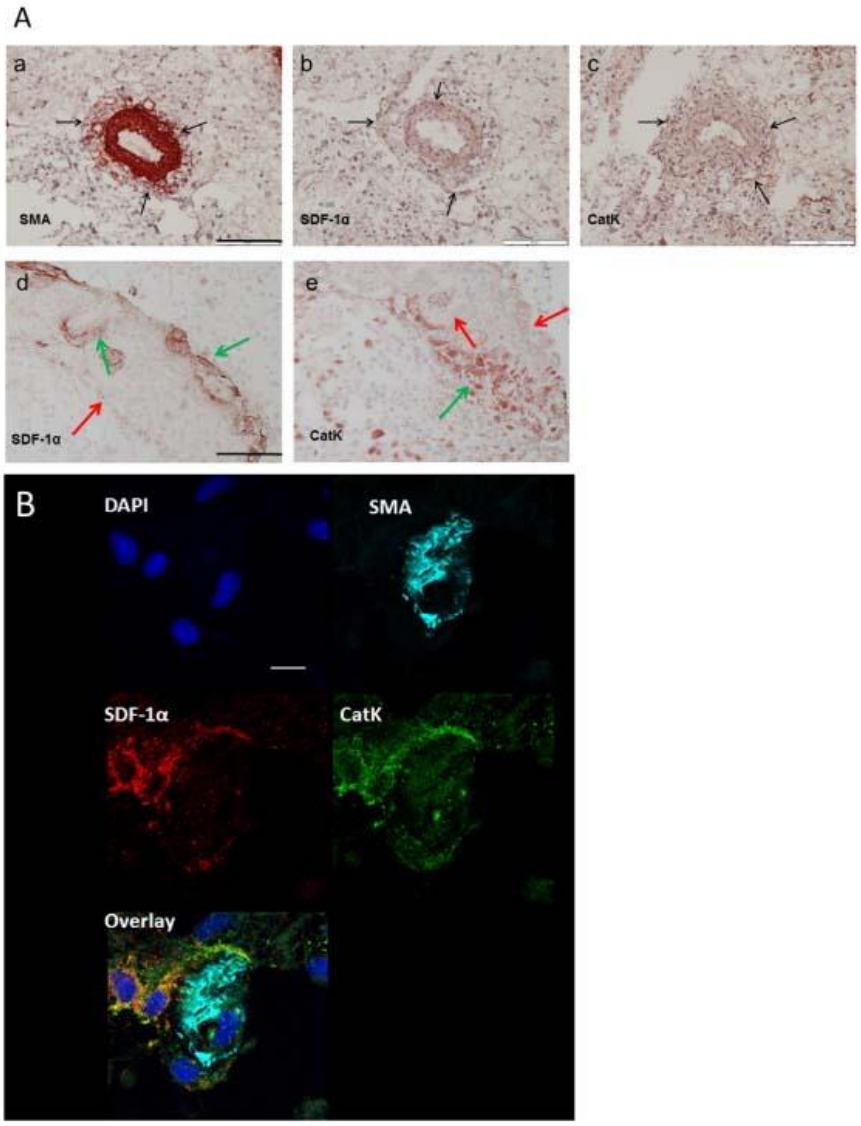


Fig. 6. Immunolocalization of SDF-1α and CatK in niches around arterioles. (A) Immunohistochemical staining of SMA (a), SDF-1α (b) and CatK (c) was performed on human serial cryostat sections of GBM, showing the expression of SDF-1α and CatK in GSLC niches around SMA-positive arterioles and in the arteriolar wall (indicated by black arrows). SMA stains smooth muscle cells of the arteriolar wall, which is the center of GSLC niches. (d, e) Inverse correlation of SDF-1α and CatK protein expression in niches in serial cryostat sections of GBM. Red arrows indicate low protein expression and green arrows indicate higher protein expression. Sections were counterstained with hematoxylin to detect nuclei. Scale bar = 100 μm. (B) Fluorescence immunohistochemical staining of SMA, SDF-1α and CatK was performed on human serial cryostat sections of GBM and imaging by confocal microscopy showed co-localization of SDF-1α (red) and CatK (green) around SMA-positive arterioles (light blue). SDF-1α and CatK were partly co-localized (yellow). Sections were counterstained with DAPI to detect the nuclei. Scale bar = 10 μm.

[40,41]. The N-terminal cleavage sites of CatK are located in the flexible region of SDF-1α that is responsible for binding to the functional site of CXCR4/CXCR7 and for triggering of signaling. It has been shown that cleavage of 2 residues from the N-terminus is sufficient to abolish activation of the receptor [42]. The remaining 2 cleavage sites are located in the globular part of the molecule at positions that are directly involved in the interactions with the N-terminal part of CXCR4/CXCR7 [43]. It is thus likely that CatK cleavage prevents SDF-1α from binding to CXCR4/CXCR7. To test whether SDF-1a cleavage by CatK inhibits chemotaxis, transwell invasion assays were performed using either SDF-1α as a chemo-attractant or the CatK-induced cleavage products of SDF-1α (Section 3.3).

3.3. CatK cleavage of SDF-1α prevents transwell invasion

Transwell invasion assays were performed with NCH421k and U87 cells to determine the chemotactic activity of SDF-1α and its cleavage products and PepC-C. The relative invasion of U87 and NCH421k cells was higher in the presence of SDF-1α and PepC-C than in the presence of reaction mixtures, SDF-1α cleavage products, synthetic SDF-1α N-terminal peptides or control conditions and this effect was significant (Fig. 3). Fig. 3 shows significant chemotactic effects of SDF-1α and PepC-C on NCH421k and U87 cells as compared to the control. There was no significant difference between the effects of SDF-1α and PepC-C (Fig. 3). Cleavage products of SDF-1α generated by CatK at pH 5.5 and 7.4, both in the complete reaction mixtures and after filtration to remove peptides larger than 3 kDa, did not show any chemotactic effects. The filtration step was performed to specifically determine the effects of SDF-1α-derived small peptides from the N-terminus (Fig. 2). These data indicate that SDF-1α cleavage by CatK at both pH 5.5 and 7.4 completely abolished the chemotactic effects of SDF-1α. To study these phenomena further, 2 small peptides from the N-terminus of SDF-1α were synthesized and tested in transwell invasion assays. Fig. 3 shows that these synthetic peptides had no chemotactic effects either alone or together. Since we did not observe any difference between the effects of complete reaction mixtures and filtrated small cleavage products, all further experiments were performed with the filtrated small cleavage products only.

3.4. CatK cleavage of SDF-1α prevents Matrigel invasion from spheroids

Invasion assays were performed in 3D to study the invasive behaviour of NCH421k cells that were growing as spheroids in Matrigel (Fig. 4A). Treatment of the spheroids with SDF-1α and PepC-C resulted in a significantly increased number of NCH421k cells that invaded Matrigel out of the spheroids, as compared to the control (Fig. 4Aa–c). CatK-induced cleavage products of SDF-1α at pH 5.5 and 7.4 did not stimulate invasion of GSLCs out of the spheroids as the invasion was similar to that in control conditions (Fig. 4Aa, d, e). This invasive pattern was observed both after 3 and 6 days.

3.5. Schematic representation of the GSLC niche

Fig. 5 shows our concept of the GSLC niche. CXCR4 and/or CXCR7-expressing GSLCs are retained around arterioles in the GSLC niche by SDF-1α/CXCR4 and/or SDF-1α/CXCR7 interactions as was found in our previous study [9]. The arteriolar wall consists of endothelial cells, pericytes, smooth muscle cells and the adventitia which consists of stroma containing extracellular matrix (ECM) and stromal cells. The GSLCs are attached to the stroma via SDF-1α/CXCR4/7 interactions. CatK activity induces cleavage and inactivation of SDF-1α, which results in migration of GSLCs out of GSLC niches.

3.6. SDF-1α and CatK expression around arterioles in GSLC niches

Chromogenic and fluorescence IHC were performed to provide supporting evidence for our concept of the GSLC niche as illustrated in Fig. 5. Human GBM serial cryostat sections were used for chromogenic IHC to localize SDF-1α and CatK in GSLC niches. Fig. 6Aa–c shows that SDF-1α and CatK are both localized around SMA-positive arterioles of GSLC niches and are also expressed in the arteriolar wall. SDF-1α and CatK were expressed around arterioles. In addition, we found SDF-1α and CatK expression in an inverse correlation in niches (Fig. 6Ad, e).

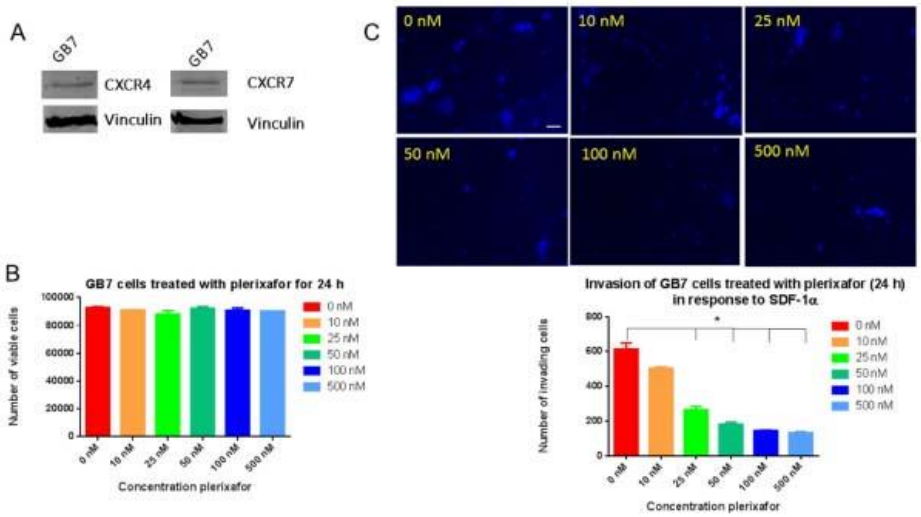


Fig. 7. CXCR4 inhibitor plerixafor inhibits invasion of CXCR4/CXCR7-expressing GB7 GSLCs. (A) Western blot data shows that GB7 GSLCs express both CXCR4 and CXCR7. Vinculin is used as loading control. (B) Cell viability assays were performed to determine toxicity of plerixafor. Treatment with 10, 25, 50, 100 and 500 nM plerixafor for 24 h did not affect cell viability. (C) Transwell invasion assays were performed with GB7 GSLCs treated with 10, 25, 50, 100 and 500 nM plerixafor for 24 h with SDF-1α in the lower chamber as chemoattractant. The data shows that plerixafor reduces the number of invading cells significantly. DAPI-stained cells were counted using ImageJ software. Scale bar = 50 μm. The error bars represent the standard error of the mean. *, $P < 0.05$.

Fluorescence IHC and confocal imaging of human GBM cryostat sections showed that SDF-1α and CatK are co-localized around SMA-positive arterioles of GSLC niches (Fig. 6B).

3.7. CXCR4 inhibitor plerixafor inhibits invasion of GSLCs

Since our data provides supporting evidence that the SDF-1α/CXCR4/CXCR7 axis is involved in retaining CXCR4/CXCR7-expressing GSLCs in SDF-1α-containing niches, we determined the effect of the CXCR4 inhibitor plerixafor on invasion of GSLCs in response to SDF-1α. Western blot analysis revealed that GB7 GSLCs express both CXCR4 and CXCR7. Vinculin was used as loading control (Fig. 7A). Next, we determined the toxicity of plerixafor by performing cell viability assays. The data shows that treatment with plerixafor does not affect cell viability after 24 h (Fig. 7B), confirming that plerixafor is not toxic for the cells. Transwell invasion assays were performed to determine the effect of plerixafor on invasion of GB7 GSLCs, which were treated with various concentrations of plerixafor for 24 h and SDF-1α was used as chemo-attractant. Fig. 7C shows a concentration-dependent effect of plerixafor with a significant reduction in the number of invading GB7 GSLCs as compared to the control and 500 nM plerixafor had the highest inhibitory effect on invasion.

4. Discussion

The present study shows that SDF-1α induces chemotactic responses of U87 GBM cells, and NCH421k and GB7 GSLCs supporting the concept that SDF-1α recruits GSLCs to the wall of arterioles, where GSLC niches are located. Our qRT-PCR data revealed that U87 cells have higher levels of SDF-1α receptor CXCR4 mRNA, whereas the NCH421k cells have higher levels of CXCR7 mRNA. However, the flow cytometry analysis showed that both U87 and NCH421k cells express high levels of CXCR4 protein and lower CXCR7 protein levels at their surface. We assume that either CXCR7 protein in NCH421k cells is mainly present intracellularly in granules or that turnover rates of the receptors in the 2 cell lines are different. In addition, our western blot analysis showed that the GB7 cells express both CXCR4 and CXCR7 in serum-free conditions. Hattermann et al. in 2010 found in serum-containing media that CXCR4 was expressed in GSLCs and differentiated GBM cells whereas CXCR7 was expressed in differentiated GBM cells [45]. Our data is in line with other studies that showed that CXCR4 and CXCR7 are essential for functioning of brain tumor cells [18–21]. U87 and NCH421k cells differ in the expression of CXCR7, but we found similar chemotactic responses in vitro towards SDF-1α (Fig. 3). GB7 GSLCs also express both CXCR4 and CXCR7 (Fig.7A) and these cells are strongly attracted towards SDF-1α (Fig. 7C). This chemoattraction was inhibited by the CXCR4 inhibitor plerixafor (Fig. 7C) which was also shown recently by Yadev et al. in their study of perivascular invasion of GBM cells and GSLCs [46], which is in line with our concept that the SDF-1α/CXCR4 axis is involved in retaining CXCR4-expressing GSLCs in SDF-1a-containing niches (Fig. 5). We have not tested the CXCR7-inhibitor CCX662 in our GSLC models. It is likely that CXCR7 is less involved in the process of invasion than CXCR4, since the SDF-1α/CXCR7 axis activates β-arrestin, resulting in scavenging of SDF-1α. The heterodimeric SDF-1α/CXCR4/CXCR7 signaling axis induces a conformational change of CXCR4 and G-proteins and blocks further signaling [18]. Since CatK activation is a complicated and highly regulated process, CXCR4/CXCR7 inhibition may be a more promising strategy to enforce GSLCs out of their niches than activation of CatK.

Protease signaling via modifications of their substrates may affect cytokine activity which is a complex feedback loop between the families of proteases and cytokines [47]. The co-localization and inverse correlation between expression of SDF-1α and CatK proteins in GSLC niches (Fig. 6) suggests that extralysosomal CatK cleaves and inactivates SDF-1α, with the consequence of the release of GSLCs from niches (Fig. 5). Extracellular SDF-1α can be explained by secretion by endothelial cells and stromal cells and is upregulated by HIF-1α and VEGF [17]. SDF-1α can be present intracellularly as well as it can be internalized after binding to CXCR7 [18]. CatK is an endolysosomal protease and is therefore present intracellularly, but can also be present extracellularly when secreted by GBM cells or endothelial cells.

CatK was found to be one of the highest differentially expressed proteases in GBM tissues and cells versus their normal counterparts [29], but we have not been able to show its activity in GBM tissue and cell lysates. This suggests that CatK activity is in vivo highly regulated by proteolytic, possibly autolytic activation of its precursor form [39], which may depend on pH and redox potential which in turn are regulated by glutathione and hydrogen peroxide. The latter inhibits the processing of the proenzyme and inactivates mature CatK [48]. CatK has already been reported as one of the proteases besides MMP-2, MMP-9, neutrophil elastase and cathepsin G, that can inactivate SDF-1α by cleaving off amino acids from the N-terminus of SDF-1α [49]. Later, Staudt et al. showed that all 11 constitutively secreted cysteine cathepsins can cleave SDF-1α to modulate the communication between HSCs and their niches in the bone marrow, and all were secreted as proteolytically inactive enzymes [39]. Most cleavages of SDF-1α were observed with CatB that is highly expressed in GBM [30,31], and, therefore, a possible cooperation between CatK and CatB in regulating chemotactic activity of SDF-1α in vivo cannot be excluded.

The N-terminal domain of SDF-1α which binds with residues 12–17 (RFFESH) to CXCR4 acts as an initial docking site for SDF-1α. After binding, the activation domain composed of amino acid residues 1–8 (KPVSLSYR) binds to the N-terminal end of the receptor, inducing a conformational change that allows binding of G-proteins to the intracellular domain of the receptor, leading to activation of signaling pathways described above [18]. Filipo et al. (2013) demonstrated that the N-terminal sequence of SDF-1α, PepC-C (KPVSLSYRCPCRFFESHIARA), is sufficient to stimulate proliferation and chemotaxis of neural stem cells from the subventricular zone to injury sites in the cortex, thus possessing full SDF-1α activity [36]. Here, we demonstrated that CatK cleaves SDF-1α at 3 positions beyond the amino acid 21 position of N-terminal PepC-C, thus completely inactivating SDF-1α activity. The two small synthetic peptides of the N-terminus of SDF-1α (KPVS and KPVSLS) did not show chemotactic activity, retaining U87 and NCH421k cell invasion at control levels (Fig. 3). In contrast, PepC-C was chemotactically active in a similar way as intact SDF-1α in invasion assays, as was shown previously [36]. It would be interesting to determine whether treatment with the two small peptides together with SDF-1α results in inhibition of the chemotactic activity of SDF-1α, as the two small peptides may be able to bind to the active site of CXCR4/7 receptors without activating them and preventing the SDF-1α binding. The bulk of the SDF-1α protein is not involved in the chemotactic activity (Fig. 2). Therefore, it may have a function in protection of the active N-terminus of SDF-1α against degradation.

In conclusion, the present study provides supporting evidence for our concept of the GSLC niche that CatK activity releases GSLCs from niches by inactivating SDF-1α and we proposed the novel therapeutic approach that disrupts SDF-1α/CXCR4 and/or SDF-1α/CXCR7 interactions to enhance GSLC migration out of niches, with subsequent loss of their stemness and sensitization to chemo-irradiation. Therefore, it is relevant to study CatK activity in more detail. An interesting question that arises is whether CatK should be inhibited, as has been suggested for many types of cancer [28], or rather upregulated. In line with this upregulation, Lopez-Otin et al. in 2007 reported that the activity of many proteases in cancer have tumor suppressing effects rather than tumorigenic effects [50]. We therefore suggest that CatK activity should be upregulated in GBM before and during chemo-irradiation, since this may sensitize GSLCs to chemo-irradiation.

Transparency document

The Transparency document associated with this article can be found, in online version.

Acknowledgements

This study was supported by a René Vogels travel grant (VVVH), a JoKolk scholarship (VVVH), the Dutch Cancer Society grant (KWF; UVA 2014-6839; VVVH, CJFVN), the Slovenian Research Agency (ARRS) Programme Grants (P1-0245 and P1-0140; TTL, MN) and ARRS Young Researchers Grant (UV, BB), and by the Fundação de Amparo à Pesquisa do Estado de São Paulo (FAPESP-12/50191-AR).

References

[1] R. Kalkan, Glioblastoma stem cells as a new therapeutic target for glioblastoma, Clin. Med. Insights Oncol. 9 (2015) 95–103.
[2] D. Schiffer, M. Mellai, L. Annovazzi, V. Caldera, A. Piazzi, T. Denysenko, A. Melcarne, Stem cell niches in glioblastoma: a neuropathological view, Biomed. Res. Int. 2014 (2014) 725921.
[3] S.E. Mir, P.C. De Witt Hamer, P.M. Krawczyk, L. Balaj, A. Claes, J.M. Niers, A.A. Van Tilborg, A.H. Zwinderman, D. Geerts, G.J. Kaspers, W. Peter Vandertop, J. Cloos, B.A. Tannous, P. Wesseling, J.A. Aten, D.P. Noske, C.J. Van Noorden, T. Wurdinger, In silico analysis of kinase expression identifies WEE1 as a gatekeeper against mitotic catastrophe in glioblastoma, Cancer Cell 18 (2010) 244–257.
[4] A.R. Rama, P.J. Alvarez, R. Madeddu, A. Aranega, ABC transporters as differentiation markers in glioblastoma cells, Mol. Biol. Rep. 41 (2014) 4847–4851.
[5] J.D. Lathia, M. Li, P.E. Hall, J. Gallagher, J.S. Hale, Q. Wu, M. Venere, E. Levy, M.R. Rani, P. Huang, E. Bae, J. Selfridge, L. Cheng, H. Guvenc, R.E. McLendon, I. Nakano, A.E. Sloan, H.S. Phillips, A. Lai, C.L. Gladson, M. Bredel, S. Bao, A.B. Hjelmeland, J.N. Rich, Laminin alpha 2 enables glioblastoma stem cell growth, Ann. Neurol. 72 (2012) 766–778.
[6] A.B. Hjelmeland, Q. Wu, S. Wickman, C. Eyler, J. Heddleston, Q. Shi, J.D. Lathia, J. Macswords, J. Lee, R.E. McLendon, J.N. Rich, Targeting A20 decreases glioma stem cell survival and tumor growth, PLoS Biol. 8 (2010) e1000319.
[7] P.J. Richardson, CXCR4 and glioblastoma, Anticancer Agents Med Chem. 16 (2015) 59–74.
[8] D. Hambardzumyan, G. Bergers, Glioblastoma: defining tumor niches, Trends Cancer 1 (2015) 252–265.
[9] V.V. Hira, K.J. Ploegmakers, F. Grevers, U. Verbovsek, C. Silvestre-Roig, E. Aronica, W. Tigchelaar, T.L. Turnsek, R.J. Molenaar, C.J. Van Noorden, CD133$^+$ and Nestin$^+$ glioma stem-like cells reside around CD31$^+$ arterioles in niches that express SDF-1alpha, CXCR4, osteopontin and cathepsin K, J. Histochem. Cytochem. 63 (2015) 481–493.
[10] P.E. Boulais, P.S. Frenette, Making sense of hematopoietic stem cell niches, Blood 125 (2015) 2621–2629.
[11] A. Ehninger, A. Trumpp, The bone marrow stem cell niche grows up: mesenchymal stem cells and macrophages move in, J. Exp. Med. 208 (2011) 421–428.
[12] O. Kollet, A. Dar, S. Shivtiel, A. Kalinkovich, K. Lapid, Y. Sztainberg, M. Tesio, R.M. Samstein, P. Goichberg, A. Spiegel, A. Elson, T. Lapidot, Osteoclasts degrade endosteal components and promote mobilization of hematopoietic progenitor cells, Nat. Med. 12 (2006) 657–664.
[13] S.J. Morrison, D.T. Scadden, The bone marrow niche for haematopoietic stem cells, Nature 505 (2014) 327–334.
[14] A.D. Lander, J. Kimble, H. Clevers, E. Fuchs, D. Montarras, M. Buckingham, A.L. Calof, A. Trumpp, T. Oskarsson, What does the concept of the stem cell niche really mean today? BMC Biol. 10 (2012) 19.
[15] B. Joddar, Y. Ito, Artificial niche substrates for embryonic and induced pluripotent stem cell cultures, J. Biotechnol. 168 (2013) 218–228.
[16] D. Zagzag, M. Esencay, O. Mendez, H. Yee, I. Smirnova, Y. Huang, L. Chiriboga, E. Lukyanov, M. Liu, E.W. Newcomb, Hypoxia- and vascular endothelial growth factor-induced stromal cell-derived factor-1alpha/CXCR4 expression in glioblastomas: one plausible explanation of Scherer's structures, Am. J. Pathol. 173 (2008) 545–560.
[17] D. Zagzag, Y. Lukyanov, L. Lan, M.A. Ali, M. Esencay, O. Mendez, H. Yee, E.B. Voura, E.W. Newcomb, Hypoxia-inducible factor 1 and VEGF upregulate CXCR4 in glioblastoma: implications for angiogenesis and glioma cell invasion, Lab. Invest. 86 (2006) 1221–1232.
[18] R. Wurth, A. Bajetto, J.K. Harrison, F. Barbieri, T. Florio, CXCL12 modulation of CXCR4 and CXCR7 activity in human glioblastoma stem-like cells and regulation of the tumor microenvironment, Front. Cell. Neurosci. 8 (2014) 144.
[19] R. Sengupta, A. Dubuc, S. Ward, L. Yang, P. Northcott, B.M. Woerner, K. Kroll, J. Luo, M.D. Taylor, R.J. Wechsler-Reya, J.B. Rubin, CXCR4 activation defines a new subgroup of Sonic hedgehog-driven medulloblastoma, Cancer Res. 72 (2012) 122–132.
[20] M.J. Walters, K. Ebsworth, R.D. Berahovich, M.E. Penfold, S.C. Liu, R. Al Omran, M. Kioi, S.B. Chernikova, D. Tseng, E.E. Mulkearns-Hubert, M. Sinyuk, R.M. Ransohoff, J.D. Lathia, J. Karamchandani, H.E. Kohrt, P. Zhang, J.P. Powers, J.C. Jaen, T.J. Schall, M. Merchant, L. Recht, J.M. Brown, Inhibition of CXCR7 extends survival following irradiation of brain tumours in mice and rats, Br. J. Cancer 110 (2014) 1179–1188.
[21] J.B. Rubin, A.L. Kung, R.S. Klein, J.A. Chan, Y. Sun, K. Schmidt, M.W. Kieran, A.D. Luster, R.A. Segal, A small-molecule antagonist of CXCR4 inhibits intracranial growth of primary brain tumors, Proc. Natl. Acad. Sci. U. S. A. 100 (2003) 13513–13518.
[22] D.G. Duda, S.V. Kozin, N.D. Kirkpatrick, L. Xu, D. Fukumura, R.K. Jain, CXCL12 (SDF1alpha)-CXCR4/CXCR7 pathway inhibition: an emerging sensitizer for anticancer therapies? Clin. Cancer Res. 17 (2011) 2074–2080.
[23] S. Kenig, M.B. Alonso, M.M. Mueller, T.T. Lah, Glioblastoma and endothelial cells cross-talk, mediated by SDF-1, enhances tumour invasion and endothelial proliferation by increasing expression of cathepsins B, S, and MMP-9, Cancer Lett. 289 (2010) 53–61.
[24] C.C. Bleul, R.C. Fuhlbrigge, J.M. Casasnovas, A. Aiuti, T.A. Springer, A highly efficacious lymphocyte chemoattractant, stromal cell-derived factor 1 (SDF-1), J. Exp. Med. 184 (1996) 1101–1109.
[25] Y. Uemae, E. Ishikawa, S. Osuka, M. Matsuda, N. Sakamoto, S. Takano, K. Nakai, T. Yamamoto, A. Matsumura, CXCL12 secreted from glioma stem cells regulates their proliferation, J. Neurooncol 117 (2014) 43–51.
[26] M. Terasaki, Y. Sugita, F. Arakawa, Y. Okada, K. Ohshima, M. Shigemori, CXCL12/CXCR4 signaling in malignant brain tumors: a potential pharmacological therapeutic target, Brain Tumor Pathol. 28 (2011) 89–97.
[27] I. Kryczek, S. Wei, E. Keller, R. Liu, W. Zou, Stroma-derived factor (SDF-1/CXCL12) and human tumor pathogenesis, Am. J. Physiol. Cell Physiol. 292 (2007) C987–C995.
[28] U. Verbovsek, C.J. Van Noorden, T.T. Lah, Complexity of cancer protease biology: cathepsin K expression and function in cancer progression, Semin. Cancer Biol. 35 (2015) 71–84.
[29] U. Verbovsek, H. Motaln, A. Rotter, N.A. Atai, K. Gruden, C.J. Van Noorden, T.T. Lah, Expression analysis of all protease genes reveals cathepsin K to be overexpressed in glioblastoma, PLoS One 9 (2014) e111819.
[30] B. Gole, P.C. Huszthy, M. Popovic, J. Jeruc, Y.S. Ardebili, R. Bjerkvig, T.T. Lah, The regulation of cysteine cathepsins and cystatins in human gliomas, Int. J. Cancer 131 (2012) 1779–1789.
[31] T.T. Lah, M.B. Duran Alonso, C.J. Van Noorden, Antiprotease therapy in cancer: hot or not? Expert Opin. Biol. Ther. 6 (2006) 257–279.
[32] N. Podergajs, H. Motaln, U. Rajcevic, U. Verbovsek, M. Korsic, N. Obad, H. Espedal, M. Vittori, C. Herold-Mende, H. Miletic, R. Bjerkvig, T.L. Turnsek, Transmembrane protein CD9 is glioblastoma biomarker, relevant for maintenance of glioblastoma stem cells, Oncotarget 7 (2016) 593–609.
[33] K. Kolosa, H. Motaln, C. Herold-Mende, M. Korsic, T.T. Lah, Paracrine effects of mesenchymal stem cells induce senescence and differentiation of glioblastoma stem-like cells, Cell Transplant. 24 (2015) 631–641.
[34] A. Torsvik, G.V. Rosland, A. Svendsen, A. Molven, H. Immervoll, E. McCormack, P.E. Lonning, M. Primon, E. Sobala, J.C. Tonn, R. Goldbrunner, C. Schichor, J. Mysliwietz, T.T. Lah, H. Motaln, S. Knappskog, R. Bjerkvig, Spontaneous malignant transformation of human mesenchymal stem cells reflects cross-contamination: putting the research field on track – letter, Cancer Res. 70 (2010) 6393–6396.
[35] M. Novinec, M. Pavsic, B. Lenarcic, A simple and efficient protocol for the production of recombinant cathepsin V and other cysteine cathepsins in soluble form in *Escherichia coli*, Protein Expr. Purif. 82 (2012) 1–5.
[36] T.R. Filippo, L.T. Galindo, G.F. Barnabe, C.B. Ariza, L.E. Mello, M.A. Juliano, L. Juliano, M.A. Porcionatto, CXCL12 N-terminal end is sufficient to induce chemotaxis and proliferation of neural stem/progenitor cells, Stem Cell Res. 11 (2013) 913–925.
[37] P. Chieco, A. Jonker, B.A. De Boer, J.M. Ruijter, C.J. Van Noorden, Image cytometry: protocols for 2D and 3D quantification in microscopic images, Prog. Histochem. Cytochem. 47 (2013) 211–333.
[38] C.A. Schneider, W.S. Rasband, K.W. Eliceiri, NIH Image to ImageJ: 25 years of image analysis, Nat. Methods 9 (2012) 671–675.
[39] N.D. Staudt, A. Maurer, B. Spring, H. Kalbacher, W.K. Aicher, G. Klein, Processing of CXCL12 by different osteoblast-secreted cathepsins, Stem Cells Dev. 21 (2012) 1924–1935.
[40] J.E. Pease, J. Wang, P.D. Ponath, P.M. Murphy, The N-terminal extracellular segments of the chemokine receptors CCR1 and CCR3 are determinants for MIP-1alpha and eotaxin binding, respectively, but a second domain is essential for efficient receptor activation, J. Biol. Chem. 273 (1998) 19972–19976.
[41] F.S. Monteclaro, I.F. Charo, The amino-terminal domain of CCR2 is both necessary and sufficient for high affinity binding of monocyte chemoattractant protein 1. Receptor activation by a pseudo-tethered ligand, J. Biol. Chem. 272 (1997) 23186–23190.
[42] M.P. Crump, J.H. Gong, P. Loetscher, K. Rajarathnam, A. Amara, F. Arenzana-Seisdedos, J.L. Virelizier, M. Baggiolini, B.D. Sykes, I. Clark-Lewis, Solution structure and basis for functional activity of stromal cell-derived factor-1; dissociation of CXCR4 activation from binding and inhibition of HIV-1, EMBO J. 16 (1997) 6996–7007.
[43] J.J. Ziarek, A.E. Getschman, S.J. Butler, D. Taleski, B. Stephens, I. Kufareva, T.M. Handel, R.J. Payne, B.F. Volkman, Sulfopeptide probes of the CXCR4/CXCL12 interface reveal oligomer-specific contacts and chemokine allostery, ACS Chem. Biol. 8 (2013) 1955–1963.
[44] E.F. Pettersen, T.D. Goddard, C.C. Huang, G.S. Couch, D.M. Greenblatt, E.C. Meng, T.E. Ferrin, UCSF chimera–a visualization system for exploratory research and analysis, J. Comput. Chem. 25 (2004) 1605–1612.
[45] K. Hattermann, J. Held-Feindt, R. Lucius, S.S. Muerkoster, M.E. Penfold, T.J. Schall, R. Mentlein, The chemokine receptor CXCR7 is highly expressed in human glioma cells and mediates antiapoptotic effects, Cancer Res. 70 (2010) 3299–3308.
[46] V.N. Yadav, D. Zamler, G.J. Baker, P. Kadiyala, A. Erdreich-Epstein, A.C. DeCarvalho, T. Mikkelsen, M.G. Castro, P.R. Lowenstein, CXCR4 increases in-vivo glioma perivascular invasion, and reduces radiation induced apoptosis: a genetic knockdown study, Oncotarget 7 (2016) 83701–83719.
[47] B. Turk, D. Turk, V. Turk, Protease signalling: the cutting edge, EMBO J. 31 (2012) 1630–1643.
[48] M. Novinec, B. Lenarcic, A. Baici, Probing the activity modification space of the cysteine peptidase cathepsin K with novel allosteric modifiers, PLoS One 9 (2014) e106642.
[49] S.Y. Cho, M. Xu, J. Roboz, M. Lu, J. Mascarenhas, R. Hoffman, The effect of CXCL12 processing on CD34$^+$ cell migration in myeloproliferative neoplasms, Cancer Res. 70 (2010) 3402–3410.
[50] C. Lopez-Otin, L.M. Matrisian, Emerging roles of proteases in tumour suppression, Nat. Rev. Cancer 7 (2007) 800–808.

Chapter 3

Discussion and Conclusions

Tumour heterogeneity is recognized as a major cause of ineffective radio- and chemotherapy and recurrence in many types of cancer, including GBM. Invasion of GBM cells into surrounding brain parenchyma is associated with the activity of proteases. Proteases degrade proteins of the ECM and process growth factors, cytokines, chemokines and cell-adhesion proteins (Section 2.1). In this doctoral dissertation, invasion-associated proteases were explored, in particular the cathepsins, MMPs and uPA, in GBM progression in relation to GBM inter- and intra-tumoural heterogeneity.

GBM tumours contain heterogeneous populations of cancer cells that also differ in their subtype (Bonavia et al., 2011; Segerman et al., 2016). In the first part of this thesis, the aim was to correlate the genotype and invasion properties of two frequently-used GBM cell lines U87 and U373, which show distinct phenotypes and differ in expression of genes associated with ECM organization, developmental processes and cell differentiation (Motaln et al., 2015). The U87 cell line is more invasive in 3D invasion models and expresses higher levels of MMPs, cysteine and serine proteases, as compared to the U373 cell line. On the basis of the GBM molecular subtype classification according to Verhaak et al. (2010) both U87 and U373 cells are of the mesenchymal subtype. Behnan et al. (2016) recently identified 12 genes for GBM genotyping instead of the 840 genes that were used until then for that purpose. Analysis of the 12 genes revealed that U373 cells have a more distinct mesenchymal feature than U87 cells, as mesenchymal genes were highly expressed in U373 cells whereas only some of these genes were expressed in U87 cells. The two cell lines also differed in the expression of genes that are associated with cellular responses to transforming growth factor beta (TGF-β). Therefore, it was surprising that U87 cells were more invasive and aggressive than U373 cells in 2D and 3D monocultures (Section 2.2.). However, the invasion and aggression behaviour was triggered in U373 cells by MSC co-culturing, possibly stimulating TGF-β-induced invasion.

Various studies have indicated that cancer-stromal cell cross-talk affects the proteolytic network and thus may affect cancer cell invasion (Sevenich & Joyce, 2014; Breznik et al., 2017a). Communication between GBM cells and infiltrating stromal cells creates a tumour-promoting microenvironment (Bonavia et al., 2011; Breznik et al., 2017a; Quail & Joyce, 2017). Here, it is reported that bone-marrow derived MSCs affect invasion of the two GBM cell lines in an opposite way. This finding is not in disagreement with the literature, as opposite effects of MSCs on the same type of tumours *in vivo* and *in vitro* has been observed before (Klopp et al., 2011; Barcellos-de-Souza et al., 2013). In GBM, both roles of MSCs in promotion (Schichor et al., 2012; Torsvik et al., 2013) and inhibition (Dasari et al., 2010; Kološa et al., 2015) of tumour growth have been reported. However, the molecular mechanisms of MSC interactions with GBM cells are not yet well defined. It is reported

here that MSCs inhibit invasion of U87 cells and enhance invasion of U373 cells *in vitro* and *in vivo*. A major cause of the opposite effects of MSCs is the heterogeneity of GBM cells, which is relevant for responses to infiltrated or exogenously applied MSCs in tumours (Section 2.2.).

To confirm the differential effects of MSCs on GBM cell invasion in a more physiological matrix, e.g. brain parenchyma *in vivo*, a novel animal model of zebrafish embryos was applied. Zebrafish models have already contributed to a better understanding of a number of pathologies, including glioma. Zebrafish xenotransplantation models have been applied to study glioma stem cell invasion (Yang et al., 2013), GBM cell heterogeneity (Welker et al., 2016) and efficacy of anti-GBM drugs (Eden et al., 2015). Zebrafish embryo brains mimic the human GBM TME with the presence of laminin and neuronal tracts that are present in early stages (Burril et al., 1995; Gutzman et al., 2008). When GBM cells were injected, rapid aggregation into tumour masses occurred in ventricles and midbrain hemispheres of zebrafish brains. GBM cells invaded the central nervous system, but they did not leave it. GBM cells in midbrain hemispheres formed elongated pseudopodia and invaded neighbouring brain areas dorsally, most likely along axonal tracts. Co-injection of GBM cells and MSCs resulted in the development of mixed tumours in zebrafish embryo brains. Intercellular interactions between GBM cells and MSCs and cell-fusion events occurred. GBM cells and MSCs used similar invasion routes in the central nervous system. The zebrafish embryo model has been successfully established and applied for addressing GBM invasion and heterogeneity (Section 2.3).

MSCs play an important immunomodulatory role in TME due to their expression of cytokines and their receptors. It was shown that MSCs in the presence of GBM cells overexpress and secrete a range of cytokines and chemokines, such as TGF-β, IL-1α and β, CXCL1-2, CXCL6, CXCL12, and CCL2/MCP1 (Motaln et al., 2012; Motaln & Turnsek, 2015). Increased levels of inflammatory cytokines enhance in an autocrine and/or paracrine manner the expression and activity of proteases in TME, affecting tumour progression (Breznik et al., 2017a). With respect to proteases, it was shown that in MSC co-cultures with U373 cells, but not with U87 cells, invasion depended on overexpression and activation of cathepsin B, which is involved in various processes of cancer progression (Hazen et al., 2000; Lah et al., 2006; Mohamed & Sloane, 2006; Mirkovic et al., 2015). It has already been demonstrated that cathepsin B is involved in the invasion of GBM cell lines and primary GBM cells since its silencing and selective inhibition impaired GBM cell invasion *in vitro* (Gole et al., 2009; 2012*)*. In NOD/SCID mice, cathepsin B was consistently localized at the invasive edges of GBM tumours (Gole et al., 2012). Cathepsin B is also known as a potential initiator of the proteolytic cascade (Lah et al., 2006; Rao Malla et al., 2013; Kos et al., 2014). Cathepsin B activates ECM-degrading MMPs (Olson & Joyce, 2015) and uPA, when bound to its membrane receptor uPAR (Mohamed & Sloane, 2006). It was found that MMP-2, -9 and-14 as well as uPA/uPAR were overexpressed in co-cultured U373 cells and not in co-cultured U87 cells. It was functionally confirmed cathepsin B, MMP-9 and MMP-14 activation by the effects of their selective inhibitors, which completely abolished the effects of MSCs on U373 cell invasion, but not on co-cultured U87 cells (Section 2.2).

Paracrine signalling between MSCs and GBM cells is mediated via growth factors, cytokines and chemokines, which are released from both cell types (Breznik et al., 2017a). The most relevant signalling protein with respect to invasion is TGF-β, which plays an important role in EMT (Pickup et al., 2013; Sinh et al., 2016). Additionally, TGF-β causes activation of invasion-related proteases cathepsin B, MMP-2 and -9 (Pickup et al., 2013; Aggarwal & Sloane, 2014). Apparently, exogenous TGF-β, released by MSCs, triggers protease expression and increased invasion by U373 cells but not by U87 cells. This

differential effect of TGF-β may be caused by alternative signalling pathways in the two phenotypically different GBM cell lines (Piek et al., 1999).

Since cathepsin B has tumour-promoting roles and elevated cathespin B protein and activity have been observed in many cancer types (Hazen et al., 2000; Lah et al., 2006; Kos et al., 2014; Mirković et al., 2015), including GBM (Strojnik et al., 1999; Colin et al., 2009; Gole et al., 2012), this cysteine protease is a potential target for anti-cancer treatment. Recently, nitroxoline was identified as reversible, selective and non-covalent inhibitor of cathepsin B that inhibits pro-tumorigenic endopeptidase activity of cathepsin B. It has been shown that nitroxoline significantly reduced cell proliferation and invasion of different cancer cell lines and abrogated tumour growth and metastasis in various mouse models (Mirković et al., 2015). Here, new selective inhibitors of cathepsin B, such as nitroxoline and its derivate - compound 17 (Sosić et al., 2013) were tested in co-cultures of MSCs and different GBM cells. When MSC/U373 co-cultured spheroids were prepared, and studied, migration of both cell types was increased and was significantly inhibited by compound 17 as well as nitroxoline. On the other hand, addition of either compound 17 or nitroxoline had no effect on the migration of cells from MSC/U87 co-culture spheroids, whereas migration of U87 monoculture spheroids was impaired by both nitroxoline and compound 17. Our results were in line with the upregulated cathepsin B levels in co-cultures of U373 cells and MSCs and increased secretion of cathepsin B in U373/MSC co-cultures. In contrast, expression of cathepsin B was not altered in co-cultures of MSCs and U87 GBM cells, when compared to U87 monocultures. Besides that, compound 17 appeared to be more effective than nitroxoline in inhibition of cancer cell invasion *in vitro* as well as impairing tumour growth *in vivo* in LPB mouse fibrosarcoma tumours (Section 2.4).

In conclusion, MSC/GBM cross-talk is different in two GBM cell lines, indicating that GBM heterogeneity has to be considered when testing new anti-GBM approaches.

In the second part of this doctoral dissertation, cysteine cathepsins were studied, in particular with respect to the expression, roles and predictive values of less explored cathepsins K and X in GBM pathobiology. High expression of cysteine cathepsins K and X at mRA and protein levels have already been linked with the progression of various types of cancers (Kos et al., 2015; Verbovšek et al., 2015).

High cathepsin K protein expression confirmed previous findings that cathepsin K mRNA was upregulated in GBM cells and tissues vs. their normal counterparts (Verbovšek et al., 2014). An association between cathepsin K mRNA expression and GBM patient's survival was not found, as was proved for several other types of cancers (Verbovšek et al., 2015). However, when GBM tumours were stratified according to the molecular subtype, high cathepsin K levels in proneural GBM subtypes showed a borderline predictive potential for poor survival.

Cathepsin X mRNA expression levels in GBM tissues were observed to be significantly higher than in lower-grade gliomas and normal brain. These results are in a line with studies of other types of cancers, such as hepatocellular carcinoma and melanoma, showing a correlation between cathepsin X overexpression in cancer tissue and advanced tumour stages (Wang et al., 2011). The highest cathepsin X expression was observed in the mesenchymal GBM subtype, which represents the most aggressive and therapy-resistant GBM subtype (Segerman et al., 2016). With respect to the survival prediction, high cathepsin X levels in serum and cancer tissue of patients with colorectal cancer and hepatocellular carcinoma, respectively, have been shown to be associated with shorter overall survival (Wang et al., 2011; Vižin et al. 2012; Kos et al., 2015). The same trend for cathepsin X mRNA levels was found in 156 GBM patients. This predictive impact was dependent on the GBM subtype. An association between cathepsin X protein expression and survival of 21 GBM patients, which were not stratified by their subtype, was not

found. The discrepancy between the two studies is most likely due to the small size and characteristics of the GBM patients' cohorts (Section 2.5).

In the present thesis, it is demonstrated that tumour-initiating GSCs are present around arterioles, defined by a thick layer of tunica media of smooth muscle cells, that express SMA, demonstrating the presence of peri-arteriolar GSC niches in GBM tissues. GSCs were identified by expressing the stem cell markers CD133 and nestin. SDF-1α and CD68 imaging confirmed that chemotactic cytokine SDF-1α and macrophages (CD68+ cells) are also present in these peri-arteriolar regions, as was already reported before (Hira et al., 2015; Roos et al., 2017). The cathepsins K and X, together with the extensively studied cathepsin B, were detected in GSC niches, seemingly produced by cancer cells and stromal cells, and likely secreted into the interstitial space. In addition, protease activity of cathepsins B, but not that of cathepsin K was detected in the same GSC niches around arterioles. Cathepsin B, X and K distribution patterns in GSC niches were analysed in both paraffin and cryostat GBM tissue sections (Section 2.6). When correlations were investigated between mRNA expression of GSC niche markers and cathepsins K and X in 156 GBM samples, it was found that cathepsins K and X mRNA expression correlated with mRNA expression of GSC niche markers. These findings indicate that cathepsins have a specific role in GSC regulation in their niches by degradation of ECM or processing of cytokines, such as SDF-1α (Section 2.7).

Cathepsins B, K and X are structurally and functionally different, but were found in the same GSC niche microenvironment in GBM tissues and share the capacity to proteolytically degrade chemokine SDF-1α *in vitro* (Staudt et al., 2012), which is present in niches. This chemokine is important for retaining HSCs in their niches and the cleavage of SDF-1α by cathepsin B, K and X caused reduction in chemotaxis of HSCs (Kollet et al., 2006; Staudt et al., 2010; 2012). It was demonstrated that SDF-1 α induces chemotactic responses of CXCR4- and CXCR7-positive GBM cells and GSCs supporting the concept that this cytokine recruits GSCs to niche regions. It was also demonstrated that cathepsin K cleaves the N-terminal site and thus inactivates SDF-1α. This implies that cathepsin K activity facilitates invasion of GSCs out of their niches (Section 2.7).

Altogether, the findings reported in this thesis show that both cathepsins, K and X, are progressively upregulated in GBM. High cathepsin X mRNA levels are associated with poor GBM patient survival. Moreover, high inter- and intra-tumoural heterogeneity of cathepisins K and X expression was observed. GBM subtype-dependent predictive values of these cathepsins were found, indicating the importance of studying and understanding the GBM heterogeneity when exploring new biomarkers. Since SDF-1α and invasion affecting cathepsin B, K and X are all present in all GSC niches, it is possible that cooperation between all three cathepsins in regulation of SDF-1α chemotactic activity exists *in vivo.*

Appendix A

Supplementary Material of Included Publications

A.1 Supplementary Material of Publication 2.2.

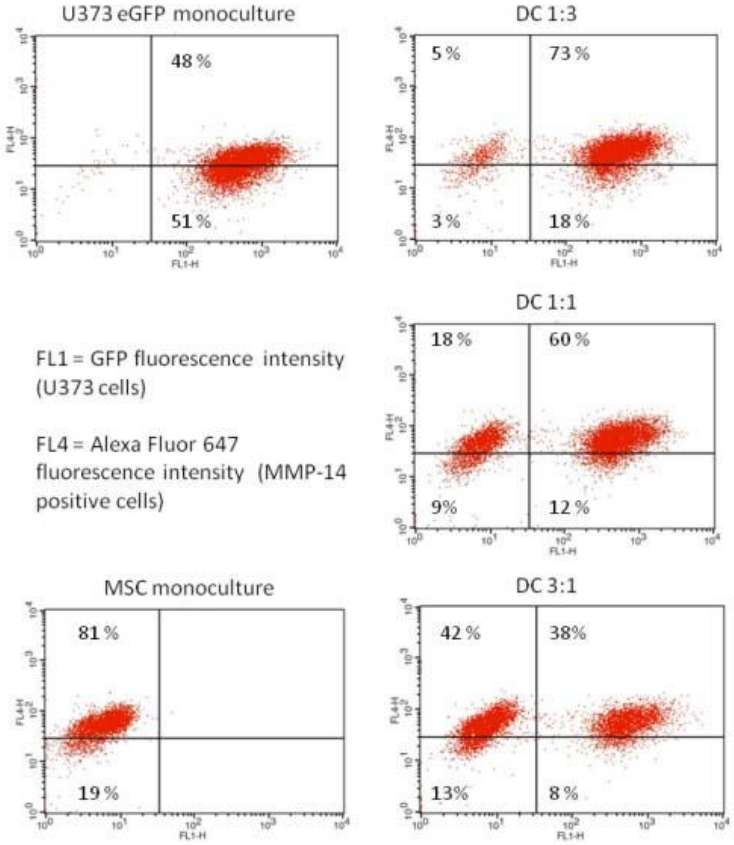
www.impactjournals.com/oncotarget/ Oncotarget, Supplementary Materials 2017

Mesenchymal stem cells differentially affect the invasion of distinct glioblastoma cell lines

SUPPLEMENTARY MATERIALS

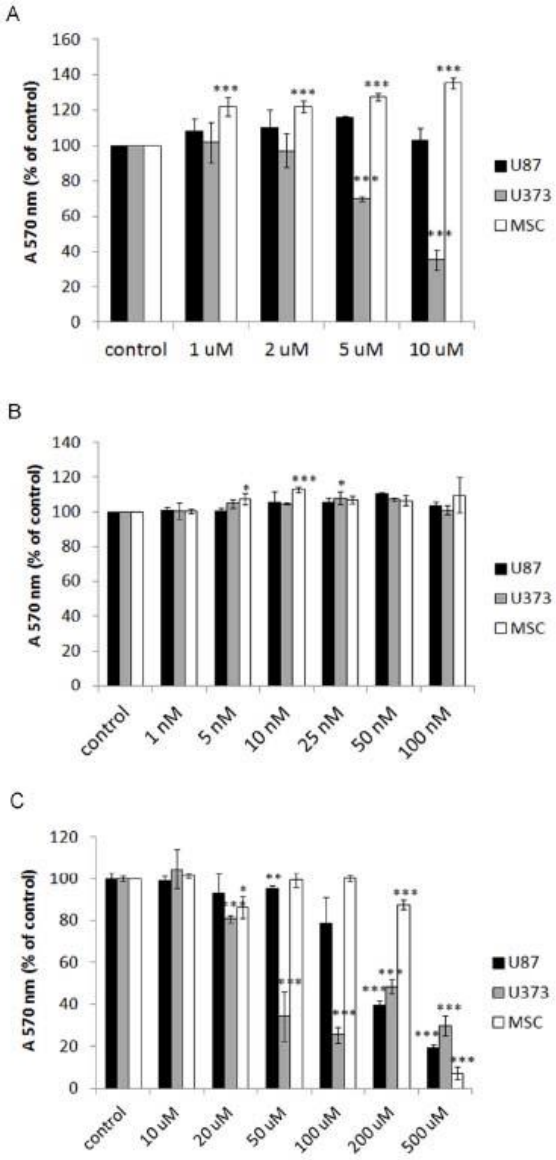
Flow cytometry analysis

Protein expression of candidate protein in each cell type was determined as percentage of cells stained positive for candidate protein out of total (stained and unstained) cells. Example of flow cytometry analysis and calculation of MMP-14 expression in co-cultured U373 eGFP cells and MSCs after 3 days in co-cultures:



MMP-14 expression in U373 cells and MSCs in DC 3-1 co-culture:
% protein expression in U373 cells = **38/(38+8)= 82,6 %**
% protein expression in MSCs = **42/(42+13)= 76,4 %**

www.impactjournals.com/oncotarget/ Oncotarget, Supplementary Materials 2017



Supplementary Figure 1: MSC and GBM (U87 and U373) cell viability in the presence of the selective protease inhibitors CA-074Me (A), MMP-9 I (B), and NSC405020 (C). Cells were plated and incubated with series of concentrations of protease inhibitors during 72 h. Cell viability was determined using MTT assays as absorbance (A) at 570 nm relative to the control (0 nM/μM of inhibitor). The inhibitor concentrations were considered non-toxic when cell viability was >95% as compared to the control. Data are means ± SD. * $P < 0.05$, ** $P < 0.01$, *** $P < 0.001$.

www.impactjournals.com/oncotarget/ Oncotarget, Supplementary Materials 2017

Supplementary Table 1: Upregulated protease genes in GBM tissue, as compared to normal brain

See Supplementary File 1

www.impactjournals.com/oncotarget/ Oncotarget, Supplementary Materials 2017

Supplementary Table 2: Expression of genes from TCGA 840 gene list [1] in U87 and U373 cells

We analyzed 6 biological replicates of U87 and 3 biological replicates of U373 cells as described in Material and Methods section. Based on the data pre-processing as done in *Verhaak et al.* [1], 517 genes were used for determination of GBM subtype: PN – proneural, NL – neural, CL – classical and MES – mesenchymal (as determined by *Verhaak et al.*, column B). Upregulated genes are shown in red. The mesenchymal subtype (MES) had the most upregulated genes in both, U87 and U373 cell lines. Genes with the expression that was filtered out during quality control are denoted with NA.

See Supplementary File 2

Supplementary Table 2 is available online at: http://www.oncotarget.com/index.php?journal=oncotarget&page=article&op=view&path[]=16041&pubmed-linkout=1

www.impactjournals.com/oncotarget/ Oncotarget, Supplementary Materials 2017

Supplementary Table 3: GO enrichment results for the 294 genes with significantly different expression levels between U87 and U373 cell lines

The enrichment p-value and the FDR corrected p-value, together with the enrichment values used for the p-value calculation using the hypergeometric model are shown.

See Supplementary File 1

www.impactjournals.com/oncotarget/ Oncotarget, Supplementary Materials 2017

Supplementary Table 4: List of TaqMan probes (Applied Biosystems) used in the qRT-PCR analyses

GENE SYMBOL	GENE NAME	TAQMAN PROBE
CAPN1	Calpain1	Hs00559804_m1
CAPN2	Calpain 2	Hs00965097_m1
CTSB	Cathepsin B	Hs00947433_m1
MMP2	MMP-2	Hs001548727_m1
MMP9	MMP-9	Hs00234579_m1
MMP14	MMP-14	Hs00237119_m1
PLAU	Urokinase-type plasminogen activator (uPA)	Hs01547054_m1
PLAUR	Urokinase-type plasminogen activator receptor (uPAR)	Hs00958880_m1
GAPDH	Glyceraldehyde 3-phosphate dehydrogenase	Assay No. 4310884E

www.impactjournals.com/oncotarget/ Oncotarget, Supplementary Materials 2017

Supplementary Table 5: List of primary antibodies and their dilutions used in the flow cytometry analysis and western blotting

PRIMARY ANTIBODY	SOURCE	Flow cytometry	Western blotting
Rabbit anti-calpain 1	Abcam (ab28258)	1:200	1:500
Rabbit anti-calpain 2	Abcam (ab39165)	1:100	1:100
Rabbit anti-cathepsin b	Krka, d.d.	1:10	1:200
Mouse anti-mmp-2	Abcam (ab3158)	1:20	1:200
Rabbit anti-mmp-9	Abcam (ab38898)	1:100	1:1000
Rabbit anti-mmp-14	Abcam (ab3644)	1:20	/
Rabbit anti-upa	Abcam (ab24121)	1:100	1:200
Rabbit anti-upar	Abcam (ab103791)	1:100	/
Mouse isotype control IgG1 κ	Abcam (ab91535)	1:10	/

Supplementary File 1

Supplementary Table 1: Upregulated protease genes in GBM tissue, as compared to normal brain.

GENESYMBOL	ENTREZ ID	GENENAME	FC CLASS1/CLASS2
CYSTEINE PROTEASES			
CFLAR	8837	CASP8 and FADD-like apoptosis regulator	1.709
CASP7	840	caspase 7, apoptosis-related cysteine peptidase	1.683
USP39	10713	ubiquitin specific peptidase 39	1.670
CASP4	837	caspase 4, apoptosis-related cysteine peptidase	1.658
MALT1	10892	mucosa associated lymphoid tissue lymphoma translocation gene 1	1.650
USP1	7398	ubiquitin specific peptidase 1	1.633
ESPL1	9700	extra spindle pole bodies homolog 1 (S. cerevisiae)	1.613
GGH	8836	gamma-glutamyl hydrolase (conjugase, folylpolygammaglutamyl hydrolase)	1.578
TNFAIP3	7128	tumor necrosis factor, alpha-induced protein 3	1.577
CASP1	834	caspase 1, apoptosis-related cysteine peptidase (interleukin 1, beta, convertase)	1.576
GMPS	8833	guanine monphosphate synthetase	1.569
CASP3	836	caspase 3, apoptosis-related cysteine peptidase	1.567
CASP6	839	caspase 6, apoptosis-related cysteine peptidase	1.558
CTSS	1520	cathepsin S	1.557
CTSO	1519	cathepsin O	1.553
PAN2	9924	PAN2 poly(A) specific ribonuclease subunit homolog (S. cerevisiae)	1.544
GFPT2	9945	glutamine-fructose-6-phosphate transaminase 2	1.528
CTSK	1513	cathepsin K	1.502
USP3	9960	ubiquitin specific peptidase 3	1.468
CTSL1	1514	cathepsin L1	1.455
CTSB	1508	cathepsin B	1.442
CAPN2	824	calpain 2, (m/II) large subunit	1.420
CTSC	1075	cathepsin C	1.339
MATRIX METALLOPROTEASES			
ADAMTS9	56999	ADAM metallopeptidase with thrombospondin type 1 motif, 9	1.693
ADAMTS5	11096	ADAM metallopeptidase with thrombospondin type 1 motif, 5	1.685
EIF3F	8665	eukaryotic translation initiation factor 3, subunit F	1.667
ADAM12	8038	ADAM metallopeptidase domain 12	1.654
ZMPSTE24	10269	zinc metallopeptidase (STE24 homolog, S. cerevisiae)	1.646
ENPEP	2028	glutamyl aminopeptidase (aminopeptidase A)	1.644
PEPD	5184	peptidase D	1.633
DPP3	10072	dipeptidyl-peptidase 3	1.632
PMPCB	9512	peptidase (mitochondrial processing) beta	1.627
RNPEP	6051	arginyl aminopeptidase (aminopeptidase B)	1.617
DNPEP	23549	aspartyl aminopeptidase	1.615
TFRC	7037	transferrin receptor (p90, CD71)	1.555
ERAP2	64167	endoplasmic reticulum aminopeptidase 2	1.498
CPM	1368	carboxypeptidase M	1.399
MMP2	4313	matrix metallopeptidase 2 (gelatinase A, 72kDa gelatinase, 72kDa type IV collagenase)	1.344

LAP3	51056	leucine aminopeptidase 3	1.338
DPYSL3	1809	dihydropyrimidinase-like 3	1.332
ADAM9	8754	ADAM metallopeptidase domain 9	1.246
AEBP1	165	AE binding protein 1	1.197
MMP9	**4318**	**matrix metallopeptidase 9 (gelatinase B, 92kDa gelatinase, 92kDa type IV collagenase)**	**1.192**
SERINE PROTEASES			
ABHD11	83451	abhydrolase domain containing 11	1.706
ABHD4	63874	abhydrolase domain containing 4	1.687
MST1	4485	macrophage stimulating 1 (hepatocyte growth factor-like)	1.661
LONP1	9361	lon peptidase 1, mitochondrial	1.642
CLPP	8192	ClpP caseinolytic peptidase, ATP-dependent, proteolytic subunit homolog (E. coli)	1.633
RHBDF1	64285	rhomboid 5 homolog 1 (Drosophila)	1.614
HTRA1	5654	HtrA serine peptidase 1	1.612
PCSK5	5125	proprotein convertase subtilisin/kexin type 5	1.568
PLAU	**5328**	**plasminogen activator, urokinase**	**1.543**
TPP1	1200	tripeptidyl peptidase I	1.523
C1RL	51279	complement component 1, r subcomponent-like	1.508
PRSS23	11098	protease, serine, 23	1.482
DAG1	1605	dystroglycan 1 (dystrophin-associated glycoprotein 1)	1.438
CTSA	5476	cathepsin A	1.426
PLAT	5327	plasminogen activator, tissue	1.396
CPVL	54504	carboxypeptidase, vitellogenic-like	1.340
SEC11A	23478	SEC11 homolog A (S. cerevisiae)	1.320
PRCP	5547	prolylcarboxypeptidase (angiotensinase C)	1.305
CFI	3426	complement factor I	1.305
BCHE	590	butyrylcholinesterase	1.271
C1S	716	complement component 1, s subcomponent	1.226
MEST	4232	mesoderm specific transcript homolog (mouse)	1.220
C1R	715	complement component 1, r subcomponent	1.174
LTF	4057	lactotransferrin	1.067
CARD8	22900	caspase recruitment domain family, member 8	1.533
THREONINE PROTEASES			
PSMA5	5686	proteasome (prosome, macropain) subunit, alpha type, 5	1.665
AGA	175	aspartylglucosaminidase	1.652
PSMA7	5688	proteasome (prosome, macropain) subunit, alpha type, 7	1.650
PSMA2	5683	proteasome (prosome, macropain) subunit, alpha type, 2	1.463
PSMB8	5696	proteasome (prosome, macropain) subunit, beta type, 8 (large multifunctional peptidase 7)	1.319
PSMB9	5698	proteasome (prosome, macropain) subunit, beta type, 9 (large multifunctional peptidase 2)	1.270
ASPARTIC PROTEASES			
	25825	beta-site APP-cleaving enzyme 2	

MIXED PROTEASES (MIXED CATALYTIC TYPE)			
CD97	976	CD97 molecule	1.533
GPR56	9289	G protein-coupled receptor 56	1.377
ELTD1	64123	EGF, latrophilin and seven transmembrane domain containing 1	1.363

*Upregulated protease genes in GBM tissue compared to normal brain tissue, after passing the criteria of P <0.05 and fold change (FC; class1/class2) >1.0.

Supplementary Table 3: GO enrichment results for the 294 genes with significantly different expression levels between U87 and U373 cell lines. The enrichment p-value and the FDR corrected p-value, together with the enrichment values used for the p-value calculation using the hypergeometric model are shown.

GO term	Description	P-value	FDR q-value	Enrichment (N, B, n, b)	Genes
GO:0071363	cellular response to growth factor stimulus	1.02E-6	4.21E-3	13.69 (292,8,16,6)	COL1A1 - collagen, type i, alpha 1 NRP1 - neuropilin 1 ABL1 - c-abl oncogene 1, non-receptor tyrosine kinase SHC1 - shc (src homology 2 domain containing) transforming protein 1 SOX9 - sry (sex determining region y)-box 9 COL4A2 - collagen, type iv, alpha 2
GO:0071560	cellular response to transforming growth factor beta stimulus	8.33E-6	1.72E-2	18.25 (292,4,16,4)	COL1A1 - collagen, type i, alpha 1 ABL1 - c-abl oncogene 1, non-receptor tyrosine kinase SOX9 - sry (sex determining region y)-box 9 COL4A2 - collagen, type iv, alpha 2
GO:0070848	response to growth factor	8.86E-6	1.22E-2	10.95 (292,10,16,6)	COL1A1 - collagen, type i, alpha 1 NRP1 - neuropilin 1 ABL1 - c-abl oncogene 1, non-receptor tyrosine kinase SHC1 - shc (src homology 2 domain containing) transforming protein 1 SOX9 - sry (sex determining region y)-box 9 COL4A2 - collagen, type iv, alpha 2
GO:0071559	response to transforming growth	7.19E-5	7.4E-2	14.60 (292,5,16,4)	COL1A1 - collagen, type i, alpha 1

	factor beta				ABL1 - c-abl oncogene 1, non-receptor tyrosine kinase SOX9 - sry (sex determining region y)-box 9 COL4A2 - collagen, type iv, alpha 2
GO:0009887	animal organ morphogenesis	1.09E-4	8.97E-2	2.84 (292,20,72,14)	TGFB3 - transforming growth factor, beta 3 COL8A2 - collagen, type viii, alpha 2 SOX9 - sry (sex determining region y)-box 9 EPHB4 - eph receptor b4 SOX4 - sry (sex determining region y)-box 4 GNAS - gnas complex locus CDH2 - cadherin 2, type 1, n-cadherin (neuronal) TGFBR2 - transforming growth factor, beta receptor ii (70/80kda) COL5A1 - collagen, type v, alpha 1 COL1A1 - collagen, type i, alpha 1 NRP1 - neuropilin 1 COL1A2 - collagen, type i, alpha 2 HOXD3 - homeobox d3 SRF - serum response factor (c-fos serum response element-binding transcription factor)
GO:0044711	single-organism biosynthetic process	3.06E-4	2.1E-1	2.43 (292,20,90,15)	TRAM2 - translocation associated membrane protein 2 GSTA4 - glutathione s-transferase alpha 4 ASL - argininosuccinate lyase SERPINH1 - serpin peptidase inhibitor, clade h (heat shock protein 47), member 1,

					(collagen binding protein 1) ADCY9 - adenylate cyclase 9 COL5A1 - collagen, type v, alpha 1 COL1A1 - collagen, type i, alpha 1 GSTK1 - glutathione s-transferase kappa 1 ACSL1 - acyl-coa synthetase long-chain family member 1 CRYL1 - crystallin, lambda 1 ATP5F1 - atp synthase, h+ transporting, mitochondrial fo complex, subunit b1 ACSL3 - acyl-coa synthetase long-chain family member 3 TCIRG1 - t-cell, immune regulator 1, atpase, h+ transporting, lysosomal v0 subunit a3 MGST2 - microsomal glutathione s-transferase 2 ATP5L - atp synthase, h+ transporting, mitochondrial fo complex, subunit g
GO:0048844	artery morphogenesis	3.26E-4	1.92E-1	24.33 (292,6,6,3)	NRP1 - neuropilin 1 JAG1 - jagged 1 SRF - serum response factor (c-fos serum response element-binding transcription factor)
GO:0045665	negative regulation of neuron differentiation	8.8E-4	4.53E-1	10.81 (292,9,12,4)	NRP1 - neuropilin 1 JAG1 - jagged 1 SOX9 - sry (sex determining region y)-box 9 PMP22 - peripheral myelin protein 22

A.2 Supplementary Material of Publication 2.5.

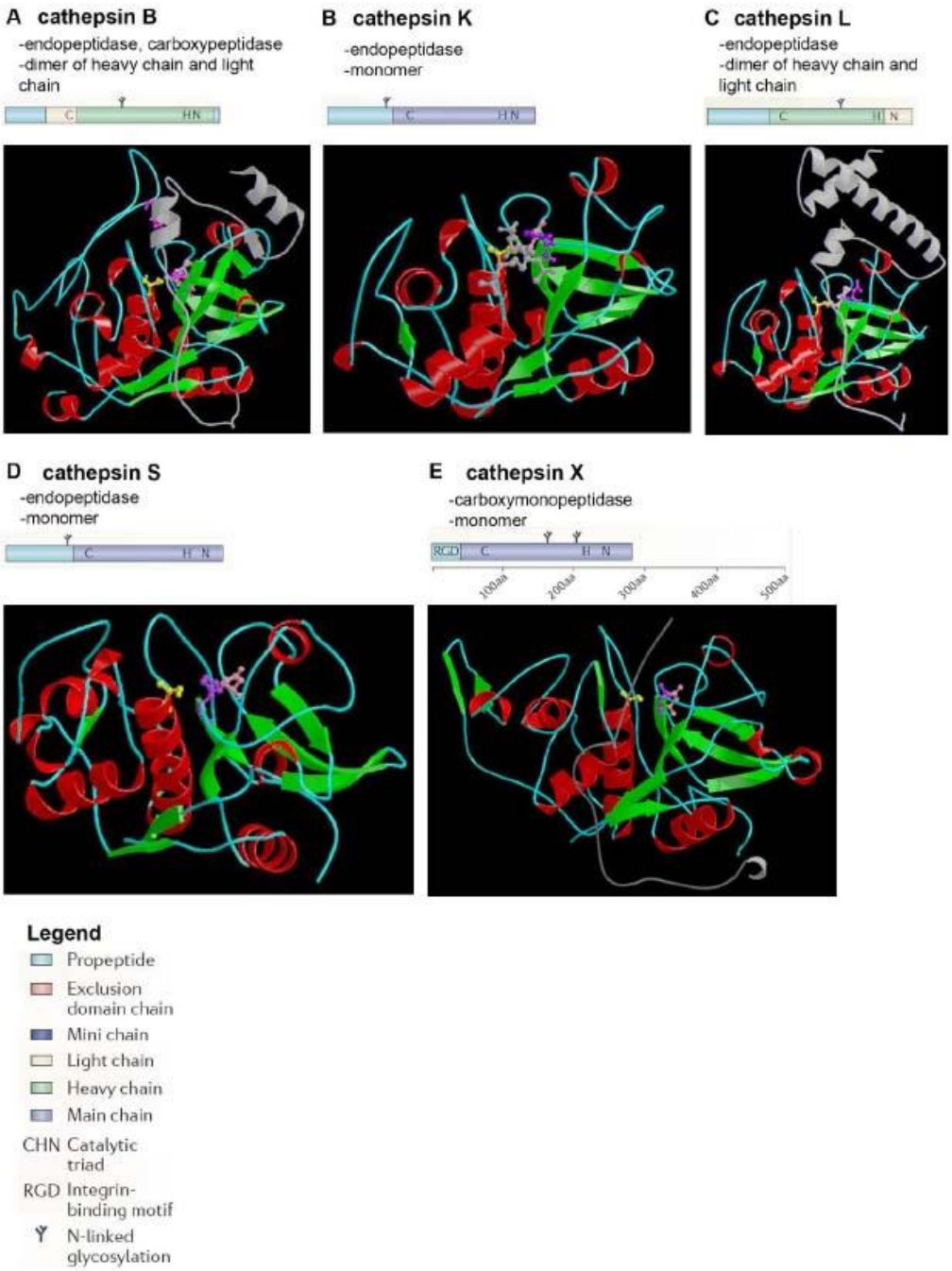


Figure S1. Relationship between catalytic activities and structures of cathepsins B, K, L, S and X. Catalytic activity, subunit structure and 3D structures of (A) cathepsin B, (B) cathepsin K, (C) cathepsin L, (D) cathepsin S and (E) cathepsin X. Subunit structures of cathepsins are taken from Olson and Joyce, Nat Rew Cancer 2015, and 3D structures are taken from MEROPS peptidase database *(https://www.ebi.ac.uk/merops/index.shtml).*

The explanations of 3D structures of cathepsins: (A) Catalytic residues are shown in ball-and-stick representation: Cys108 in yellow, His278 in purple and Asn298 in pink. His189 on the occluding loop is shown in purple in ball-and-stick representation. The propeptide is shown in grey; (B) Catalytic residues are shown in ball-and-stick representation: Cys133 in yellow, His276 in purple and Asn296 in pink. E-64 is shown in grey in ball-and-stick representation; (C) Catalytic residues are shown in ball-and-stick representation: Cys138 (engineered to be serine) in yellow, His276 in purple and Asn300 in pink. The propeptide is shown in grey; (D) Catalytic residues are shown in ball-and-stick representation: Cys139 (engineered to be serine) in yellow, His278 in purple and Asn298 in pink; (E) One subunit of the dimer is shown. Catalytic residues are shown in ball-and-stick representation: Cys92 in yellow, His241in purple and Asn261 in pink. The propeptide is shown in grey.

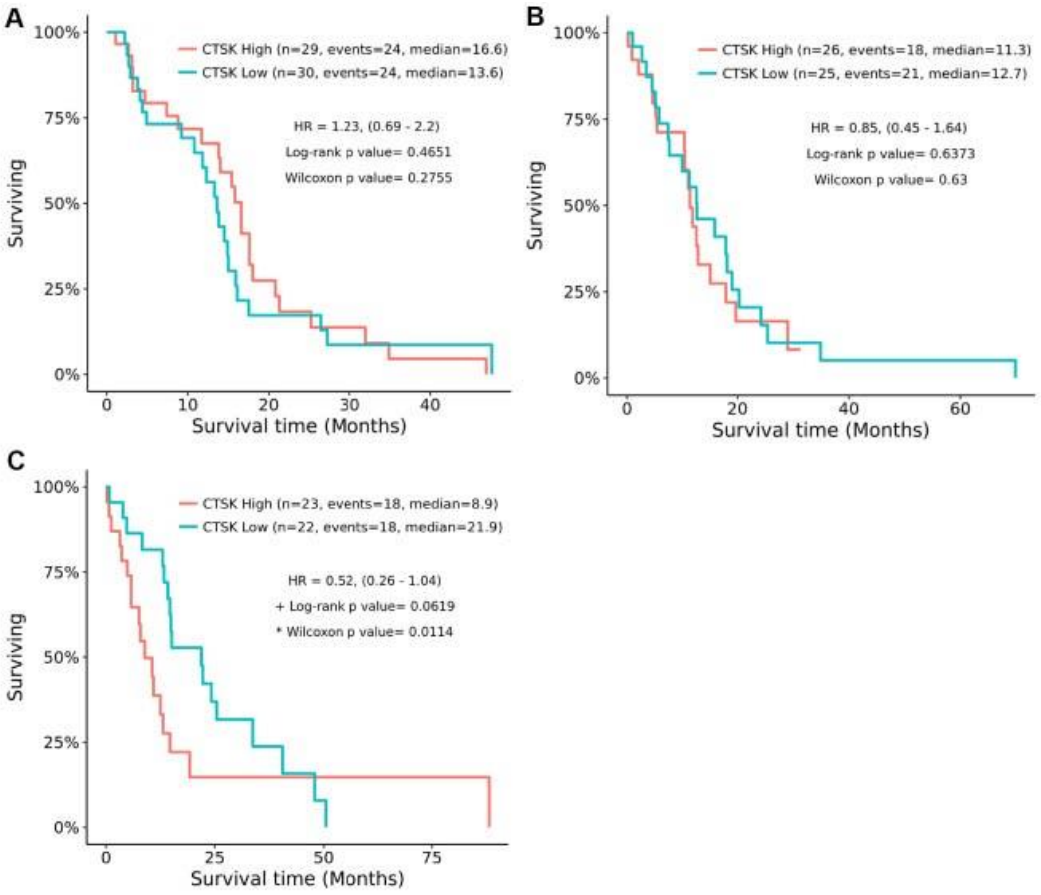


Figure S2. Kaplan-Meier survival curves for overall survival time with respect to cathepsin K mRNA levels. Cathepsin K mRNA expression did not correlate with GBM survival in classical (A) and mesenchymal (B) subtypes. In the proneural subtype (C) cathepsin K has limited p value ($P < 0.0619$ by Log rank and $P < 0.0114$ value by Wilcoxon analysis), which may be considered to be potentially significant. Kaplan-Maier survival curves were obtained from GlioVis data portal [33]. GBM were stratified into two groups, tumors with high and tumors with low cathepsin K expression, using median value as cutoff.

Table S1. Comparison of prognostic significance of measured variables by COX proportional hazard model in 21 GBM patients.

Variable	Hazard ratio	P value	Hazard ratio 95 % CI
Age (years)	1.03	0.43	(0.96-1.09)
Gender (M/F)	1.03	0.96	(0.33-3.22)
CTSK protein expr. (%)	1.03	0.16	(0.99-1.07)
CTSX protein expr. (%)	0.91	0.15	(0.85-0.98)

CI: confidence interval; M/F: male/female

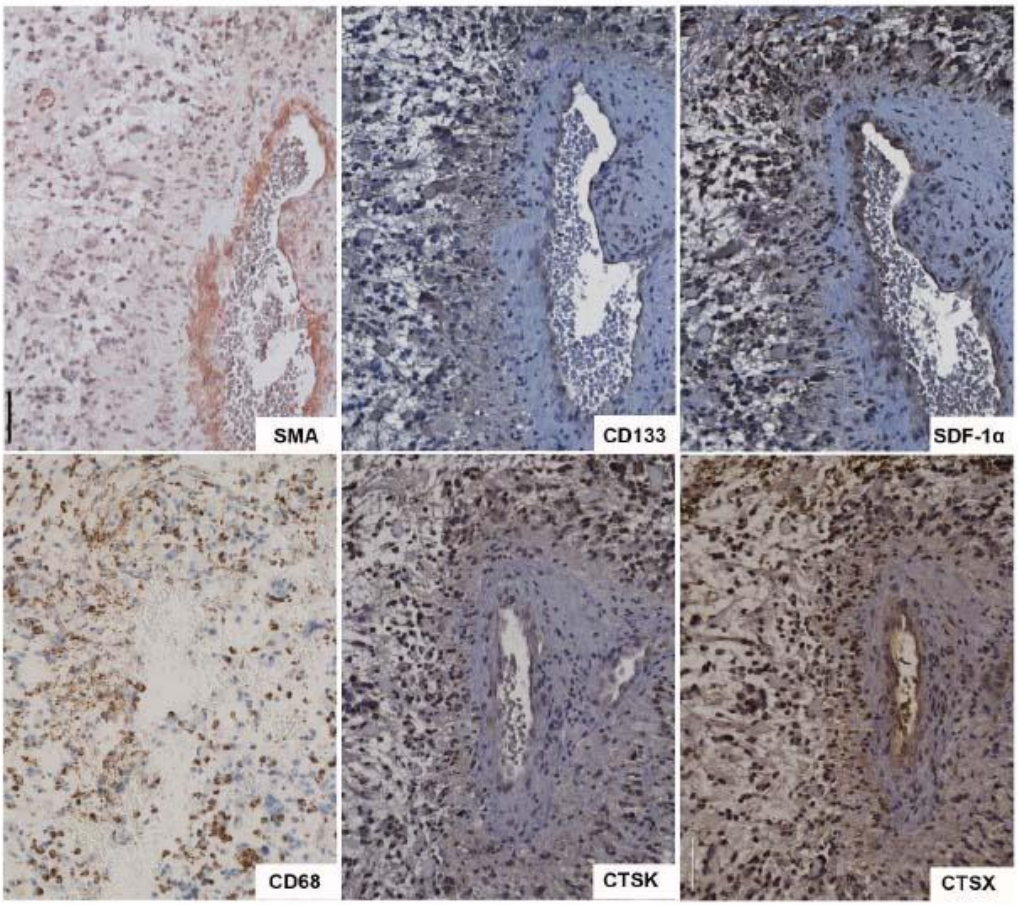


Figure S3. High-magnification images of serial paraffin-embedded GBM sections labelled for GSC niche markers SMA, CD133 and SDF-1*α*, macrophage marker CD68 and cathepsins K and X. Immunohistochemical labelling of SMA was performed with AEC as substrate (red colour) and of the other proteins with DAB as substrate (brown colour). Cell nuclei were stained using hematoxylin (blue/purple). Scale bar = 50 µm.

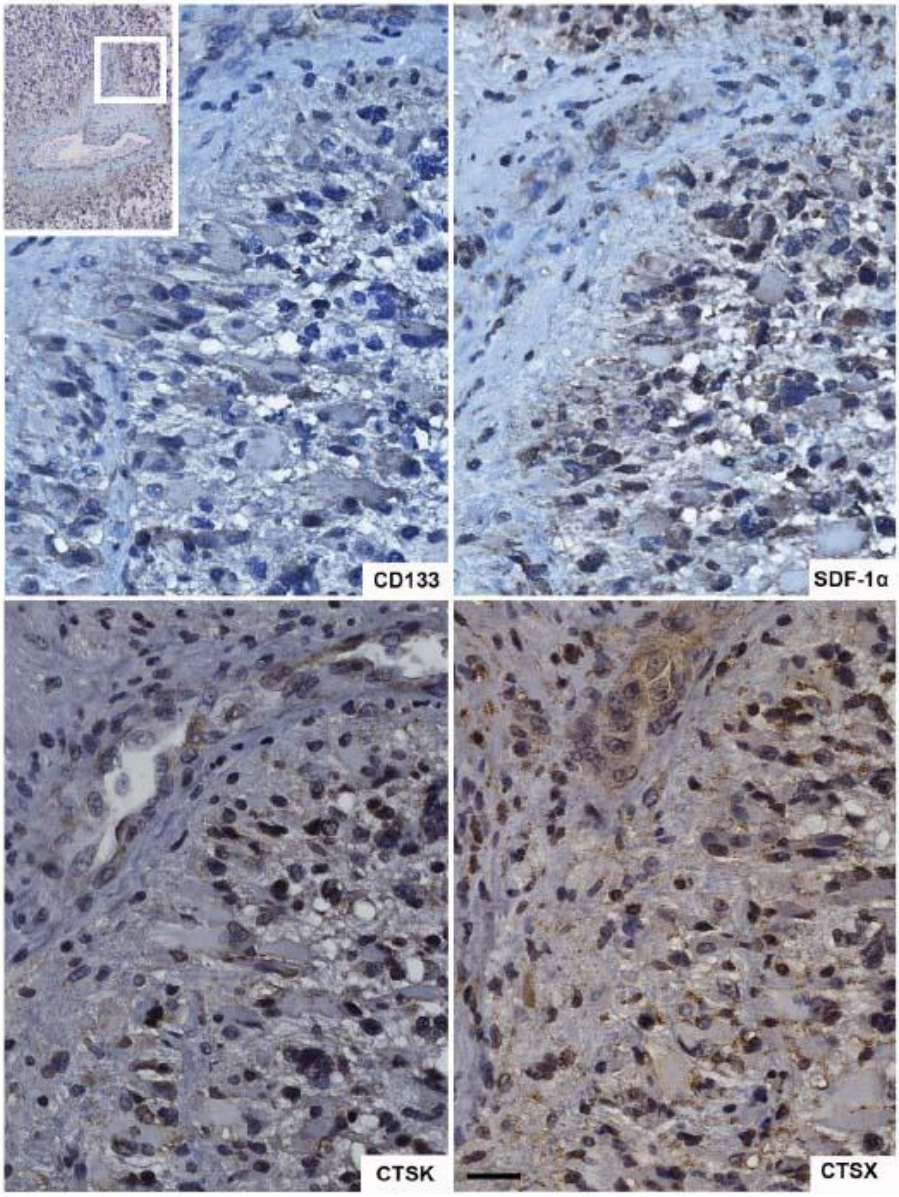


Figure S4. High-magnification images of serial paraffin-embedded GBM sections labelled for GSC niche markers CD133 and SDF-1α and cathepsins K and X. Region around the arteriole as shown in upper left corner of the Figure was magnified. Immunohistochemical labelling of proteins was performed with DAB as substrate (brown colour). Cell nuclei were stained using hematoxylin (blue/purple). Scale bar = 20 µm.

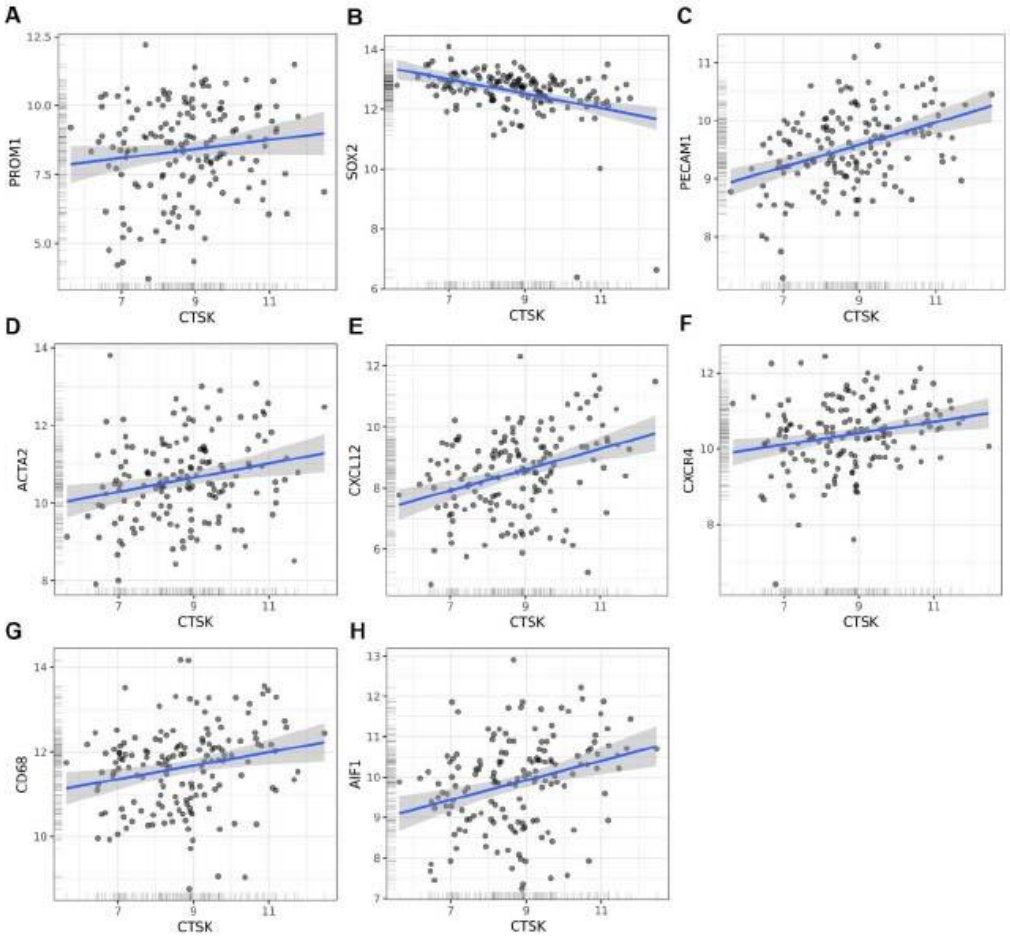


Figure S5. Correlation of microarray-based gene expression level of cathepsin K and GSC stem cell niche markers. Cathepsin K expression did not correlate with the expression of GSC markers CD133 (i.e. PROM1) (A), but it negatively correlated with the other GSC marker SOX2 (B). We observed positive correlation of cathepsin K expression with the expression of GSC niche markers: endothelial marker CD31 (i.e. PECAM1) (C), α-smooth muscle actin marker SMA (i.e. ACTA2) (D), chemotactic cytokine SDF-1α (i.e. CXCL12) (E) and its receptor CXCR4 (F), the macrophage/microglia markers CD68 (G) and Iba1 (i.e. AIF1) (H). Trend lines indicate linear regression estimates. Log2-tarsformed mRNA expression data were obtained via GlioVis portal.

Table S2. Characteristics of the 21 globlastoma (GBM) patients, operated at the Department of Neurosurgery of the University of Ljubljana, University Medical Centre Ljubljana, Slovenia. 6 out of 21 patients were females (median age 60.5 years), the mean age of males was 62 years.

Number	Gender	Age at the time of operation (years)	Survival (months)	Newly-diagnosed or reccurent	Therapy (radio- or chemotrerapy with temozolomide)
1	M	46	17	Newly-diagnosed	Radiotherapy (60 Gy) + temozolomide, adjuvant temozolomide therapy
2	M	81	7	Newly-diagnosed	Radiotherapy (30 Gy)
3	F	48	8	Newly-diagnosed	Radiotherapy (60 Gy) + temozolomide, adjuvant temozolomide therapy
4	F	62	32	Newly-diagnosed	Radiotherapy (60 Gy) + temozolomide, adjuvant temozolomide therapy
5	M	81	0	Newly-diagnosed	/
6	M	43	21	Newly-diagnosed	Radiotherapy (60 Gy) + temozolomide, adjuvant temozolomide therapy
7	F	56	15	Newly-diagnosed	Radiotherapy (60 Gy) + temozolomide, adjuvant temozolomide therapy
8	M	54	3	Newly-diagnosed	Radiotherapy (60 Gy) + temozolomide, without adjuvant temozolomide therapy
9	M	55	26	Newly-diagnosed	Radiotherapy (60 Gy) + temozolomide, adjuvant temozolomide therapy
10	M	75	17	Newly-diagnosed	Radiotherapy (60 Gy) + temozolomide, adjuvant temozolomide therapy
11	M	66	8	Newly-diagnosed	Radiotherapy (60 Gy) + temozolomide, adjuvant temozolomide therapy
12	M	59	16	Newly-diagnosed	Radiotherapy (60 Gy) + temozolomide, adjuvant temozolomide therapy
13	F	59	16	Newly-diagnosed	Radiotherapy (60 Gy) + temozolomide, without adjuvant temozolomide therapy
14	F	66	8	Newly-diagnosed	Radiotherapy (60 Gy) + temozolomide, adjuvant temozolomide therapy

15	**F**	**67**	**3**	Newly-diagnosed	Radiotherapy (30 Gy)
16	**M**	**53**	**12**	Newly-diagnosed	Radiotherapy (60 Gy) + temozolomide, adjuvant temozolomide therapy
17	**M**	**59**	**1**	Newly-diagnosed	Without therapy
18	**M**	**65**	**13**	Newly-diagnosed	Radiotherapy (60 Gy) + temozolomide, adjuvant temozolomide therapy
19	**M**	**62**	**12**	Newly-diagnosed	Radiotherapy (60 Gy) + temozolomide, adjuvant temozolomide therapy
20	**M**	**71**	**12**	Newly-diagnosed	Radiotherapy (30 Gy) + temozolomide, adjuvant temozolomide therapy
21	**M**	**80**	**9**	Newly-diagnosed	Radiotherapy (30 Gy)

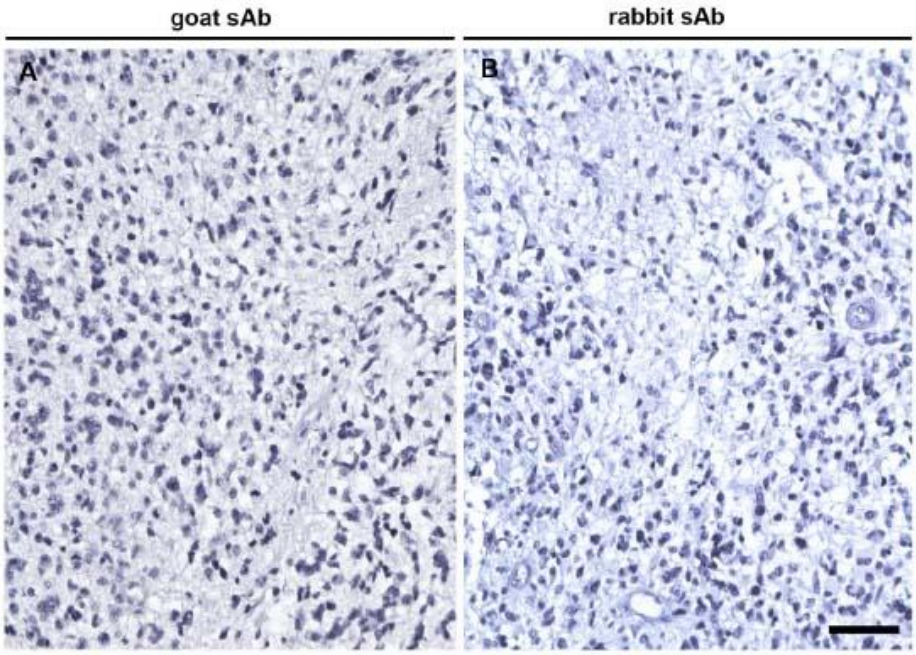


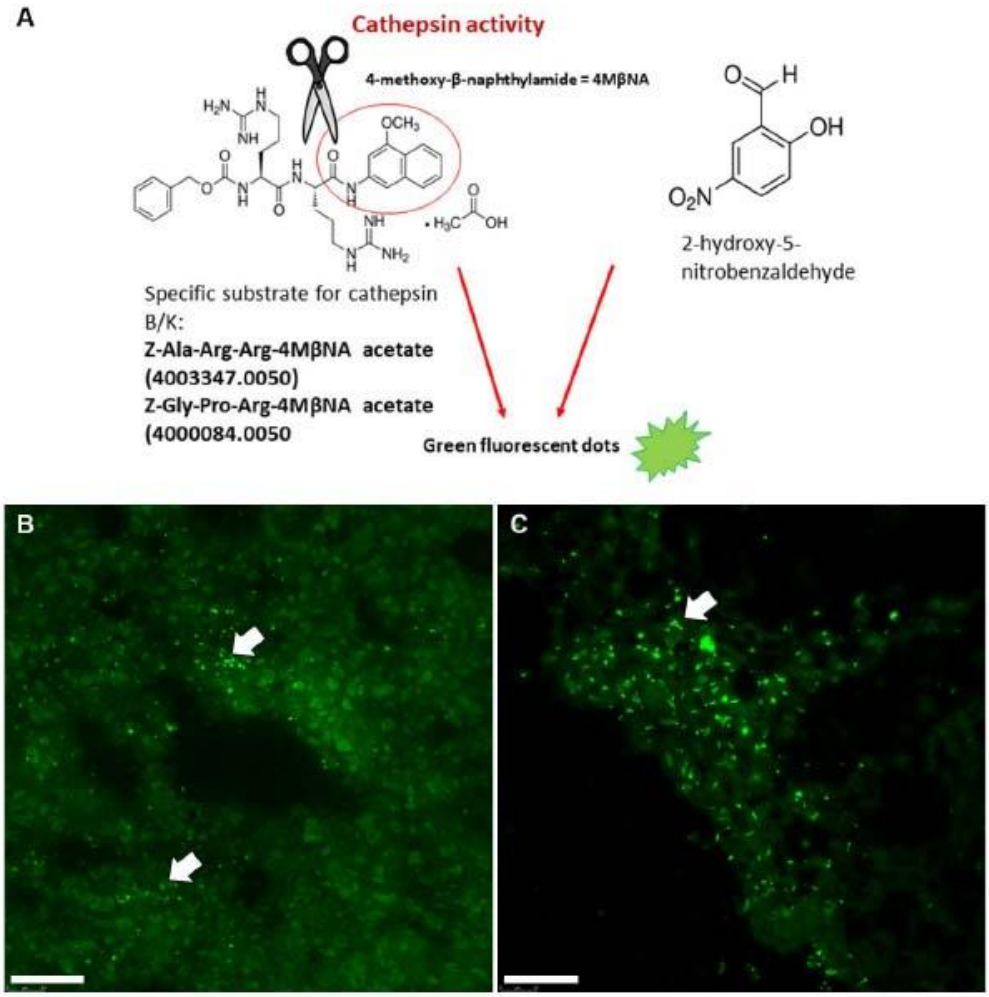
Figure S6. Control incubations of paraffin-embedded GBM sections for IHC.

Control incubations were performed in the absence of primary antibodies and with goat (A) or rabbit (B) secondary horse-radish-peroxidase–conjugated antibodies (sAb) in the final dilution of 1:200. Scale bar = 50 µm.

A.3 Supplementary Material of Publication 2.6.

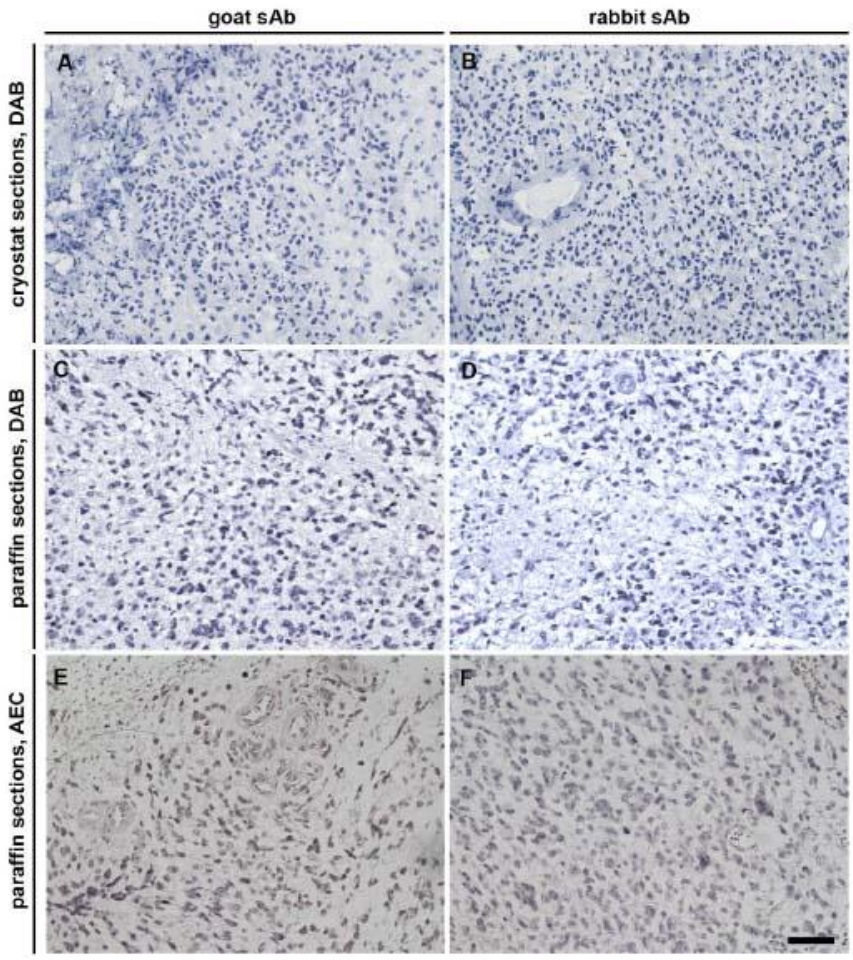
Supplementary Table 1. Details of the 21 GBM patients operated at the Department of Neurosurgery of the University of Ljubljana, University Medical Centre Ljubljana, Slovenia.

	Patient number	Gender	Age at the time of operation
1	NIB48	M	46
2	NIB50	M	81
3	NIB52	F	48
4	NIB55	F	62
5	NIB56	M	81
6	NIB65	M	43
7	NIB68	F	56
8	NIB70	M	54
9	NIB71	M	55
10	NIB74	M	75
11	NIB77	M	66
12	NIB78	M	59
13	NIB81	F	59
14	NIB82	F	66
15	NIB83	F	67
16	NIB87	M	53
17	NIB91	M	59
18	NIB93	M	65
19	NIB95	M	62
20	NIB96	M	71
21	NIB 98	M	80



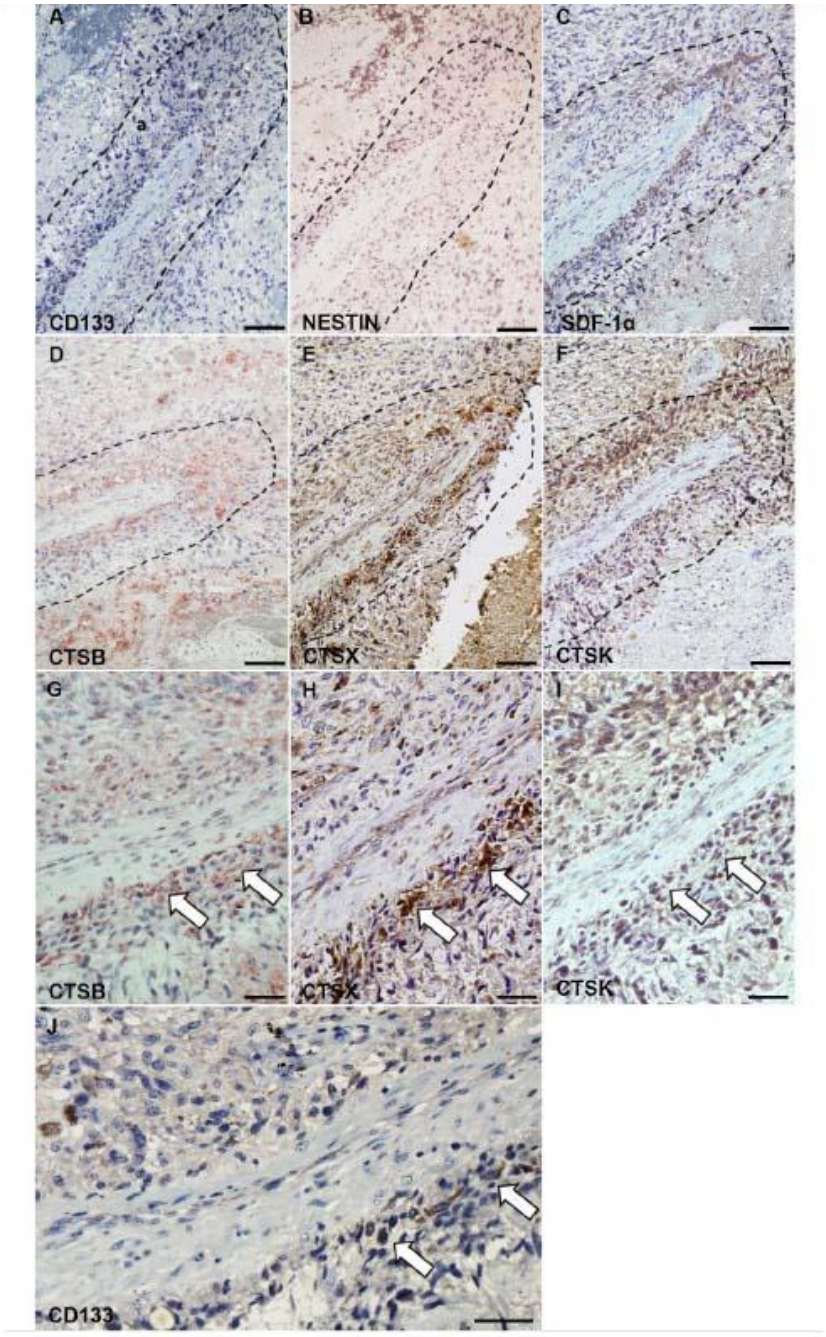
Supplementary Figure 1. Procedure for localization of cathepsin B and K activity with the use of metabolic mapping and selective fluorogenic substrates.

(A) The principle of the monitoring of cathepsin activity in GBM cryostat sections. The method is based on detection of green fluorescent product (dots) obtained after coupling of cleaved 4MβNA with 2-hydroxy-5-nitrobenzaldehyde. (B) Green fluorescent dots represent protease activity in GBM sections as indicated by arrows. Green fluorescent background is due to non-specific binding of 2-hydroxy-5-nitrobenzaldehyde to $-NH_2$ groups of proteins. (C) After 50-60 min, recrystallization of the final reaction product starts and the formation of needle-like crystals begins (arrow). Thus, the images have to be capture before recrystallization starts to occur. Scale bar = 50 µm.



Supplementary Figure 2. Control incubations for IHC of cryostat and paraffin-embedded GBM sections.

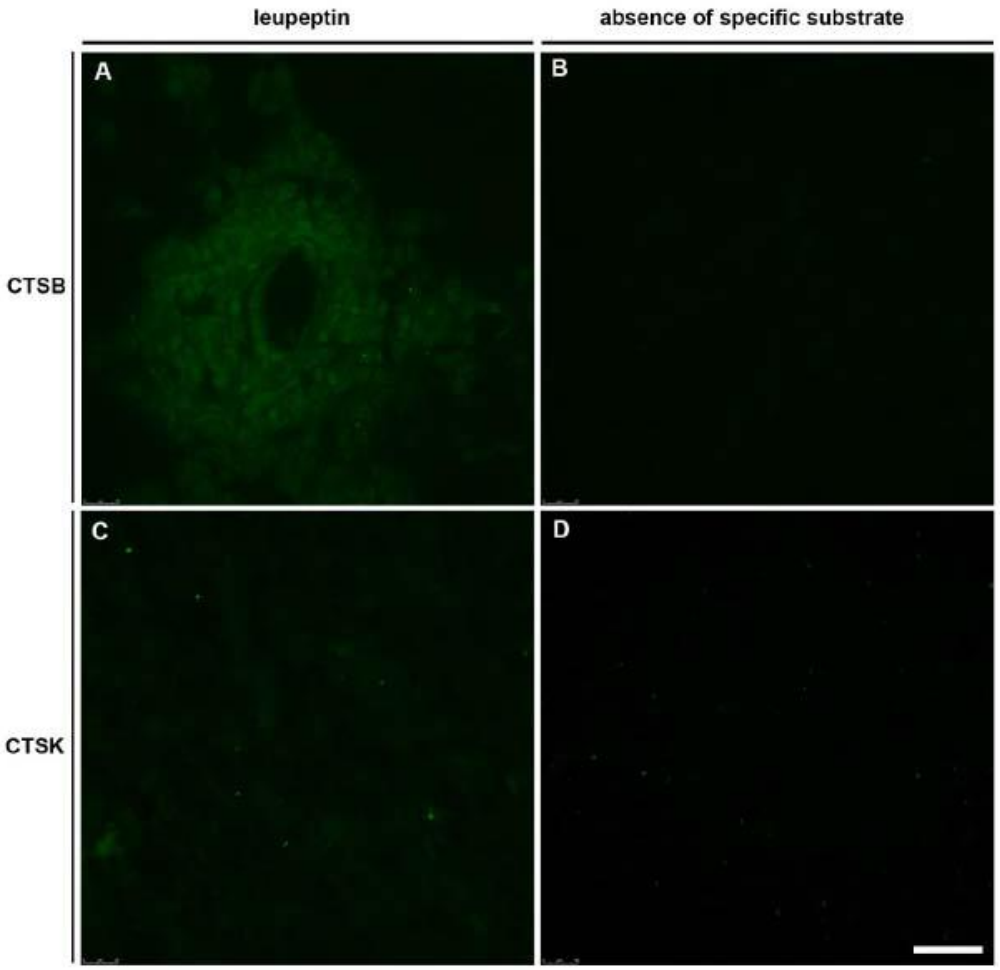
Control incubations were performed in the absence of primary antibodies and with goat (A, C, E) or rabbit (B, D, F) secondary horse-radish-peroxidase–conjugated antibodies (sAb) in the final dilution of 1:200. Immunohistochemical labelling was detected using DAB substrate (A-D) or AEC substrate (E, F). Cell nuclei were counterstained using haematoxylin (blue/purple). Scale bar = 50 µm.



Supplementary Figure 3. Low-magnification images of serial paraffin-embedded GBM sections labelled for GSC niche markers and cathepsins. Low-magnification images of Figure 3 are presented.

Cathepsins B (D, G), X (E, H) and K (F, I) are highly expressed within GSC niches (A-C) and their expression was co-localised with CD133-positive cells (A, D-F, G-J), as indicated by arrows. Immunohistochemical labelling of nestin (B) and cathepsin B (D,G) was performed with AEC as

substrate (red colour) and of the other proteins (A, C, E, F, H, J) with DAB as substrate (brown colour). Cell nuclei were counterstained using haematoxylin (blue/purple). a = arteriole. **A-F**: scale bar = 100 µm; **G-J**: scale bar = 50 µm.



Supplementary Figure 4. Control incubations of cryostat GBM sections for cathepsin B and K activity using metabolic mapping.

The specificity of the reaction was verified by incubation in the presence of the cathepsin inhibitor leupeptin (5 µM) (A, C) or in the absence of specific substrates for cathepsin B (B) and cathepsin K (D). Scale bar = 50 µm.

Appendix B

Permissions for Reproduction of Included Publications

B.1 Permission for Reproduction of Publication 2.7.



Copyright Clearance Center RightsLink®

Home | Create Account | Help

Title: Cathepsin K cleavage of SDF-1α inhibits its chemotactic activity towards glioblastoma stem-like cells

Author: Vashendriya V.V. Hira,Urška Verbovšek,Barbara Breznik,Matic Srdič,Marko Novinec,Hala Kakar,Jill Wormer,Britt Van der Swaan,Brigita Lenarčič,Luiz Juliano,Shwetal Mehta,Cornelis J.F. Van Noorden,Tamara T. Lah

Publication: Biochimica et Biophysica Acta (BBA) - Molecular Cell Research

Publisher: Elsevier

Date: March 2017

Copyright © 2017, Elsevier

LOGIN

If you're a copyright.com user, you can login to RightsLink using your copyright.com credentials. Already a RightsLink user or want to learn more?

Please note that, as the author of this Elsevier article, you retain the right to include it in a thesis or dissertation, provided it is not published commercially. Permission is not required, but please ensure that you reference the journal as the original source. For more information on this and on your other retained rights, please visit: https://www.elsevier.com/about/our-business/policies/copyright#Author-rights

BACK | CLOSE WINDOW

Copyright © 2017 Copyright Clearance Center, Inc. All Rights Reserved. Privacy statement. Terms and Conditions.
Comments? We would like to hear from you. E-mail us at customercare@copyright.com

References

Aggarwal, N. & Sloane, B.F. (2014). Cathepsin B: multiple roles in cancer. *Proteomics Clinical Applications*, 8(5-6), 427-37. doi: 10.1002/prca.201300105

Barcellos-de-Souza, P., Gori, V., Bambi, F. & Chiarugi, P. (2013). Tumor microenvironment: bone marrow-mesenchymal stem cells as key players. *Biochimica et Biophysica Acta*, 1836(2), 321-35. doi: 10.1016/j.bbcan.2013.10.004

Behnan, J., Isakson, P., Joel, M., Cilio, C., Langmoen, I.A., Vik-Mo, E.O. & Badn, W. (2014). Recruited brain tumor-derived mesenchymal stem cells contribute to brain tumor progression. *Stem Cells*, 32(5), 1110-23. doi: 10.1002/stem.1614

Behnan, J., Stangeland, B., Hosainey, S.A., Joel, M., Olsen, T.K., Micci, F., Glover, J.C., Isakson, P. & Brinchmann, J.E. (2017). Differential propagation of stroma and cancer stem cells dictates tumorigenesis and multipotency. *Oncogene*, 36(4), 570-584. doi: 10.1038/onc.2016.230

Beier, D., Hau, P., Proescholdt, M., Lohmeier, A., Wischhusen, J., Oefner, P.J., Aigner, L., Brawanski, A., Bogdahn, U. & Beier, C.P. (2007). CD133(+) and CD133(-) glioblastoma-derived cancer stem cells show differential growth characteristics and molecular profiles. *Cancer Research*, 67(9), 4010-5. doi: 10.1158/0008-5472.CAN-06-4180

Bjerkvig, R., Johansson, M., Miletic, H. & Niclou, S.P. (2009). Cancer stem cells and angiogenesis. *Seminars in Cancer Biology*, 19(5), 279-84. doi: 10.1016/j.semcancer.2009.09.001

Bonavia, R., Inda, M.M., Cavenee, W.K. & Furnari, F.B. (2011). Heterogeneity maintenance in glioblastoma: a social network. *Cancer Research*, 71(12), 4055-60. doi: 10.1158/0008-5472.CAN-11-0153

Borovski, T., De Sousa E Melo, F., Vermeulen, L. & Medema, J.P. (2011). Cancer stem cell niche: the place to be. *Cancer Research*, 71(3), 634-9. doi: 10.1158/0008-5472.CAN-10-3220

Brennan CW, Verhaak RG, McKenna A, Campos B, Noushmehr H, … Chin L; TCGA Research Network. (2013). The somatic genomic landscape of glioblastoma. *Cell*, 155(2), 462-77. doi: 10.1016/j.cell.2013.09.034

Breslin, S. & O'Driscoll, L. (2016). The relevance of using 3D cell cultures, in addition to 2D monolayer cultures, when evaluating breast cancer drug sensitivity and resistance. *Oncotarget*, 7(29), 45745-45756. doi: 10.18632/oncotarget.9935

Breznik, B., Motaln, H. & Turnšek, T.L. (2017). Proteases and cytokines as mediators of interactions between cancer and stromal cells in tumours. *Biological Chemistry*, 398(7), 709-719. doi: 10.1515/hsz-2016-0283

Breznik, B, Motaln, H., Vittori, M., Rotter, A. & Lah Turnšek, T. (2017). Mesenchymal stem cells differentially affect the invasion of distinct glioblastoma cell lines. *Oncotarge*t, 8(15), 25482-25499. doi: 10.18632/oncotarget.16041

Breznik, B., Limback, C., Kos, J., Khurshed, M., Bošnjak, R., J., Lah Turnšek, T. & Van Noorden. (in revision). Cysteine cathepsins B, X and K expression in peri-arteriolar glioblastoma stem cell niches. *Journal of Histochemistry and Cytochemistry*

Breznik, B., Limback, C., Porčnik, A., Blejec, A., Koprivnikar Krajnc, M., Bošnjak, R., Kos, J., Van Noorden, C.J.F. & Lah Turnšek, T. (in revision). Cathepsins K and X in glioblastoma progression and survival. *International Journal of Molecular Sciences*

Burrill, J.D. & Easter SS Jr. (1995). The first retinal axons and their microenvironment in zebrafish: cryptic pioneers and the pretract. *The Journal of Neuroscience*, 15(4), 2935-47.

Butowski, N., Colman, H., De Groot, J.F., Omuro, A.M., Nayak, L., … Prados, M. (2016). Orally administered colony stimulating factor 1 receptor inhibitor PLX3397 in recurrent glioblastoma: an Ivy Foundation Early Phase Clinical Trials Consortium phase II study. *Neuro Oncology*, 18(4), 557-64. doi: 10.1093/neuonc/nov245

Cabarcas, S.M., Mathews, L.A., & Farrar, W.L. (2011). The cancer stem cell niche — there goes the neighborhood? *International Journal of Cancer*, 129(10), 2315–2327. doi: 10.1002/ijc.26312

Calabrese, C., Poppleton, H., Kocak, M., Hogg, T.L., Fuller, C., … Gilbertson, R.J. (2007). A perivascular niche for brain tumor stem cells. Cancer Cell, 11(1), 69-82. doi: 10.1016/j.ccr.2006.11.020

Campos, B., Wan, F., Farhadi, M., Ernst, A., Zeppernick, F., … Herold-Mende C. (2010). Differentiation therapy exerts antitumor effects on stem-like glioma cells. *Clinical Cancer Research*, 16(10), 2715-28. doi: 10.1158/1078-0432.CCR-09-1800

Cassidy, J.W., Caldas, C. & Bruna, A. (2015). Maintaining Tumor Heterogeneity in Patient-Derived Tumor Xenografts. *Cancer Research*, 75(15):2963-8. doi: 10.1158/0008-5472.CAN-15-0727

Claes, A., Idema, A.J. & Wesseling, P. (2007). Diffuse glioma growth: a guerilla war. *Acta Neuropathologica*, 114(5):443-58. doi: 10.1007/s00401-007-0293-7

Colin, C., Voutsinos-Porche, B., Nanni, I., Fina, F., Metellus, P., … Figarella-Branger, D. (2009). High expression of cathepsin B and plasminogen activator inhibitor type-1 are strong predictors of survival in glioblastomas. *Acta Neuropathologica*, 118(6), 745-54. doi: 10.1007/s00401-009-0592-2

Cuddapah, V.A., Robel, S., Watkins, S. & Sontheimer, H. (2014). A neurocentric perspective on glioma invasion. *Nature Reviews Neuroscience*, 15(7), 455-65. doi: 10.1038/nrn3765

Czarnek, N., Clark, K., Peters, K.B. & Mazurowski MA. (2017). Algorithmic three-dimensional analysis of tumor shape in MRI improves prognosis of survival in glioblastoma: a multi-institutional study. *Journal of Neurooncology*, 132(1), 55-62. doi: 10.1007/s11060-016-2359-7

Dasari, V.R., Kaur, K., Velpula, K.K., Gujrati, M., Fassett, D., Klopfenstein, J.D, Dinh, D.H. & Rao, J.S. (2010). Upregulation of PTEN in glioma cells by cord blood mesenchymal stem cells inhibits migration via downregulation of the PI3K/Akt pathway. *PLoS One*, 5(4), e10350. doi: 10.1371/journal.pone.0010350

Domanska, U.M., Kruizinga, R.C., Nagengast, W.B., Timmer-Bosscha, H., Huls, G., de Vries, E.G. & Walenkamp, A.M. (2013). A review on CXCR4/CXCL12 axis in oncology: no place to hide. *European Journal of Cancer*, 49(1):219-30. doi: 10.1016/j.ejca.2012.05.005

Eden, C., Ju, B., Murugesan, M., Phoenix, T., Nimmervoll, B., … Gilbertson, R.J. (2015). Orthotopic models of pediatric brain tumors in zebrafish. *Oncogene,* 34(13), 1736-42. doi: 10.1038/onc.2014.107

Eden, C., Ju, B., Murugesan, M., Phoenix, T., Nimmervoll, B., Tong, Y., … Gilbertson, R.J. (2015). Orthotopic models of pediatric brain tumors in zebrafish. *Oncogene,* 34(13), 1736-42. doi: 10.1038/onc.2014.107

Ellis, H.P., Greenslade, M., Powell, B., Spiteri, I., Sottoriva, A. & Kurian, K.M. (2015). Current Challenges in Glioblastoma: Intratumour Heterogeneity, Residual Disease, and Models to Predict Disease Recurrence. *Frontiers in Oncology*, 5, 251. doi: 10.3389/fonc.2015.00251

Flannery, T., McQuaid, S., McGoohan, C., McConnell, R.S., McGregor, G., **...** Johnston, P.G. (2006). Cathepsin S expression: An independent prognostic factor in glioblastoma tumours--A pilot study. *International Journal of Cancer,* 119(4), 854–60. doi: 10.1002/ijc.21911

Friedl, P. & Wolf, K. (2003). Tumour-cell invasion and migration: diversity and escape mechanisms. *Nature Reviews Cancer*, 3(5), 362-74. doi: 10.1038/nrc1075

Fukuda, M.E., Iwadate, Y., Machida, T., Hiwasa, T., Nimura, Y., ... Seki, N. (2005). Cathepsin D is a potential serum marker for poor prognosis in glioma patients. *Cancer Research*, 65(12), 5190-4. doi: 10.1158/0008-5472.CAN-04-4134

Gallego, O. (2015). Nonsurgical treatment of recurrent glioblastoma. *Current Oncology*, 22(4), e273-81. doi: 10.3747/co.22.2436

Gattazzo, F., Urciuolo, A. & Bonaldo, P. (2014). Extracellular matrix: a dynamic microenvironment for stem cell niche. *Biochimica et Biophysica Acta*, 1840(8), 2506-19. doi: 10.1016/j.bbagen.2014.01.010

Goffart, N., Lombard, A., Lallemand, F., Kroonen, J., Nassen, J., **...** Rogister, B. (2017). CXCL12 mediates glioblastoma resistance to radiotherapy in the subventricular zone. *Neuro-Oncology*, 19(1), 66-77. doi: 10.1093/neuonc/now136

Gole, B., Durán Alonso, M.B., Dolenc, V. & Lah, T. (2009). Post-translational regulation of cathepsin B, but not of other cysteine cathepsins, contributes to increased glioblastoma cell invasiveness *in vitro*. *Pathology Oncology Research*, 15(4), 711-23. doi: 10.1007/s12253-009-9175-8

Gole, B., Huszthy, P.C., Popović, M., Jeruc, J., Ardebili, Y.S., Bjerkvig, R. & Lah, T.T. (2012) The regulation of cysteine cathepsins and cystatins in human gliomas. *International Journal of Cancer*, 131(8), 1779-89. doi: 10.1002/ijc.27453

Gutzman, J.H., Graeden, E.G., Lowery, L.A., Holley, H.S. & Sive, H. (2008). Formation of the zebrafish midbrain-hindbrain boundary constriction requires laminin-dependent basal constriction. *Mechanisms of Development*, 125(11-12). 974-83. doi: 10.1016/j.mod.2008.07.004

Hambardzumyan, D. & Bergers, G. (2015). Glioblastoma: Defining Tumor Niches. *Trends in Cancer*, 1(4), 252-265. doi: 10.1016/j.trecan.2015.10.009

Hanahan, D. & Coussens, L.M. (2012). Accessories to the crime: functions of cells recruited to the tumor microenvironment. *Cancer Cell*, 21(3), 309-22. doi: 10.1016/j.ccr.2012.02.022

Hazen, L.G., Bleeker, F.E., Lauritzen, B., Bahns, S., Song, J., Jonker, A., Van Driel, B.E., Lyon, H., Hansen, U., Köhler, A. & Van Noorden, C.J. (2000). Comparative localization of cathepsin B protein and activity in colorectal cancer. *The Journal of Histochemistry and Cytochemistry*, 48(10), 1421-30. doi: 10.1177/002215540004801012

Hira, V.V., Ploegmakers, K.J., Grevers, F., Verbovšek, U., Silvestre-Roig, C., … Van Noorden C.J. (2015). CD133+ and Nestin+ Glioma Stem-Like Cells Reside Around CD31+ Arterioles in Niches that Express SDF-1α, CXCR4, Osteopontin and Cathepsin K. *The Journal of Histochemistry and Cytochemistry*, 63(7), 481-93. doi: 10.1369/0022155415581689

Hira, V.V., Verbovšek, U., Breznik, B., Srdič, M., Novinec, M., Kakar, H., Wormer, J., der Swaan, B.V., Lenarčič, B., Juliano, L., Mehta, S., Van Noorden, C.J. & Lah TT. (2017). Cathepsin K cleavage of SDF-1α inhibits its chemotactic activity towards

glioblastoma stem-like cells. *Biochimica et Biophysica Acta*, 1864(3), 594-603. doi: 10.1016/j.bbamcr.2016.12.021

Hira, V.V.V., Wormer, J.R., Kakar, H., Breznik, B., Van der Swaan, B., Hulsbos, R., Tigchelaar, W, Tonar, Z., Khurshed, M., Molenaar, R.J. & Van Noorden, C.J.F. (2018). Peri-arteriolar glioblastoma stem cell niches express bone marrow hematopoietic stem cell niche proteins. *The Journal of Histochemistry and Cytochemistry,* 22155417749174. doi: 10.1369/0022155417749174

Hossain, A., Gumin, J., Gao, F., Figueroa, J., Shinojima, N., Takezaki, T., Priebe, W., Villarreal, D., Kang, S.G., Joyce, C., Sulman, E., Wang, Q., Marini, F.C., Andreeff, M., Colman, H. & Lang, F.F. (2015). Mesenchymal Stem Cells Isolated From Human Gliomas Increase Proliferation and Maintain Stemness of Glioma Stem Cells Through the IL-6/gp130/STAT3 Pathway. *Stem Cells*, 33(8), 2400-15. doi: 10.1002/stem.2053

Huszthy, P.C., Daphu, I., Niclou, S.P., Stieber, D., Nigro, J.M., Sakariassen, P.Ø., Miletic, H., Thorsen, F. & Bjerkvig, R. (2012). In vivo models of primary brain tumors: pitfalls and perspectives. *Neuro-Oncology*, 14(8):979-93. doi: 10.1093/neuonc/nos135

Johnson, B.E., Mazor, T., Hong, C., Barnes, M., Aihara, K., … Costello, J.F. (2014). Mutational analysis reveals the origin and therapy-driven evolution of recurrent glioma. *Science*, 343(6167), 189-193. doi: 10.1126/science.1239947

Kalluri, R. (2003). Basement membranes: structure, assembly and role in tumour angiogenesis. *Nature Reviews Cancer*, 3(6), 422-33. doi: 10.1038/nrc1094

Kenig, S., Alonso, M.B., Mueller, M.M. & Lah, T.T. (2010) Glioblastoma and endothelial cells cross-talk, mediated by SDF-1, enhances tumour invasion and endothelial proliferation by increasing expression of cathepsins B, S, and MMP-9. *Cancer Letters*, 2010, 289(1), 53-61. doi: 10.1016/j.canlet.2009.07.014

Kenig, S., Frangež, R., Pucer, A. & Lah, T. (2011). Inhibition of cathepsin L lowers the apoptotic threshold of glioblastoma cells by up-regulating p53 and transcription of caspases 3 and 7. *Apoptosis*, 16(7), 671-82. doi: 10.1007/s10495-011-0600-6

Kimlin, L.C., Casagrande, G. & Virador, V.M. (2013). In vitro three-dimensional (3D) models in cancer research: an update. *Molecular Carcinogenesis*, 52(3), 167-82. doi: 10.1002/mc.21844

Klopp, A.H., Gupta, A., Spaeth, E., Andreeff, M. & Marini, F. 3rd. (2011). Concise review: Dissecting a discrepancy in the literature: do mesenchymal stem cells support or suppress tumor growth? *Stem Cells*, 29(1), 11-9. doi: 10.1002/stem.559

Kollet, O., Dar, A., Shivtiel, S., Kalinkovich, A., Lapid, K., … Lapidot, T. (2006). Osteoclasts degrade endosteal components and promote mobilization of hematopoietic progenitor cells. *Nature Medicine*, 12(6), 657-64. doi: 10.1038/nm1417

Kološa, K., Motaln, H., Herold-Mende, C., Koršič, M. & Lah, T.T. (2015). Paracrine effects of mesenchymal stem cells induce senescence and differentiation of glioblastoma stem-like cells. *Cell Transplantation*, 24(4), 631-44. doi: 10.3727/096368915X687787

Kos, J., Mitrović, A. & Mirković, B. (2014). The current stage of cathepsin B inhibitors as potential anticancer agents. *Future Medical Chemistry*, 6(11), 1355-71. doi: 10.4155/fmc.14.73

Kos, J., Vižin, T., Fonović, U.P. & Pišlar, A. (2015). Intracellular signaling by cathepsin X: molecular mechanisms and diagnostic and therapeutic opportunities in cancer. *Seminars in Cancer Biology*, 31, 76-83. doi: 10.1016/j.semcancer.2014.05.001.

Lah, T.T., Durán Alonso, M.B. & Van Noorden, C.J. (2006) Antiprotease therapy in cancer: hot or not? *Expert Opinion on Biological Therapy*, 6(3), 257-79. doi: 10.1517/14712598.6.3.257

Lathia, J.D., Gallagher, J., Heddleston, J.M., Wang, J., Eyler, C.E., Macswords, J., Wu, Q., Vasanji, A., McLendon, R.E., Hjelmeland, A.B. & Rich, J.N. (2010). Integrin

alpha 6 regulates glioblastoma stem cells. *Cell Stem Cell*, 6(5), 421-32. doi: 10.1016/j.stem.2010.02.018

Lathia, J.D., Mack, S.C., Mulkearns-Hubert, E.E., Valentim, C.L. & Rich, J.N. (2015). Cancer stem cells in glioblastoma. *Genes & Development*, 29(12), 1203-17. doi: 10.1101/gad.261982.115

López-Otín, C. & Bond, J.S. (2008). Proteases: multifunctional enzymes in life and disease. *The Journal of Biological Chemistry.* 283(45), 30433-7. doi: 10.1074/jbc.R800035200

López-Otín, C. & Matrisian, L.M. (2007). Emerging roles of proteases in tumour suppression. *Nature Reviews Cancer*, 7(10), 800-8. doi: 10.1038/nrc2228

López-Otín, C. & Overall, C.M. (2002). Protease degradomics: a new challenge for proteomics. Nature Reviews *Molecular Cell Biology*, 3(7), 509-19. doi: 10.1038/nrm858

Louis, D.N., Perry, A., Reifenberger, G., von Deimling, A., Figarella-Branger, D., Cavenee, W.K., Ohgaki, H., Wiestler, O.D., Kleihues, P. & Ellison, D.W. (2016). The 2016 World Health Organization Classification of Tumors of the Central Nervous System: a summary. *Acta Neuropathologica*, 131(6), 803-20. doi: 10.1007/s00401-016-1545-1

Ludwig, K. & Kornblum, H.I. (2017). Molecular markers in glioma. *Journal of Neurooncology.* doi: 10.1007/s11060-017-2379-y. [Epub ahead of print]

MacRae, C.A. & Peterson, R.T. (2015). Zebrafish as tools for drug discovery. *Nature Reviews Drug Discovery*, 14(10):721-31. doi: 10.1038/nrd4627

Mason, S.D. & Joyce, J.A. (2011). Proteolytic networks in cancer. T*rends in Cell Biology*, 21(4), 228-37. doi: 10.1016/j.tcb.2010.12.002

Meng, J., Li, P., Zhang, Q., Yang, Z. & Fu, S. (2014). A radiosensitivity gene signature in predicting glioma prognostic via EMT pathway. *Oncotarget*, 5(13), 4683-93. doi: 10.18632/oncotarget.2088

Mentlein, R., Hattermann, K. & Held-Feindt, J. (2012). Lost in disruption: role of proteases in glioma invasion and progression. *Biochimica et Biophysica Acta*, 1825(2), 178-85. doi: 10.1016/j.bbcan.2011.12.001

Mirković, B., Markelc, B., Butinar, M., Mitrović, A., Sosič, I., … Kos, J. (2015). Nitroxoline impairs tumor progression in vitro and in vivo by regulating cathepsin B activity. *Oncotarget*, 6(22):19027-42. doi: 10.18632/oncotarget.3699

Mitrović, A., Sosič, I., Kos, Š., Tratar, U.L., Breznik, B., Kranjc, S., Mirković, B., Gobec, S., Lah, T., Serša, G. & Kos, J. (2017). Addition of 2-(ethylamino)acetonitrile group to nitroxoline results in significantly improved anti-tumor activity *in vitro* and *in vivo*. *Oncotarget*, 8(35), 59136-59147. doi: 10.18632/oncotarget.19296

Mohamed, M.M. & Sloane, B.F. (2006). Cysteine cathepsins: multifunctional enzymes in cancer. *Nature Reviews Cancer*, 6(10), 764-75. doi: 10.1038/nrc1949

Motaln, H. & Turnsek, T.L. (2015). Cytokines play a key role in communication between mesenchymal stem cells and brain cancer cells. *Protein and Peptide Letters*, 22(4), 322–331.

Motaln, H., Gruden, K., Hren, M., Schichor, C., Primon, M., Rotter, A. & Lah, T.T. (2012). Human mesenchymal stem cells exploit the immune response mediating chemokines to impact the phenotype of glioblastoma. *Cell Transplantation*, 21(7), 1529-45. doi: 10.3727/096368912X640547

Motaln, H., Koren, A., Gruden, K., Ramšak, Ž., Schichor, C. & Lah, T.T. (2015). Heterogeneous glioblastoma cell cross-talk promotes phenotype alterations and enhanced drug resistance. *Oncotarget*, 6(38), 40998-1017. doi: 10.18632/oncotarget.5701.

Mueller, M.M. & Fusenig, N.E. (2004). Friends or foes - bipolar effects of the tumour stroma in cancer. *Nature Reviews Cancer*, 4(11), 839-49. doi:10.1038/nrc1477

Ohgaki, H. & Kleihues, P. (2013). The definition of primary and secondary glioblastoma. Clin Cancer Research, 19(4), 764-72. doi: 10.1158/1078-0432.CCR-12-3002.

Olson, O.C. & Joyce, J.A. (2015). Cysteine cathepsin proteases: regulators of cancer progression and therapeutic response. *Nature Reviews Cancer*, 15(12), 712-29. doi: 10.1038/nrc4027

Patel, A.P., Tirosh, I., Trombetta, J.J., Shalek, A.K., Gillespie, S.M., … Bernstein, B.E. (2014). Single-cell RNA-seq highlights intratumoral heterogeneity in primary glioblastoma. *Science*, 344(6190), 1396-401. doi: 10.1126/science.1254257

Phillips, H.S., Kharbanda, S., Chen, R., Forrest, W.F., Soriano, R.H., Wu, T.D., Misra, A., Nigro, J.M., Colman ,H., Soroceanu, L., Williams, P.M., Modrusan, Z., Feuerstein, B.G. & Aldape, K. (2006). Molecular subclasses of high-grade glioma predict prognosis, delineate a pattern of disease progression, and resemble stages in neurogenesis. *Cancer Cell*, 9(3), 157-73. doi:10.1016/j.ccr.2006.02.019

Pickup, M., Novitskiy, S. & Moses, H.L. (2013). The roles of TGFβ in the tumour microenvironment. *Nature Reviews Cancer*, 13(11), 788-99. doi: 10.1038/nrc3603

Piek, E., Westermark, U., Kastemar, M,, Heldin, C.H., van Zoelen, E.J., Nistér, M. & Ten Dijke, P. (1999). Expression of transforming-growth-factor (TGF)-beta receptors and Smad proteins in glioblastoma cell lines with distinct responses to TGF-beta1. *International Journal of Cancer*, 80(5).756-63.

Placone, A.L., Quiñones-Hinojosa, A. & Searson, P.C. (2016). The role of astrocytes in the progression of brain cancer: complicating the picture of the tumor microenvironment. *Tumour Biology*, 37(1), 61-9. doi: 10.1007/s13277-015-4242-0.

Plaks, V., Kong, N. & Werb, Z. (2015). The cancer stem cell niche: how essential is the niche in regulating stemness of tumor cells? *Cell Stem Cell*, 16(3), 225-38. doi: 10.1016/j.stem.2015.02.015

Podergajs, N., Motaln, H., Rajčević, U., Verbovšek, U., Koršič, M., Obad, N., Espedal, H., Vittori, M., Herold-Mende, C., Miletic, H., Bjerkvig, R. & Turnšek, T.L. (2016). Transmembrane protein CD9 is glioblastoma biomarker, relevant for maintenance of glioblastoma stem cells. *Oncotarget*, 7(1):593-609. doi: 10.18632/oncotarget.5477

Quail, D.F. & Joyce, J.A. (2017) The Microenvironmental Landscape of Brain Tumors. *Cancer Cell*, 31(3), 326-341. doi: 10.1016/j.ccell.2017.02.009.

Rama, A.R., Alvarez, P.J., Madeddu, R. & Aranega, A. (2014). ABC transporters as differentiation markers in glioblastoma cells. *Molecular Biology Reports*, 41(8), 4847-51. doi: 10.1007/s11033-014-3423-z

Rao Malla, R., Gopinath, S., Alapati, K., Gorantla, B., Gondi, C.S. & Rao, J.S. (2013). Knockdown of cathepsin B and uPAR inhibits CD151 and α3β1 integrin-mediated cell adhesion and invasion in glioma. *Molecular Carcinogenesis*, 52(10), 777-90. doi: 10.1002/mc.21915

Rape, A., Ananthanarayanan, B. & Kumar, S. (2014). Engineering strategies to mimic the glioblastoma microenvironment. *Advanced Drug Delivery Reviews*, 79-80, 172-83. doi: 10.1016/j.addr.2014.08.012

Rauch, U. (2004). Extracellular matrix components associated with remodeling processes in brain. *Cellular and Molecular Life Sciences*, 61(16), 2031-45. doi: 10.1007/s00018-004-4043-x

Rauch, U. (2007). Brain matrix: structure, turnover and necessity. *Biochemical Society Transactions*, 35(Pt 4), 656-60. doi: 10.1042/BST0350656

Rawlings, N.D., Barrett, A.J. & Finn, R. (2016).Twenty years of the MEROPS database of proteolytic enzymes, their substrates and inhibitors. *Nucleic Acids Research*, 44*(D1),* D343-50. doi: 10.1093/nar/gkv1118

Renovanz, M. & Kim, E.L. (2014). Intratumoral heterogeneity, its contribution to therapy resistance and methodological caveats to assessment. *Frontiers in Oncology*, 4, 142. doi: 10.3389/fonc.2014.00142

Ricklefs, F., Mineo, M., Rooj, A.K., Nakano, I., Charest, A., Weissleder, R., Breakefield, X.O., Chiocca, E.A., Godlewski, J. & Bronisz, A. (2016). Extracellular Vesicles from High-Grade Glioma Exchange Diverse Pro-oncogenic Signals That Maintain Intratumoral Heterogeneity. *Cancer Research*, 76(10), 2876-81. doi: 10.1158/0008-5472.CAN-15-3432

Roos, A., Ding, Z., Loftus, J.C. & Tran, N.L. (2017). Molecular and Microenvironmental Determinants of Glioma Stem-Like Cell Survival and Invasion. *Frontiers in Oncology*, 7, 120. doi: 10.3389/fonc.2017.00120

Sayegh, E.T., Kaur, G., Bloch, O. & Parsa, A.T. (2014). Systematic review of protein biomarkers of invasive behavior in glioblastoma. *Molecular Neurobiology*, 49(3), 1212-44. doi: 10.1007/s12035-013-8593-5

Scherer, H. J. (1938). Structural development in gliomas. The *American Journal of Cancer,* 34(3), 333–351.

Schichor, C., Albrecht, V., Korte, B., Buchner, A., Riesenberg, R., … Tonn JC. (2012). Mesenchymal stem cells and glioma cells form a structural as well as a functional syncytium *in vitro*. *Experimental Neurology*, 234(1), 208-19. doi: 10.1016/j.expneurol.2011.12.033

Segerman, A., Niklasson, M., Haglund, C., Bergström, T., Jarvius, M., … Westermark, B. (2016). Clonal Variation in Drug and Radiation Response among Glioma-Initiating Cells Is Linked to Proneural-Mesenchymal Transition. *Cell Reports*, 17(11), 2994-3009. doi: 10.1016/j.celrep.2016.11.056.

Sevenich, L, & Joyce, J.A. (2014) Pericellular proteolysis in cancer. *Genes and Development*, 28(21), 2331-47. doi: 10.1101/gad.250647.114

Singh, S.K., Clarke, I.D., Terasaki, M., Bonn, V.E., Hawkins, C., Squire, J. & Dirks, P.B. (2003). Identification of a cancer stem cell in human brain tumors. *Cancer Research*, 63(18), 5821-8.

Singh, S.K., Fiorelli, R., Kupp, R., Rajan, S., Szeto, E., … Mehta, S. (2016). Post-translational Modifications of OLIG2 Regulate Glioma Invasion through the TGF-β Pathway. *Cell Reports*, 16(4), 950-66. doi: 10.1016/j.celrep.2016.06.045

Sosič, I., Mirković, B., Arenz, K., Stefane, B., Kos, J. & Gobec, S. (2013). Development of new cathepsin B inhibitors: combining bioisosteric replacements and structure-based design to explore the structure-activity relationships of nitroxoline derivatives. *Journal of Medical Chemistry*, 56(2), 521-33. doi: 10.1021/jm301544x

Staudt, N.D., Aicher, W.K., Kalbacher, H., Stevanovic, S., Carmona, A.K., Bogyo, M. & Klein, G. (2010). Cathepsin X is secreted by human osteoblasts, digests CXCL-12 and impairs adhesion of hematopoietic stem and progenitor cells to osteoblasts. *Haematologica*, 95(9), 1452-60. doi: 10.3324/haematol.2009.018671

Staudt, N.D., Maurer, A., Spring, B., Kalbacher, H., Aicher, W.K. & Klein G. (2012). Processing of CXCL12 by different osteoblast-secreted cathepsins. *Stem Cells and Development,* 21(11), 1924-35. doi: 10.1089/scd.2011.0307

Strojnik, T., Kavalar, R., Trinkaus, M. & Lah, T.T. (2005). Cathepsin L in glioma progression: comparison with cathepsin B. *Cancer Detectiona and Prevention*, 29(5), 448-55. doi: 10.1016/j.cdp.2005.07.006

Strojnik, T., Kos, J., Zidanik, B., Golouh, R. & Lah, T. (1999) Cathepsin B immunohistochemical staining in tumor and endothelial cells is a new prognostic factor for survival in patients with brain tumors. *Clinical Cancer Res*earch, 5(3), 559-67.

Tajnšek, U., Motaln, H., Levičar, N., Rotter, A. & Lah Turnšek, T. (2013). The duality of stem cells: Double-edged sword in tumor evolution and treatment. In: Resende RR, Ulrich H (eds) *Trends in Stem Cell Proliferation and Cancer Research*. Springer Science+Business Media, Dordrecht, pp 391–433.

Thoma, C.R., Zimmermann, M., Agarkova, I., Kelm, J.M. & Krek, W. (2014). 3D cell culture systems modeling tumor growth determinants in cancer target discovery. *Advanced Drug Delivery Reviews*, 69-70, 29-41. doi: 10.1016/j.addr.2014.03.001

Tobia, C., Gariano, G., De Sena, G. & Presta, M. (2013). Zebrafish embryo as a tool to study tumor/endothelial cell cross-talk. *Biochimica et Biophysica Acta*, 1832(9):1371-7. doi: 10.1016/j.bbadis.2013.01.016

Torsvik, A. & Bjerkvig, R. (2013). Mesenchymal stem cell signaling in cancer progression. *Cancer Treatment Reviews*, 39(2),180-8. doi: 10.1016/j.ctrv.2012.03.005

Turk, B., Turk, D. & Turk, V. (2012). Protease signalling: the cutting edge. The EMBO Journal. 31(7), 1630-43. doi: 10.1038/emboj.2012.42

Ulrich, T.A., de Juan Pardo, E.M. & Kumar, S. (2009). The mechanical rigidity of the extracellular matrix regulates the structure, motility, and proliferation of glioma cells. *Cancer Reseach*, 69(10), 4167-74. doi: 10.1158/0008-5472.CAN-08-4859

Van Meir, E.G., Hadjipanayis, C.G., Norden, A.D., Shu, H.K., Wen, P.Y. & Olson, J.J. (2010). Exciting new advances in neuro-oncology: the avenue to a cure for malignant glioma. *CA: A Cancer Journal for Clinicians*, 60(3), 166-93. doi: 10.3322/caac.20069

Verbovšek, U., Motaln, H., Rotter, A., Atai, N.A., Gruden, K., Van Noorden, C.J. & Lah, T.T. (2014). Expression analysis of all protease genes reveals cathepsin K to be overexpressed in glioblastoma. *PLoS One*, 9(10), e111819. doi: 10.1371/journal.pone.0111819

Verbovšek, U., Van Noorden, C.J. & Lah, T.T. (2015). Complexity of cancer protease biology: Cathepsin K expression and function in cancer progression. *Seminars in Cancer Biology*, 35, 71-84. doi: 10.1016/j.semcancer.2015.08.010

Verhaak, R.G., Hoadley, K.A., Purdom, E., Wang, V., Qi, Y., Wilkerson, ... Hayes, D.N., Cancer Genome Atlas Research Network (2010). Integrated genomic analysis identifies clinically relevant subtypes of glioblastoma characterized by abnormalities in PDGFRA, IDH1, EGFR, and NF1. *Cancer Cell*, 17(1), 98-110. doi: 10.1016/j.ccr.2009.12.020

Vittori, M., Breznik, B., Gredar, T., Hrovat, K., Bizjak Mali, L. & Lah TT. (2016). Imaging of human glioblastoma cells and their interactions with mesenchymal stem cells in the zebrafish (Danio rerio) embryonic brain. *Radiology and Oncology*, 50(2), 159-67. doi: 10.1515/raon-2016-0017

Vittori, M., Motaln, H. & Turnsek, T.L. (2015) The study of glioma by xenotransplantation in zebrafish early life stages. *The Journal of Histochemistry and Cytochemistry*, 63(10), 749-61. doi: 10.1369/0022155415595670

Vizin, T., Christensen, I.J., Nielsen, H.J. & Kos, J. (2012). Cathepsin X in serum from patients with colorectal cancer: relation to prognosis. *Radiology and Oncology*, 46(3), 207-12. doi: 10.2478/v10019-012-0040-0

Wang, J., Cao, Z., Zhang, X.M., Nakamura, M., Sun, M., Hartman, J., Harris, R.A., Sun,Y. & Cao, Y. (2015). Novel mechanism of macrophage-mediated metastasis revealed in a zebrafish model of tumor development. *Cancer Research*, 75(2):306-15. doi: 10.1158/0008-5472.CAN-14-2819

Wang, J., Chen, L., Li, Y. & Guan, X.Y. (2011). Overexpression of cathepsin Z contributes to tumor metastasis by inducing epithelial-mesenchymal transition in hepatocellular carcinoma. *PLoS One*, 6(9), e24967. doi: 10.1371/journal.pone.0024967

Wang, J., Sakariassen, P.Ø., Tsinkalovsky, O., Immervoll, H., Bøe, S.O., … Enger PØ. (2008). CD133 negative glioma cells form tumors in nude rats and give rise to CD133 positive cells. *International Journal of Cancer*, 122(4). 761-8. doi: 10.1002/ijc.23130

Wang, Q., Hu, B., Hu, X., Kim, H., Squatrito, M., … Verhaak, R.G.W. (2017). Tumor Evolution of Glioma-Intrinsic Gene Expression Subtypes Associates with Immunological Changes in the Microenvironment. *Cancer Cell*, 32(1), 42-56.e6. doi: 10.1016/j.ccell.2017.06.003

Welker, A.M., Jaros, B.D., Puduvalli, V.K., Imitola, J., Kaur, B. & Beattie, C.E. (2016). Standardized orthotopic xenografts in zebrafish reveal glioma cell-line-specific characteristics and tumor cell heterogeneity. *Disease Models & Mechanisms*, 9(2), 199-210. doi: 10.1242/dmm.022921

White, R., Rose, K. & Zon, L. (2013). Zebrafish cancer: the state of the art and the path forward. *Nature Reviews Cancer,* 13(9), 624-36. doi: 10.1038/nrc3589

Wolf, K. & Friedl, P. (2011). Extracellular matrix determinants of proteolytic and non-proteolytic cell migration. *Trends in Cell Biology*, 21(12), 736-44. doi: 10.1016/j.tcb.2011.09.006

Wu, A., Wei, J., Kong, L.Y., Wang, Y., Priebe, W., Qiao, W., Sawaya, R. & Heimberger, A.B. (2010). Glioma cancer stem cells induce immunosuppressive macrophages/microglia. *Neuro-Oncology*, 12(11), 1113-25. doi: 10.1093/neuonc/noq082

Yamada, K.M. & Cukierman, E. (2007). Modeling tissue morphogenesis and cancer in 3D. *Cell*, 130(4), 601-10. doi: 10.1016/j.cell.2007.08.006

Yang, X.J., Cui, W., Gu, A., Xu, C., Yu, S.C., Li, T.T., Cui, Y.H., Zhang, X. & Bian, X.W. (2013). A novel zebrafish xenotransplantation model for study of glioma stem cell invasion. *PLoS On*e, 8(4), e61801. doi: 10.1371/journal.pone.0061801

Ye, X. & Weinberg, R.A. (2015). Epithelial-Mesenchymal Plasticity: A Central Regulator of Cancer Progression. *Trends in Cell Biology*, 25(11), 675-86. doi: 10.1016/j.tcb.2015.07.012

Zhang, B., Shimada, Y., Kuroyanagi, J., Nishimura, Y., Umemoto, N., Nomoto, T., Shintou, T., Miyazaki, T. & Tanaka, T. (2014). Zebrafish xenotransplantation model for cancer stem-like cell study and high-throughput screening of inhibitors. *Tumour Biology*, 35(12), 11861-9. doi: 10.1007/s13277-014-2417-8

Zhu, T.S., Costello, M.A., Talsma, C.E., Flack, C.G., Crowley, J.G., **...** Fan, X. (2011). Endothelial cells create a stem cell niche in glioblastoma by providing NOTCH ligands that nurture self-renewal of cancer stem-like cells. *Cancer Research*, 71(18), 6061-72. doi: 10.1158/0008-5472.CAN-10-4269

Bibliography

Publications Related to the Thesis

Breznik, B, Motaln, H., Vittori, M., Rotter, A. & Lah Turnšek, T. (2017). Mesenchymal stem cells differentially affect the invasion of distinct glioblastoma cell lines. *Oncotarge*t, 8(15), 25482-25499. doi: 10.18632/oncotarget.16041

Breznik, B., Limback, C., Kos, J., Khurshed, M., Bošnjak, R., J., Lah Turnšek, T. & Van Noorden. (in revision). Cysteine cathepsins B, X and K expression in peri-arteriolar glioblastoma stem cell niches. *Journal of Histochemistry and Cytochemistry*

Breznik, B., Limback, C., Porčnik, A., Blejec, A., Koprivnikar Krajnc, M., Bošnjak, R., Kos, J., Van Noorden, C.J.F. & Lah Turnšek, T. (in revision). Cathepsins K and X in glioblastoma progression and survival. *International Journal of Molecular Sciences*

Breznik, B., Motaln, H. & Lah Turnšek, T. (2017). Proteases and cytokines as mediators of interactions between cancer and stromal cells in tumours. *Biological Chemistry*, 398(7), 709-719. doi: 10.1515/hsz-2016-0283

Hira, V.V., Verbovšek, U., Breznik, B., Srdič, M., Novinec, M., Kakar, H., Wormer, J., der Swaan, B.V., Lenarčič, B., Juliano, L., Mehta, S., Van Noorden, C.J. & Lah TT. (2017). Cathepsin K cleavage of SDF-1α inhibits its chemotactic activity towards glioblastoma stem-like cells. *Biochimica et Biophysica Acta*, 1864(3), 594-603. doi: 10.1016/j.bbamcr.2016.12.021

Mitrović, A., Sosič, I., Kos, Š., Tratar, U.L., Breznik, B., Kranjc, S., Mirković, B., Gobec, S., Lah, T., Serša, G. & Kos, J. (2017). Addition of 2-(ethylamino)acetonitrile group to nitroxoline results in significantly improved anti-tumor activity *in vitro* and *in vivo*. *Oncotarget*, 8(35), 59136-59147. doi: 10.18632/oncotarget.19296

Vittori, M., Breznik, B., Gredar, T., Hrovat, K., Bizjak Mali, L. & Lah TT. (2016). Imaging of human glioblastoma cells and their interactions with mesenchymal stem cells in the zebrafish (Danio rerio) embryonic brain. *Radiology and Oncology*, 50(2), 159-67. doi: 10.1515/raon-2016-0017

Other Publications

Hira, V.V.V., Wormer, J.R., Kakar, H., Breznik, B., Van der Swaan, B., Hulsbos, R., Tigchelaar, W, Tonar, Z., Khurshed, M., Molenaar, R.J. & Van Noorden, C.J.F. (2018). Peri-arteriolar glioblastoma stem cell niches express bone marrow hematopoietic stem cell niche proteins. *The Journal of Histochemistry and Cytochemistry,* 22155417749174. doi: 10.1369/0022155417749174

Pillat, M.M., Oliveira, M.N., Motaln, H., Breznik, B., Glaser, T., Lah, T.T. & Ulrich, H. (2016). Glioblastoma-mesenchymal stem cell communication modulates expression patterns of kinin receptors: Possible involvement of bradykinin in information flow. *Cytometry Part A*, 89(4), 365-75. doi: 10.1002/cyto.a.22800

Vittori, M., Breznik, B., Hrovat, K., Kenig, S. & Lah, T.T. (2017). RECQ1 Helicase Silencing Decreases the Tumour Growth Rate of U87 Glioblastoma Cell Xenografts in Zebrafish Embryos. *Genes (Basel)*, 8(9). pii: E222. doi: 10.3390/genes8090222

Biography

The author of this thesis, Barbara Breznik, was born on 21st October 1989 in Novo mesto. She finished Primary school Loka and High school Črnomelj. In 2008, she enrolled in Uniform master's study programme Pharmacy at the Faculty of Pharmacy, University of Ljubljana. She defended her master thesis, entitled *Establishment and characterization of in vitro tumour invasion models using the cell line U-87* in July 2013. The master thesis was performed under the supervision of Prof. Janko Kos and Bojana Mirković.

In October 2013, she enrolled in the PhD program Nanosciences and Nanotechnologies at the Jožef Stefan International Postgraduate School and started her PhD research as a young researcher at the Department of Genetic Toxicology and Cancer Biology at the National Institute of Biology under the supervision of Prof. Tamara Lah Turnšek. She spent part of her PhD training abroad, at the Department of Medical Biology at the Academic Medical Center Amsterdam for 3 months. There, she was trained in histology technics under the supervision of Prof. Cornelis van Noorden. She presented her work at several international conferences and meetings, such as Glioma Invasion Forum, Conference on Translational Oncology, Summer School on Proteases and their Inhibitors, EORTC Pathobiology annual meetings and EMBO conference. The PhD candidate attended several workshops on the topics qPCR, confocal microscopy, survival analysis, scientific writing and cancer biology.

She has been involved in various international projects, such as the European Programme of Cross-Border Cooperation for Slovenia-Italy GLIOMA and Brazilian National Council of Technological and Scientific Development-founded project: The Relevance of the Bradykinin system and Related Purinergic Signalling Pathways in GBM Cells upon Co-culturing with Human Mesenchymal Stem Cells. She is a management committee substitute in EU-founded COST action 16119: *In vitro 3-D total cell guidance and fitness.*